Simplicity of supercooled liquids

Experimental investigations inspired by the isomorph theory

Schmidt, Lisa Anita Roed

Publication date:
2018

Document Version
Publisher's PDF, also known as Version of record

Citation for published version (APA):
Schmidt, L. A. R. (2018). *Simplicity of supercooled liquids: Experimental investigations inspired by the isomorph theory*. Roskilde Universitet.

PhD thesis

by Lisa Anita Roed Schmidt

Simplicity of supercooled liquids

Experimental investigations inspired by the isomorph theory

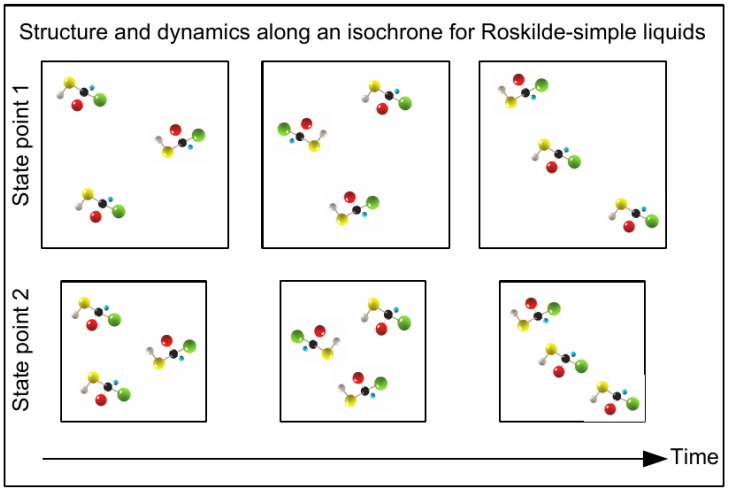

Supervisor: Kristine Niss
Co-supervisor: Bo Jakobsen

Glass & Time, Physics, IMFUFA, Department of Science and Environment, Roskilde University, Denmark

October 31, 2018

Abstract

This thesis investigates simple behavior of supercooled liquids inspired by the isomorph theory's predictions for Roskilde-simple liquids. Van der Waals liquids are expected to be Roskilde simple, whereas hydrogen-bonded liquids are not. Four investigations are presented.

1) A liquid obeys isochronal superposition if its dynamics is invariant along the isochrones. We develop quantitative measures of isochronal superposition and use them on the four van der Waals-bonded liquids, polyphenyl ether, diethyl phthalate, tetramethyl tetraphenyl trisiloxane, and dibutyl phthalate, and the two hydrogen-bonded liquids, glycerol and 1,2,6 hexanetriol. We conclude that the van der Waals liquids obey isochronal superposition to a higher degree than the hydrogen-bonded liquids. This confirms a prediction of the isomorph theory.

2) The van der Waals-bonded liquid, polyphenyl ether, is studied using specific heat spectroscopy under high pressure. The results are compared to similar dielectric results to test if the isochrones from the two methods coincide. We conclude that the ratio between the two time scales is independent of both temperature and pressure, which is a greater simplicity than predicted by the isomorph theory.

3) Aging following jumps in temperature is studied for the hydrogen-bonded liquids, glycerol and 1,2,6 hexanetriol, and the van der Waals-bonded liquid, diethyl phthalate. Two tests of single-parameter aging (the measured quantity and the clock rate are controlled by the same parameter) are generalized. We conclude that all studied liquids have single-parameter aging to a good approximation.

4) The isomorph theory predicts that Roskilde-simple liquids come into instantaneous equilibrium following a jump from a state point on an isochrone to another state point on the same isochrone. Our preliminary measurements on the van der Waals-bonded liquid, polyphenyl ether, confirms this prediction.

As an overall conclusion, the van der Waals liquids follow the predictions from the isomorph theory, with several of the liquids showing even greater simplicity. The hydrogen-bonded liquids also have simple behavior to a good approximation.

Abstract in Danish

Denne afhandling undersøger simpel opførsel af underafkølede væsker inspireret af isomorph teoriens forudsigelser for Roskilde-simple væsker. Van der Waals bundne væsker forventes at være Roskilde simple, mens hydrogen bundne væsker ikke er. Fire undersøgelser præsenteres.

1) En væske opfylder isochronal superposition, hvis dens dynamik er invariant langs en isokron. Vi udvikler kvantitative mål af isochronal superposition og anvender dem på de fire van der Waals bundne væsker, polyphenyl ether, diethyl phthalate, tetramethyl tetraphenyl trisiloxane, og dibutyl phthalate, og de to hydrogen bundne væsker, glycerol og 1,2,6 hexanetriol. Vi konkluderer, at van der Waals væskerne har isochronal superposition i større grad end de hydrogen bundne væsker. Dette bekræfter en forudsigelse fra isomorph teorien.

2) Vi undersøger den frekvensafhængige varmefylde ved høje tryk for den van der Waals bundne væske, polyphenyl ether. Resultaterne sammenlignes med lignende dielektriske resultater for at teste om isokronerne for de to metoder er sammenfaldende. Vi konkluderer, at forholdet mellem de karakteristiske tider er uafhængigt af både temperatur og tryk, hvilket er en simplere opførsel end forudsagt af isomorph teorien.

3) "Aging"-opførslen efterfulgt af temperatur ændringer undersøges for de hydrogen bundne væsker, glycerol og 1,2,6 hexanetriol, og den van der Waals bundne væske, diethyl phthalate. To tests af "én"-parameter aging (den målte størrelse og raten kontrolleres af den samme parameter) generaliseres. Vi konkluderer, at alle de undersøgte væsker har tilnærmelsesvis "én"-parameter aging.

4) Isomorph teorien forudsiger, at Roskilde-simple væsker kommer instantant i ligevægt efter et spring fra et punkt på en isokron til et andet punkt på den samme isokron. Vores foreløbige målinger på den van der Waals bundne væske polyphenyl ether bekræfter denne forudsigelse.

Den samlede konklusion er, at de van der Waals bundne væsker følger forudsigelserne fra isomorph teorien, og at nogle af dem har endnu simplere opførsel. De hydrogen bundne væsker har også tilnærmelsesvis simpel opførsel.

Preface

This PhD project was carried out in the "Glass & Time" group at Roskilde University while enrolled in The Doctoral School of Science and Environment. The PhD project was supervised by Professor Kristine Niss and co-supervised by Doctor Bo Jakobsen. The PhD project was partly funded by the Danish Council for Independent Research (Sapere Aude: Starting Grant) and partly by The Danish National Research Foundation's Grant No. DNRF61. The PhD project was initiated on December 16, 2012, and submitted October 31, 2018, with approximately 3 years of absence due to illness, two occurrences of maternity leave, and absence due to illness of my children. The working time of this PhD project thus lasted the three years of the Danish PhD program, including courses of 30 ECTS points and teaching obligations.

In the thesis, I use the term "we" both when I am writing about work done together with co-workers, but also when it is my own thoughts, decisions, and conclusions that are described. This is due to the convention in the field and to acknowledge the great work of my co-workers who I collaborated with during the investigations. However, I, of course, take responsibility for everything stated in the thesis.

The first investigation in this PhD thesis regarding isochronal superposition was initiated during my Master's Thesis, where dielectric measurements were obtained and preliminary quantitative measures of the degree of isochronal superposition was proposed. During my PhD, a paper was written (Paper 1), where the data analysis and theories were improved. Pressure-volume-temperature measurements were done as part of this PhD project.

As part of my PhD project, I spent three months at the Technical University of Denmark (DTU) in the Terahertz group led by Professor Peter Uhd Jepsen, resulting in a pilot project of terahertz time-domain spectroscopy on our types of liquids. Unfortunately, the project did not result in usable measurements due to instability of the measurement equipment, and it is therefore not presented in this thesis.

Acknowledgements

First of all, I want to thank Professor Kristine Niss, not just for being a great supervisor, but also for encouraging me to get a PhD degree and believing in me. Furthermore, I am very grateful for the large independence I was given in the investigations, which made it possible to pursue my own ideas in the experiments. Last, but not least, I want to thank her for her understanding that life is not always easy. I also want to thank my supervisor, Doctor Bo Jakobsen, for great supervision, especially in relation to the specific heat investigation.

I want to thank Professor Jeppe Dyre for giving me the opportunity to be a part of the "Glass & Time" group. It has been very fruitful to collaborate closely with everyone in the group, which, I am sure, has improved the quality of my investigations. I, of course, also want to thank all the members of the "Glass & Time" group, especially Tina Hecksher for many nice discussions and help in relation to the aging investigation.

I want to thank the workshop at Roskilde University: Preben Olsen, Ebbe H. Larsen, and Torben Rasmussen, for helping me with the development of new sample cells, and improvements of the high-pressure setup. It has been very productive to have such a close collaboration with the workshop. One of my largest thanks goes to Ib Høst Pedersen, who has been an indescribable help in relation to the high-pressure setup.

Furthermore, I want to thank all other people at IMFUFA, especially my office mate Johanne Gudmand-Højer, for great company during the years.

In relation to the investigation at DTU, I want to thank Peter Uhd Jepsen for giving me the opportunity to be a part of the Terahertz group, and for his supervision. Furthermore, I want to thank the Terahertz group for helping me with experiments and theory, and for the pleasant company during the months I spent at DTU.

Last, but not least, I want to thank my family for their support and understanding, especially my husband, Claus. I want to thank my two sons, Max and Lui, not necessarily for making my life easier in the last couple of years, but for showing me that hard work pays off. Furthermore, it is a joy to see them experiment with physics, like the flow of non-viscous liquids.

Contents

Chapter 1

Introduction

It is popular knowledge that in general, a system can be in three possible states; a gas, a liquid, and a solid state. What is not as well known is that in the solid state, the system can be in either a crystalline state or a glass state, even though we are surrounded by glasses in our everyday life such as window glass and different kinds of candy. A glass is solid like a crystal, but contrary to the crystalline state, the molecules are not ordered in a crystal lattice. Instead, they are disordered, as in the liquid state [1]. This thesis focuses on the glassy state, and the supercooled liquid state preceding the glassy state, by experimentally testing molecular liquids for various properties. Even though materials in the glass state are very common, this state is far from fully understood. This implies that fundamental research is still to be done in this field, as with the work in the present PhD project.

To produce a glass of a molecular liquid, the liquid is first supercooled, which happens when it is cooled at a cooling rate fast enough to avoid crystallization at the melting point, as illustrated in Figure 1.1 [2]. The supercooled liquid is in a (metastable) equilibrium state [3], with a viscosity increasing dramatically as the temperature is lowered [4]. If a perturbation (e.g. a temperature change or a mechanical perturbation) is applied to the supercooled liquid, it falls out of equilibrium, and a relaxation towards equilibrium follows. A characteristic time for the relaxation is called the relaxation time (τ). As with the viscosity, the relaxation time increases dramatically when the liquid is being supercooled [5]. At a certain temperature, referred to as the glass transition temperature (T_g), the liquid freezes and forms a glass. This happens when the relaxation time is so long that the system can not reach equilibrium within a given time scale, and thereby falls out of equilibrium [6]. A glass is, therefore, just a supercooled liquid that has not had time to equilibrate. The glass transition temperature depends on the cooling rate – the faster the cooling rate, the higher T_g. The conventional glass transition temperature is often characterized as the temperature where the relaxation time is 100 s [5].

The glass transition may also be reached by increasing pressure [1]. Since

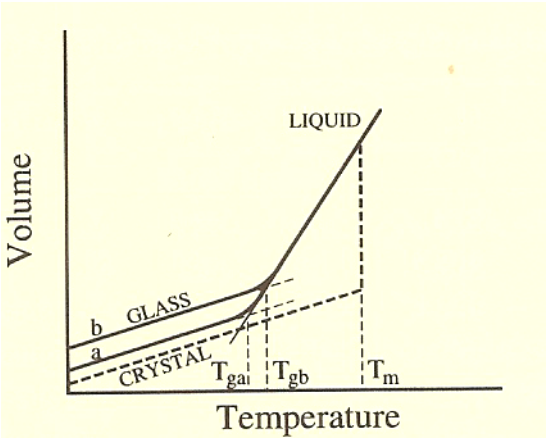

Figure 1.1: An illustration of the glass formation reached by cooling. As the liquid is cooled, the volume decreases. At the melting temperature (T_m), the liquid may turn into a crystal, implying that the volume decreases discontinuously (dashed curve). If the cooling rate is fast enough, crystallization is avoided, and the liquid becomes supercooled. In this case, the volume continues decreasing with the same thermal expansion coefficient as in the liquid state. By cooling further, the liquid turns into a glass at the glass transition temperature (T_g). This is detected as the temperature where the slope, and thereby the thermal expansion coefficient, changes. A glass is just a supercooled liquid that has not had time to reach equilibrium, which implies that the glass transition temperature depends on the cooling rate, i.e. a fast cooling rate results in a high T_g. Figure from Debenedetti (1996), page 242 [5].

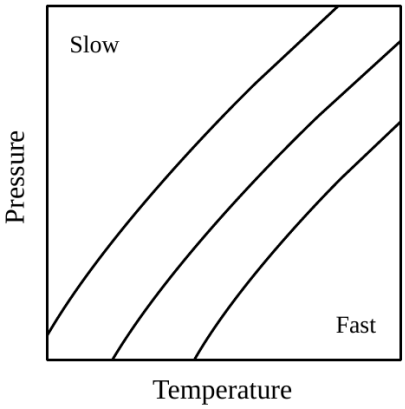

Figure 1.2: Illustration of isochrones, which are lines in the phase diagram, where all points have the same relaxation time. Here, three isochrones are illustrated. The relaxation time increases with decreasing temperature and/or increasing pressure.

both decreasing temperature and increasing pressure can lead to a supercooled liquid and thereby a glass, there will be different state points, i.e. points in the temperature/pressure diagram, which have the same relaxation time τ. This leads to the definition of isochrones, which are lines in the temperature/pressure phase diagram where all points have the same relaxation time [7]. Figure 1.2 illustrates isochrones in the temperature/pressure phase diagram. Note that the isochrones may also be considered in the temperature/density phase diagram.

To study the behavior along isochrones and other parts of the two-dimensional phase diagram, high-pressure measurements are needed. In the last couple of decades, experimental high-pressure studies have revealed findings like density scaling [8–15] and isochronal superposition [13, 14, 16–21]. Furthermore, the isomorph theory suggested a decade ago [22–27] predicts simple behavior of the so-called Roskilde-simple liquids along isochrones. The above findings suggest that high-pressure measurements and isochrones are important in the study and understanding of supercooled liquids. Several of the experimental investigations show differences in van der Waals and hydrogen-bonded liquids' ability to obey isochronal superposition and density scaling, with van der Waals liquids having the largest ability. This suggests a difference between hydrogen-bonded liquids and van der Waals-bonded liquids, and their simplicity. This is also supported by the isomorph theory where van der Waals-bonded liquids are expected to be Roskilde simple, but hydrogen-bonded liquids are not.

The present PhD thesis investigates the simplicity of supercooled liquids, where both simplicity predicted from the isomorph theory is tested, but also simple behavior that is not directly predicted from the theory. Furthermore, both van der Waals and hydrogen-bonded liquids are studied to examine the

difference in simplicity of the two types of liquids. Below, the structure of the thesis, including the investigations, is presented.

1.1 Structure of the thesis

The first chapters are introductory chapters which are relevant for several of the investigations. Chapter 2 provides an introduction to the temperature/pressure dependence of supercooled liquids and the isomorph theory. In this PhD project, the molecular liquids are studied by use of both linear response functions like dielectric spectroscopy, and non-linear responses, like aging following jumps in temperature. Chapter 3 gives an introduction to the formalism of these response functions. Chapter 4 provides experimental details that are relevant for several of the investigations.

Four investigations are presented in this PhD thesis: isochronal superposition, specific heat spectroscopy under high pressure, single-parameter aging, and isochronal jump. Each of the four investigations can be read independently of each other.

All of the investigations examine the simplicity of supercooled liquids inspired by predictions from the isomorph theory. The isochronal superposition and isochronal jump investigations both directly test predictions from the isomorph theory. The specific heat and aging investigations are inspired by the isomorph theory, and test simpler behavior than predicted by the isomorph theory. The isochronal superposition and the aging investigations both directly compare the simplicity of van der Waals and hydrogen-bonded liquids. Our hypothesis, followed by the earlier experimental high-pressure investigations, as well as the isomorph theory, is that van der Waals liquids have simpler behavior than hydrogen-bonded liquids. Chapters 5 - 8 show the four investigations:

- Isochronal Superposition (Chapter 5): This investigation is directly inspired by a prediction of the isomorph theory and compares hydrogen-bonded liquids and van der Waals liquids' ability to obey isochronal superposition. Furthermore, we develop measures to quantify to which degree the liquids obey isochronal superposition. The results are published in Paper 1.

- Specific heat spectroscopy under high pressure (Chapter 6): In this investigation, we adapt specific heat spectroscopy to high pressures. The results are compared to similar dielectric results to test if the isochrones from the two measuring methods coincide. The results are published in Paper 2.

- Single-parameter aging (Chapter 7): We study aging following jumps in temperature for hydrogen-bonded and van der Waals-bonded liquids, and investigate whether the liquids have so-called single-parameter aging using a generalized version of single-parameter aging tests derived in Ref. [28].

The results are published at arXiv in Paper 3, which is also submitted to the Journal of Physical Chemistry.

- Isochronal jump (Chapter 8): This investigation directly tests a prediction of the isomorph theory. In order to make the isochronal jump, several improvements are made at the pressure setup. This chapter describes these improvements, and shows and discusses the preliminary measurements of the isochronal jump.

Chapter 9 provides concluding remarks of the above investigations in relation to the isomorph theory and the simplicity of the liquids. Appendices A - C show details from the investigations, and Appendix D provides reprints of the three papers made in relation to this PhD project.

Chapter 2

Temperature and pressure dependence

The combined temperature and pressure dependence of supercooled liquids have become increasingly interesting with the experimental findings of density scaling and isochronal superposition [8–21]. These findings were given a theoretical background by the proposal of the isomorph theory a decade ago. This predicted isochronal superposition, density scaling, and instantaneous equilibrium following a jump from one state point on an isochrone to another state point on the same isochrone (an isochronal jump), and other predictions for a group of liquids called Roskilde-simple liquids [22–27]. Van der Waals liquids are expected to be Roskilde-simple liquids while hydrogen-bonded liquids are not. The experimental investigations also suggest a difference in these two classes of liquids' ability to obey isochronal superposition and density scaling.

Section 2.1 first describes some experimental findings that suggest simple behavior of liquids. Section 2.2 gives a short overview of the isomorph theory, where Roskilde-simple liquids, isomorphs and predictions from the theory are described.

2.1 Experimental findings

A liquid obeys density scaling if the relaxation time τ varies with density ρ and temperature T in the following way [25]

$$\tau = F(\rho^\gamma/T) \tag{2.1}$$

where γ is a constant and F is a function. This implies that when τ is plotted as a function of ρ^γ/T for different state points in the phase diagram, τ will collapse onto one master curve. An example of density scaling is seen in Figure 2.1 (left). Computer simulations and experiments have shown that for large

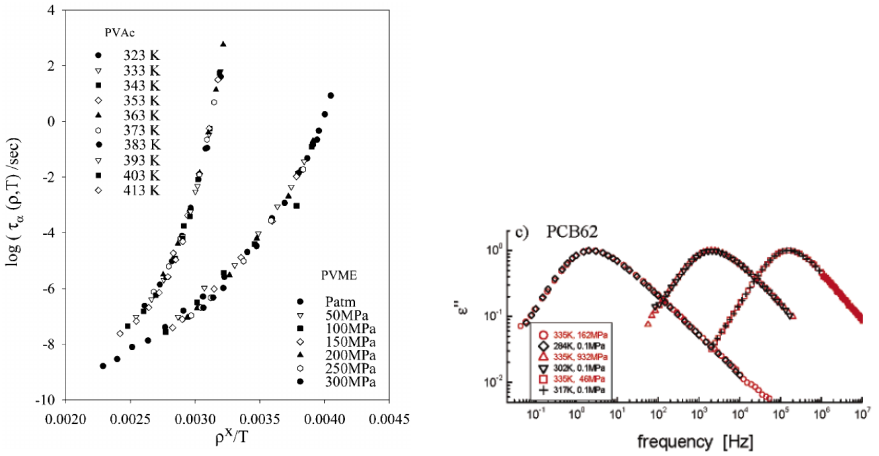

Figure 2.1: Left: Example of density scaling for two liquids (poly(vinylmethylether) (PVME) and poly(vinylacetate) (PVAc)). The data collapse onto one master curve when the relaxation times are plotted against ρ^γ/T. Figure from Alba-Simionesco *et al.* (2004) [9]. Right: Example of isochronal superposition for the liquid chlorinated biphenyl (PCB62). The relaxation spectra for state points on the same isochrone have the same shape. Figure from Ngai *et al.* (2005) [20].

variations in density ρ (more than ≈ 10 %), γ may depend on density implying $\tau = F(h(\rho)/T)$, where h is some function of ρ [27, 29]. Density scaling has been confirmed in experiments by e.g. Dreyfus *et al.* (2004) [10], Casalini & Roland (2004) [11], Alba-Simionesco *et al.* (2004) [9], and Roland *et al.* (2008) [13] which show that density scaling holds for several liquids including van der Waals liquids. Roland *et al.* (2008) [13] also show that density scaling fails if the liquid is hydrogen bonded.

A liquid obeys isochronal superposition if the shape of the relaxation is the same when the relaxation time is the same. An example of isochronal superposition is seen in Figure 2.1 (right). Isochronal superposition has been experimentally investigated in for example Tölle (2001) [16], Roland *et al.* (2003) [17], Pawlus *et al.* (2003) [18], and Ngai *et al.* (2005) [20]. Several of the investigations suggest that van der Waals-bonded liquids obey isochronal superposition, whereas hydrogen-bonded liquids do not. In Chapter 5, we examine van der Waals and hydrogen-bonded liquids' ability to obey isochronal superposition.

2.2 Isomorph theory

The isomorph theory is developed by the theory part of the Glass & Time group at Roskilde University [22–27]. The theory predicts that the so-called Roskilde-simple liquids have isomorphs in the phase diagram along which the dynamics and structure in reduced units are invariant. Isomorphs are thus lines in the phase diagram with e.g. the same reduced relaxation time. Below, a short introduction to Roskilde-simple liquids, isomorphs, and some predictions of the theory is given. It is furthermore introduced how our investigations relate to the isomorph theory.

2.2.1 Roskilde-simple liquids

To define Roskilde-simple liquids, we look at the contributions to the energy E and the pressure p in a system. It is well known that the energy is a sum of the kinetic energy K depending on the particles momenta ($\mathbf{p}_i$) and potential energy U depending on the particles positions ($\mathbf{r}_i$) [30]. The pressure p also has two contributions depending respectively on the particles momenta ($\mathbf{p}_i$) and positions ($\mathbf{r}_i$) [30, 31]

$$p = Nk_BT(\mathbf{p}_1, ..., \mathbf{p}_n)/V + W(\mathbf{r}_1, ..., \mathbf{r}_n)/V \tag{2.2}$$

where N is the number of particles, k_b is the Boltzmann constant, T is the temperature, V is the volume, and W is the virial defined as [30]

$$W = -\frac{1}{3}\sum \mathbf{r}_i \cdot \nabla_{\mathbf{r}_i} U \tag{2.3}$$

At a given state point, W and U fluctuate in time. Roskilde-simple liquids are defined as liquids that have strong correlations between W and U [32, 33]. Figure 2.2 shows an example of the correlation of W and U in a system with strong correlations. The degree of these WU-correlations is determined by the correlation coefficient (R) [22, 34]

$$R = \frac{\langle \Delta W \Delta U \rangle}{\sqrt{\langle (\Delta W)^2 \rangle}\sqrt{\langle (\Delta U)^2 \rangle}} \tag{2.4}$$

where $-1 \leq R \leq 1$ and $\Delta W(t) = W(t) - \langle W \rangle$. $\langle\rangle$ denotes thermal ensemble averages [22]. A liquid is defined to have strong WU-correlations and thereby be Roskilde simple if $R > 0.9$ [22, 35]. This definition is pragmatic, but has been shown to be reasonable.

Computer simulations have shown that van der Waals-bonded liquids are Roskilde simple. More specifically polymers, pure metals, small molecules, and crystals have been investigated in computer simulations and shown to be Roskilde simple [22, 23, 36–40]. Thus, also in experiments we expect that van der Waals liquids are Roskilde simple [25, 41]. In 2011, Gundermann *et al.* [42] showed that the van der Waals-bonded liquid tetramethyl tetraphenyl

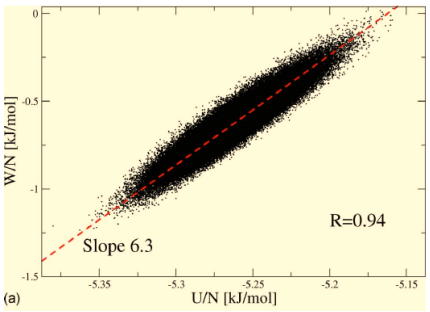

Figure 2.2: The fluctuations of the virial W and the potential energy U over time at a given state point plotted against each other. Due to the strong correlations of W and U, the points form an elongated ellipse. Figure from Bailey *et al.* (2008) [22].

trisiloxane (DC704) is, in fact, Roskilde simple, as they measured the correlation coefficient to be $R = 0.9 \pm 0.2$.

On the other hand, computer simulations simulating hydrogen-bonded and ionic liquids show that these are not Roskilde simple [22, 23, 43]. In several of the investigations in the present thesis, we use both van der Waals-bonded liquids and hydrogen-bonded liquids to test whether the results from computer simulations also apply to real liquids.

2.2.2 Isomorphs

Roskilde-simple liquids have isomorphs, which are lines in the phase diagram with a number of invariant properties, usually in reduced units [25]. A continuous curve in the phase diagram on which any two state points are isomorphic defines an isomorph. To define isomorphic state points and thereby isomorphs, it is necessary to introduce reduced coordinates. For any microscopic configuration $\mathbf{R} = (\mathbf{r}_1, ..., \mathbf{r}_N)$ of a thermodynamic state point with density ρ, the reduced coordinates are defined

$$\tilde{\mathbf{R}} = \rho^{1/3}\mathbf{R} \tag{2.5}$$

To define when two state points (T_1, ρ_1) and (T_2, ρ_2) are isomorphic, we first look at two of their microscopic configurations, $\mathbf{R}^{(1)}$ and $\mathbf{R}^{(2)}$. The original isomorph theory from 2009 suggests that the state points are isomorphic if whenever the microscopic configurations have identical reduced coordinates i.e. $\tilde{\mathbf{R}}^{(1)} = \tilde{\mathbf{R}}^{(2)}$, they have proportional configurational NVT Boltzmann factors [25]

$$e^{-U(\mathbf{R}^{(1)})/k_BT_1} = C_{12}e^{-U(\mathbf{R}^{(2)})/k_BT_2} \tag{2.6}$$

where the constant C_{12} only depends on the state points and not on the microconfigurations.

The isomorph definition was modified in 2014 [44], and it is now defined as

$$U(\mathbf{R}_a) < U(\mathbf{R}_b) \Rightarrow U(\lambda\mathbf{R}_a) < U(\lambda\mathbf{R}_b) \tag{2.7}$$

where λ is a scalar and $\mathbf{R}_a$ and $\mathbf{R}_b$ are two different microscopic configurations at the same state point. This definition is a generalization of the original definition (Eq. (2.6)), with the original definition being the first-order approximation of the new definition [45].

Due to the definition of isomorphs, the structure and dynamics in reduced units are the same along the isomorphs resulting in a number of invariant properties, e.g. the average relaxation time in reduced units [25]. The reduced units, however, make little difference for viscous liquids. For example, the relaxation time in reduced units is $\tilde{\tau} = \rho^{1/3}T^{1/2}K \cdot \tau$, where K is a constant [25]. When the temperature changes about 30% and the density changes about 20%, the variation of the factor $\rho^{1/3}T^{1/2}K$ is entirely insignificant compared to the relaxation time variation for glass-forming liquids (about 100 billion %). Thus, the difference between using the actual relaxation time and the relaxation time in reduced units is very small, and the isochrones, therefore, are approximately isomorphs (however, note that all liquids have isochrones, but only Roskilde-simple liquids are expected to have isomorphs). For further isomorph invariants, see Gnan *et al.* (2009) [25] and Dyre (2014) [27].

Since Roskilde-simple liquids have isomorphs and, thereby, a number of invariant properties along these, it is expected that Roskilde-simple liquids have simpler physics than other liquids [25, 35].

2.2.3 Predictions

The number of invariant properties along isomorphs leads to several predictions for Roskilde-simple liquids. Density scaling, as mentioned, is an example, (Eq. (2.1)), which follows from the isomorph theory because the factor $\frac{\rho^\gamma}{T}$ and the relaxation time τ are approximately constant along the isomorphs [25].

The prediction of isochronal superposition for Roskilde-simple liquids follows from the isomorphs' invariance of the relaxation time and the dynamics and thereby the relaxation spectrum, respectively [27]. Isochronal superposition is tested for both van der Waals and hydrogen-bonded liquids in Chapter 5.

As mentioned, the relaxation time is invariant along an isochrone, however, the relaxation time associated with different response functions may differ. Following the isomorph theory, an isochrone determined by the relaxation time for one response function must also be an isochrone for another response function, however, with another characteristic time associated. This means that isochrones for various response functions must coincide; a prediction which is tested in Chapter 6.

The isomorph theory also gives predictions about physical aging, i.e. the structural relaxation of the liquid following a jump in temperature and/or pressure. First of all, the theory predicts that the system comes into equilibrium

instantaneously when jumping from one state point on an isochrone to another state point on the same isochrone (an isochrone jump) [25, 27]. This follows naturally from the proportional Boltzmann factors at these state points (Eq. (2.6)). Furthermore, the theory predicts that jumps from one isochrone to another isochrone along different paths should have the same relaxation curve. We test these predictions in Chapter 8.

Chapter 7 shows an investigation of aging following temperature jumps, where it is tested whether the studied liquids have so-called single-parameter aging, where both the structural relaxation and the measured property depend on the same parameter. Single-parameter aging is not linked to the isomorph theory, but work is done to investigate the connection between isomorph theory and aging (see Dyre (2018) [46]). However, our hypothesis, inspired from the isomorph theory, is that van der Waals liquids have simpler behaivior than hydrogen-bonded liquids, also in aging. We test this hypothesis in Chapter 7.

Chapter 9 follows up on the results of the investigations in relation to the isomorph theory and the simplicity of the studied liquids.

Chapter 3

Experimental observables

In the investigations in this PhD thesis, the supercooled liquids are experimentally studied by use of response functions. An equilibrium supercooled liquid exposed to a perturbation will relax toward a new equilibrium; it responds to the perturbation. The experimental measuring methods study this response. For example, a change in temperature (a perturbation) results in a change of volume (a response).

When a system is exposed to an input, it will result in an output. In response theory, the relation between the input and the output is investigated. If the input is sufficiently small, the output will depend linearly on the input, and it is called linear response. Dielectric spectroscopy, which is used for several of the investigations in the present thesis, is one of the most studied linear response functions in glass science. Furthermore, specific heat spectroscopy used in the present investigations is also an example of a linear response function. If, on the other hand, the input is large, the response will be non-linear. Aging, where the liquid is studied following a jump in temperature (and/or pressure) is an example of this.

The formalism of linear response is described in Section 3.1, and Section 3.2 describes dielectric spectroscopy as an example of a linear response function. Section 3.3 describes the formalism of the non-linear response due to a change in temperature. This is also referred to as aging and is used for the investigations in Chapter 7 and Chapter 8.

3.1 Linear response

To study linear response, we look at the relation between an input $I(t)$ and an output $O(t)$ which can be described by [47]

$$O(t) = \int_{-\infty}^{t} \mu(t - t')I(t')dt' \tag{3.1}$$

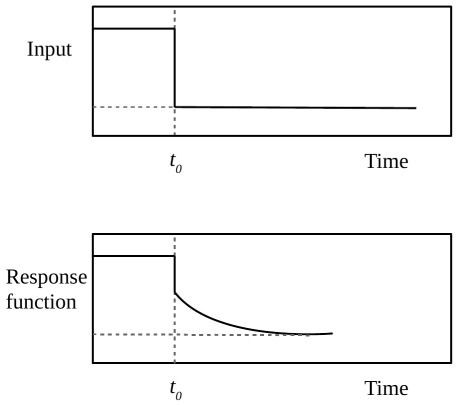

Figure 3.1: Illustration of a linear response following a Heaviside input. The response consists of an instantaneous contribution and a relaxation part.

where μ is called the memory function. We assume that no change in input leads to no change in output, resulting in $\mu = 0$ if $t < t'$. Substituting $t'' = t - t'$ and changing t'' to t' gives

$$O(t) = \int_0^\infty \mu(t')I(t-t')dt' \tag{3.2}$$

As an example, we consider an input with a sudden change from 0 to I_0 at time $t = 0$, which can be expressed by a Heaviside function $H(t)$

$$I(t) = I_0 H(t) = I_0 \cdot \begin{cases} 0 & \text{for } t \leq 0 \\ 1 & \text{for } t > 0 \end{cases} \tag{3.3}$$

Applying the Heaviside input gives

$$O(t) = \int_0^\infty \mu(t')I_0 H(t-t')dt' = I_0 \int_0^\infty \mu(t')dt' = I_0 R(t) \tag{3.4}$$

where $R(t)$ is the response function in the time domain implying [47]

$$\frac{dR(t)}{dt} = \mu(t) \tag{3.5}$$

Figure 3.1 shows an example of a response function following a Heaviside input, where the response consists of an instantaneous contribution and a relaxation part.

If the input is a harmonic oscillating function $I(t) = I_0 e^{i(\omega t + \varphi_I)}$, the linear response may be considered in the frequency domain. The output will, in this

case, also be harmonic, oscillating with the same frequency as the input, but with a possible phase shift relative to the input:

$$O_0 e^{i(\omega t+\varphi_O)} = R(\omega) I_0 e^{i(\omega t+\varphi_I)} \tag{3.6}$$

Using the relation between the memory function and the response function in the time domain (Eq. (3.5)), the following relationship between the response function in the time domain and the response function in the frequency domain is established [47]

$$R(\omega) = \int_0^\infty \mu(t') e^{-i\omega t'} dt' = \int_0^\infty \frac{dR(t')}{dt'} e^{-i\omega t'} dt' \tag{3.7}$$

In this PhD thesis, two types of linear response methods are used; dielectric spectroscopy and specific heat spectroscopy. Below dielectric spectroscopy is described as an example of a linear response function.

3.2 Dielectric spectroscopy

The measuring method used for the major part of the investigations is dielectric spectroscopy. Here, the liquid is placed in a parallel-plate capacitor to which an external electrical field is applied. For an empty parallel-plate capacitor, the relation between the capacitance (C), the vacuum permittivity (ε_0), the area of the plates (A), and the distance between the plates (d) is [48]

$$C_{\text{empty}} = \frac{\varepsilon_0 A}{d} \tag{3.8}$$

The capacitance of a parallel-plate capacitor filled with sample liquid with the frequency-dependent dielectric constant ε is [48]

$$C = \varepsilon \cdot C_{\text{empty}} = \frac{\varepsilon_0 \varepsilon A}{d} \tag{3.9}$$

where it is assumed that the used liquids are dielectrics (the electrons are attached to each individual molecule in the liquids). The used liquids are furthermore considered to be isotropic liquids, i.e. liquids whose properties are the same in all directions, and polar liquids, i.e. the molecules have a dipole moment without an applied field [48].

To define ε, we consider how the charge distribution of the molecules in the molecular liquid are affected by an applied electric field. The molecules, and thereby the molecular liquid, are affected by two mechanisms: stretching and rotating. A detailed description and discussion of these mechanisms are, for example, provided in Ref. [49]. The two mechanisms result in a polarization of the dielectrics, which is measured in polarization $\mathbf{P}$ defined as the dipole moment per unit volume [48]. Provided that the applied field $\mathbf{E}$ is not too

strong for most substances (so-called linear dielectrics), the polarization $\mathbf{P}$ is proportional to $\mathbf{E}$. This is the case here and the relationship is

$$\mathbf{P} = \varepsilon_0 \chi_e \mathbf{E} \tag{3.10}$$

where χ_e is the electric susceptibility of the dielectric relating to the dielectric constant as $\varepsilon = 1 + \chi_e$ [48]. The above equation shows a linear response function with $\mathbf{E}$ being the input, $\mathbf{P}$ being the output and χ_e being the response. In our experiments, we apply a harmonic oscillating electric field, noting $\mathbf{E} = E_0 e^{i(\omega t + \varphi_E)}$. The output will also be harmonic oscillating with the same frequency as the input, but with a possible phase difference giving

$$P_0 e^{i(\omega t + \varphi_P)} = \varepsilon_0 \chi_{e,0} e^{i\varphi_{\chi_e}} E_0 e^{i(\omega t + \varphi_E)} \tag{3.11}$$

The stretching happens almost instantaneously, and the frequency dependence of χ_e is caused by the rotational mechanism. To further understand what happens when we apply the electric field, we look at the amplitudes and the phases of the above equation at a fixed frequency, respectively:

$$P_0 = \varepsilon_0 \chi_{e,0} E_0 \Leftrightarrow \varepsilon_0 \chi_{e,0} = \frac{P_0}{E_0} \tag{3.12}$$

$$\varphi_P = \varphi_{\chi_e} + \varphi_E \Leftrightarrow \varphi_{\chi_e} = \varphi_P - \varphi_E \tag{3.13}$$

At low frequencies, the molecules have enough time to adjust to the electric field, and thereby rotate themselves to align. The amplitude of χ_e thereby reaches a (high) plateau, since the polarization is large. At higher frequencies, the molecules do not have time to align themselves with the field, and the amplitude of χ_e goes towards a new lower plateau. Between the two plateaus, the motion of the polar molecules are out of phase with the applied field, resulting in a so-called loss peak for the electric susceptibility. The frequency of this loss peak is dependent on the relaxation time of the liquid and thereby on the temperature/pressure, since the molecules' ability to rotate depends on the viscosity of the liquid.

The electrical displacement field $\mathbf{D}$, which is the field caused by the applied field and the polarization, is defined as [48]

$$\mathbf{D} = \varepsilon_0 \mathbf{E} + \mathbf{P} \tag{3.14}$$

which, for linear dielectrics, can be reduced to (using Eq. (3.10))

$$\mathbf{D} = \varepsilon_0 \varepsilon \mathbf{E} \tag{3.15}$$

The frequency-dependent dielectric constant ε is thereby defined by the proportionality constant between the applied field $\mathbf{E}$ and the displacement field $\mathbf{D}$. This is also an example of linear response with $\mathbf{E}$ being the input, $\mathbf{D}$ being the output, and ε the response. Equivalent to χ_e, ε is also frequency dependent.

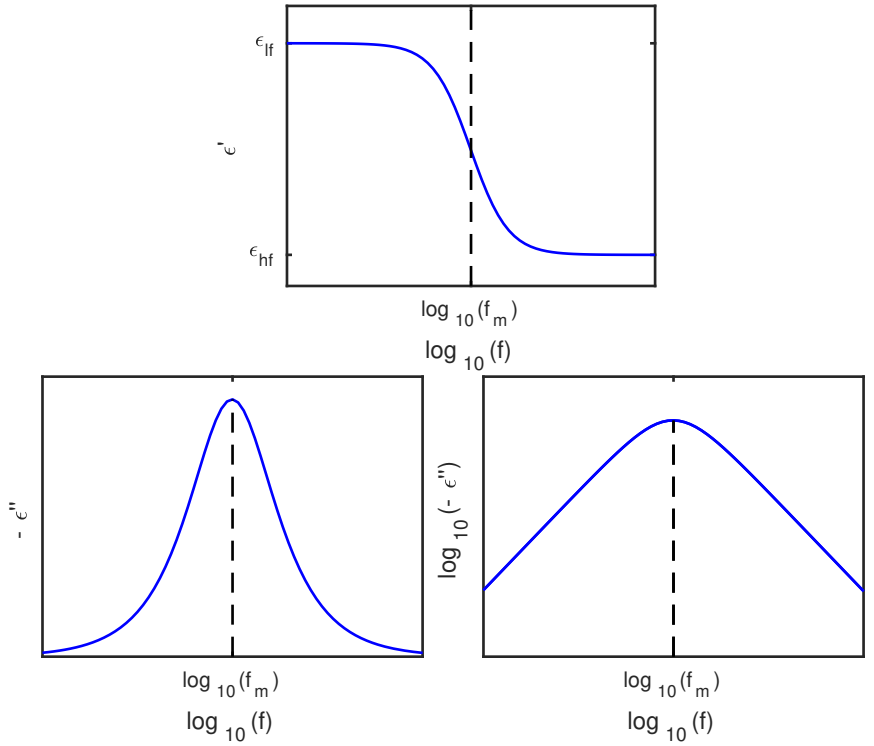

Figure 3.2: Illustration of the frequency-dependent dielectric constant. Top: The real part of the dielectric relaxation spectrum. Bottom, left: The negative imaginary part of the dielectric relaxation spectrum. Bottom, right: The logarithm of the negative imaginary part of the dielectric relaxation spectrum.

At low frequencies, the real part of the dielectric constant approaches the equilibrium value (ε_{lf}) immediately, because the molecules rotate to align with the field. At higher frequencies, the molecules do not have enough time to align themselves with the field, and the real part of the dielectric constant approaches a new, lower value (ε_{hf}). The real part of the dielectric constant is illustrated in Figure 3.2 (top). The difference between ε_{lf} and ε_{hf} is called the dielectric strength $\Delta\varepsilon$. Between the two plateaus, the motion of the polar molecules are out of phase with the applied field. The dielectric constant therefore shows a loss peak. Figure 3.2 (bottom) illustrates the typical frequency dependence of the negative imaginary dielectric constant ($-\varepsilon''$). The relaxation is called the α-relaxation, and the loss peak is also referred to as the α-peak. The frequency at the maximum of the α-peak is also called the loss peak frequency and is noted f_m in this thesis. We define a characteristic time of the relaxation as $\tau = 1/(2\pi f_m)$, which we refer to as the relaxation time. Note that f_m and thereby τ for the different response functions might differ (as we, for example,

show for the relaxation times found from respectively dielectric spectroscopy and specific heat spectroscopy in Chapter 6).

The spectra may show β-relaxation on the right side of the peak (since they are faster than α-relaxations) due to minor motions in the liquids. Furthermore, conductivity may affect the spectra on the left side of the peak as a straight line.

3.3 Non-linear response – aging

Non-linear response is the response of a system following a large perturbation. In our investigation of aging (Chapter 7), the applied perturbation is a (large) jump in temperature, where we examine how the liquid equilibrates afterwards. This relaxation is called structural relaxation. Note that the isochronal jump investigation (Chapter 8) is also a study of aging, where we study jumps in both temperature and pressure, and combinations of the two. However, in this formal description of the non-linear response, only pure temperature jumps are considered. Note that aging may also refer to the changing of chemical relations over time, but here, only pure physical aging is studied.

To study aging, the liquid has to be close to the glass transition temperature. A chosen property of the liquid is monitored as a function of time, e.g. the volume, the dielectric loss at a fixed frequency, etc. Remember that a system in the glass state is out of equilibrium, and it will therefore relax towards the (metastable) equilibrium state, i.e. the supercooled liquid state. When performing a temperature jump to a temperature just below the glass transition temperature, the liquid will therefore relax. Figure 3.3 illustrates aging in the temperature/volume diagram.

If the jump is performed to a temperature too far below T_g, it will be impossible for the liquid to reach equilibrium (and maybe even to relax towards equilibrium on a observable time scale). Since the relaxation time changes dramatically with temperature, aging can only be observed in a small temperature range. Note that if the jumps are performed in a temperature range above the glass transition temperature, the structural relaxation will be too fast to be measurable.

In the following description of the formalism of aging, we consider an instantaneous jump in temperature (which is also what we aim for in our experiments). We furthermore assume that the liquid is in equilibrium before the jump is initiated, and that the relaxation is monitored until the new equilibrium is reached. Following a jump from a temperature T_1 to a temperature T_2 leads to an instantaneous change of a measured property p followed by a relaxation towards equilibrium at T_2 as illustrated in Figure 3.4 (left). Note that this relaxation looks like the linear response in Figure 3.1. The instantaneous change stems from the atomic vibrations, while the following relaxation towards equilibrium is due to structural changes in the liquid [50]. The slope of the studied property as a function of temperature, $\partial p/\partial T$, has one value in the

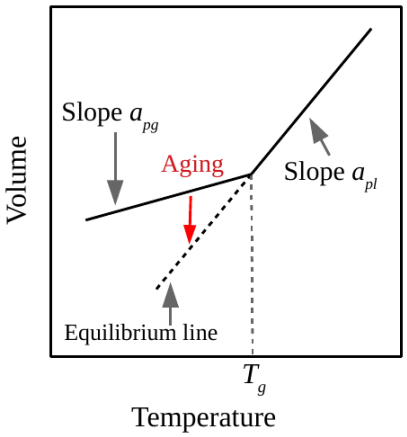

Figure 3.3: Illustration of aging. Following a jump in temperature to a temperature just below the glass transition temperature, the liquid will first be out of equilibrium in the glass state. It will then equilibrate towards the supercooled liquid state. This relaxation is called structural relaxation and is also referred to as aging.

(supercooled) liquid state (α_{pl}), and another value in the glass state (α_{pg}), as illustrated in Figure 3.3. The first instantaneous change depends on the characteristic slope in the glass state α_{pg}, while the structural relaxation depends on both the characteristic slope in the supercooled liquid state α_{pl} and in the glass state, α_{pg} as illustrated in Figure 3.4.

The non-linearity is seen already at small temperature jumps (actually, it is difficult to perform a linear response using temperature jumps, but an example is seen in Ref. [51]). When studying temperature up and down jumps of equal size to the same temperature, the non-linearity is clearly visible, as illustrated in Figure 3.5. This is where the non-linear response differs from linear responses. This non-linearity arises because the relaxation rate is structure-dependent, and evolves with time. During a down jump, the relaxation rate decreases as the structure ages. On the contrary, during an up jump, the relaxation rate increases as the structure ages [50, 52].

The standard formalism for describing the structural relaxation is called the Tool-Narayanaswamy (TN) formalism, and is presented below. First, we define the normalized relaxation function, $R(t)$. $R(t)$ is defined as the time-dependent distance to equilibrium at the end temperature T_2 over the overall change of the measured property from T_1 to T_2

$$R(t) = \frac{p(t, T_2) - p(\infty, T_2)}{p(\infty, T_1) - p(\infty, T_2)} \tag{3.16}$$

From this definition, it is seen that $R(0) = 1$ and that $R(t) \to 0$ as $t \to \infty$.

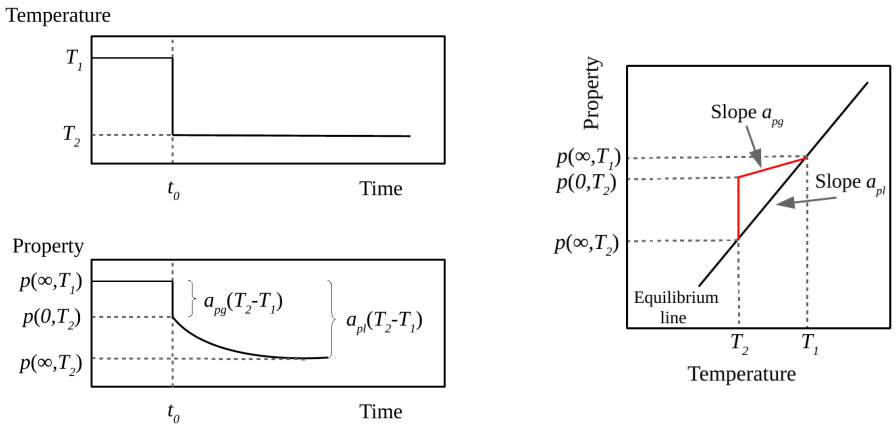

Figure 3.4: Aging following an instantaneous jump in temperature from T_1 to T_2. The change of the monitored property ($p(t,T)$) consists of an instantaneous change (from $p(\infty,T_1)$ to $p(0,T_2)$), depending on the characteristic slope in the glass state α_{pg}, and a relaxation towards equilibrium depending on both the characteristic slope in the supercooled liquid state α_{pl} and the glass α_{pg} as shown on the figures. Left: The change of property as a function of time. Right: The change of property as a function of temperature, seen as the red line. Remember that the temperature change from T_1 to T_2 is instantaneous. Figures adapted from Scherer (1986) [50].

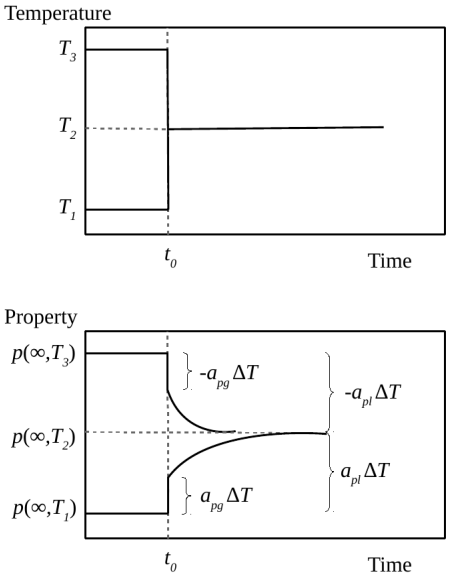

Figure 3.5: Illustration of a temperature up and a temperature down jump of equal size to the same temperature. The non-linearity is clearly visible. Figure adapted from Scherer (1986) [50].

3.3.1 Tool-Narayanaswamy formalism

In the 1940s, Tool [53, 54] first described the non-linearity of the structural relaxation using a parameter called the fictive temperature T_f. In 1971, Narayanaswamy [55] further developed on this approach.

Narayanaswamy's idea was that linearity can be re-established by introducing a material time ξ. ξ may be thought of as a time measured on a clock with a clock rate $\gamma(t)$ that itself evolves with time [52]. The material time is defined from the structural clock rate γ and the actual time t as [50, 52, 55]

$$d\xi = \gamma(t)dt \Leftrightarrow \xi = \int_0^t \gamma(t)dt \tag{3.17}$$

In this approach, it is assumed that the non-linearity of the structural relaxation occurs only because of the non-linearity of the relaxation rate. The model, therefore, for example, assumes that the system has time-temperature-superposition, implying that the equilibrium relaxation spectra are temperature invariant.

The TN-formalism implies that the normalized relaxation function $R(t)$ is a unique function of the material time ξ, giving [52, 55]

$$R(t) = \phi(\xi(t)) \tag{3.18}$$

with $\phi(\xi)$ being a unique function independent of temperature and time. This implies that when R is plotted as a function of ξ for different jumps in temperature, the curves collapse onto one master curve.

The TN-formalism introduced a single-parameter assumption in terms of the fictive temperature T_f. The hypothesis is that both the measured property $p(t)$ and the clock rate $\gamma(t)$ of the structural relaxation are controlled by the same parameter. We refer to this property as single-parameter aging, which we develop tests for in Chapter 7.

The TN-formalism is usually tested using analytical functions and fitting to these to find, for example, the material time [28, 50, 55]. The single-parameter aging tests we develop in Chapter 7 have the advantage that one does not explicitly need to calculate the material time. We, furthermore, do not need to make any assumptions regarding the shape of the relaxation curve ϕ.

Chapter 4

Experimental details

This chapter describes experimental details relevant for the four investigations: isochronal superposition, frequency-dependent specific heat under high pressure, aging following temperature jumps, and isochronal jump. All experiments were conducted in the laboratory at Roskilde University.

Section 4.1 describes the pressure setup used for the isochronal superposition, the specific heat, and the isochronal jump investigations. The electronic equipment used for all investigations are described in Section 4.2, however, only the standard configuration used for the investigations of isochronal superposition and aging are shown. Different configurations are used for the isochronal jump and the specific heat investigations, which are described in the respective chapters. The liquids for the four investigations are described in Section 4.3. The aging measurements and some of the specific heat measurements are performed in an atmospheric pressure cryostat at Roskilde University. For further details on this cryostat, see Ref. [56]. In this thesis, the cryostat is referred to as a standard RUC cryostat.

4.1 Pressure setup

The pressure setup consists of several parts, with the pressure vessel being the heart of the setup. The pressure vessel is type MV1 from Unipress Equipment in Warsaw, Poland, and is illustrated in Figure 4.1. The maximal pressure is 600 MPa, and the temperature range is 173 K to 393 K. The sample cell, which differs for the different investigations, is placed in the pressure chamber in the middle of the pressure vessel which contains a pressure medium (we use a silicon oil). The pressure vessel is connected to a high pressure pump via a metal capillary entering at the bottom of the vessel leading the pressure medium to the pressure vessel. The pump is the type U111 from Unipress Equipment in Warsaw, Poland. The maximal pressure is 700 MPa. The pressure is controlled directly at the pump, allowing for automatic pressure rise. The release of the

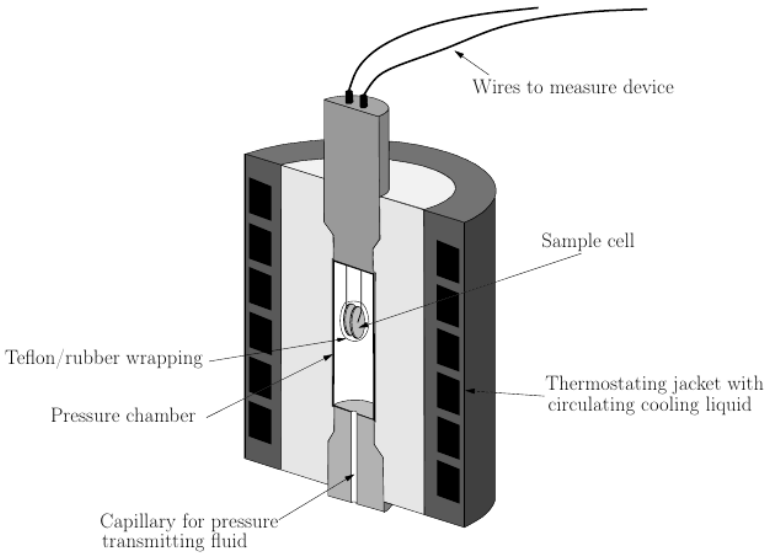

Figure 4.1: Cross section of the pressure vessel. The sample cell is placed in the pressure chamber, which is filled with pressure medium. The pressure is delivered through a metal capillary at the bottom of the vessel. The thermal liquid flows around the pressure chamber in the walls of the pressure vessel. The wires connecting the sample cell to the electrical equipment passes through the plug in the top of the pressure vessel. Figure from Gundermann (2013) [57].

pressure is done manually by the opening of a valve. When the pressure is set, it is kept stable by the pump ensuring that the pressure increases to the desired pressure again when the pressure decreases more than 3 MPa from the desired value. The setting of 3 MPa is the smallest margin permitted. This limited pressure stability affects the measurements, and is clearly visible in several of the investigations.

The pressure vessel is connected to a thermal bath, specifically a Julabo F81-ME, which ensures a temperature stability of ± 0.02 K in the thermal bath [58]. The thermal medium used for the measurements is a mixture of water and glycol, resulting in the temperature range of 233 K to 333 K. The bath ensures that the thermal liquid with a selected temperature circulates around in the sides of the vessel, ensuring a stable temperature.

The top of the pressure vessel, called the plug, has feed-throughs to connect the sample cell to the electrical equipment. A thermocouple is placed in the plug close to the sample environment, where the temperature is measured (as this temperature may be different from the temperature in the thermal bath). The temperature measured using the thermocouple is used for the isochronal superposition investigation and the specific heat investigation. For the isochronal jump investigation, we developed an internal temperature regulation, which allows for a temperature measurement inside the pressure chamber (see Section 8.2.3).

The pump, the thermal bath, the thermocouple, and the electrical measurement equipment are connected to a computer where the pressure, the temperatures, and the electrical signals are detected. Additionally, the thermal bath and the electrical equipment are controlled from the computer.

When performing the measurements, the pressure vessel is wrapped in Styrofoam to prevent ice formation, and to maintain a stable temperature. Figure 4.2 shows the pressure setup, and Figure 4.3 shows the pressure vessel. All investigations performed at this pressure setup (including investigations of the setup itself) are in Refs. [57, 59–64].

The pressure setup also allows for pressure-volume-temperature (PVT) measurements, which are used for the isochronal superposition investigation (described in Section 5.2).

4.2 Electronic measurement equipment

The electrical measurement equipment consists of a LCR meter and a multimeter working with a generator, which, together, measures in the frequency range of 10^{-3} Hz - 10^{6} Hz. The commercial LCR meter, an Agilent E4980A, measures the capacitance of the sample cell directly in the frequency range of 10^{2} Hz - 10^{6} Hz. A custom-built setup with a frequency generator in combination with an Agilent 3458A multimeter measures in the frequency range of 10^{-3} Hz - 10^{2} Hz. See Ref. [65] for further details. There is an automatic switch between the LCR meter and the multimeter at 100 Hz. The multimeter and frequency

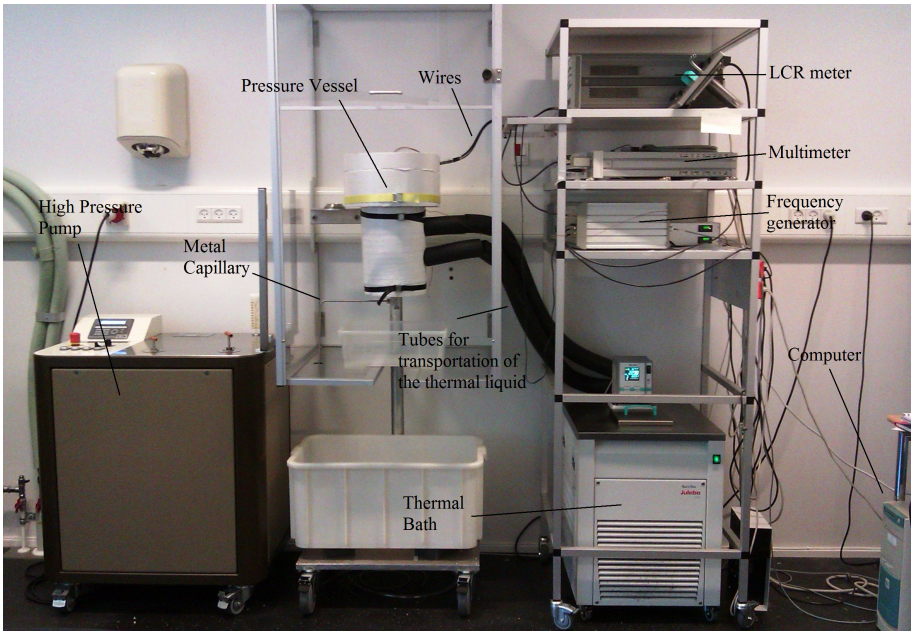

Figure 4.2: The pressure setup. Picture from Roed (2012) [59].

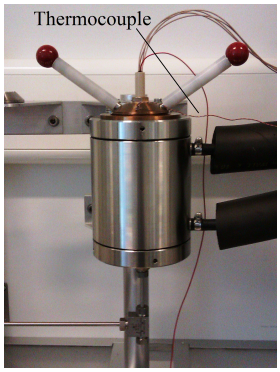

Figure 4.3: The pressure vessel. Picture from Roed (2012) [59].

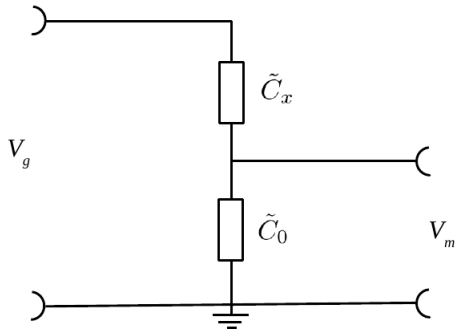

Figure 4.4: The configuration of the electrical equipment used for measuring the capacitance of the sample cell $\tilde{C}_x$. $\tilde{C}_0$ illustrates a prebox with a known capacitor and resistor in parallel.

generator are used for all four investigations. For the dielectric measurements in the isochronal superposition investigation and the aging investigation, the configuration is described below. For the specific heat measurements and the dielectric measurements in the isochronal jump investigation, the multimeter and the frequency generator are used in different configurations described in the respective chapters (6 and 8).

The configuration of the electronic equipment is illustrated in Figure 4.4. The frequency generator supplies a voltage V_g. The supplied voltage is harmonic oscillating $V_g = V_0 \cos(\omega t + \phi_{V_g})$. To calculate in the electrical circuit, we use a complex notation, $\tilde{V}_g$, defined as

$$V_g = \mathrm{Re}(\tilde{V}_g) = \mathrm{Re}(V_0 e^{i(\omega t + \phi_{V_g})}) \tag{4.1}$$

The multimeter measures the voltage V_m, which is the voltage over a known prebox, consisting of a known capacitor and resistor in parallel. The sample has capacitance $\tilde{C}_x$, while the prebox has capacitance $\tilde{C}_0$. Since V_g and $\tilde{C}_0$ are known, and V_m is measured, the capacitance of the sample cell ($\tilde{C}_x$) can be calculated as

$$\tilde{V}_g \cdot \frac{1}{\frac{1}{\tilde{C}_x} + \frac{1}{\tilde{C}_0}} = \tilde{V}_m \cdot \tilde{C}_0 \Leftrightarrow \tag{4.2}$$

$$\tilde{C}_x = \tilde{C}_0 \cdot \frac{\tilde{V}_m}{\tilde{V}_g - \tilde{V}_m} \tag{4.3}$$

Before this calculation, the exact value of $\tilde{C}_0$ is found by a calibration. For more details on the calibration, see Ref. [59].

Liquid	Bonding	T_g (K)	$\Delta\varepsilon$	Investigations	Density
5PPE	vdW	245 [67]	~ 2 [68]	IS, SH, IJ	Ref. [57]
Glycerol	H	193 [69]	~ 60	IS, Aging	Ref. [70]
DEP	vdW	187 [69]	~ 8	IS, Aging	This work
1,2,6-HT	H	203 [71]	~ 40	IS, Aging	This work
DC704	vdW	211 [67]	~ 0.2 [67]	IS. Ref. [66]	Ref. [57]
DBP	vdW	177 [7]	~ 8	IS. Ref. [7]	Ref. [70]

Table 4.1: The liquids studied. "H" is hydrogen-bonded and "vdW" is van der Waals-bonded. Where no reference is given, $\Delta\varepsilon$ is from the measurements used for the isochronal superposition investigation. "IS" is isochronal superposition, "SH" is specific heat, and "IJ" is isochronal jump. Where no references are given, data are obtained in relation to this work. Details on the density data are given in Section 5.2.2.

4.3 Liquids

This section describes the liquids used in the four investigations performed at Roskilde University. Measurements on the four of the liquids, polyphenyl ether (5PPE), glycerol, diethyl phthalate (DEP), and 1,2,6 hexanetriol (1,2,6-HT), are performed in relation to this PhD. For the isochronal superposition investigation (Chapter 5), dielectric data on tetramethyl tetraphenyl trisiloxane (DC704) and dibutyl phthalate (DBP) are also used. The DC704 data was compiled for the article Nielsen *et al.* (2010) [66] and was measured in the laboratory at Silesian University, Katowice, Poland. The DBP data was compiled for the article Niss *et al.* (2007) [7] and was measured in the laboratory LCP, in Orsay.

Figure 4.5 shows the molecular structure of the liquids. The intermolecular bonds of 5PPE, DEP, DC704, and DBP are van der Waal bonds, and they are, therefore, expected to be Roskilde simple. The intermolecular bonds in glycerol and 1,2,6-HT are hydrogen bonds, and they are, therefore, not expected to be Roskilde simple. Table 4.1 gives an overview of the used liquids including their bonding, T_g at atmospheric pressure, dielectric strength $\Delta\varepsilon$, which investigations they are used in, and where density data for the liquids are obtained.

It is well known that the hydrogen-bonded liquids, especially, can absorb water. Therefore, the liquids are placed in an exicator before use to extract water. The exact exicator times are stated under the experimental details for each investigation. In the table, we stated T_g=193 K at atmospheric pressure for glycerol, however, it seems to vary, which is possibly due to the amount of water in the liquid (as an example, T_g is found to be approximately 185 K in the aging investigation (Chapter 7)).

5PPE

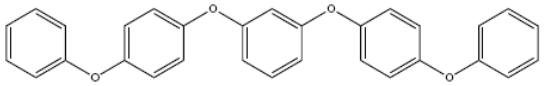

Glycerol

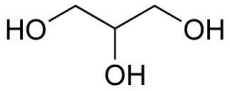

DEP

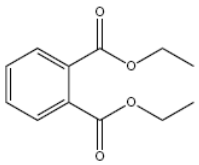

1,2,6-HT

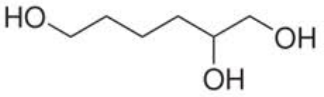

DC704

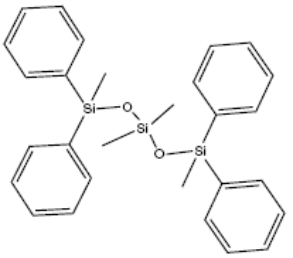

DBP

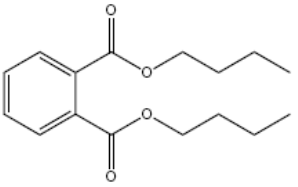

Figure 4.5: The molecular structure of the liquids.

Chapter 5

Isochronal superposition

The isochronal superposition investigation was initiated in my Master Thesis (Ref. [59]), where the dielectric measurements were obtained, and a quantitative measure of isochronal superposition was proposed. As part of this PhD project, the measures of isochronal superposition were improved to include temperature and density changes. In order to include density, pressure-volume-temperature (PVT) measurements were made in relation to this PhD project. Furthermore, a paper about isochronal superposition was written (Paper 1). This chapter about isochronal superposition was written after the paper, and several sections are therefore identical or similar to sections in the article.

A liquid obeys isochronal superposition if its dynamics is invariant along the isochrones. More precisely, a liquid obeys isochronal superposition if the complex, frequency-dependent response function $R(\omega, Q)$ in question at state point Q can be written

$$R(\omega, Q) = R_0(Q)\tilde{R}(\omega, \tau(Q)) + K_0(Q) \tag{5.1}$$

Here $R_0(Q)$ and $K_0(Q)$ are state-point dependent real constants. The function $\tilde{R}(\omega, \tau(Q))$ describes the shape of the relaxation spectrum; this function depends on the state point Q only via its relaxation time $\tau(Q)$. For the imaginary part of the response function, isochronal superposition implies

$$R''(\omega, Q) = R_0(Q)\tilde{R}''(\omega, \tau(Q)) \tag{5.2}$$

Tölle (2001) first demonstrated isochronal superposition for a single liquid, orthoterphenyl, in data for the intermediate scattering function determined by neutron scattering [16]. Soon after, systematic investigations of isochronal superposition were initiated by Roland *et al.* (2003) [17] and Ngai *et al.* (2005) [20] using dielectric spectroscopy. These seminal papers showed isochronal superposition for the van der Waals liquids studied, but reported that hydrogen-bonded liquids often violate isochronal superposition. The isomorph theory also suggests such a difference between the two types of liquids, since Roskilde-simple

liquids are predicted to obey isochronal superposition, where van der Waals liquids are expected to be Roskilde simple, but hydrogen-bonded liquids are not. Our hypothesis, which is tested in this investigation, is, therefore, that van der Waals liquids obey isochronal superposition better than hydrogen-bonded liquids. Note that the isomorph theory does not predict anything about hydrogen-bonded liquids.

We studied four van der Waals liquids: polyphenyl ether (5PPE), diethyl phthalate (DEP), dibutyl phthalate (DBP), and tetramethyl tetraphenyl trisiloxane (DC704), as well as two hydrogen-bonded liquids: 1,2,6 hexanetriol (1,2,6-HT) and glycerol (details on the liquids are given in Section 4.3). The six liquids are all studied previously, also by use of dielectric spectroscopy under high pressure [18, 57, 72–75].

By visually comparing the imaginary part of response functions along a liquid's isochrones, the analysis of isochronal superposition has traditionally followed the age-old method for investigating time-temperature superposition (TTS). Appendix A.1 shows this type of qualitative analysis on our data. This investigation takes the analysis one step further by suggesting two measures of the degree of isochronal superposition – such measures are relevant because one does not expect any liquid to obey isochronal superposition with mathematical rigor. They are furthermore useful when comparing different liquids' ability to obey isochronal superposition, since the measurements of the different liquids may vary in temperature and pressure range, and we expect that measurements taken at state points close to each other are more identical than measurements taken at state points far from each other.

Section 5.1 defines our measures of isochronal superposition. In Section 5.2, the pressure-volume-temperature measurements are presented, and the densities are estimated for the used liquids. We study isochronal superposition by use of dielectric spectroscopy, and the measurements are presented in Section 5.3, including a discussion about the difficulties when comparing different liquids using dielectric spectroscopy. Section 5.4 shows the shape parameters used for the measures of isochronal superposition, and Section 5.5 shows the results of the measures. Section 5.6 provides concluding remarks on the investigation.

5.1 Measures of the degree of isochronal superposition

To develop quantitative measures of isochronal superposition, we first consider perfect isochronal superposition. A loss peak, in principle, is characterized by infinitely many shape parameters $X, Y, Z, ...$ In practice, a few parameters are enough to characterize the shape, for instance, fitting-model based parameters like the stretching exponent β, the Havriliak-Negami parameters, the Cole-Davidson β_{CD}, etc., or model-independent parameters like the half width at half depth or the loss peak area in a log-log plot. Perfect isochronal superposition is

characterized by constant shape parameters along an isochrone:

$$0 = dX|_\tau = dY|_\tau = dZ|_\tau = ... \tag{5.3}$$

in which $|_\tau$ signals that the variation is considered at constant relaxation time.

In order to determine how much a given shape parameter X varies along an isochrone, we assume that a metric ds has been defined in the thermodynamic phase diagram. Since $d\ln X = dX/X$ gives the relative change of X, the rate of relative change of X along an isochrone is given by the operator L defined by

$$L(X) \equiv \left| \frac{d\ln(X)}{ds} \right|_\tau \tag{5.4}$$

We now need to define a reasonable metric ds. A state point is characterized by its temperature T and pressure P, so one option is $ds^2 = dT^2 + dP^2$. However, this metric depends on the unit system used, which is not acceptable. This problem may be solved by using logarithmic distances, i.e., defining $ds^2 = (d\ln(T))^2 + (d\ln(P))^2$. Actually, using pressure is not optimal because there are numerous decades of pressures below ambient pressure where little change of the physics take place; furthermore, a logarithmic pressure metric does not allow for negative pressures. For these reasons, we instead quantify state points by their temperature and density ρ, and use the following metric

$$ds^2 \equiv (d\ln(T))^2 + (d\ln(\rho))^2 \tag{5.5}$$

Equations (5.4) and (5.5) define a quantitative measure of isochronal superposition. In practice, suppose an experiment results in data for the shape parameter X along an isochrone. This gives a series of numbers $X_1, X_2, ...$, corresponding to the state points $(T_1, \rho_1), (T_2, \rho_2), ...$ Since $\ln(X_{i+1}) - \ln(X_i) = \ln(X_{i+1}/X_i)$, etc., the discrete version of the right-hand side of Eq. (5.4) is

$$L(X_{i+1/2}) = \left| \frac{\ln(X_{i+1}/X_i)}{\sqrt{\ln^2(T_{i+1}/T_i) + \ln^2(\rho_{i+1}/\rho_i)}} \right| \tag{5.6}$$

An alternative measure of isochronal superposition corresponding to the purely temperature-based metric $ds^2 = (d\ln(T))^2$ is defined by

$$L_T(X) \equiv \left| \frac{d\ln(X)}{d\ln(T)} \right|_\tau \tag{5.7}$$

This measure is considered because density data are not always available. If the density-scaling exponent $\gamma \equiv (d\ln(T)/d\ln(\rho))|_\tau$ [25] is known for the range of state points in question, Eq. (5.5) implies $ds^2 = (d\ln(T))^2(1+1/\gamma^2)$. This leads to the following relation between the two isochronal superposition measures

$$L(X) = \frac{L_T(X)}{\sqrt{1+1/\gamma^2}} \tag{5.8}$$

This relation is useful in the (common) situation where gamma is reported in the literature, but the original density data are difficult to retrieve.

5.2 Pressure-volume-temperature (PVT) measurements

In order to use the measure $L(X)$ of isochronal superposition, the density of the liquids at different state points are necessary. In order to find the density as function of pressure and temperature, pressure-volume-temperature (PVT) data are needed. PVT data are available for DBP and glycerol in Ref. [70]. PVT measurements for DC704 and for 5PPE are from Refs. [42] and [57]. PVT measurements on 1,2,6-HT and DEP are performed in relation to the present investigation and are described in the following section.

5.2.1 Equipment and method

The PVT measurements on 1,2,6-HT and DEP are performed at the pressure equipment at Roskilde University (see Section 4.1). A special plug for the pressure vessel is used for this purpose, which is illustrated together with the sample cell and the pressure vessel in Figure 5.1. The sample cell consists of a sample container shaped as a cylinder with the diameter 20 mm and height 41 mm. One of the ends of the cylinder functions as a floating piston to transmit the pressure into the sample. The piston is sealed by a rubber o-ring to avoid mixing up sample and pressure liquid. The other end of the sample cell has a de-aerating screw, which is used to prevent air in the container. The maximum pressure of the sample cell is 600 MPa and the temperature ranges from 253.15 K to 353.15 K (however, the maximum temperature with the used cooling bath is 333 K (Section 4.1)).

The displacement of the piston is measured by use of a rod connected to the piston. The displacement of this rod is measured by a "linear variable displacement transformer" (LVDT). The LVDT used to measure the displacement of the piston is the type PAn 20s, and the corresponding measuring bridge is the type MPL701. The maximum displacement of the piston is 20 mm.

To perform measurements, the clean sample cell is first weighed (M_{empty}). The de-aerating screw is tightened and the container is filled with sample liquid. The piston is then placed carefully in the sample container. The sample cell is turned around so the de-aerating screw is pointing upwards. The de-aerating screw is loosened and the piston is pushed until the piston and the sample cell coincides (resulting in first air and then sample liquid coming out of the valve of the de-aerating screw). The de-aerating screw is tightened, and the sample cell is weighed again (M_{filled}). The rod is connected to the sample cell, and the sample cell is then connected to the plug.

The weight of the sample liquid is calculated, $M_{\text{sample}} = M_{\text{filled}} - M_{\text{empty}}$. The specific volume ($V_{\text{sp}} = 1/\rho$) at room temperature and ambient pressure is

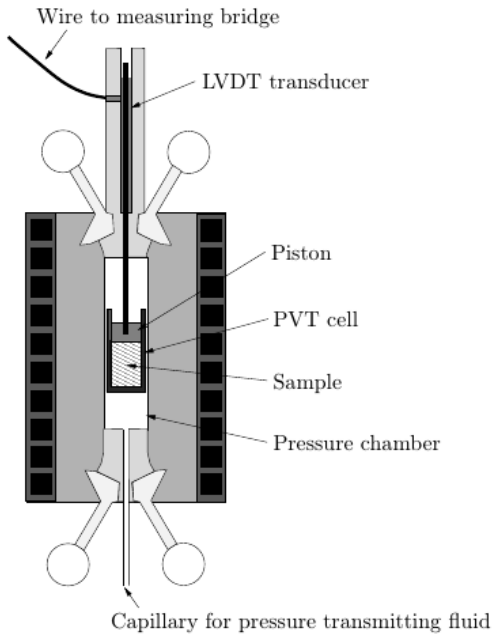

Figure 5.1: Illustration of the plug and sample cell used for PVT measurements. Figure from Gundermann (2013) [57].

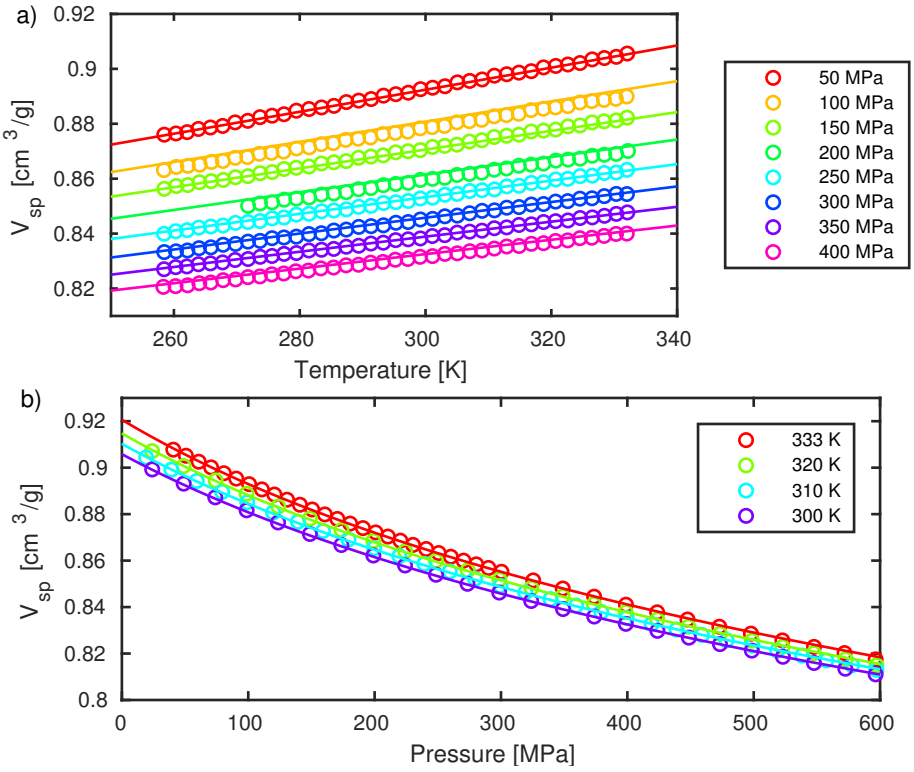

Figure 5.2: PVT measurements on 1,2,6-HT. The lines show the fit to the Tait-equation. (a) Data along isobars. (b) Data along isotherms.

therefore

$$V_{\mathrm{sp}} = \frac{V_{\mathrm{sample}}}{M_{\mathrm{sample}}} = \frac{\pi \cdot h \cdot r^2}{M_{\mathrm{sample}}} \tag{5.9}$$

where V_{sample} is the volume of the sample container and thereby the volume of the liquid at room temperature and ambient pressure. h is the height of the cylinder and r is the radius of the cylinder.

When the temperature and pressure are changed, the volume of the sample changes and the piston moves. The specific volume V_{sp} is then calculated as

$$V_{\mathrm{sp}} = \frac{(h - D) \cdot \pi \cdot r^2}{M_{\mathrm{sample}}} \tag{5.10}$$

where D is the measured displacement of the piston.

Figure 5.2 shows the PVT measurements on 1,2,6-HT, which are performed along both isobars and isotherms. Figure 5.3 shows the PVT measurements on DEP, which are performed along isobars.

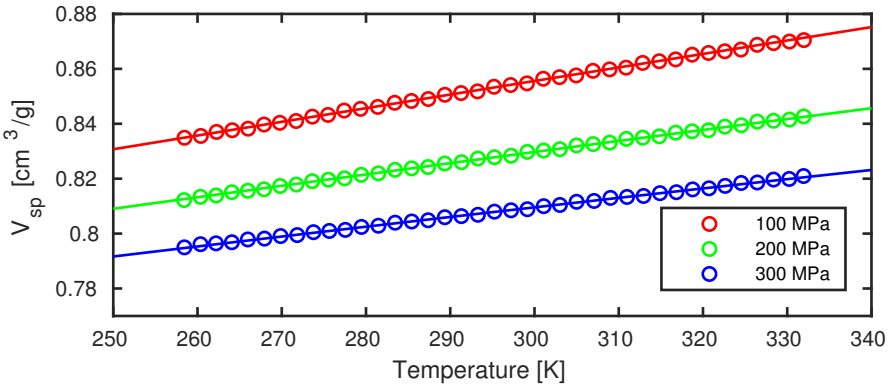

Figure 5.3: PVT measurements along isobars on DEP. The lines show the fit to the Tait-equation.

5.2.2 Extrapolation using the Tait-equation

The state points where the respective PVT measurements and dielectric measurements can be performed are often not the same. Figure 5.4 shows the situation for 1,2,6-HT and DEP, where only one state point for DEP overlaps between the two methods. Therefore, an extrapolation of the PVT data is necessary in order to determine the density at the state points used. The PVT data are fitted to the Tait-equation of state, which show the specific volume as a function of temperature and pressure. The used Tait-equation is [57]:

$$V_{\mathrm{sp}} = v_0 \cdot e^{\alpha_0 \cdot T} \cdot \left(1 - C \cdot \ln\left(1 + \frac{P}{b_0 \cdot e^{-b_1 \cdot T}}\right)\right) \tag{5.11}$$

where T is the temperature in Celsius and P is the pressure in MPa.

For 1,2,6-HT a fit to the Tait equation is made with both the data performed along isobars and the data performed along isotherms. The used parameters for the Tait equation is the average of the parameters found from, respectively, the isobar and the isotherm fit. Figure 5.2 shows the fit of the Tait equation with the average values. For DEP, the fit to the Tait equation is seen in Figure 5.3.

The PVT data for glycerol and DBP are seen in Figure 5.5, where also the fits to the Tait equation are shown. For DC704 and 5PPE, the fitting parameters to the Tait equation are given in Refs. [42] and [57]. The fitting parameters to the Tait equation for all the used liquids are shown in Table 5.1.

5.3 Dielectric measurements

For the investigation of isochronal superposition, we use the imaginary part of the spectra obtained by dielectric measurements. Dielectric measurements have been obtained by us on the four liquids: 5PPE, DEP, glycerol and 1,2,6-HT, in

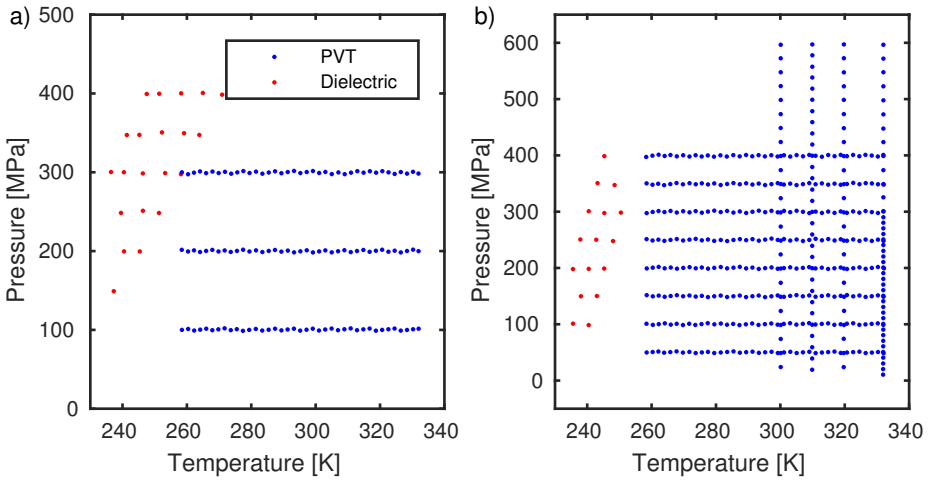

Figure 5.4: The state points where the respective PVT measurements and dielectric measurements are performed for DEP (a) and for 1,2,6-HT (b).

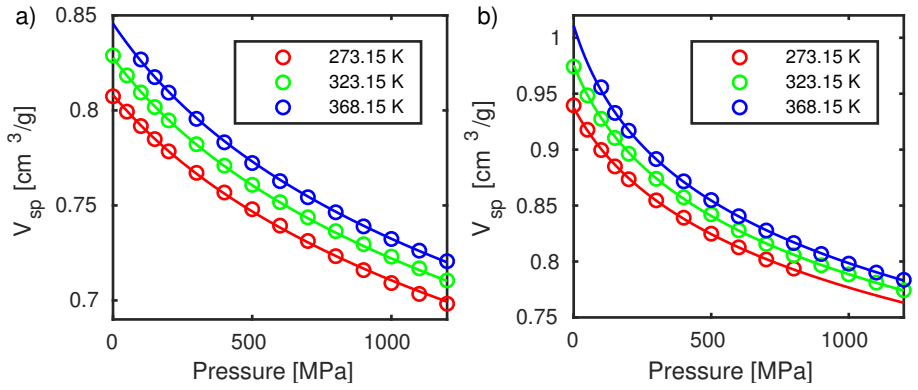

Figure 5.5: PVT data for glycerol and DBP from Bridgman (1932) [70], and fits to the Tait-equation. (a) Glycerol. (b) DBP.

Liquid	v_0	a_0	C	b_0	b_1	Ref.
1,2,6-HT	0.894	$4.9 \cdot 10^{-4}$	0.085	269	0.0029	This work
Glycerol	0.808	$4.8 \cdot 10^{-4}$	0.112	519	0.0018	Ref. [70]
5PPE	0.822	$6.5 \cdot 10^{-4}$	0.095	285	0.0043	Ref. [57]
DEP	0.874	$7.4 \cdot 10^{-4}$	0.103	235	0.0046	This work
DC704	0.920	$7.1 \cdot 10^{-4}$	0.088	188	0.0048	Ref. [57]
DBP	0.938	$7.9 \cdot 10^{-4}$	0.093	189	0.0050	Ref. [70]

Table 5.1: The parameters for the Tait-equation (Eq. (5.11)) for the different liquids.

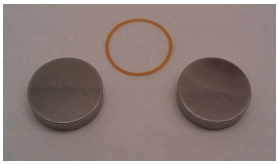

Figure 5.6: The sample cell used for the dielectric measurements. Picture from Roed (2012) [59].

relation to Ref. [59], while the data on DC704 are from Ref. [66] and the data on DBP are from Ref. [7].

For the dielectric measurements obtained by us in relation to Ref. [59], the used equipment is described in Section 4.1 and Section 4.2. Glycerol was in an exicator for 20 hours and 1,2,6-HT was in the exicator for two hours before use. Glycerol, 1,2,6-HT, and DEP were acquired from Sigma Aldrich and 5PPE was acquired from Santovac. The sample cell consists of two round stainless steel plates with a diameter of 19.5 mm, separated by a 0.05 mm thick Kapton spacer, which has an inner diameter of 17.5 mm and outer diameter of 19.5 mm. Figure 5.6 shows the sample cell. The sample cell is wrapped in Teflon tape and rubber to avoid mixing with the pressure fluid. For further details about the measurements, see Ref. [59].

Measurements on DEP and 5PPE were performed at several temperatures along 7 and 5 isobars, respectively. With the liquids 1,2,6-HT and glycerol, we discovered crystallization, which was detected by a drop in the dielectric signal. For these liquids, we therefore performed the final measurements with a new sample directly on selected isochrones.

For each liquid, state points which are approximately on the same isochrone are chosen for the investigation. These raw data are shown for all six liquids in Figure 5.7. We identify state points on the same isochrone as state points with the same value loss peak frequency, f_m, corresponding to a relaxation time $\tau = \frac{1}{2\pi f_m}$. This results in 2-5 isochrones with 3-6 state points each for each liquid. See Appendix A.2 for details on the selected isochrones.

When using dielectric spectroscopy, the amplitude of the signal is strongly sample dependent. Figure 5.8 illustrates the size of the signal for the liquids studied in this work and the overall experimental situation. Hydrogen-bonded liquids generally have a much larger dipole moment than van der Waals liquids, which leads to much better dielectric relaxation signals for the former liquids.

Another factor which differs from sample to sample is the area in the phase diagram where measurements can be performed. The equipment has a temperature, a pressure, and a frequency range, which give some general limits. The temperature and pressure dependence of the relaxation time is sample dependent, and the part of the phase diagram where the α-relaxation is present in the available frequency range therefore varies. Figure 5.9 illustrates this, and it is also clear from the raw data in Figure 5.7. By using a measure of isochronal

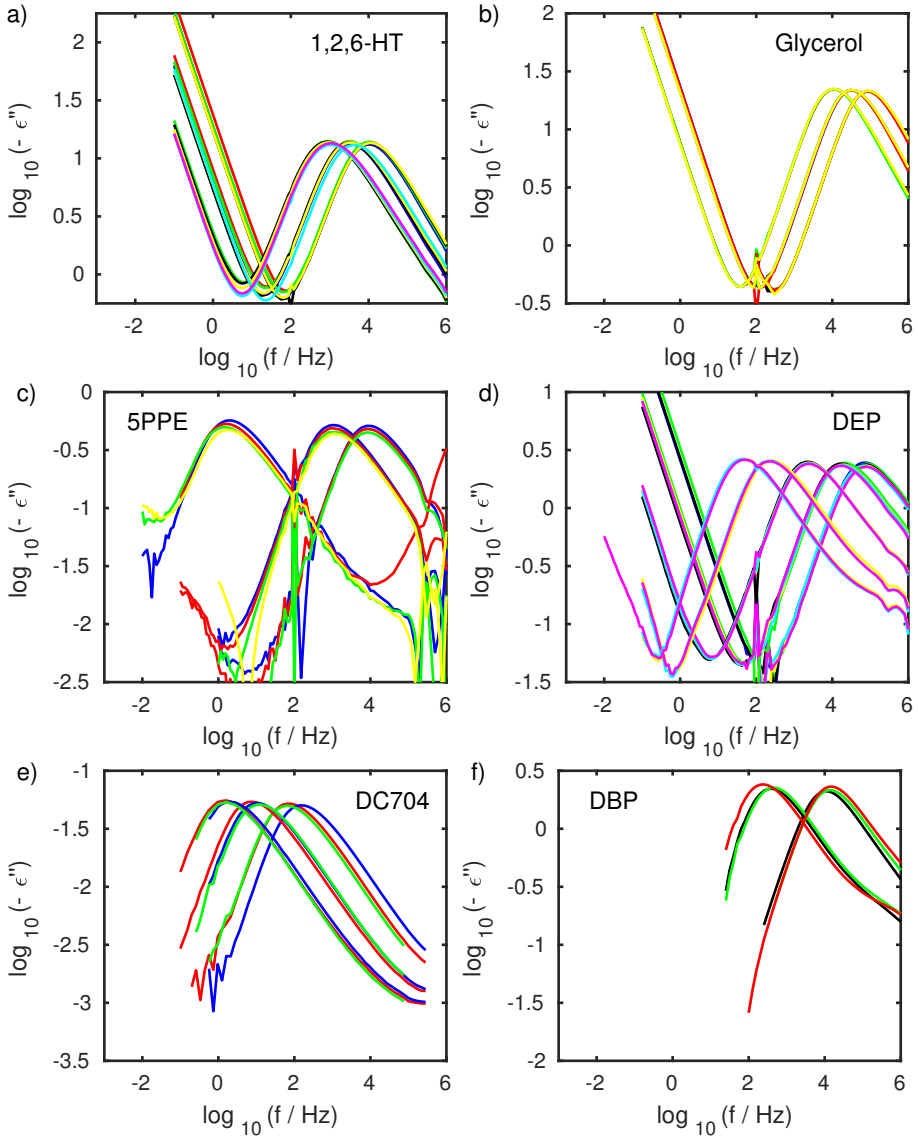

Figure 5.7: Raw data of the six studied liquids. The figures show the measurements which are selected to be on approximate isochrones. Each color represents a pressure. The figures illustrate that there are differences in noise and signal between the liquids. Furthermore, it is seen that the frequency range where the measurements are performed is different for the different liquids.

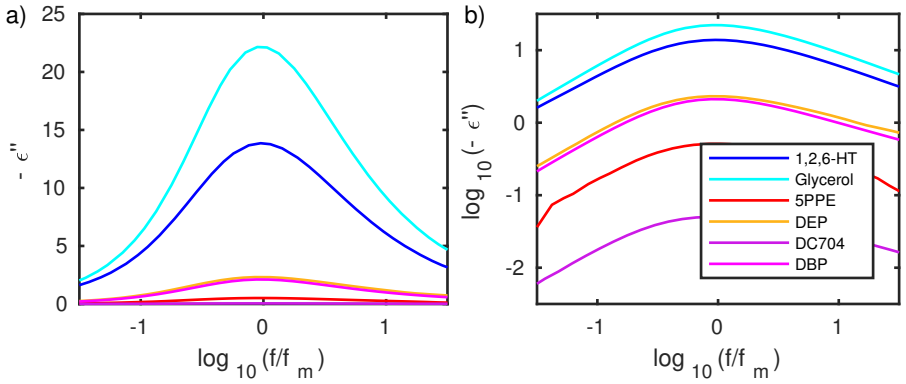

Figure 5.8: The figures show one relaxation spectrum for each of the used liquids on, respectively, a linear and a log scale. It is seen that the hydrogen-bonded liquids (the blue spectra) have better signal than the van der Waals liquids. The spectrum of DC704 is not visible in figure (a), because the signal is too low compared to the other liquids.

superposition, it is possible to take this challenge into account in term of the temperature and density difference (see Section 5.1).

5.4 Shape parameters

To use the measures of the degree of isochronal superposition on the measurements, shape parameters of the dielectric spectra are needed. We use three different shape parameters, the half width at half depth $W_{1/2}$, the area of dielectric loss over maximum loss in a log-log plot A, and the model-dependent shape parameter β_{DC} from the Cole-Davidson fitting function.

5.4.1 Half width at half depth $W_{1/2}$

As one shape parameter we use the half width at half depth, $W_{1/2}$, defined as the number of decades of frequency from the frequency of maximum dielectric loss to the higher frequency (denoted $f_{1/2}$) where the loss value is halved [69]:

$$W_{1/2} \equiv \log_{10}(f_{1/2}/f_m) \tag{5.12}$$

The $W_{1/2}$-values are plotted in Figure 5.10 (a) as functions of temperature for each isochrone studied. This figure suggests that isochronal superposition is not obeyed for the two hydrogen-bonded liquids (blue), since there is a clear change of $W_{1/2}$ as temperature changes. The figure suggests that the four van der Waals liquids obey isochronal superposition. There is more scatter in the values for the van der Waals liquids than for the hydrogen-bonded liquids, which is

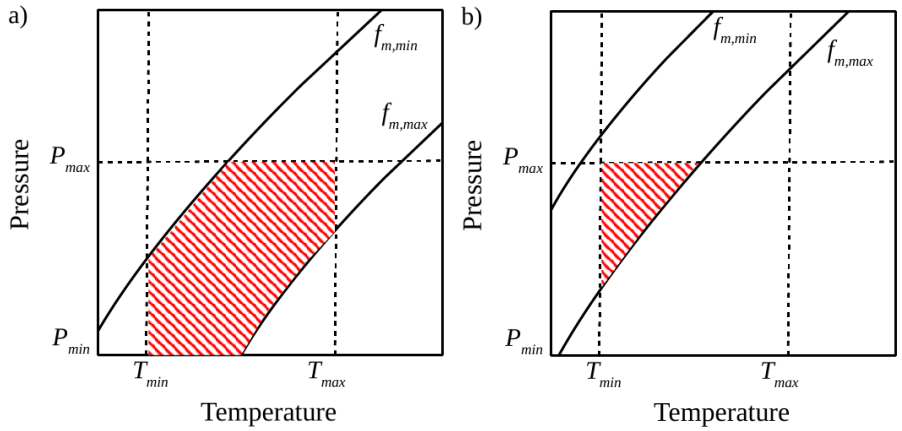

Figure 5.9: Illustration of measuring area on two different liquids. The red shaded area illustrates the part of the phase diagram where the α-peak can be measured. The pressure, temperature, and frequency range are determined by the equipment. However, the frequency at the α-relaxation (f_m) at each state point depends on the liquid. Two liquids are illustrated: the glass transition temperature T_g is lower for the liquid in (b) than the liquid in (a).

due to the smaller dielectric signals (see Figure 5.8). From Figure 5.10 (a) it is also seen that $W_{1/2}$ is almost constant at all state points for DEP and DC704, suggesting that isochronal superposition in these cases is a consequence of TTS (or more specifically, time-temperature-pressure superposition). However, the isochrones are separated from one another in the case of 5PPE and DBP (just as they are in the case of 1,2,6-HT and glycerol). This shows that isochronal superposition can apply even when the spectra broaden upon supercooling, which is also supported by earlier works where isochronal superposition has been found for systems without TTS [66, 76].

In Figure 5.10 (b), $W_{1/2}$ for all the data (i.e., also measurements that are not on the chosen isochrones) is shown as a function of f_m. It is seen that the $W_{1/2}$-values for DEP and DC704 especially are close to being the identical when f_m is the same. This is also the case for 5PPE and DBP at some values of f_m, but not all. For glycerol and 1,2,6-HT, on the other hand, $W_{1/2}$ seems to vary for all values of f_m. If the liquid obeys isochronal superposition, then $W_{1/2}$ has to be the same when f_m is the same. Thus, we can see directly from this figure that glycerol and 1,2,6-HT deviate from isochronal superposition.

5.4.2 Area of dielectric loss over maximum loss in a log-log plot A

As a second, model-independent shape parameter, we used the area of dielectric loss over maximum loss in a log-log plot, denoted by A. We integrated from

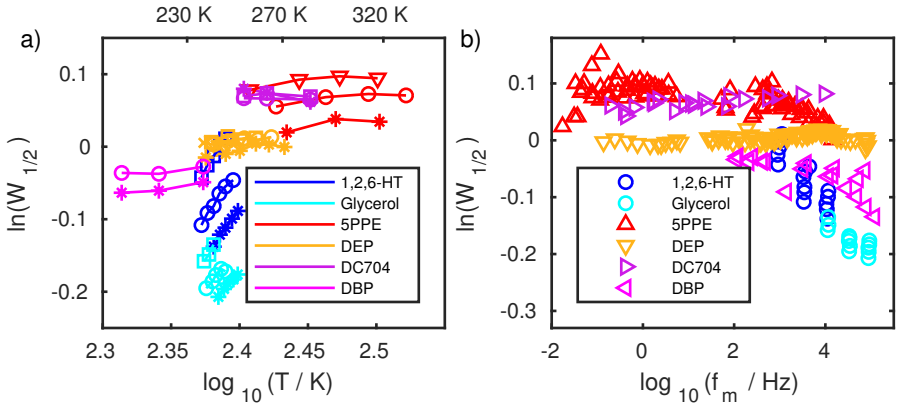

Figure 5.10: Half width at half depth ($W_{1/2}$). (a) $W_{1/2}$ as a function of temperature for each isochrone. Blue: 1,2,6-HT, stars: $\log_{10}(f_m) \simeq 4.0$, circles: $\log_{10}(f_m) \simeq 3.6$, squares: $\log_{10}(f_m) \simeq 3.0$. Cyan: glycerol, stars: $\log_{10}(f_m) \simeq 5.0$, circles: $\log_{10}(f_m) \simeq 4.5$, squares: $\log_{10}(f_m) \simeq 4.1$. Red: 5PPE, stars: $\log_{10}(f_m) \simeq 4.0$, circles: $\log_{10}(f_m) \simeq 3.1$, triangles: $\log_{10}(f_m) \simeq 0.2$. Orange: DEP, stars: $\log_{10}(f_m) \simeq 4.9$, circles: $\log_{10}(f_m) \simeq 4.3$, squares: $\log_{10}(f_m) \simeq 3.4$, triangles: $\log_{10}(f_m) \simeq 2.4$, crosses: $\log_{10}(f_m) \simeq 1.7$. Purple: DC704, stars: $\log_{10}(f_m) \simeq 2.0$, circles: $\log_{10}(f_m) \simeq 1.0$, squares: $\log_{10}(f_m) \simeq 0.3$. Magenta: DBP, stars $\log_{10}(f_m) \simeq 4.1$, circles: $\log_{10}(f_m) \simeq 2.6$. (b) $W_{1/2}$ as a function of f_m for all the measurements. If the liquids obey isochronal superposition $W_{1/2}$ has to be the same when f_m is the same.

-0.4 decades below the loss peak frequency to 1.0 decade above it. This was done by adding data for the logarithm of the dielectric loss taken at -0.4, -0.2, 0.2, 0.4, 0.6, 0.8, and 1.0 decades relative to the loss peak frequency:

$$A = |\sum_{i=1}^{7} \log_{10}(\tilde{\varepsilon}_{j+1}(\tilde{f}_i))| \tag{5.13}$$

where $\tilde{\varepsilon} = \frac{\varepsilon''}{\varepsilon''_{max}}$ and $\tilde{f} = \frac{f}{f_m}$. This area measure focuses on the high-frequency side of the peak. This is motivated in part by the occasional presence of dc conductivity on the low-frequency side of the peak, in part by the fact that for molecular liquids, this side of the peak is generally characterized by a slope close to unity, i.e., it varies little from liquid to liquid [77].

5.4.3 β_{DC} from the Cole-Davidson fitting function

As a third parameter, we used the model-dependent shape parameter β_{DC} from the Cole-Davidson fitting function [78]

$$\tilde{\varepsilon}(\omega) = \varepsilon_\infty + \frac{\Delta\varepsilon}{(1 + i\omega\tau)^{\beta_{CD}}} \tag{5.14}$$

For all spectra, we have fitted from half a decade on the low-frequency side of f_m to one decade on the high-frequency side of f_m. This interval is chosen so that all spectra are fitted in the same size of interval. The fits are shown in Figure 5.11. Below the measures are used on the found shape parameters.

5.5 Results

For a quantitative isochronal superposition analysis, we apply the L and L_T operators to the shape parameter $W_{1/2}$ seen in Figure 5.12. Both measures are considerably higher for the hydrogen-bonded liquids than for the van der Waals liquids; thus the latter obey isochronal superposition to a higher degree than the hydrogen-bonded liquids. We see from Figure 5.12 that the two measures $L(W_{1/2})$ and $L_T(W_{1/2})$ lead to similar overall pictures and the same conclusion.

In Figure 5.13, the measures $L(A)$ and $L_T(A)$ are shown. Clearly, the measures are higher for the hydrogen-bonded liquids than for the van der Waals liquids. Thus, also with respect to the area shape parameter, the van der Waals liquids obey isochronal superposition to a higher degree than the hydrogen-bonded liquids.

Results from using the L operators on the model-dependent shape parameter β_{DC} from the Cole-Davidson fitting function are shown in Figure 5.14. It is seen that also with respect to the model-dependent shape parameter β_{CD}, the van der Waals liquids obey isochronal superposition to a higher degree than the hydrogen-bonded liquids.

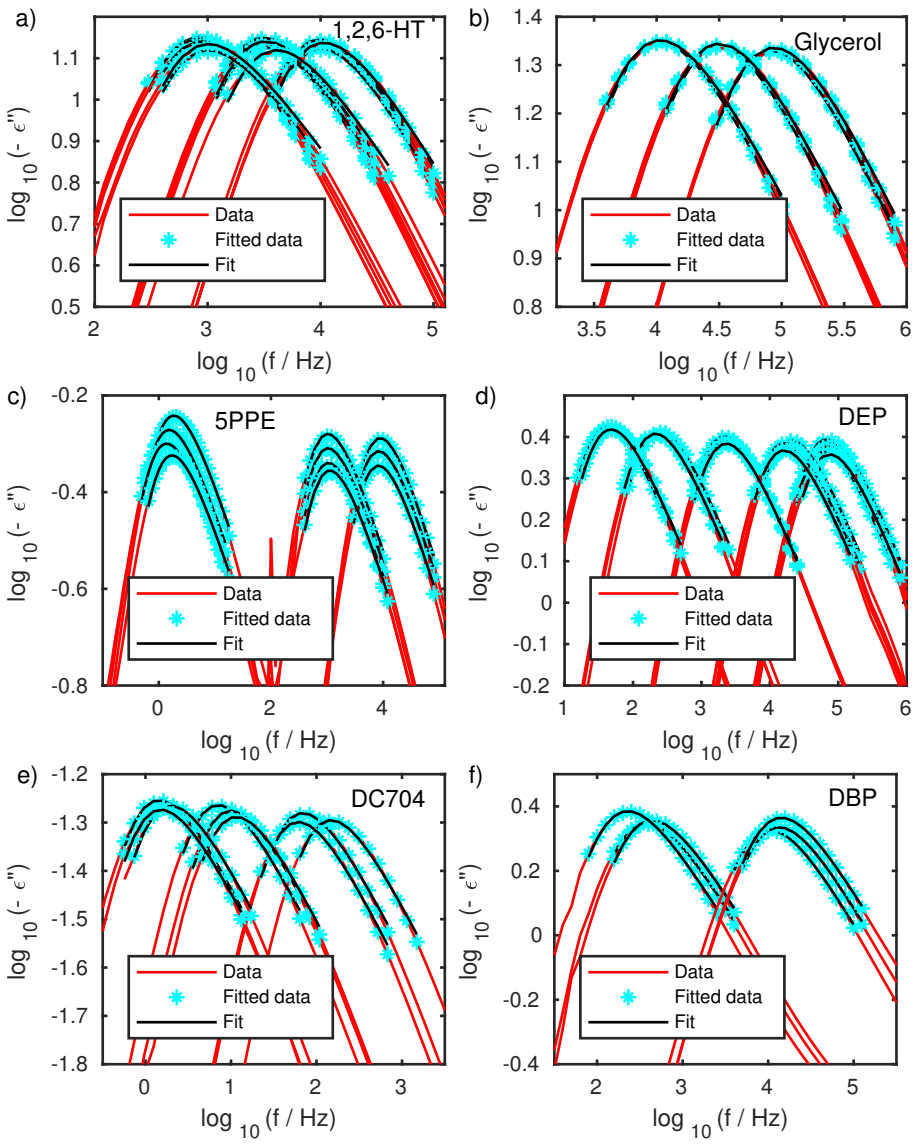

Figure 5.11: Cole-Davidson fit. The raw data, the part of the raw data which is used for the fit and the Cole-Davidson fit.

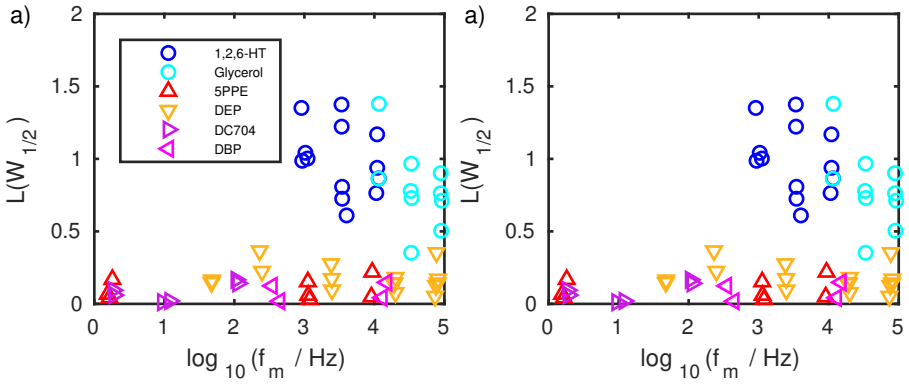

Figure 5.12: The measures of isochronal superposition based on the half width at half depth of the dielectric loss peak, $W_{1/2}$. (a) The measure $L(W_{1/2})$ giving the rate of relative change of $W_{1/2}$ along an isochrone. (b) The measure $L_T(W_{1/2})$.

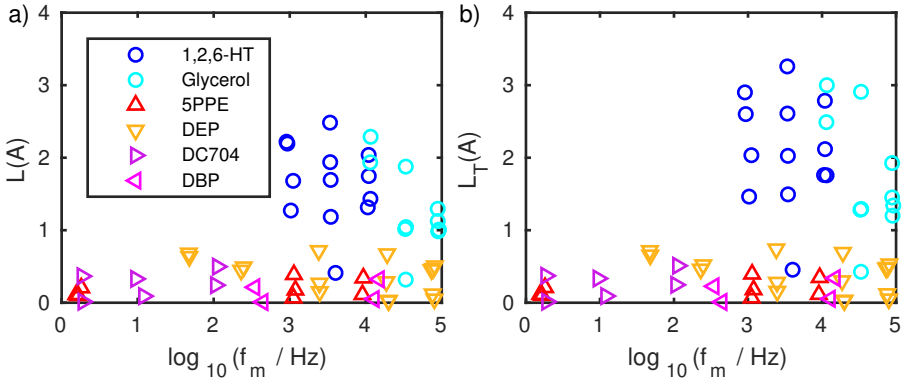

Figure 5.13: The measures of isochronal superposition based on the area A of the dielectric loss peak plotted in a normalized log-log plot, obtained by integrating from -0.4 to +1.0 decades around the loss-peak frequency. (a) The measure $L(A)$. (b) The measure $L_T(A)$.

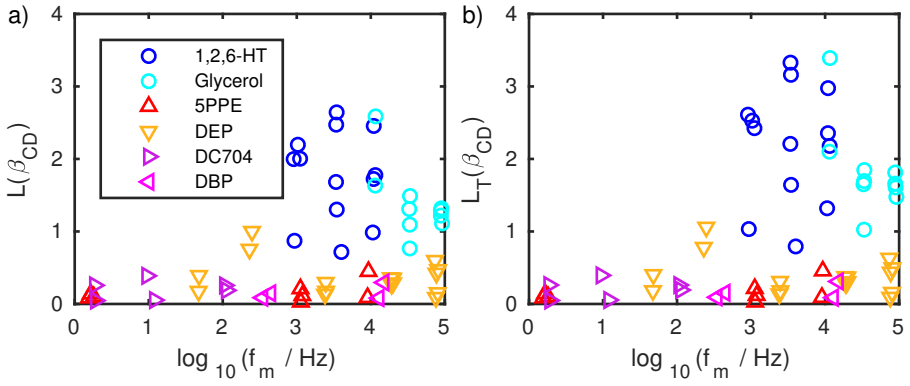

Figure 5.14: The measures of isochronal superposition based on the shape parameter of the Cole-Davidson function β_{CD}. (a) The measure $L(\beta_{CD})$. (b) The measure $L_T(\beta_{CD})$.

It is not straightforward to estimate the systematic uncertainties involved in the measurements, but an attempt to do so is presented in the next section.

5.5.1 Uncertainty in the measures

We made an attempt to find the experimental uncertainty in the measurements to estimate an error bar for the measures. Note that there are many different ways to estimate the error bars, and this is just one way to do it.

We find the error bars for the shape parameter (X) using the relative deviation of the shape parameter of two measurements at the same state point. We then fit a power law to the maximum relative deviation for each liquid against the dielectric strength of the liquid (we use a fit since we do not have two measurements at the same state point for DC704 and DBP). The maximum deviations are used, because the measurements at the same state points are performed right after each other, and we expect that the deviation would be larger if the two measurements were totally independent.

The fitted power law is used to find the relative deviation p for each liquid, which is then used to calculate the error bar of the shape parameter σ_X for each liquid in this way

$$\sigma_X = X \cdot p \tag{5.15}$$

where p is the relative deviation found by the fitted power law.

We then find the error bar of $\ln(X)$ ($\sigma_{\ln(X)}$) in the following way

$$\sigma_{\ln(X)} = \ln(X) - \ln(X \cdot (1-p)) = \ln\left(\frac{1}{1-p}\right) \tag{5.16}$$

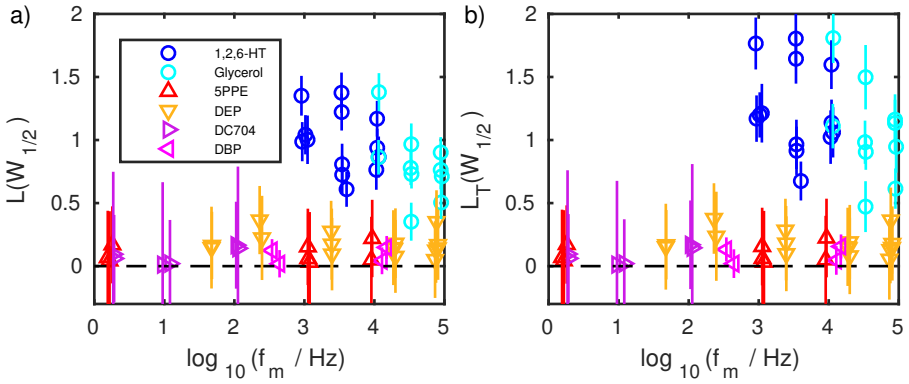

Figure 5.15: The measures based on $W_{1/2}$ with error bars. (a) The measure $L(W_{1/2})$. (b) The measure $L_T(W_{1/2})$.

The error bar of the measure $L(X)$ ($\sigma_{L(X)}$) is then found as

$$\sigma_{L(X_{i+1/2})} = \frac{\sqrt{2} \cdot \sigma_{\ln(X)}}{\sqrt{\ln^2(T_i/T_{i+1}) + \ln^2(\rho_i/\rho_{i+1})}} \tag{5.17}$$

where we use a standard method for calculating the error bar of a sum of (or difference between) two numbers. In the error bar, we do not take uncertainties in the temperature and density into account.

The error bar of the measure $L_T(X)$ ($\sigma_{L_T(X)}$) is found as

$$\sigma_{L_T(X_{i+1/2})} = \frac{\sqrt{2} \cdot \sigma_{\ln(X)}}{\ln(T_i/T_{i+1})} \tag{5.18}$$

The Figures 5.15 and 5.16 show the measures with these error bars. If the liquid obeys isochronal superposition, both measures must be zero within the experimental uncertainty. This is the case for the four van der Waals liquids, but not for the two hydrogen-bonded liquids.

5.6 Concluding remarks

To summarize, we have proposed two measures of isochronal superposition that quantify the relative change of a given relaxation-spectrum shape parameter along an isochrone. To use the measures, PVT data were obtained for DEP and 1,2,6-HT. The measures were tested for six liquids with regard to two model-independent shape parameters characterizing dielectric loss peaks, the half width at half depth and the loss-peak area in a normalized log-log plot, and one model-dependent shape parameter, the Cole-Davidson β_{CD}. The two measures

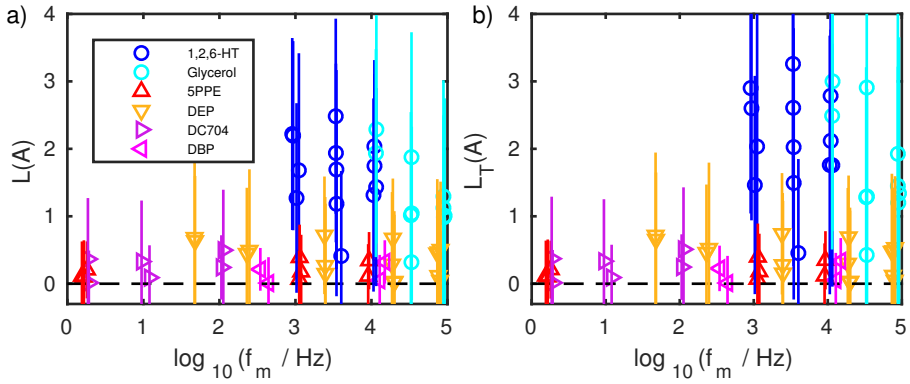

Figure 5.16: The measures based on A with error bars. (a) The measure $L(A)$. (b) The measure $L_T(A)$.

lead to similar overall pictures; in particular, both support the conclusion that van der Waals liquids obey isochronal superposition to a higher degree than hydrogen-bonded liquids.

The conclusion that van der Waals liquids obey isochronal superposition better than hydrogen-bonded liquids is not new. This was reported as a clear tendency in the pioneering papers on isochronal superposition from 2003 and 2005 by Roland *et al.* [17] and Ngai *et al.* [20]. In the present investigation, we have focused on systems with no visible beta relaxation or excess wing. Capaccioli *et al.* [76] demonstrated isochronal superposition in systems with beta relaxation, suggesting that the beta and alpha relaxations are connected.

The results are discussed in relation to the isomorph theory in Chapter 9.

Chapter 6

High-pressure specific heat spectroscopy

The aim of this investigation was to compare relaxation times found from specific heat measurements and dielectric measurements, respectively, in the two-dimensional phase diagram inspired by the study in Jakobsen *et al.* (2012) [79], where the characteristic times for several measuring methods including dielectric and specific heat along the atmospheric isobar were studied. To study frequency-dependent specific heat under high pressure, we adapted our method of measuring specific heat [80] to the high-pressure equipment at Roskilde University as part of the present investigation. The dielectric measurements done in relation to the isochronal superposition investigation (Chapter 5) were conducted in the same pressure setup, which gave us an unique possibility to compare the results from the two measuring methods at high pressures. In relation to this investigation, a paper was written (Paper 2). Some sections in this chapter are similar to sections from the paper.

The glass transition has classically been investigated by calorimetry, where the glass transition is observed as a drop in specific heat, when the slow degrees of freedom are no longer accessible on the experimental timescale. However, the realization that specific heat is time/frequency dependent and shows relaxation is surprisingly young, and dates back to the early 1980s [81–86]. The experimental use of specific heat as a spectroscopic technique studying the complex frequency-dependent specific heat dates back to the work by Birge and Nagel [83] and Christensen [84] in 1985. However, the number of experimental studies of the dynamics in viscous liquids as seen from frequency-dependent specific heat are limited. The following list is not comprehensive but covers, to the best of our knowledge, all groups having addressed the issue Refs. [80, 83, 84, 87–92]. To the best of our knowledge, only one previous study of frequency-dependent specific heat at elevated pressures exists, in which Leyser *et al.* (1995) [93] investigated orthoterphenyl 20 years ago in a limited pressure range up to 105

MPa.

The heat capacity (C) of a substance is the amount of heat (Q) needed to raise the temperature of the substance by one Kelvin [94]

$$C = \frac{Q}{\Delta T} \tag{6.1}$$

The specific heat used here is the heat capacity per volume. The specific heat can be measured under isobaric or isochoric conditions, for example, leading to respective isobaric c_p and isochoric c_v specific heat. In this investigation, it is the longitudinal specific heat (c_l) which is measured [95, 96]. The longitudinal specific heat c_l is related to the isochoric specific heat c_v by

$$c_l = \frac{K_S + \frac{4}{3}G}{K_T + \frac{4}{3}G} c_v \tag{6.2}$$

where K_S is the adiabatic bulk modulus, K_T is the isothermal bulk modulus, and G is the shear modulus. The isochoric specific heat c_v is related to the isobaric specific heat c_p by

$$c_p = \frac{K_S}{K_T} c_v \tag{6.3}$$

At state points where relaxation occurs, G will differ from 0, which means that c_p and c_l differ. However, the difference of the characteristic timescale is very small, implying that c_l is approximately equal to c_p [79, 95].

Our experimental method [80, 96] is based on a NTC-termistor (negative temperature coefficient termistor), which is a temperature-dependent resistor. In this setup, the termistor acts both as a heat generator and as a thermometer. The thermistor is placed in the middle of a container filled with sample liquid, implying that the thermistor is surrounded by the sample. This experimental method is based on the thermal effusivity, which determines the liquid's ability to take up heat from parts of its surface and transport it away [80]. The effusivity (e) depends on the heat conductivity λ and the specific heat c of the sample liquid in this way: $e = \sqrt{\lambda c}$.

In this investigation, the specific heat is investigated in the thermal thick limit, meaning that the boundaries of the sample cell do not affect the measurements [80, 96]. In the thermal thick limit, the sample size (here > 5 mm) is much larger than the heat diffusion length l_D which is defined as $l_D = \sqrt{\frac{D}{i\omega}}$, where D is the heat diffusivity. Jakobsen *et al.* (2010) [80] states that a realistic value of D is 0.1 mm^2/s, resulting in l_D between 0.05 and 1.6 mm in the used frequency range for our measurements.

The sections 6.1 – 6.3 describe the specific heat measurements. Section 6.1 provides the experimental details. This section furthermore describes our new sample cell for specific heat measurements at high pressures. Section 6.2 describes how the specific heat is derived from the measured signal. This is by no means trivial, and requires several assumptions. In Section 6.3 we use two

alternative ways of finding the specific heat from the measured signal. Section 6.4 shows the results of the specific heat measurements and compares them to dielectric measurements taken under the same conditions. Section 6.5 provides the concluding remarks of this investigation.

6.1 Experimental details

The specific heat measurements are performed at two different setups. The two setups are the high-pressure equipment at Roskilde University (see Section 4.1) and a standard RUC cryostat (described in Ref. [56]). The measurements on the standard RUC cryostat are taken at atmospheric pressure with varying temperature. The measurements on the pressure equipment are done with both varying pressure and temperature. The used liquid is polyphenyl ether (5PPE) from Santovac. Before use, the liquid was placed in an exicator for one hour until no bubbles were seen. Further details on 5PPE are given in Section 4.3. Former investigations utilizing the same experimental method at atmosheric pressure, Jakobsen *et al.* (2010) [80] and Jakobsen *et al.* (2012) [79], are also made with 5PPE as sample liquid, which made it perfect for testing the new high-pressure sample cell.

6.1.1 Sample cells

Different sample cells are used for the two setups. They are both made as cylinders. A NTC-termistor (type U23UD from Bowthorpe Thermometrics) is placed in the middle of the cylinder, with wires going out of the side of the cylinder (illustrated in Figure 6.1). The sample cell is filled with the sample liquid and the thermistor is thereby surrounded by the liquid. The thermistor has a radius of approximately 0.2 mm.

Pressure setup

The sample cell for the pressure setup was developed as part of this investigation, see the illustration in Figure 6.1. Figure 6.2 shows the working drawing of the cell. It is made in polyetheretherketone (PEEK). The top and the bottom of the sample cell are also made in PEEK with rubber o-rings in the sides, which work as pistons to transmit the pressure into the sample liquid. One of the pistons has a valve, which makes it possible to remove air from the sample cell after filling it. The cylinder can be divided in the middle to remove the sample liquid and clean the sample cell. The o-rings in the pistons should, in principle, keep the sample and the pressure liquid from mixing. However, in order to secure the sample, the sample cell was packed in three layers of teflon tape and rubber.

The size of the sample cell ensures that there are 10 mm to the closest sides, which means that we are in the thick limit.

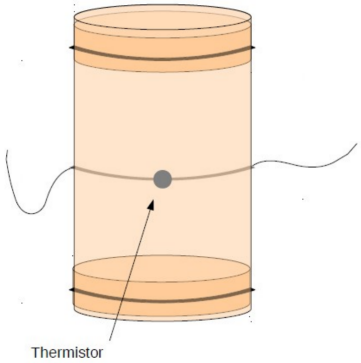

Figure 6.1: Illustration of the new specific heat sample cell for the high-pressure equipment. Note that this illustration does not give the right dimensions of the thermistor, since the thermistor is actually quite small and barely visible.

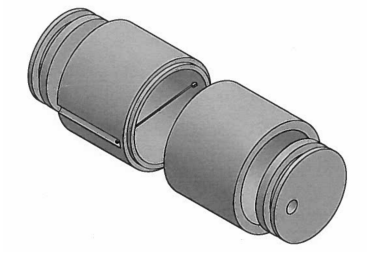

Figure 6.2: Working drawing made by the workshop at Roskilde University of the new specific heat sample cell for the high-pressure equipment.

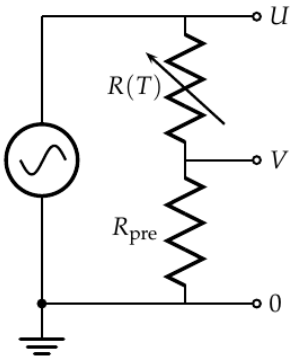

Figure 6.3: The electrical setup. $R(T)$ is the thermistor and R_{pre} is a temperature-independent resistor. Figure from Jakobsen (2011) [97].

Standard setup

The sample cell for the standard RUC setup is made as a cylinder with bottom in copper and a lid in PEEK. The size of the sample cell insures that there are 5 mm to the closest sides. This sample cell is used before in Ref. [79].

6.1.2 Electronic measurement equipment

The electric equipment consists of a frequency generator and one or two multimeters, the same as described in Section 4.2, but used in a different configuration. When measuring specific heat, we utilize that the multimeters can measure all harmonic components of the signals.

Figure 6.3 shows the used electrical setup, where $R(T)$ is the thermistor. A temperature-independent resistor (R_{pre}) is placed in series with the thermistor. The size of R_{pre} is measured directly by the use of a multimeter before measurements are started. During the measurements, the voltage V over R_{pre} and the voltage U generated from the frequency generator are measured. The measurements at the pressure equipment are performed using two multimeters so that the two voltages U and V are measured at the same time. The measurements at the standard RUC setup are performed using one multimeter. This means that the voltage V is measured first, and the voltage U is measured afterwards. The two-multimeter configuration is preferred due to more precise measurements and due to the time it takes to perform the measurements.

The current in this system is (following Ohms law $V = R \cdot I$)

$$I(t) = \frac{U(t)}{R_{\text{pre}} + R(T(t))} \tag{6.4}$$

and

$$I(t) = \frac{V(t)}{R_{\text{pre}}} \tag{6.5}$$

By combining the above equations, the voltage divider equation is derived

$$V(t) = \frac{R_{\text{pre}}}{R_{\text{pre}} + R(T(t))} U(t) \tag{6.6}$$

In Section 6.2, we show how to derive the specific heat from the measured voltages.

6.1.3 Measuring protocol

The measurements are conducted at different temperatures along isobars. For each measuring series, the voltage amplitude is chosen so that the corresponding temperature amplitude is constant at the different temperatures. The measurements are started at the highest temperature, and measurements are then taken at the different temperatures while going down in temperature. After each temperature step there is a waiting time of at least four hours before measurements are performed to ensure that the liquid is in equilibrium. For the measuring series at atmospheric pressure (0.1 MPa) on the pressure setup, measurements are also performed while going up in temperature again.

Four different datasets with varying temperature are made at the pressure equipment:

- 0.1 MPa with a temperature amplitude around 0.96 K
- 0.1 MPa with a temperature amplitude around 0.55 K
- 150 MPa with a temperature amplitude around 0.96 K
- 300 MPa with a temperature amplitude around 0.96 K

Three different datasets are made using the standard RUC cryostat, where measurements are performed at atmospheric pressure with three different temperature amplitudes:

- Temperature amplitude around 0.95 K
- Temperature amplitude around 0.75 K
- Temperature amplitude around 0.55 K

The measurement series at atmospheric pressure are done with variable temperature amplitude to determine how the temperature amplitude affects the temperature of the sample near the thermistor, and thereby, to determine an effective temperature of the sample. Section 6.2.5 describes how this effective temperature is determined. The measurements are conducted at the standard

RUC setup with a known sample cell to investigate whether the new sample cell for the pressure setup gives correct results. The results at 0.1 MPa from the two different setups are therefore compared in Section 6.2.6 together with data from a previous study (Jakobsen *et al.* (2012) [79]).

First, Section 6.2 shows how we derive the specific heat from the voltage measurements. This is shown for the dataset from the pressure setup at 0.1 MPa with the temperature amplitude around 0.96 K. The same data analysis is used for all other datasets except the dataset at 300 MPa, where the data analysis is therefore also shown and described in Section 6.3.

6.2 Deriving the specific heat from the measurements

The used experimental method is argued and described in detail in Jakobsen *et al.* (2010) [80], which is also the main reference to this section, where an overview over the initial data analysis is given. The purpose of this initial data analysis is to come from the measured voltages ($V(t)$ and $U(t)$) to the frequency-dependent specific heat (c_l), which is by no means trivial. The results are shown in Section 6.4.

The principle of this experimental method is that a harmonic varying heat current with angular frequency ω and complex amplitude P is generated in the thermistor, and thereby at the surface in contact with the liquid. The generated heat flows through the liquid, and results in a harmonic temperature oscillation at the surface between the liquid and thermistor with complex amplitude δT. The thermal impedance is defined as the ratio of the complex amplitude of a harmonic temperature oscillation δT, and the harmonic varying heat current with complex amplitude P

$$Z_{\text{liq}} = \frac{\delta T}{P} \tag{6.7}$$

In the thermal thick limit the thermal impedance at an inner radius r_1 is described by

$$Z_{\text{liq}} = \frac{1}{4\pi\lambda r_1(1+\sqrt{i\omega r_1^2 c_l/\lambda})} \tag{6.8}$$

where c_l is the longitudinal specific heat and λ is the heat conductivity. Using a thick sample, Z_{liq} is independent on the mechanical boundary conditions [96].

The next sections derives the specific heat from the measured voltages, which requires a number of steps because we need to take the structure of the thermistor into account. These steps are stated below to give an overview of the analysis:

- Find the measured thermal impedance $Z_2 = \frac{T_2}{P_2}$ from the measured voltages (Section 6.2.2).

  - Find the power components directly from the power produced in the thermistor.
  - Find the temperature components and thereby Z_2, using the temperature dependence of the thermistor, the most significant components of the measured voltages and an iterative solution technique.

- Find Z_{liq} from the measured Z_2 (Section 6.2.3).
  - Derive a model of the system including the thermistor.
  - Fit the model to the measured Z_2, letting c_l be constant, i.e., the fit will only be correct in the non-relaxation range at high temperatures.
  - Extrapolate the fitting parameters from high temperatures to estimate them at the low temperatures where relaxation occurs.
  - Calculate Z_{liq} using the extrapolated fitting parameters.

- Calculate the frequency-dependent specific heat $c_l(\omega)$ (Section 6.2.4).
  - Estimate the heat conductivity λ from $Z_{\mathrm{liq},0}$.
  - Calculate $c_l(\omega)$ from Eq. (6.8).
  - Find a characteristic time from the loss peak of the imaginary part of the relaxation spectrum $-c_l''$.
  - Determine error-bar due to "hump" in spectra.

- Find the effective temperature of sample (Section 6.2.5).

All the above steps are performed for each measurement, i.e., for all temperatures (except the extrapolation of the fitting parameters which involves measurements at all temperatures along the different isobars).

First, we describe the complex notation used for the harmonic oscillating signals.

6.2.1 Complex notation

In the following, we use a complex notation to describe the periodic signals $A(t)$ of, e.g., the voltages. This is more complex than, for example, the signals used for dielectric spectroscopy, since this system is not linear. This complex notation, which is based on Ref. [97] is described here.

A time-dependent periodic signal can be written

$$A(t) = A_0 + |A_1|\cos(\omega t + \phi_1) + ... + |A_n|\cos(n\omega t + \phi_n) \tag{6.9}$$

where A_0 and $|A_k|$ are the amplitudes and ϕ_k are the phases. Using complex notation, the periodic signal can be written as

$$A(t) = \frac{1}{2}(A_0 + A_0 + |A_1|e^{i(\omega t+\phi_1)} + |A_1|e^{-i(\omega t+\phi_1)} + ...+ |A_n|e^{i(n\omega t+\phi_n)} + |A_n|e^{-i(n\omega t+\phi_n)}) \tag{6.10}$$

By introducing a complex amplitude $A_k = |A_k|e^{i\phi_k}$ and the notation $E_k = e^{ik\omega t}$ gives

$$A(t) = \frac{1}{2}\left(A_0 + A_1E_1 + ... + A_nE_n + c.c.\right) \tag{6.11}$$

where *c.c.* means the complex conjugated of all terms. The complex conjugated of $|A_n|e^{i(n\omega t+\phi_n)}$ is $|A_n|e^{-i(n\omega t+\phi_n)}$.

6.2.2 Thermal impedance Z_2

The principle in the measuring method is that an electrical current with cyclic frequency ω_e is applied through a resistor, which produces a combined constant and $2\omega_e$ component heating (since $P \propto I^2$):

$$P \propto \left(\frac{1}{2}(I_1e^{i\omega_e t} + I_1e^{-i\omega_e t})\right)^2 = \frac{1}{4}I_1^2(2 + e^{i2\omega_e t} + e^{-i2\omega_e t}) \tag{6.12}$$

This gives rise to a combined temperature dc offset and temperature oscillation at $2\omega_e$ (since the heat current results in a temperature change of the resistor), which size depends on the environment, i.e. the sample liquid. Since the temperature oscillation occurs at $2\omega_e$, the thermal impedance that is of interest is $Z_2 = \frac{T_2}{P_2}$. This method is referred to as a $3\omega_e$-technique because the temperature oscillation creates a pertubation of the resistance at frequency $2\omega_e$, implying that the voltage across the thermistor contains a $3\omega_e$ component (and an additional ω_e).

In order to find the thermal impedance Z_2 of the system, the power component P_2 and the temperature component T_2 need to be found. These components are found from the measured voltages $U(t)$ and $V(t)$. Up to fourth-order harmonics are included in the input voltage $U(t)$ and the voltage over the pre-resistor $V(t)$ in this analysis:

$$U(t) = \frac{1}{2}(U_0 + U_1E_1 + U_2E_2 + U_3E_3 + U_4E_4 + c.c.) \tag{6.13}$$

$$V(t) = \frac{1}{2}(V_0 + V_1E_1 + V_2E_2 + V_3E_3 + V_4E_4 + c.c.) \tag{6.14}$$

where $E_k = e^{ik\omega_e t}$ and *c.c.* means complex conjugated.

The power components

First, the power components are found. Up to fourth-order harmonics are included in the power (heat current) $P(t)$:

$$P(t) = \frac{1}{2}(P_0 + P_1E_1 + P_2E_2 + P_3E_3 + P_4E_4 + c.c.) \tag{6.15}$$

The power (which results in a heat current) produced in the thermistor when a current runs through it is (since in general $P = I \cdot V$)

$$P(t) = I(t)(U(t) - V(t)) = \frac{(U(t) - V(t))V(t)}{R_{\text{pre}}} \tag{6.16}$$

using Eq. (6.5). The power components are found directly from the measured $U(t)$ and $V(t)$ using Eq. (6.16) [80]

$$P_0 = \frac{1}{R_{\text{pre}}}\left(W_0V_0 + \frac{1}{2}\text{Re}(W_1V_1^* + W_2V_2^* + W_3V_3^* + W_4V_4^*)\right) \tag{6.17}$$

$$P_1 = \frac{1}{R_{\text{pre}}}(W_1V_0 + V_1W_0 + \frac{1}{2}(W_2V_1^* + W_1^*V_2 + W_3V_2^* + W_2^*V_3 + W_3^*V_4 + W_4V_3^*)) \tag{6.18}$$

$$P_2 = \frac{1}{R_{\text{pre}}}\left(W_0V_2 + W_2V_0 + \frac{1}{2}(W_1V_1 + W_1^*V_3 + W_2^*V_4 + W_3V_1^* + W_4V_2^*)\right) \tag{6.19}$$

$$P_3 = \frac{1}{R_{\text{pre}}}\left(W_0V_3 + W_3V_0 + \frac{1}{2}(W_1V_2 + W_2V_1 + W_1^*V_4 + W_4V_1^*)\right) \tag{6.20}$$

$$P_4 = \frac{1}{R_{\text{pre}}}\left(W_0V_4 + W_4V_0 + \frac{1}{2}(W_1V_3 + W_2V_2 + W_3V_1)\right) \tag{6.21}$$

where $W = U - V$ and $*$ means complex conjugated.

The temperature components and thermal impedance

Now the temperature components are found. Up to fourth-order harmonics are included in the temperature $T(t)$:

$$T(t) = \frac{1}{2}(T_0 + T_1E_1 + T_2E_2 + T_3E_3 + T_4E_4 + c.c.) \tag{6.22}$$

In order to find the temperature components (and thereby the thermal impedance Z_2), the temperature dependence of the thermistor is important. For a large range of temperatures the thermistor's temperature dependence is well described by

$$R(T) = R_\infty e^{T_a/T} \tag{6.23}$$

where T_a is the activation temperature and R_∞ is the infinite temperature limiting resistance [80].

To a first order approximation, the resistance around a certain temperature T_{cryo}, which is the temperature of the surrounding environment (for example a cryostat or a vessel) can be described by

$$R(T) = R_0(1 + \alpha_1\Delta T) \tag{6.24}$$

where $\Delta T = T - T_{\text{cryo}}$. R_0 and α_1 is considered constant at a given T_{cryo} and $\alpha_1 = -\frac{T_a}{T_{\text{cryo}}^2}$ [80].

To a second order approximation, the resistance around T_{cryo} is

$$R(T) = R_0(1 + \alpha_1\Delta T + \alpha_2\Delta T^2) \tag{6.25}$$

where $\alpha_2 = \frac{\alpha_1^2}{2} - \frac{\alpha_1}{T_{\text{cryo}}}$ [80].

Combining the voltage divider equation (Eq. (6.6)) with the second order approximation of the thermistor (Eq. (6.25)) gives the following expression for the voltage $V(t)$:

$$V(t) = \frac{1}{A+1}(1 - a\Delta T + b\Delta T^2)U \tag{6.26}$$

where $A = \frac{R_0}{R_{\text{pre}}}$, $a = \frac{A\alpha_1}{1+A}$, and $b = (\frac{A\alpha_1}{1+A})^2 - \frac{A\alpha_2}{1+A}$ [80].

When combining this equation for $V(t)$ (Eq. (6.26)) and the fourth-order harmonics of $\Delta T(t)$ and $U(t)$ (respectively Eq. (6.22) and Eq. (6.13)), a large number of terms are obtained for $V(t)$. Jakobsen *et al.* (2010) [80] performed a numerical inspection of which terms that are most significant, which is the first and third harmonics of the measured voltage, with following expressions

$$V_1 = \frac{1}{A+1}\left(U_1 - aT_0U_1 - \frac{1}{2}aT_2U_1^* + X_1\right) \tag{6.27}$$

where

$$X_1 = -aT_1U_0 + bT_0^2U_1 + \frac{1}{2}bT_2T_2^*U_1 + bT_0T_2U_1^* \tag{6.28}$$

and

$$V_3 = \frac{1}{A+1}\left(-\frac{1}{2}aT_2U_1 + U_3 + X_3\right) \tag{6.29}$$

where

$$X_3 = -\frac{1}{2}aT_4U_1^* + \frac{1}{4}bT_2^2U_1^* + bT_0T_2U_1 + bT_0T_4U_1^* \tag{6.30}$$

with X_1 and X_3 being minor terms.

An iterative solution technique is used to solve these equations in order to find T_2, and thereby the thermal impedance Z_2. Just as T_2 and Z_2 is found at each temperature, the iterative solution technique is also done for each temperature.

Iterative solution technique

First, the equations for V_1 and V_3 (Eq. (6.27) and Eq. (6.29)) are rewritten to isolate, respectively, A and T_2:

$$A = \frac{U_1 - aT_0U_1 - \frac{1}{2}aT_2U_1^* + X_1}{V_1} - 1 \tag{6.31}$$

$$T_2 = -2\frac{V_3(A+1) - (U_3 + X_3)}{aU_1} \tag{6.32}$$

The steps of the iterative solution technique are:

- Set $T_0 = T_1 = T_2 = T_4 = 0$ (and thereby $X_1 = 0$ following Eq. (6.28) and $X_3 = 0$ following Eq. (6.30)).

- Estimate A from Eq. (6.31). An initial estimate of the thermistor values T_a and $A_\infty (= \frac{R_\infty}{R_{\text{pre}}})$ are then estimated using the found A, since $A(T) = A_\infty e^{T_a/T}$ (Eq. (6.23)). An initial estimate of α_1, α_2, a, and b are then calculated.
- An initial T_2 is then found from Eq. (6.32) with the estimated value of A.
- Calculate an initial $Z_2 = \frac{T_2}{P_2}$ using the initial T_2 and the power component P_2 (Eq. (6.19)).
- The other Z-components are found using $Z_1(\omega) = Z_2(\omega/2)$, $Z_4(\omega) = Z_2(2\omega)$, and using an extrapolation of Z_2 to zero frequency, which equals Z_0 [80].
- T_0, T_1, and T_4 are then estimated using $Z_n = \frac{T_n}{P_n}$, where the power components are found from Eqs. (6.17), (6.18), and (6.21).
- The estimated values for T_0, T_1, T_2, T_4, α_1, and α_2 are then used to determine a new estimate of A using Eq. (6.31), which is then used to find new estimates of T_a, α_1, α_2, a, and b. These are then used to make a new estimate of T_2, and thereby Z_2, T_1, T_4, and T_0.
- This process is repeated until convergence.

In the following, only the thermal impedance Z_2 is used and the notation is therefore now changed so that $Z = Z_2$ and $\omega = 2\omega_e$.

Figure 6.4 shows an example of Z. The figure shows how relaxation affects Z, as Z is shown at the temperatures 266.3 K and 252.7 K, where relaxation occurs at the low temperature, but not at the high temperature. Note that the relaxation does not affect the spectra much, as the difference between the two spectra is very small.

6.2.3 Model of the thermal impedance

In this section, we show how we get from the measured thermal impedance Z to the thermal impedance of the liquid Z_{liq}. In our case, the thermal impedance at an inner radius r_1 of the sample is described by (rewriting Eq. (6.8))

$$Z_{\text{liq}} = \frac{\delta T(r_1)}{P(r_1)} = \frac{1}{4\pi\lambda r_1(1+\sqrt{i\omega r_1^2 c_l/\lambda})} = Z_{\text{liq},0}\frac{1}{1+\sqrt{i\omega\tau_l}} \tag{6.33}$$

where $Z_{\text{liq},0} = \frac{1}{4\pi\lambda r_1}$ and $\tau_l = \frac{r_1^2 c_l}{\lambda}$. The radius r_1 is the radius of the thermistor.

This model of Z_{liq} can not be used directly, however, since the measured thermal impedance Z is also affected by the structure of the thermistor, illustrated in Figure 6.5. The thermistor consists of a core with radius r_0, where the heat current is generated and where the temperature is measured. Around this core is a glass capsule with outer radius r_1 which is the part of the thermistor that

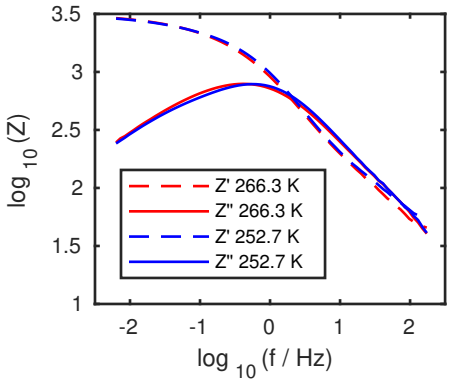

Figure 6.4: The thermal impedance of the system Z as a function of frequency at the temperatures 266.3 K and 252.7 K. The measurements are taken at atmospheric pressure, on the pressure equipment. Relaxation occurs at the low temperature, but not at the high temperature. Note that the difference is small.

is in contact with the liquid. Therefore the measured heat current $P(r_0)$ and temperature amplitude $\delta T(r_0)$ may be different from the heat current $P(r_1)$ and temperature amplitude $\delta T(r_1)$, which determines the thermal impedance of the liquid $Z_{\text{liq}} = \frac{\delta T(r_1)}{P(r_1)}$. The model of Z_{liq} (Eq. (6.33)) is therefore extended into a model of the thermal impedance of the system Z, which takes the structure of the thermistor into account, as illustrated in the thermal network in Figure 6.5 (right). The glass capsule layer has heat conductivity λ_b and specific heat c_b. This glass capsule is solid, which implies that the specific heat is frequency independent [80]. The heat diffusion through this capsule layer is well described by a thermal transfer matrix $\mathbf{T}^{\text{th}} = \mathbf{T}^{\text{th}}(\lambda_b, c_b, r_1, r_0)$ in the following way [96]

$$\begin{pmatrix} \delta T(r_1) \\ P(r_1)/i\omega \end{pmatrix} = \mathbf{T}^{\text{th}} \begin{pmatrix} \delta T(r_0) \\ P(r_0)/i\omega \end{pmatrix} \tag{6.34}$$

The components of the thermal transfer matrix are shown in Christensen & Dyre (2008) [96].

Using the thermal transfer matrix gives the following relationship between the thermal impedance at the boundary between the core and the capsule layer Z_{r_0} and the thermal impedance of the liquid Z_{liq} [80]

$$Z_{r_0} = \frac{1}{i\omega} \frac{T_{12}^{\text{th}} - T_{22}^{\text{th}} i\omega Z_{\text{liq}}}{T_{11}^{\text{th}} - T_{21}^{\text{th}} i\omega Z_{\text{liq}}} \tag{6.35}$$

Furthermore, a small part of the generated power is stored in the core of the thermistor. The heat capacity of the core is taken to be [80]

$$C_{\text{core}} = \frac{4}{3}\pi r_0^3 c_b \tag{6.36}$$

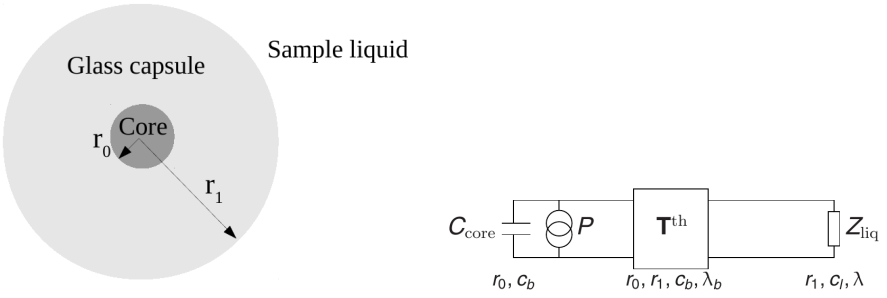

Figure 6.5: Left: Illustration of the thermistor, which consists of a core with radius r_0, and a glass capsule with outer radius r_1. The glass capsule is in contact with the liquid. Right: Thermal network model of the system used to derive Z_{liq} from the measured Z. Network model from Jakobsen *et al.* (2010) [80].

The measured thermal impedance of the system Z is related to Z_{r_0} in this way [80]

$$\frac{1}{Z} = i\omega C_{\text{core}} + \frac{1}{Z_{r_0}} \tag{6.37}$$

Using the Eqs. (6.33), (6.35), (6.36) and (6.37) the measured Z is related to Z_{liq}. The model formed by these equations has six parameters; $r_0, r_1, \lambda_b, c_b, \lambda$ and c_l. During the fitting of the model, we use a frequency-independent c_l, implying that the fit of this model is only valid in the region where c_l is frequency-independent, i.e., at temperatures above the relaxation part of the temperature range (an attempt to make a fit with a frequency-dependent c_l is made in Section 6.3.2). The number of independent parameters are only five [80], and they are chosen to be:

$$\tau_l = r_1^2 \frac{c_l}{\lambda},\ \tau_b = r_1^2 \frac{c_b}{\lambda_b},\ r = \frac{r_0}{r_1},\ c = \frac{c_l}{c_b},\ Z_{\text{liq},0} = \frac{1}{4\pi\lambda r_1} \tag{6.38}$$

This five parameter model is fitted to the measured thermal impedance Z for all state points using a least-square algorithm, keeping the five fitting parameters as free parameters. Since the fit is not correct when c_l is frequency-dependent, an extrapolation for each of the five parameters is made using the parameters at high temperatures in order to determine the values of the parameters at low temperatures where relaxation occurs. These extrapolated values are then used to calculate Z_{liq} using the measured thermal impedance and the Eqs. (6.33), (6.35), (6.36) and (6.37).

In the former investigations using the same model for the thermal impedance (e.g. Refs. [79, 80]), all parameters have been free when fitting the model of the thermal impedance of the system to the measured Z. The parameter r is then chosen as a constant, determined as the mean value of the fitting parameter r at

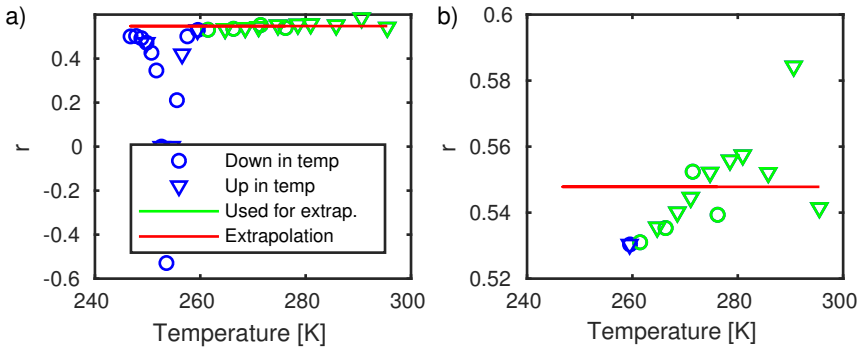

Figure 6.6: The fitting parameter r from a fit with all parameters free. Measurements are taken while going down in temperature and up again. The figure to the right shows a zoom of the high-temperature data. There seems to be a linear temperature dependence of r. The red line shows the mean value of r at the high temperatures.

high temperatures. This is also done in this investigation, but when looking at the fitting parameter r from the fit where all parameters are free, it is seen that there is a linear temperature dependence of r at the high temperatures as seen in Figure 6.6. This suggests that the usual extrapolation method is maybe not the correct choice to use with our data. One could consider an extrapolation of r found by a linear function. However, the value of r should not change with temperature, since we do not expect the radii of the thermistor to change with temperature, as it is solid. We therefore choose to fix the value of r. This is done by performing the fit with all parameters free, and then fix r as the mean value of the fitting parameter r from the high temperatures. The fit is then made again with r fixed, keeping the other four parameters free. Appendix B.1 shows how the different determinations of r affects the measurements, which suggest that a fixed r is correct.

All the fitting parameters from the fit with r fixed are shown in Figure 6.7. From the figures, it is clear at which temperature interval relaxation occurs, since the behavior of the fitting parameters starts deviating from the behavior at high temperatures. The figures also shows the relative error from the fit (σ_r), which shows that the model does not give a good fit at low temperatures. Figure 6.7 also shows the extrapolation of the fitting parameters. The parameters τ_b, τ_l and c seem to have a linear temperature dependence, and the parameters are therefore fitted to linear functions, which are used for the extrapolations. The parameters of $Z_{\mathrm{liq},0}$ are fitted by a second degree polynomial. Note that the functions used for extrapolation are chosen ad hoc. The extrapolations of the fitting parameters are used to calculate the liquid's thermal impedance Z_{liq} at the different state points. An example of the found Z_{liq} is shown together with the measured Z in Figure 6.8.

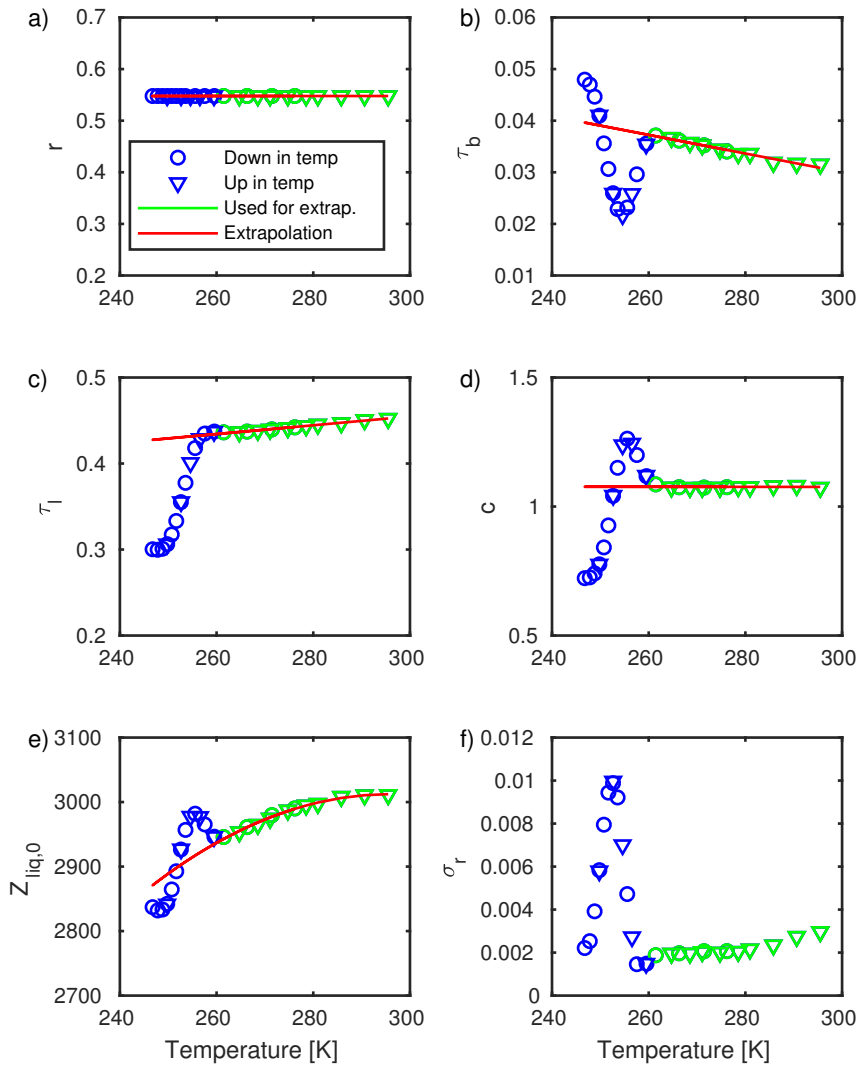

Figure 6.7: The fitting parameters and the extrapolation. The dataset is from the pressure equipment at atmospheric pressure. Measurements are taken while going down in temperature and up again. The high-temperature values are used for extrapolation. r is kept constant, τ_b, τ_l and c are expolated using linear functions, and $Z_{\mathrm{liq},0}$ is extrapolated using a second degree polynomial.

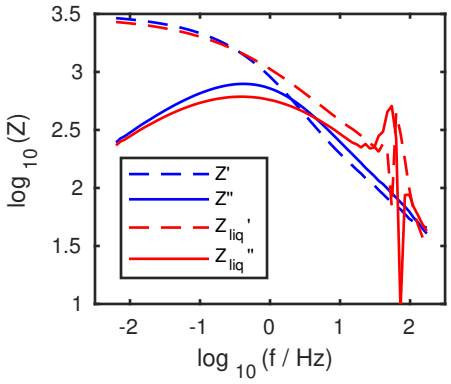

Figure 6.8: The thermal impedance of the system Z and the thermal impedance of the liquid Z_{liq} as a function of frequency at the temperature 266.3 K.

6.2.4 Specific heat

In order to find the specific heat, we first find the heat conductivity λ. λ is found using Z_{liq}. Rewriting Eq. (6.33)

$$\frac{1}{Z_{\text{liq}}} = Y_{\text{liq}} = \frac{1}{Z_{\text{liq},0}}(1 + \sqrt{i\omega r_1^2 c_l/\lambda}) \tag{6.39}$$

where $\frac{1}{Z_{\text{liq},0}} = 4\pi\lambda r_1$. If we know $Z_{\text{liq},0}$, we can find λ. When c_l is frequency-independent, the frequency term in Eq. (6.39) can be cancelled by taking the difference between the real and the imaginary part of the admittance Y'_{liq} and Y''_{liq}

$$\frac{1}{Z_{\text{liq},0}} = Y'_{\text{liq}} - Y''_{\text{liq}} \tag{6.40}$$

This is also valid in the relaxation range at low frequencies where c_l reaches its non-complex equilibrium value. Figure 6.9 (a) shows $Y'_{\text{liq}} - Y''_{\text{liq}}$ as a function of frequency for the measurements. The figure shows that the low-frequency limit is not reached for all the measurements. Figure 6.9 (b) shows the inverse of this low-frequency limit of $Y'_{\text{liq}} - Y''_{\text{liq}}$, which equals $Z_{\text{liq},0}$. Since the low-frequency limit is not reached for the measurements at temperatures with relaxation, an extrapolation of $Z_{\text{liq},0}$ from the high temperatures is used.

It is important to notice that $Z_{\text{liq},0}$ is also found as one of the fitting parameters. Figure 6.10 shows the used $Z_{\text{liq},0}$ together with the fitting parameter $Z_{\text{liq},0}$. As seen, these two $Z_{\text{liq},0}$'s differ. Appendix B.2 shows the results using the two different $Z_{\text{liq},0}$. The value of $Z_{\text{liq},0}$ especially affects the low-frequency part of the spectra, and the spectra with $Z_{\text{liq},0}$ found from the low-frequency limit of Z_{liq} seems to give a more correct result. In this investigation, as well as in former investigations using the same method and model [79, 80], $Z_{\text{liq},0}$ found from the low-frequency value is used.

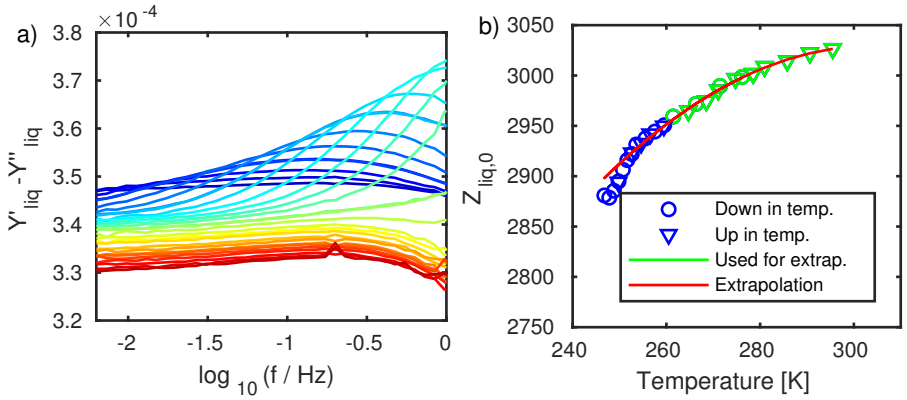

Figure 6.9: (a) $Y'_{\mathrm{liq}} - Y''_{\mathrm{liq}}$ as a function of frequency. $Z_{\mathrm{liq},0}$ is found as the low-frequency limit. However, for some of the curves, this low-frequency limit is outside the measured frequency range. The temperature span of the measurements are from 295.5 K (red) to 246.8 K (blue). (b) $Z_{\mathrm{liq},0}$ found from the low frequency limit of $Y'_{\mathrm{liq}} - Y''_{\mathrm{liq}}$ as a function of temperature and extrapolation.

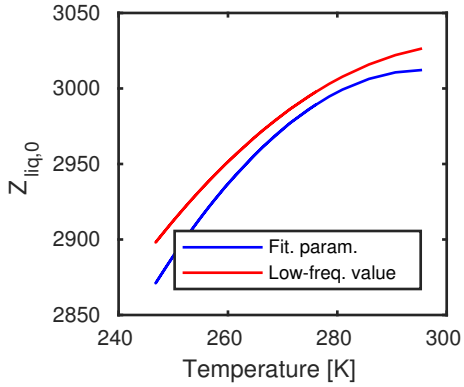

Figure 6.10: $Z_{\mathrm{liq},0}$ found using the low-frequency value of $Y'_{\mathrm{liq}} - Y''_{\mathrm{liq}}$ and $Z_{\mathrm{liq},0}$ found from the fitting parameters as functions of temperature.

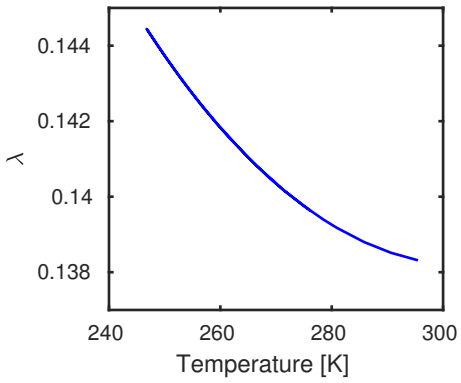

Figure 6.11: The heat conductivity λ of the liquid as a function of temperature.

The heat conductivity λ is now calculated as

$$\lambda = \frac{1}{4\pi r_1 Z_{\text{liq},0}} \tag{6.41}$$

and is showed as a function of temperature in Figure 6.11.

Using the value of λ, the specific heat c_l is calculated by rewriting Eq. (6.33)

$$c_l(\omega) = \frac{\lambda}{i\omega r_1^2}\left(\frac{Y_{\text{liq}}}{2\pi\lambda r_1} - 1\right)^2 \tag{6.42}$$

From the model of Z, only the value of the parameter $r = \frac{r_0}{r_1}$ is determined. The value of r_1 is chosen so that c_l (or more precisely, the DC specific heat c_0) gives the literature value at room temperature [80, 98]. This is only done for the datasets at atmospheric pressure. At higher pressures, the value of r_1 from atmospheric pressure is used.

Figure 6.12 shows the real part (c_l') and the imaginary part ($-c_l''$) of c_l for all measurements at atmospheric pressure. The low-frequency limit of c_l' determines the DC specific heat of the liquid [80], which is shown in Figure 6.13. In Figure 6.12, a "hump" appears in the high-temperature data of $-c_l''$. We believe that this hump might be a consequence of the thermistor not being perfectly round (but it may be due to other things). We make an attempt to subtract this hump from our data. Figure 6.14 (a) shows the high-temperature spectra, where the hump is found as the mean value of these spectra. Figure 6.14 (b) shows the data ($-c_l''$) with the hump subtracted. The spectra shown in the further analysis are the spectra with the hump subtracted, however, the hump is used to find an error-bar of the relaxation time found from the spectra. We define the relaxation time τ from the maximum frequency of loss peak as $\tau = \frac{1}{2\pi f_m}$. To find f_m, a second degree polynomial is fitted to the peak in $-c_l''$. This is done for the spectra both with and without the hump subtracted. For each temperature, the final value of f_m is determined as the mean value of

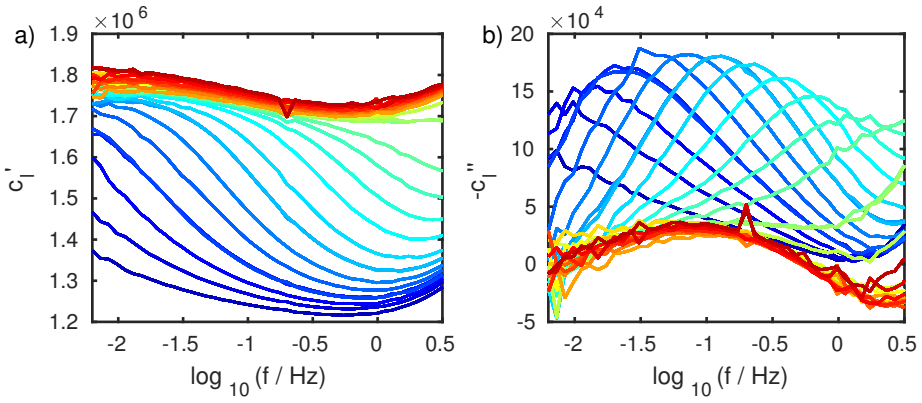

Figure 6.12: The real part (c_l') and the imaginary part ($-c_l''$) of the longitudinal specific heat as a function of frequency. The temperature span of the measurements are from 295.5 K (red) to 246.8 K (blue).

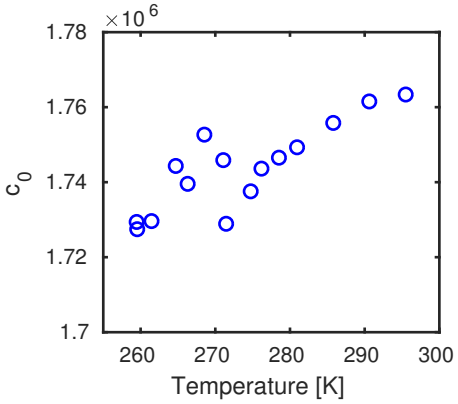

Figure 6.13: The DC specific heat c_0 as a function of temperature.

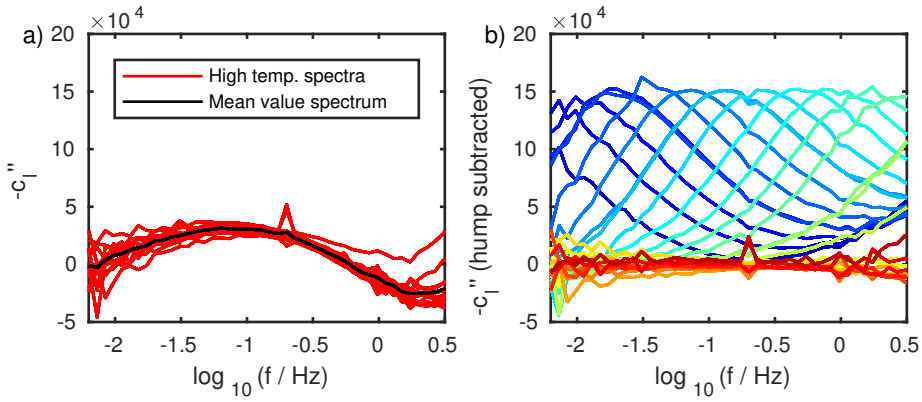

Figure 6.14: Correction for hump. (a) High-temperature data of the imaginary part of the specific heat used to find the hump. (b) The imaginary part of the specific heat with the hump subtracted. The temperature span of the measurements are from 295.5 K (red) to 246.8 K (blue).

the value of f_m from the spectrum with the hump and f_m from the spectrum with the hump subtracted. The two values of f_m are used to span an error-bar. Figure 6.15 shows f_m and τ as functions of temperature. Note that the error bar due to the hump is small.

The described initial analysis is made with all datasets, except the dataset at 300 MPa from the pressure setup, which is analyzed in Section 6.3. First, the effective temperature of the sample is found.

6.2.5 The effective temperature of the sample

Each measurement is done at a fixed temperature of the surrounding environment T_{cryo}, which is the temperature in the cryostat or the pressure vessel. However, the current through the thermistor results, besides the temperature oscillation, in an constant temperature rise T_0. The effective temperature at the thermistor is therefore $T_{\text{cryo}} + T_0$, however, the effective temperature of the sample (at the outer radius of the glass capsule) is lower since the temperature decays as a function of time. We make an attempt to estimate this effective temperature, which is inspired by the way it is done in Jakobsen *et al.* (2012) [79, 99]. Here, we utilize that the decay of the DC temperature T_0 is the same as the decay of the temperature oscillation T_2.

The measurements on the standard RUC cryostat are conducted with three different temperature amplitudes: 0.55 K, 0.75 K, and 0.95 K in order to determine how the temperature amplitude affects the temperature of the sample. The loss peak frequencies f_m are shown in Figure 6.16 as a function of the temperature at the cryostat. The correction of the temperature is found in the following way: f_m is plotted as a function of the temperature $T = T_{\text{cryo}} + a \cdot T_0$,

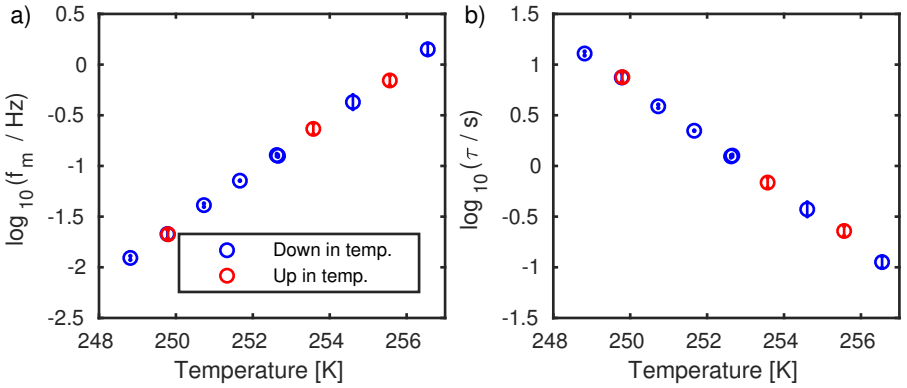

Figure 6.15: (a) The loss peak frequency f_m as a function of temperature. (b) The relaxation time τ as a function of temperature.

where T_{cryo} is the temperature of the surrounding environment, i.e., the cryostat, T_0 is the DC contribution to the temperature rise (which depends on temperature amplitude), and a is a constant between 0 and 1. The exact value of a is determined as the value which makes the values of f_m collapse into one curve. We conclude that $a = 0.5$ gives the best result, which is shown in Figure 6.16.

With the pressure equipment, measurements are taken with two temperature amplitudes at 0.1 MPa (0.96 K and 0.55 K), however, only a few measurements are taken with 0.55 K. Figure 6.17 shows the temperature correction analysis with the constant $a = 0.5$ for these datasets. We conclude that $a = 0.5$ is also a good choice for the pressure equipment. The temperatures mentioned in the following are the corrected temperatures $T = T_{\text{cryo}} + 0.5 \cdot T_0$.

6.2.6 Measurements from different equipments

The measurements from the pressure setup and the standard RUC setup are compared in Figure 6.18, where the loss peak frequencies are plotted as a function of temperature for the dataset at atmospheric pressure with temperature amplitude 0.96 K from the pressure setup, and the dataset with temperature amplitude 0.95 K from the standard RUC cryostat. The figure also includes data on 5PPE from Jakobsen *et al.* (2012) [79, 100]. The temperature dependence of the loss peak frequencies seems to be the same for all datasets. There is a temperature shift, which is probably due to the temperature calibration of the different equipment.

The results for the datasets from the pressure equipment are shown in Section 6.4. First, the analysis of the measurements along the 300 MPa isobar is shown.

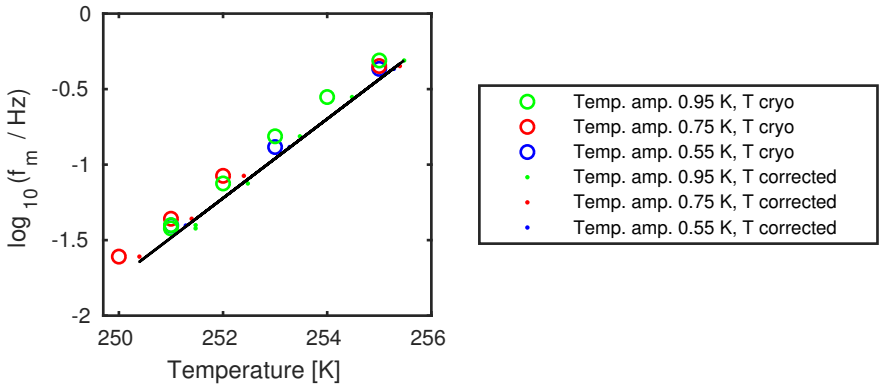

Figure 6.16: The loss peak frequencies f_m as a function of temperature from the standard RUC cryostat. The black line is a linear fit of f_m as a function of the corrected temperature.

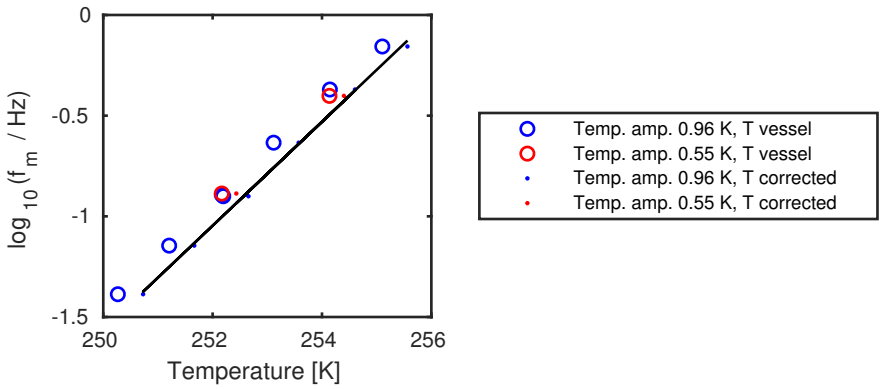

Figure 6.17: The loss peak frequencies f_m as a function of temperature from the pressure setup. The black line is a linear fit of f_m as a function of the corrected temperature.

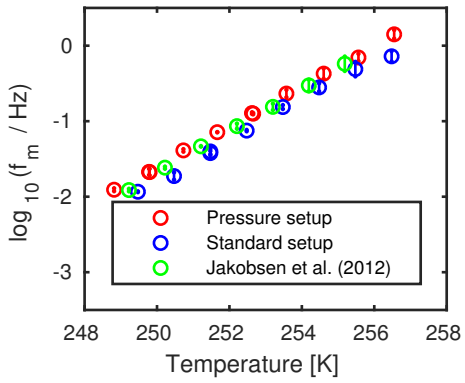

Figure 6.18: The loss peak frequencies from the two different setups at atmospheric pressure. The figure also includes data from Jakobsen *et al.* (2012) [79, 100].

6.3 Data analysis 300 MPa

All datasets except the dataset at 300 MPa are treated as described in the above Section 6.2. The reason that the data analysis of the dataset at 300 MPa can not be done in this way is that the measurements are not made at temperatures high enough above the temperatures with relaxation, due to the temperature range of the setup. This can be realized by looking at the fitting parameters from the datasets at 0.1 MPa, 150 MPa, and 300 MPa together in Figure 6.19. The data analysis of this dataset is done with two different approaches: an attempt to estimate the extrapolations from the extrapolations of fitting values at 0.1 MPa and 150 MPa, and an extended fit of the thermal impedance, which includes the frequency-dependent specific heat. The two approaches are described in the next sections.

6.3.1 Extrapolations estimated from 0.1 MPa and 150 MPa

To investigate whether the extrapolations from the datasets at 0.1 MPa and 150 MPa can be used to estimate the parameters for 300 MPa, a test is first conducted where the extrapolations of parameters at 0.1 MPa are used to determine the parameters for the dataset at 150 MPa.

As seen in Figure 6.19 (a) and (b) the parameters τ_l and τ_b seem to have almost the same temperature dependence and thereby slope for 0.1 MPa and 150 MPa. The slope of the parameter c (Figure 6.19 (c)) also seems to be similar for the two pressures. For τ_l and τ_b, a fit is made to the parameters at high temperatures from 150 MPa with the slope fixed to the slope found from 0.1 MPa. We tried the same method for the parameter c, but this does not

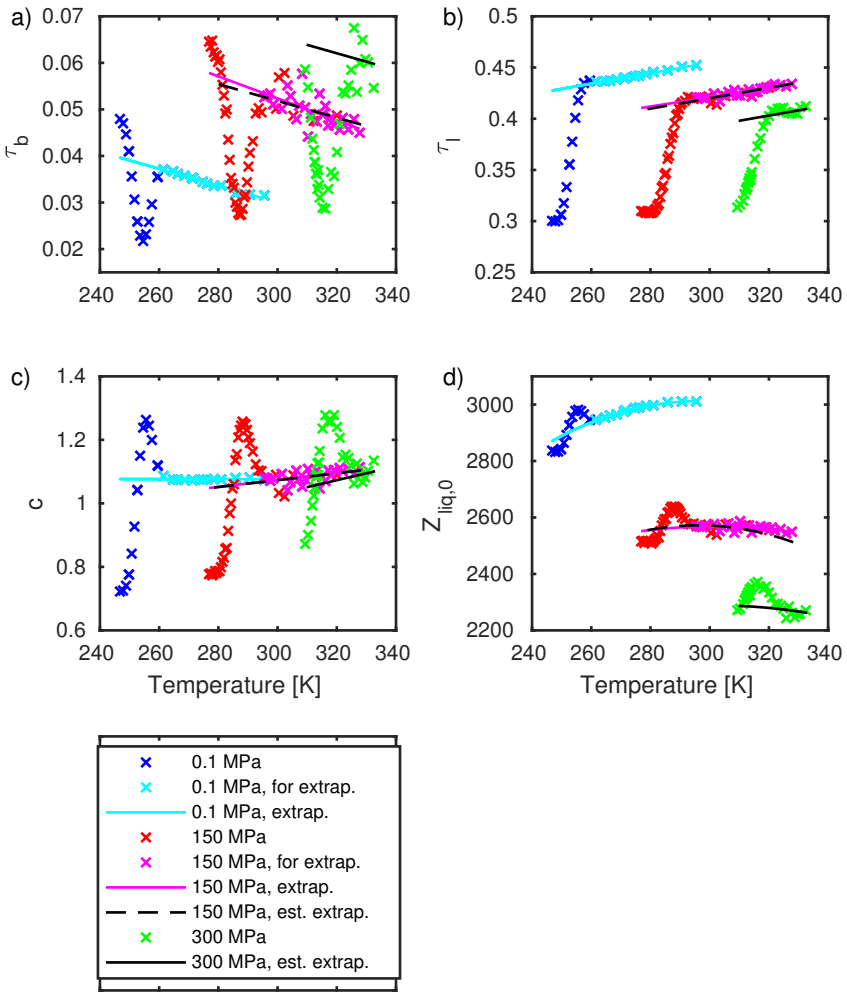

Figure 6.19: The fitting parameters for the three datasets from the pressure setup. It is clear that measurements are not made at high enough temperatures for the 300 MPa dataset to make extrapolations. Furthermore, the estimated extrapolations for 150 MPa and 300 MPa are shown.

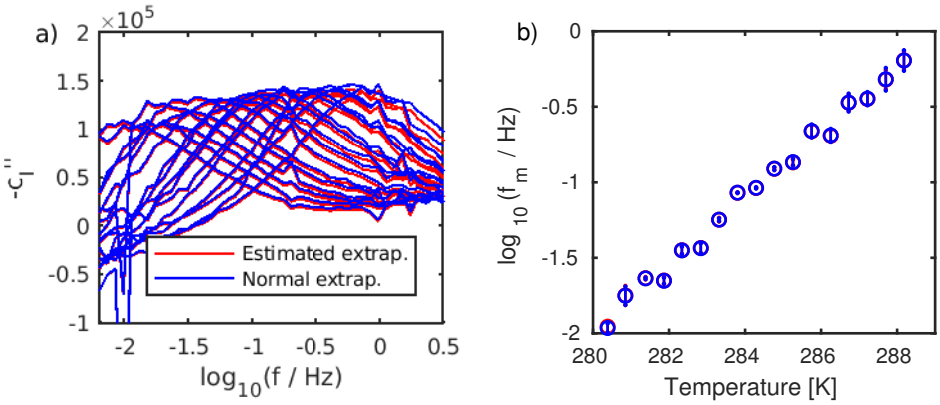

Figure 6.20: The result of the data analysis of the dataset of 150 MPa in the normal way and by estimating the extrapolations from the extrapolations from 0.1 MPa. (a) The imaginary part of the specific heat as a function of frequency for the temperatures with relaxation. (b) The loss peak frequency as a function of temperature.

give a correct result. We therefore use the "original" extrapolation of c from 150 MPa. For $Z_{\mathrm{liq},0}$ (Figure 6.19 (d)) the polynomial from 0.1 MPa is shifted in the vertical direction to match the fitting values for 150 MPa. These new extrapolations are seen in Figure 6.19 as the black dashed lines.

The result of the 150 MPa data using the extrapolations estimated from the 0.1 MPa data is shown in Figure 6.20, together with the result using the extrapolations determined from the 150 MPa parameters. The figure shows that the spectra from the two data treatments only deviates a bit, and that the loss peak frequencies are almost identical. This shows that it should be possible to determine the extrapolations for 300 MPa from the extrapolations at 0.1 MPa and 150 MPa. In Figure 6.20 (b), it is also worth noticing that the loss peak frequencies are not a perfect monetonic function of temperature, which they should be. This is due to the stability of the pressure (see Section 4.1).

Extrapolations are now found for the dataset at 300 MPa. For the parameters τ_l and τ_b, fits are made to the parameters from the highest temperatures at 300 MPa, with the slope fixed to the slope from 0.1 MPa. For $Z_{\mathrm{liq},0}$ the polynomial from 150 MPa is shifted in the vertical direction to match the fitting values for 300 MPa. For the parameter c, we assume that the slope has a linear pressure dependence. The estimated extrapolations are seen in Figure 6.19 as the black lines. The results from this data treatment are seen in Figure 6.21 and Figure 6.22.

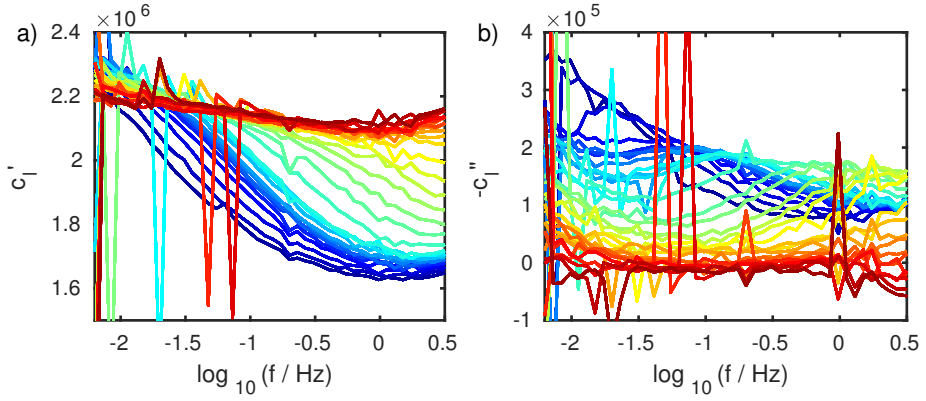

Figure 6.21: The real and the imaginary part of the specific heat at 300 MPa. These spectra are found using the extrapolations from 0.1 MPa and 150 MPa. The temperature span of the measurements are from 332.5 K (red) to 309.3 K (blue). It is clear that there is more noise in these spectra than the spectra at 0.1 MPa, which is due to the stability of the pressure.

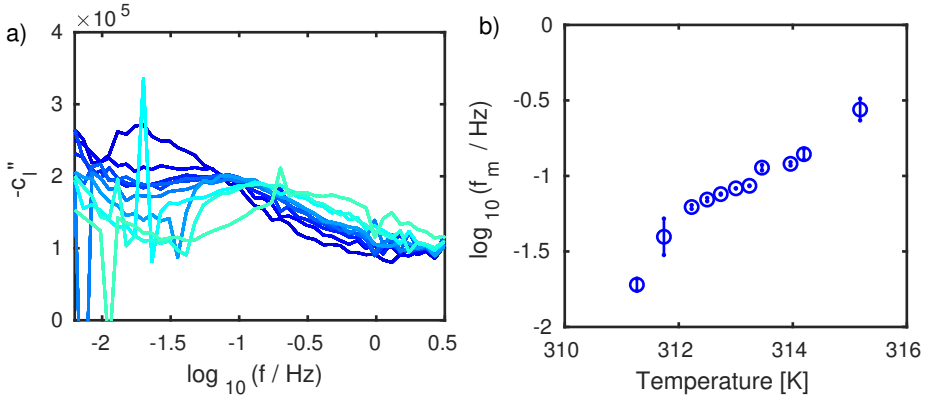

Figure 6.22: Data from 300 MPa. (a) The imaginary part of the specific heat at temperatures with relaxation. (b) The loss peak frequencies (f_m) as a function of temperature.

6.3.2 Including frequency-dependent specific heat in the fit

As another attempt to find the specific heat at 300 MPa, we extend the fit of the model of the thermal impedance of the liquid (Z_{liq}) used in Section 6.2.3. In the former data analysis, we use a frequency-independent specific heat in the fit of Z, and it, therefore, does not give correct results in the part of the temperature range where the specific heat depends on frequency. We therefore extend the fit to include a frequency-dependent specific heat.

A Cole-Davison model [78] is used to describe the frequency-dependence of the specific heat

$$c_{\text{model}} = c_\infty + \frac{c_0 - c_\infty}{(1 + i\omega\tau_c)^\beta} \Leftrightarrow \tag{6.43}$$

$$c_{\text{model}} = c_0 \cdot \left((1 - \tilde{c}) + \frac{\tilde{c}}{(1 + i\omega\tau_c)^\beta} \right) \tag{6.44}$$

where

$$\tilde{c} = 1 - \frac{c_\infty}{c_0} \tag{6.45}$$

c_0 is the low-frequency limit of c_l' and c_∞ is the high-frequency limit of c_l. At high temperatures where no relaxation occurs $c_0 = c_l$. In the model of Z_{liq}

$$Z_{\text{liq}} = Z_{\text{liq},0} \cdot \frac{1}{1 + \sqrt{i\omega\tau_l}} \tag{6.46}$$

c_l already occurs in $\tau_l = r_1^2 \frac{c_l}{\lambda}$. We therefore use a normalized version of c_{model}

$$c_{\text{model,normalized}} = \frac{c_{\text{model}}}{c_0} = (1 - \tilde{c}) + \frac{\tilde{c}}{(1 + i\omega\tau_c)^\beta} \tag{6.47}$$

which means that the model fitted to the thermal impedance of the liquid (Z_{liq}) is

$$Z_{\text{liq}} = Z_{\text{liq},0} \cdot \frac{1}{1 + \sqrt{i\omega\tau_l \cdot c_{\text{model,normalized}}}} \tag{6.48}$$

By implementing the frequency-dependent specific heat in the fit, three extra parameters are now present: $\tilde{c}$, τ_c and β. However, we chose to fix the shape parameter β and the model therefore ends up with seven independent parameters namely r, c, τ_b, τ_l, $Z_{\text{liq},0}$, $\tilde{c}$ and τ_c.

The model of the thermal impedance including the frequency-dependent c_l is fitted to Z at temperatures with relaxation. The five initial parameters r, c, τ_b, τ_l, and $Z_{\text{liq},0}$ are then used to calculate Z_{liq} using the model for Z_{liq} (Eq. (6.33)).

To investigate whether this new fit gives reliable results, a test is first done with the dataset at 0.1 MPa. First, the value for the parameter β is chosen. This is done in two ways: β is found by fitting c_{model} to a nice spectrum with peak in the middle of the available frequency range (gives $\beta = 0.52$), and β is

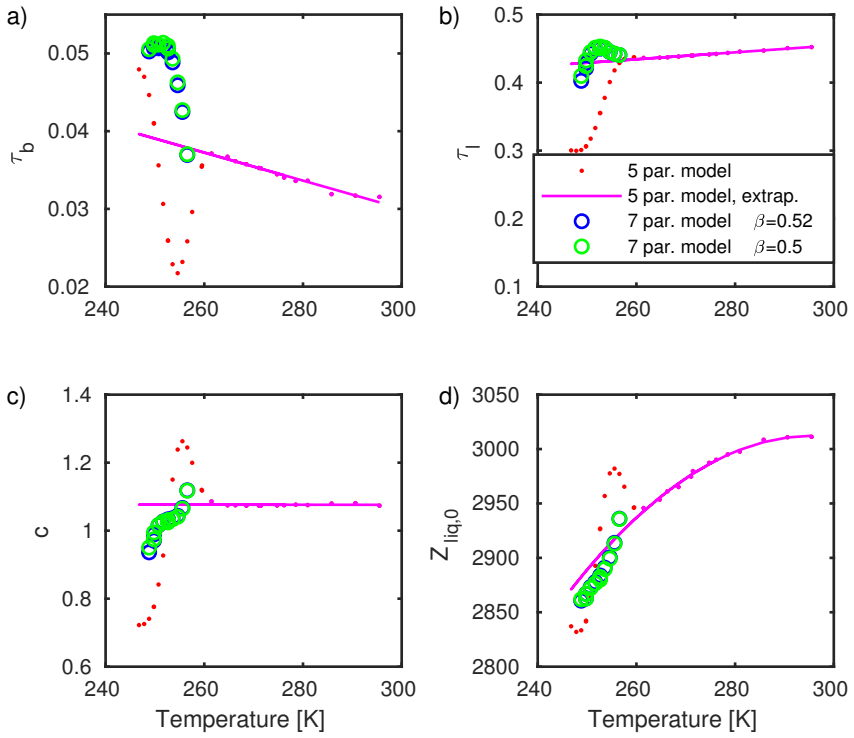

Figure 6.23: The fitting parameters of the dataset at 0.1 MPa from the pressure setup. The fitting parameters from the five-parameter fit, the extrapolation, and the fitting parameters using the seven-parameter fit with respectively $\beta = 0.52$ and $\beta = 0.5$ are shown. It is clear that the two models do not give the same values.

chosen to be 0.5 (following the results of Ref. [69]). The seven-parameter model is then fitted to Z in the temperature range with relaxation. The parameters found using the seven-parameter fit are compared to the values found using the five-parameter fit in Figure 6.23. It is clear that the fitting parameters from the two different approaches are not the same. The results using respectively the five-parameter fit and the seven-parameter fit (with respectively $\beta = 0.52$ and $\beta = 0.5$) are shown in Figure 6.24. It is seen that the loss peak frequencies differ a bit, but we conclude that it is resonable to use the seven-parameter model.

The seven-parameter fit is now used on the dataset at 300 MPa. β is found in three ways: β is found by fitting c_{model} to a nice spectrum with peak in the middle of the available frequency range using the spectra found using the extrapolations from 0.1 MPa and 150 MPa (gives $\beta = 0.32$), β is found by fitting c_{model} to a nice spectrum with peak in the middle of the available

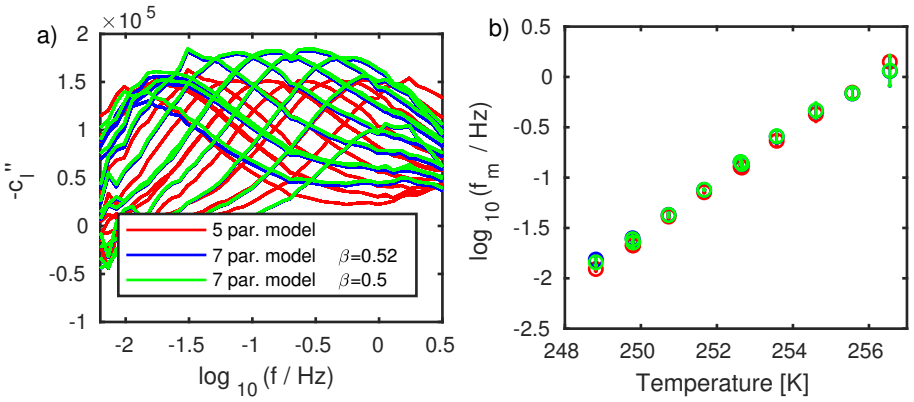

Figure 6.24: The result of the data analysis of the dataset at 0.1 MPa using respectively the five-parameter model and the seven-parameter model with respectively $\beta = 0.52$ and $\beta = 0.5$. (a) The imaginary part of the specific heat as a function of frequency for the temperatures with relaxation. (b) The loss peak frequencies as a function of temperature.

frequency range using spectra found using the actual fitting parameters from the five-parameter fit (gives $\beta = 0.79$), and β is chosen to be 0.5. The fitting parameters are shown in Appendix B.3. Figure 6.25 show the results using the seven-parameter fit.

The final loss peak frequencies at 300 MPa are chosen as the mean value of the loss peak frequencies determined in the different ways. The error bars are chosen as respectively the lowest and the highest found loss peak frequencies.

6.4 Results

Figure 6.26 shows the results of the frequency-dependent specific heat at high pressures. Examples of the imaginary part of the frequency-dependent specific heat ($-c_l''$) at 0.1 MPa and 150 MPa are shown in Figure 6.26 (a). The spectra at 300 MPa are not shown, since there are four different spectra and they contain noise. The relaxation time identified from the loss peak frequencies for all measurements along the three isobars are shown as a function of temperature in Figure 6.26 (b). There is approximately a 0.1 decade uncertainty due to the limited pressure stability of the pressure setup on 3 MPa (see Section 4.1).

The results are compared to dielectric measurements taken in relation to the isochronal superposition investigation (Chapter 5) and thereby in the same setup and under the same conditions. Figure 6.27 shows the relaxation time as a function of temperature for the specific heat measurements and for the dielectric measurements. The dielectric measurements are performed along the isobars 0.1 MPa, 100 MPa, 200 MPa, 300 MPa, and 400 MPa. The fact that

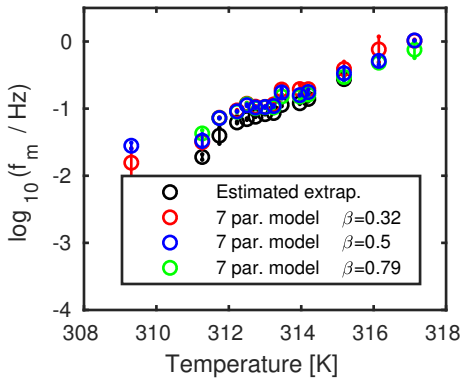

Figure 6.25: The loss peak frequencies as a function of temperature of the dataset at 300 MPa using the seven-parameter model with respectively $\beta = 0.32$, $\beta = 0.5$, and $\beta = 0.79$ together with the results using the extrapolations estimated from 0.1 MPa and 150 MPa.

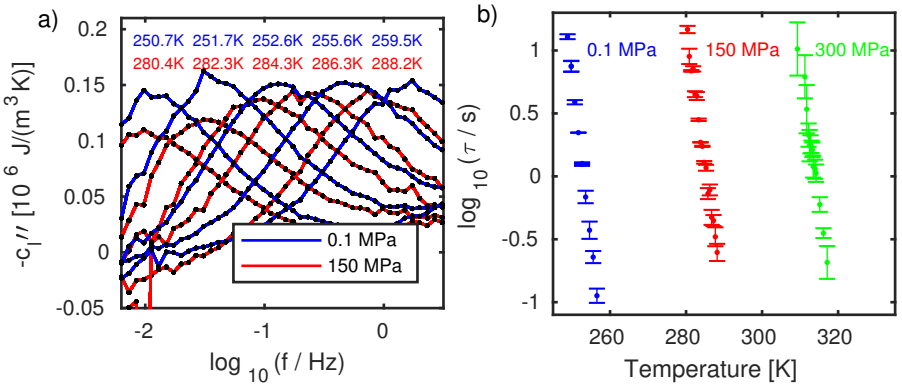

Figure 6.26: Specific heat data. (a) The imaginary part of the longitudinal specific heat at the indicated temperatures and pressures. (b) The relaxation time τ, based on the loss-peak frequency, as a function of temperature for all studied temperatures and pressures.

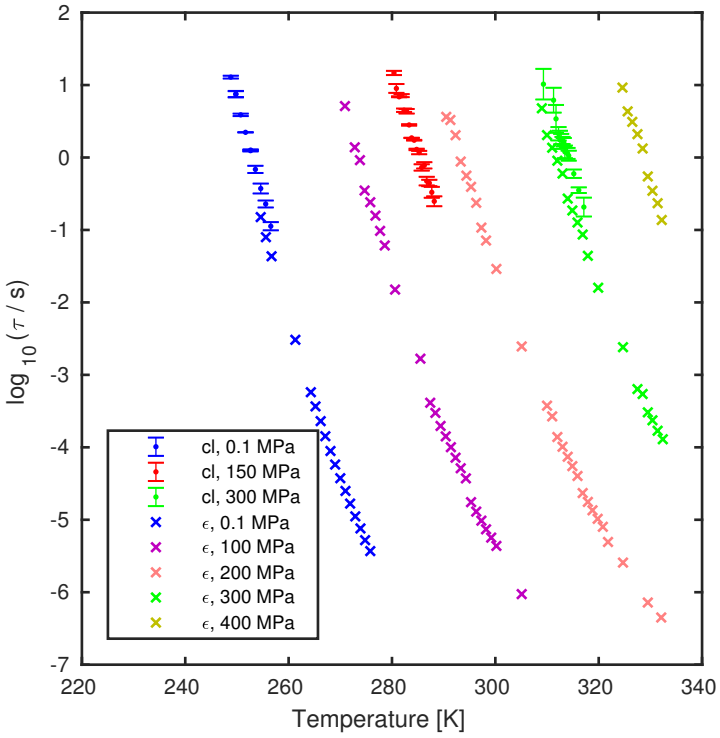

Figure 6.27: Comparison of the relaxation times τ for the specific heat measurements (same data as on Figure 6.26 (b)) and the dielectric measurements at the indicated pressures.

these measurements are taken under the same thermal and pressure conditions gives a unique possibility for directly comparing the temperature and pressure dependence of the time scale from dielectric and specific heat measurements over a rather wide pressure range. It is seen that the temperature dependence of the relaxation time closely follow each other at all investigated pressures. It is also seen that the dielectric relaxation time is faster than the specific heat relaxation time at all pressures, which was also shown for ambient pressure in Jakobsen *et al.* (2012) [79].

Figure 6.28 shows the same data using isochrones, i.e. the lines in the phase diagram with the same relaxation time. The isochrones are illustrated for both methods and it is seen that the isochrones from the two response functions are parallel.

The main result on our specific heat measurements is, together with a similar investigation at atmospheric pressure (Ref. [79]), that the relation between the relaxation times found from the dielectric measurements and the specific heat τ_ϵ/τ_{c_l} is constant within error bars for all investigated temperatures and

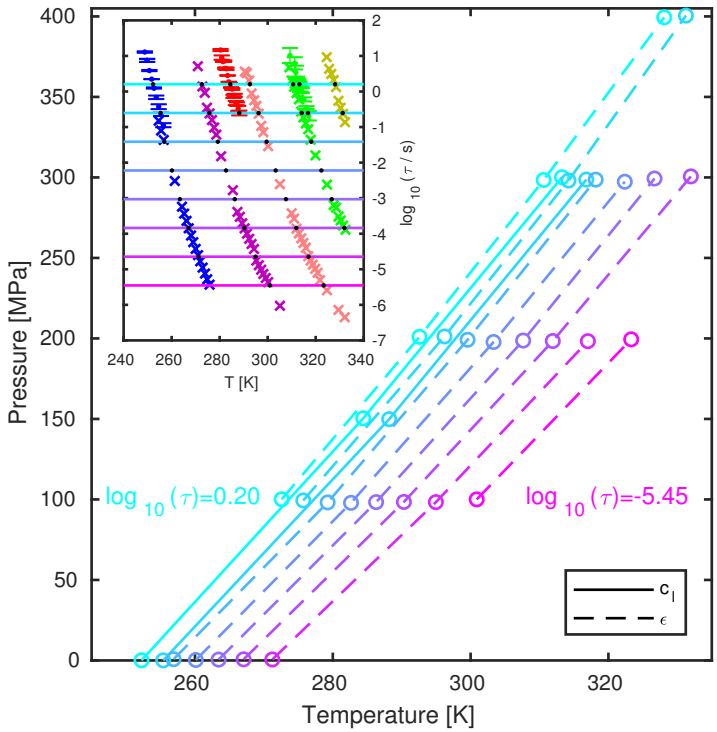

Figure 6.28: Isochrones for specific heat (full lines) and dielectric (dashed lines). The two slowest isochrones are found for both the specific heat and dielectric, but the six fastest isochrones are only found for the dielectric measurements. The inset show the same data as Figure 6.27 where the vertical lines illustrate eight chosen relaxation times. The temperatures used for the isochrones are found by interpolation (indicated by small solid points in the insert).

pressures for the investigated liquid. Combining the data from our study and the study at atmospheric pressure (Ref. [79]) gives $\log_{10}(\tau_\epsilon/\tau_{c_l}) = -0.4 \pm 0.1$ with the major contribution of the uncertainty coming from the pressure instabilities.

The parallel isochrones imply that an isochrone for one response function is also a isochrone for the other response function, however, with different relaxation times associated, since the dielectric relaxation time is faster than the specific heat relaxation time. Furthermore, it is seen here that the separation of the time scales seems to be constant within the investigated part of the phase diagram.

6.5 Concluding remarks

We have adapted our specific heat measuring method to a high-pressure setup and performed specific heat spectroscopy measurements over an unprecedented pressure range. The measurements are analysed using a fit to the five-parameter model from Ref. [80] with few adjustments. Furthermore, we implement a frequency-dependent specific heat in the fit to the model leading to a seven-parameter model. This model seems to give reliable results and is used to find the specific heat along the 300 MPa isobar.

We compared our data to dielectric data obtained in relation to the isochronal superposition investigation (Chapter 5) in the same pressure setup and thereby under identical pressure/thermal conditions. We conclude that the characteristic time scale of the specific heat and the dielectric relaxation follow each other closely as function of temperature at all investigated pressures, and that isochrones for the two response functions coincide with the dielectric relaxation being the fastest. These findings are discussed in relation to the isomorph theory in Chapter 9.

Chapter 7

Single-parameter aging

This investigation studies aging following temperature jumps for three supercooled liquids close to the glass transition. During these temperature jumps, the liquids are brought out of equilibrium, and the study of aging is a study of how the properties of a system changes over time as it equilibrates towards equilibrium, as introduced in Section 3.3.

The analysis of our data is based on the Tool-Narayanaswamy (TN) aging formalism, which we introduced in Section 3.3.1. The TN-formalism interprets aging in terms of a material time ξ. The material time may be thought of as a time measured on a clock with a clock rate that changes with time as the liquid ages. The material time is defined from the clock rate $\gamma(t)$ by [50, 55, 101]

$$d\xi = \gamma(t)dt \tag{7.1}$$

Inspired by Tool, Narayanaswamy introduced a single-parameter aging assumption in terms of a fictive temperature. The central hypothesis of single-parameter aging is that the clock-rate out of equilibrium, $\gamma(t)$, depends only on one structural parameter, and that this parameter also controls the measured quantity. Hecksher *et al.* (2015) [28] derived two tests of the single-parameter assumption, which we use for our analysis. These tests have the advantage that one does not need to calculate the material time explicitly in order to test for single-parameter aging. Furthermore, if a liquid has single parameter aging, one of the single-parameter aging tests can be used to predict relaxation curves. During the present investigation, these tests are generalized to work also for jumps ending at different temperatures.

The aim of the present investigation was to test the different liquids for single-parameter aging, using the generalized tests of single-parameter aging. The liquids used in the former investigation, Hecksher *et al.* (2015) [28], are all van der Waals liquids, which are all shown to have single-parameter aging to a good approximation. In the present investigation, we also study whether two hydrogen-bonded liquids have single-parameter aging. The difference between van der Waals-bonded liquids and hydrogen-bonded liquids is of interest in

relation to the isomorph theory [25, 27], which predicts that van der Waals liquids have simple behavior along isochrones, whereas no predictions are given for hydrogen-bonded liquids. The isomorph theory inspired our hypothesis that van der Waals liquids have simpler behavior than hydrogen-bonded liquids also in aging.

Furthermore, we performed larger jumps than in the previous investigation to test if single-parameter aging break down with larger jumps. This chapter is written simultaneously with the paper about aging (Paper 3). Some sections will therefore be similar.

Section 7.1 introduces aging experiments, including the importance of times and temperatures in such an experiment. Section 7.2 gives the experimental details of the experiment, including a description of the sample cell with temperature regulation and the measuring protocol. Section 7.3 shows the dielectric equilibrium spectra, where an attempt to find the clock rate is made. The aging measurements are presented in Section 7.4, where the initial data treatment of the measurements are performed. The single-parameter aging tests derived in Hecksher *et al.* (2015) [28] are generalized in Section 7.5, and the results are shown in Section 7.6. Section 7.7 reflects on the aging investigation and discusses the generalized single-parameter tests.

7.1 Study of aging

The study of aging is a study of how the properties of a system, e.g. a supercooled liquid, changes over time as it relaxes towards equilibrium [50]. The aging considered here is purely physical aging, i.e. the change is only related to physical changes of the system. In relation to supercooled liquids, aging is indeed interesting, because the viscous liquid relaxes towards equilibrium when a perturbation is applied. The temperature of the liquid when a large perturbation is applied is important in relation to aging experiments. For temperatures above T_g, the liquid will equilibrate fast, and there is no time to measure how the liquid equilibrates (which, of course, depends on the time it takes to take a measurement). On the other hand, if the temperature is too far below T_g the liquid will equilibrate so slowly that changes are not observable on laboratory time scales, or the liquid will not fully reach equilibrium in the experimental timescale (this depends, of course, of the time scale of the experiment). Due to the strong temperature dependence of the relaxation time, this can easily be impossible. The ideal temperature of the supercooled liquid in relation to aging experiments is below, but close to, the glass transition temperature.

In typical aging experiments on supercooled liquids, the perturbation is often applied by a temperature jump, i.e. a step up or down in temperature. We aim for this step in temperature to be instantaneous following the tradition for aging investigations at Roskilde University (e.g. Refs. [28, 51, 52]). However, since an instantaneous temperature change is not physically achievable, we aim for the new temperature to be reached, and be constant and homogeneous throughout

the sample before any structural changes take place in the sample, i.e. the structural relaxation time of the liquid should be much larger than the time it takes to change the temperature. Furthermore, a good temperature control is needed to keep the temperature stable before and after the jump. Note that aging can be studied in other ways, for example, by cooling the sample with a constant, fast cooling rate from a temperature (high) above T_g to a temperature just below T_g e.g. in Refs. [102, 103].

Following a jump on temperature, the relaxation towards equilibrium is monitored by measuring a physical quantity as a function of time. The requirements for this physical quantity are that it should be measured accurately, and that it should be fast to measure so that no structural relaxation takes place in the liquid during the time it takes to take a measurement. Furthermore, the quantity should be strongly temperature dependent, so that even small temperature changes are easy to measure. The dielectrics of the liquid satisfy these requirements, and have been used for aging measurements before by, e.g. Schlosser and Schönhals [104], Loidl and Lunkenheimer *et al.* [102, 105–107], Richert *et al.* [103], Alegría *et al.* [108–110], and Cangialosi *et al.* [111]. In this investigation, the dielectric loss at a fixed frequency is used. This fixed frequency is chosen to be on the right flank of the α-peak above any visual contributions from possible β-processes, such as excess wings.

As introduced in Section 3.3, aging is non-linear, even for small temperature steps. This is due to the fact that the structure of the system changes as it approaches equilibrium, and the aging rate is structure dependent [50]. For a jump down in temperature, the structural relaxation becomes slower as time evolves, whereas for a jump up in temperature, the structural relaxation becomes faster as time evolves.

7.2 Experimental details

The two hydrogen-bonded liquids, 1,2,6-hexanetriol (1,2,6-HT) and glycerol, together with the van der Waals-bonded liquid diethyl phthalate (DEP), were used for this investigation. 1,2,6-HT and DEP were both achieved from Sigma-Aldrich and were placed in an excicator for two hours before use. Glycerol was achieved from Fluka and was placed in an excicator for 20 hours before use. Details on the liquids are given in Section 4.3.

7.2.1 Sample cell – microregulator

In order to change the temperature fast, we use a specially-designed microregulator as sample cell [28, 47, 51, 52] illustrated in Figure 7.1. The microregulator consists of a parallel-plate capacitor placed in top of a peltier element, which is used to control the temperature. A NTC-thermistor is placed in the lowest capacitor plate, which is used to monitor the temperature. The microregulator is placed in a main cryostat (a standard RUC cryostat [56]). When performing

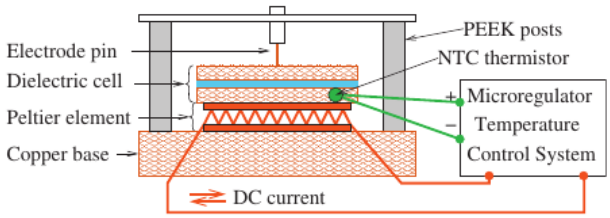

Figure 7.1: Illustration of the microregulator. Figure from Hecksher *et al.* (2010) [52].

the aging measurements, the temperature of the cryostat is kept constant, while the microregulator is used to keep the temperature stable and make jumps around the temperature of the cryostat. By using the microregulator, the temperature fluctuations are kept below 100 μK and the characteristic thermal equilibrium time is 2 s. More details are given in Ref. [52]. The capacitor consists of two copper plates with a diameter of 10 mm (1 mm thick) separated by four kapton spacers. The spacers are 0.5 mm x 0.5 mm and have a height of 0.05 mm. This gives an empty capacitance on 14 pF. The electrical equipment used for measuring the capacitance is described in Section 4.2.

Before use, the microregulator with sample cell is placed in ethanol for one hour, and afterwards it is dried in the cryostat for 20 hours. To fill the capacitor, a drop of the liquid is placed at the gap between the two capacitor plates and the liquid then flows into the capacitor.

The hydrogen-bonded liquids especially can absorb water, and for all liquids, the cryostat is therefore heated to 300 K beforehand to evaporate any possible water in the cryostat. Just before the sample cell is placed in the cryostat, the cryostat is flushed with liquid nitrogen, and the temperature is set between 245-265 K (which is below the melting temperature of water). The microregulator with sample liquid is then placed in the cryostat, while the temperature stabilizes. It is ensured that the liquids do not take in water during the measurements, since reproducibility is ensured.

7.2.2 Measuring protocol

The temperature is first lowered to the temperature where we want to make temperature jumps around, which is just below the glass transition temperature. In practice, dielectric equilibrium spectra are obtained at different temperatures while lowering the temperature to find the right starting temperature. The starting temperature for this experiment is a couple of degrees below the glass transition temperature.

When the starting temperature is reached, the microregulator is turned on to keep the temperature stable. The sample then anneals until no change of the dielectric properties is seen, which can result in several weeks of waiting

time. When the liquid is in equilibrium, the jumps are performed. After each jump, it is ensured that the liquid is in equilibrium before performing the next jump (however, the starting temperature for DEP was too low, and equilibrium is therefore not reached for several jumps). The typically measuring protocol is a down jump, an up jump, an up jump, and down jump. The size of the temperature jumps vary from 2 K to 8 K. For most measurements, we can assume that no structural changes take place in the liquids during the temperature jump, however, for measurements starting at the highest temperatures where the relaxation time is 150-250 s (depending on liquid), some structural relaxation may occur during the measurements.

During the jumps, the relaxation is monitored by the dielectric loss at a fixed frequency as a function of time. The measuring time is 3-20 s for each point, depending on the fixed frequency (different frequencies are used for the different liquids). This means that we can assume that no structural changes take place in the liquids during the measurements, however, for measurements starting at the highest temperatures, some structural relaxation may occur during the first measuring points.

7.3 Dielectric spectra results – estimation of γ_{eq}

The purpose of the equilibrium spectra is partly to find the right temperatures at which to perform the aging measurements. The liquid has to be below the glass transition, and we use that the relaxation time must be above 100 s, which roughly corresponds to $\log_{10}(f_m) < -3$, where f_m is the frequency at the maximum of the α-peak. Furthermore, the measurements are used to estimate the frequency at the maximum f_m at the temperatures where the peak is outside the available frequency range (which is the temperatures where the aging measurements are performed). Actually, it is the equilibrium dielectric clock rate γ_{eq} that we want to estimate, which is defined as the inverse of the dielectric relaxation time τ defined from f_m as

$$\gamma_{\text{eq}} = \frac{1}{\tau} = 2\pi f_m \tag{7.2}$$

Remember that the material time for the TN-formalism is defined from the clock rate γ, which is actually the structural clock rate. By using the dielectric clock rate, we assume an internal clock exists, meaning that the two clock rates are proportional [52, 79].

Equilibrium dielectric spectra for the three liquids are shown in Figure 7.2. For DEP, it is seen that the sample begins to crystallize at high temperatures (the height of the α-peak decreases drastic), however, these spectra are taken during reheating of the sample after the aging measurements, and it has no effect on the aging data.

In order to estimate the clock rate γ_{eq} for temperatures where the α-peak is outside the measurable frequency range, it is first investigated whether the

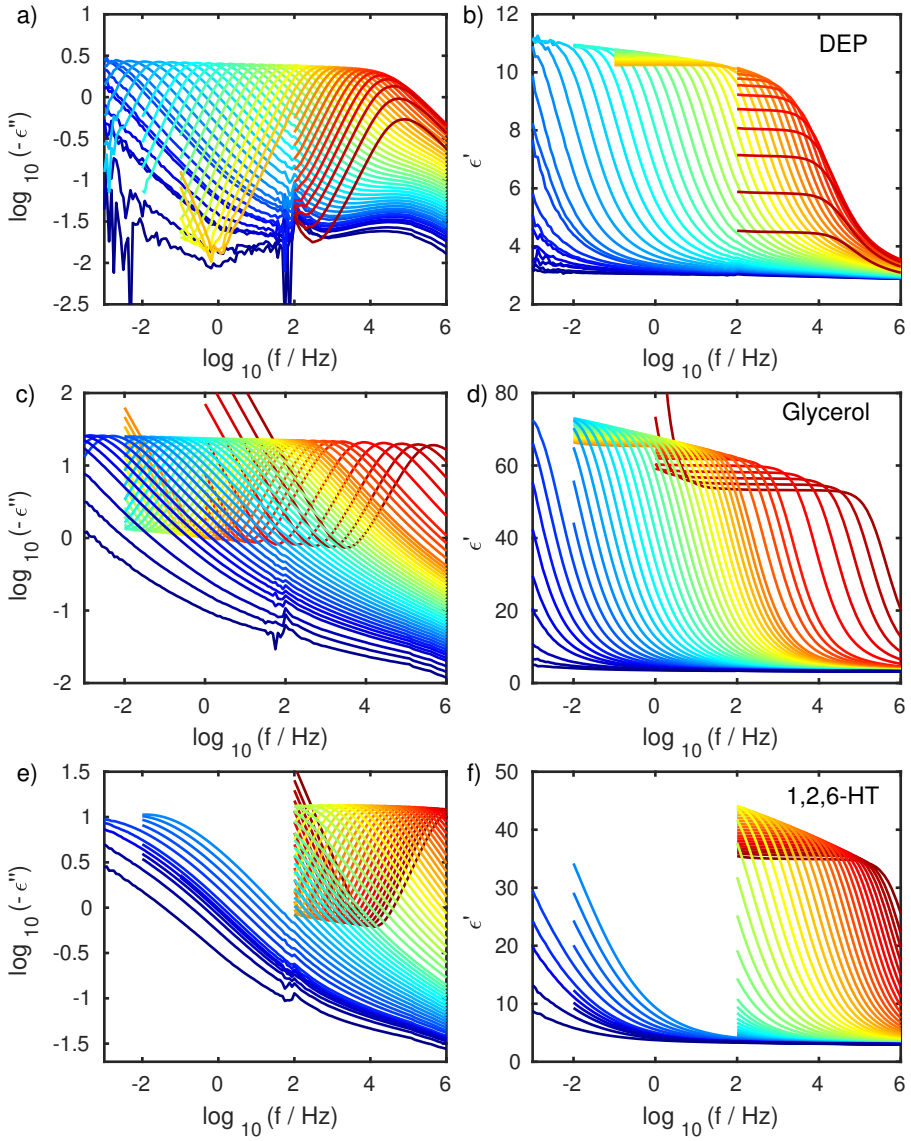

Figure 7.2: Dielectric equilibrium spectra for the three used liquids. Left: The imaginary part. Right: The real part. The temperature span for DEP is 215 K to 174.2 K. The temperature span for glycerol is 245 K to 176.2 K. The temperature span for 1,2,6-HT is 265 K to 188.8 K.

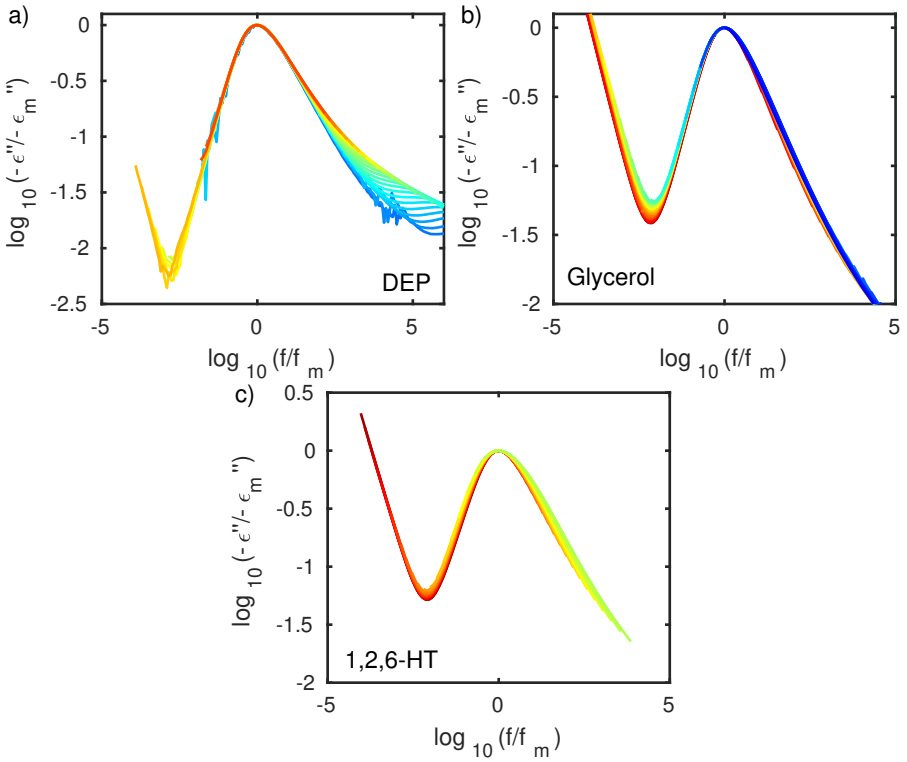

Figure 7.3: Investigation of time temperature superposition (TTS) for the liquids. (a) DEP. (b) Glycerol. (c) 1,2,6-HT.

liquids obey time temperature superposition (TTS), which is the case if the imaginary part of the spectra has the same shape at all temperatures. The loss peak frequency f_m is found by fitting a second degree polynomial to the peak. Figure 7.3 shows the spectra superimposed to investigate TTS. It is seen that the liquids do not obey TTS.

In order to find γ_{eq}, we use several methods: a shift-factor method described below, and extrapolations of four fitting functions. The below investigation of estimations of γ_{eq} is shown for glycerol. The shift-factor method requires that the liquid obeys TTS, however, only for a limited temperature range. First, the shift-factor is found in the following way: A main spectrum is chosen, which has to be a spectrum where the α-peak is visible. The spectra from the lower temperatures are shifted to the right until they are on top of the chosen main spectrum. This is done by hand. It gives a shift-factor $a(T)$ depending on temperature. The spectra and the shifted spectra are seen in Figure 7.4. Assuming that the horizontal shift of the right flank of the spectrum equals the

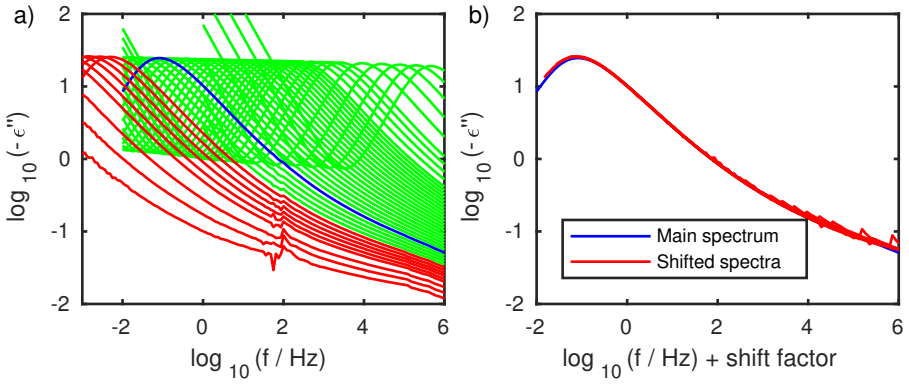

Figure 7.4: Shift-factor method for glycerol. (a) The equilibrium spectra. The blue spectrum is the "main" spectrum. The red spectra are "shifted" to the right to place them in top of the main spectrum. (b) The shifted spectra.

horizontal shift of the maximum frequency of the α-peak, we have

$$\log_{10}(f_m(T)) = \log_{10}(f_{m,\text{main}}) + a(T) \tag{7.3}$$

where $f_{m,\text{main}}$ is the frequency of the loss peak of the main spectrum. The estimations of γ_{eq} at temperatures where the aging measurements are performed are shown together with γ_{eq} for temperatures where the α-peak is visible in the dielectric spectra in Figure 7.5. The figure furthermore show extrapolations of τ from four fitting functions. τ from the temperatures ranging from 185 K to 195 K are used for the fits. The fitting functions are:

- Vogel-Fulcher-Tammann (VFT): $\tau(T) = \tau_0 \exp\left(\frac{A}{T-T_0}\right)$
- Avramov: $\tau(T) = \tau_0 \exp\left(\frac{B}{T^n}\right)$
- Parabolic: $\tau(T) = \tau_0 \exp\left(J^2\left(\frac{1}{T} - \frac{1}{T_0}\right)^2\right)$
- Second degree polynomial: $\log_{10}(\tau(T)) = aT^2 + bT + c$

It is seen that the different methods give different values of γ_{eq}. Using one of the generalized single-parameter aging tests (which we derive in Section 7.5), we can also estimate γ_{eq}. In Section 7.5, this γ_{eq} is compared to γ_{eq} from VFT.

7.4 Aging measurements – initial data treatment

This section shows the aging measurements and the initial data treatment. Four datasets are made, one with DEP and 1,2,6-HT respectively, and two with

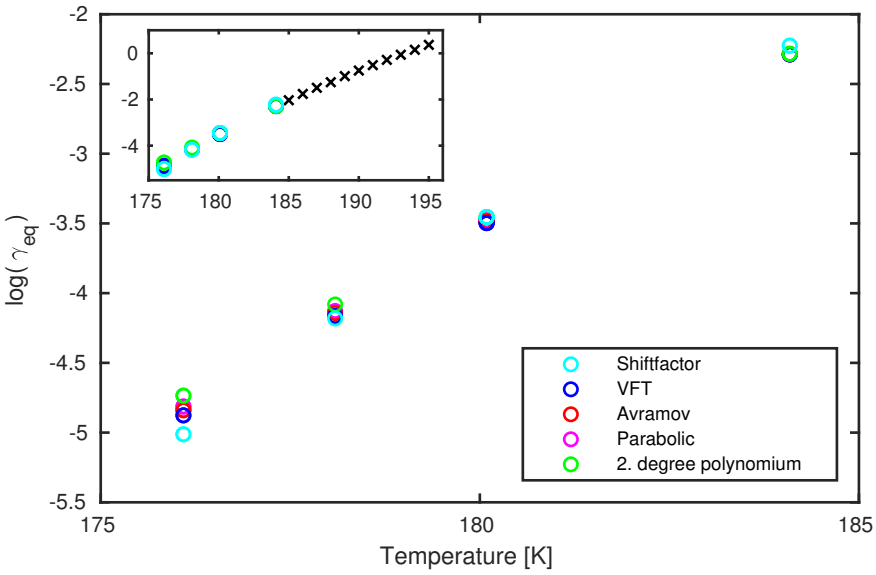

Figure 7.5: Estimated clock rates γ_{eq} for glycerol as a function of temperature at the temperatures at which aging measurements are performed. The insert shows the estimations together with γ_{eq} found directly from the α-peak shown as black crosses.

glycerol. Details are seen in the tables below where liquid, measuring frequency, measuring time for each point, jumps, annealing times t_{anneal}, and estimated relaxation times τ_{eq} are stated.

DEP, measuring frequency 0.133 Hz (measuring time 15 s)

End temp.	Jump	$\log_{10}(t_{anneal})$	$\log_{10}(\tau_{\text{eq}})$
182.2 K	178.2 K → 182.2 K	3.7 (≈ 1.4 hours)	2.2 (≈ 2.7 min)
180.2 K	178.2 K → 180.2 K	4.5 (≈ 9 hours)	3.2 (≈ 0.5 hours)
178.2 K	182.2 K → 178.2 K	5.4 (≈ 70 hours)	4.2 (≈ 4.2 hours)
	180.2 K → 178.2 K	5.3 (≈ 55 hours)	

Glycerol, measuring frequency 0.1 Hz (measuring time 20 s)

End temp.	Jump	$\log_{10}(t_{anneal})$	$\log_{10}(\tau_{\text{eq}})$
184.1 K	180.1 K → 184.1 K	3.7 (≈ 1.4 hours)	2.3 (≈ 3 min)
	176.1 K → 184.1 K	3.9 (≈ 2.2 hours)	
180.1 K	184.1 K → 180.1 K	4.8 (≈ 18 hours)	3.6 (≈ 1.2 hours)
	178.1 K → 180.1 K	4.8 (≈ 18 hours)	
	176.1 K → 180.1 K	5.0 (≈ 30 hours)	
178.1 K	180.1 K → 178.1 K	5.5 (≈ 90 hours)	4.3 (≈ 5.5 hours)
176.1 K	184.1 K → 176.1 K	6.3 (≈ 550 hours)	4.9 (≈ 23 hours)
	180.1 K → 176.1 K	6.2 (≈ 440 hours)	

Glycerol, measuring frequency 1 Hz (measuring time 3 s)

End temp.	Jump	$\log_{10}(t_{anneal})$	$\log_{10}(\tau_{\text{eq}})$
184.0 K	182.0 K → 184.0 K	3.7 (≈ 1.4 hours)	2.3 (≈ 3 min)
182.0 K	184.0 K → 182.0 K	4.2 (≈ 4.4 hours)	3.0 (≈ 0.3 hours)
	180.0 K → 182.0 K	4.3 (≈ 5.5 hours)	
180.0 K	182.0 K → 180.0 K	4.7 (≈ 14 hours)	3.6 (≈ 1.2 hours)

1,2,6-HT, measuring frequency 1 Hz (measuring time 3 s)

End temp.	Jump	$\log_{10}(t_{anneal})$	$\log_{10}(\tau_{\text{eq}})$
195.2 K	193.0 K → 195.2 K	5.4 (≈ 70 hours)	2.4 (≈ 4 min)
193.0 K	195.2 K → 193.0 K	5.5 (≈ 88 hours)	3.0 (≈ 0.3 hours)
	190.9 K → 193.0 K	5.5 (≈ 88 hours)	
190.9 K	193.0 K → 190.9 K	5.8 (≈ 175 hours)	3.6 (≈ 1 hour)

For further notation, the jump sizes and temperatures are shown in round numbers, e.g. the temperature 182.1 K is denoted 182 K etc.

Figure 7.6 shows the spectra at the temperatures between which the jumps are performed, together with the measuring frequency for the different liquids. For DEP, there is a lot of noise in the measurements at the two lowest temperatures (174 K and 176 K).

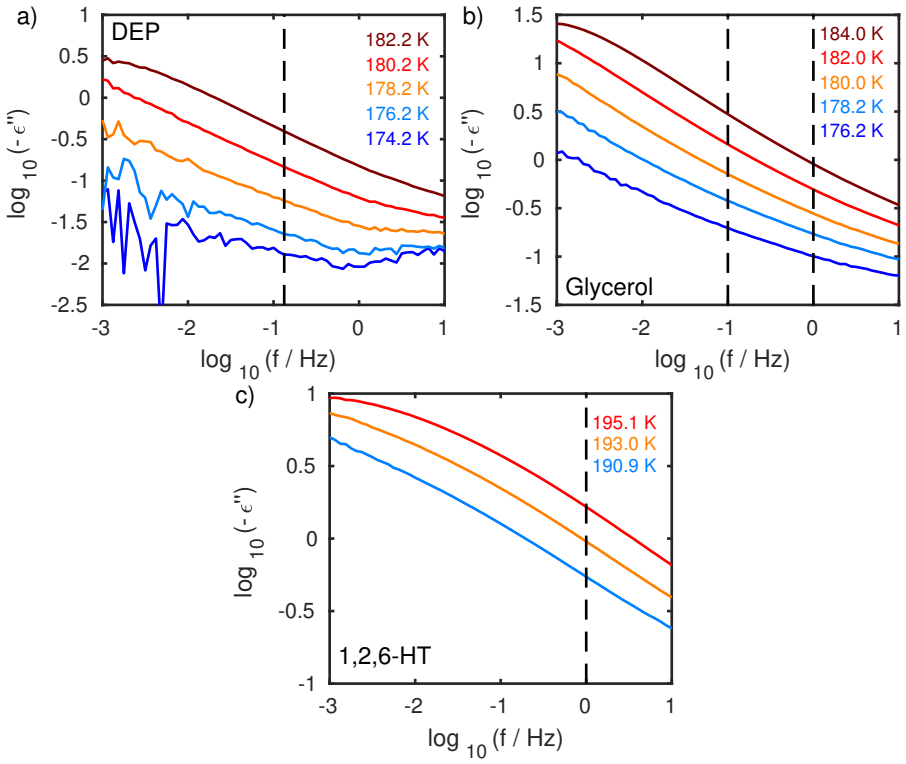

Figure 7.6: The imaginary part of the dielectric equilibrium spectra at the temperatures between which the jumps are performed. The black lines illustrate the measuring frequencies. (a) DEP. (b) Glycerol. (c) 1,2,6-HT.

The measuring protocols, together with the raw data, are shown in Figure 7.7. The color notation is that up jumps are reddish, and down jumps are bluish. Several jumps are made twice, which made it possible to check for reproducibility, but only the first is used in the further data treatment. For DEP, it is seen again that there is a lot of noise at the two lowest temperatures, and it is furthermore seen that the liquid does not fully reach equilibrium at these temperatures. Therefore, the jumps to and from these temperatures (174 K and 176 K), which are brownish and grayish, are not used in the further investigation.

As seen in Figure 7.7, the raw data consists of many data points. The raw data are averaged in order to reduce the noise. Figure 7.8 shows an example of this for DEP. The averaging is done on a logarithmic scale. The first number of raw data are kept, then the $\log_{10}(time)$-scale is divided into a number of equally sized intervals in which the raw data are averaged. Here, the first 11 raw data points are kept, then the $\log(time)$-scale is divided into 79 equal sized intervals in which the raw data are averaged.

Figures 7.9 (left) show the data as a function of time on a logarithmic scale. Jumps ending at the same temperature reach the same equilibrium value. Jumps starting at the same temperature start at the same value, however, this is not visible in the figure due to the instantaneous contribution to the aging (see Section 3.3). Note that same size up and down jumps are not symmetrical, which is due to the non-linearity already seen with small jumps.

For further data treatment, some notation is now introduced. Each jump is performed from a starting temperature T_{start}, and ends at an end temperature T_{end}. The measured time-dependent quantity is denoted $X(t) = \log_{10}(-\varepsilon''(f_{\text{measure}}, t))$. When the liquid is in equilibrium at T_{end} as $t \to \infty$, the measured quantity is denoted X_{eq}. Figure 7.10 shows X_{eq} as a function of temperature for the four datasets. The time-dependent distance to equilibrium at T_{end} is denoted $\Delta X(t) = X(t) - X_{\text{eq}}$. $\Delta X(0)$ thereby defines the total change of the measured quantity from T_{start} to T_{end}.

The normalized relaxation function $R(t)$ is defined as the time-dependent distance to equilibrium over the overall change from start to end of the measured quantity [50, 55]

$$R(t) = \frac{\Delta X(t)}{\Delta X(0)} \tag{7.4}$$

From the definition, it is seen that $R(0) = 1$ and that $R(t) \to 0$ as $t \to \infty$. Figure 7.9 (right) shows the normalized relaxation function as a function of temperature for all jumps.

As mentioned, jumps that do not reach equilibrium at all are not used in the further data treatment. However, all jumps are adjusted by an "equilibrium error", which essentially is an adjustment of the end point of $\log_{10}(-\varepsilon''(f_{\text{measure}}))$, i.e. X_{eq}. This equilibrium error is found by hand. Figure 7.11 shows an example of the error for DEP. The results are barely affected, and for clarity of the figures, the error bar is not shown further.

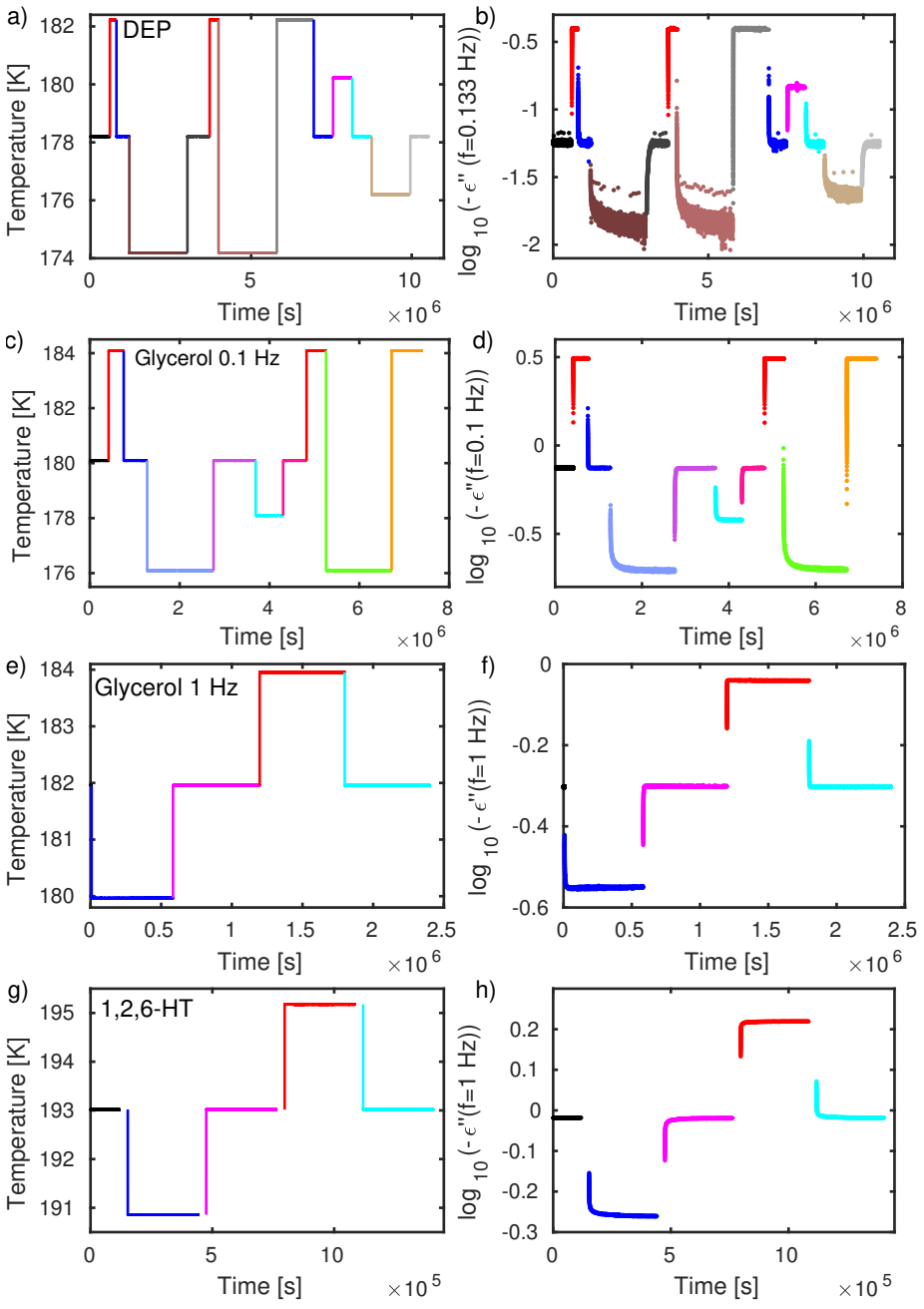

Figure 7.7: Raw measurements. Left: Temperature as a function of time. Right: The measured quantity $\log_{10}(-\varepsilon''(f_{\text{measure}}))$ at the fixed measuring frequency as a function of time.

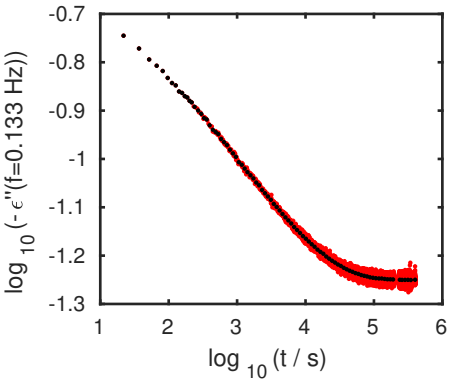

Figure 7.8: Example of averaged data for DEP. The red points show the raw data, and the black points show the averaged data.

7.5 Generalized single-parameter tests

Hecksher *et al.* (2015), [28] first derived the two tests of single-parameter aging. These tests requires two jumps to the same temperature. In Hecksher *et al.* (2015) [28] they only use these two jumps in their analysis. We take the analysis one step further by including jumps to different temperatures and thereby generalize the tests. The below derivation of the generalized tests is inspired by Hecksher *et al.* (2015) [28].

The tests are based on the TN-formalism (see Section 3.3.1). As described, the idea of the TN-formalism is that a material time (ξ) can be defined from the clock rate $\gamma(t)$ [28, 50, 55]

$$d\xi = \gamma(t)dt \tag{7.5}$$

As mentioned, the material time may be thought of as a time measured on a clock with a clock rate that evolves with time. The TN-formalism implies that the normalized relaxation function $R(t)$ is a unique function of the material time ξ [28, 55]

$$R(t) = \phi(\xi) \tag{7.6}$$

The time derivative of R is given by $\dot{R} = \phi'(\xi)\gamma(t)$, since $d\xi/dt = \gamma(t)$. Since ξ is a unique function of R, $\phi'(\xi)$ is also a unique function of R. We denote this negative function by $-F(R)$ giving

$$\dot{R} = -F(R)\gamma(t) \tag{7.7}$$

Hecksher *et al.* (2015) [28] introduce the single-parameter assumption, by assuming that both the measured quantity $X(t)$ and the clock rate $\gamma(t)$ are controlled by the same parameter $Q(t)$. Hecksher *et al.* assumed that the temperature jumps are small, so that it is reasonable to Taylor expand both

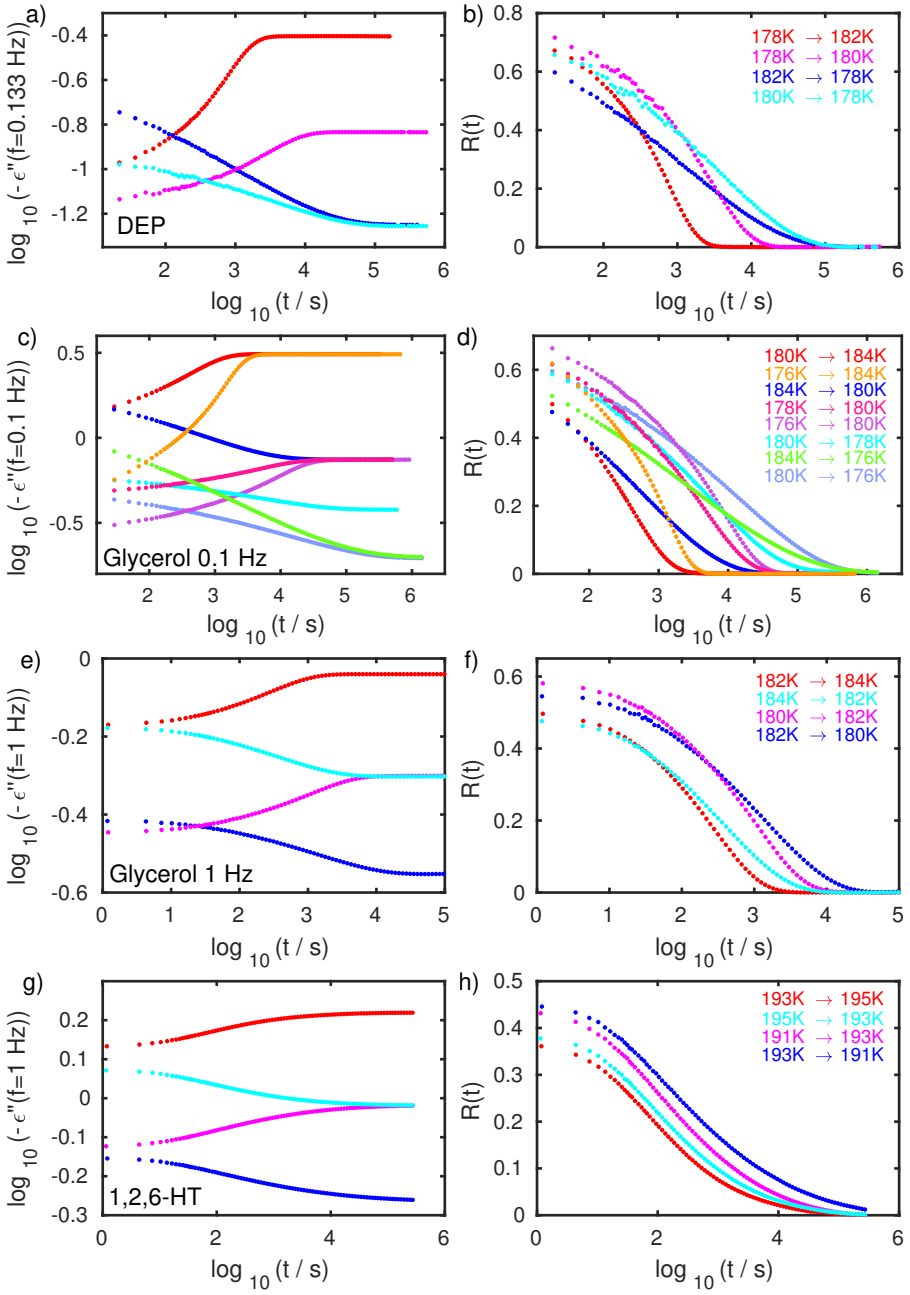

Figure 7.9: Measurements. Left: $\log_{10}(-\varepsilon''(f_{\text{measure}}))$ as a function of time. Right: The normalized relaxation function $R(t)$.

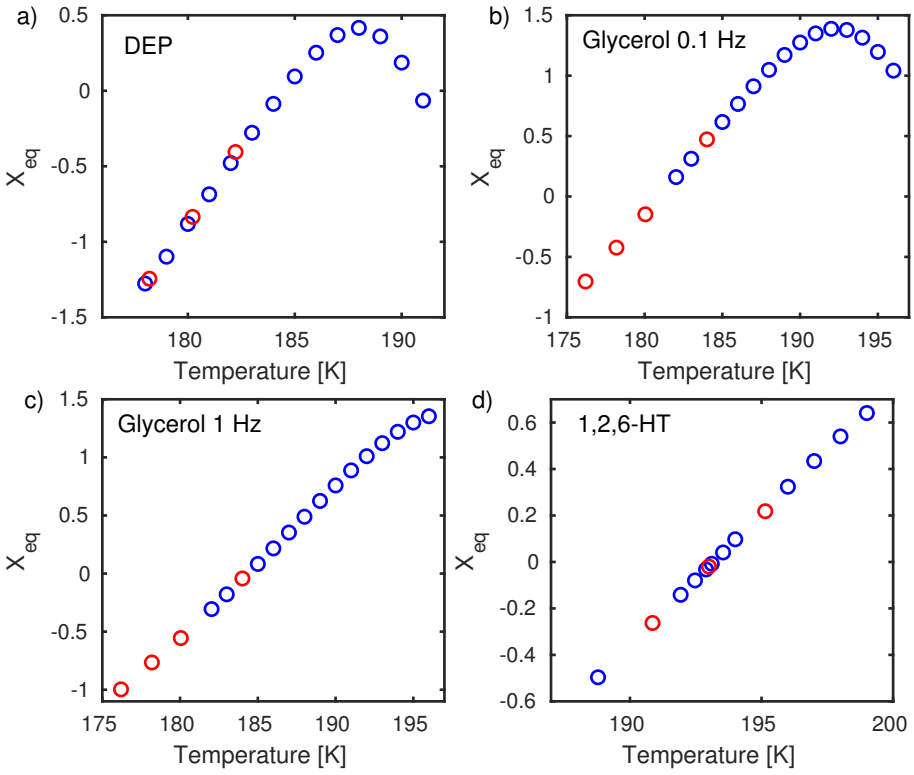

Figure 7.10: The measured quantity at equilibrium at the end temperature (X_{eq}) as a function of temperature. The red circles indicate the temperatures at which the jumps are performed.

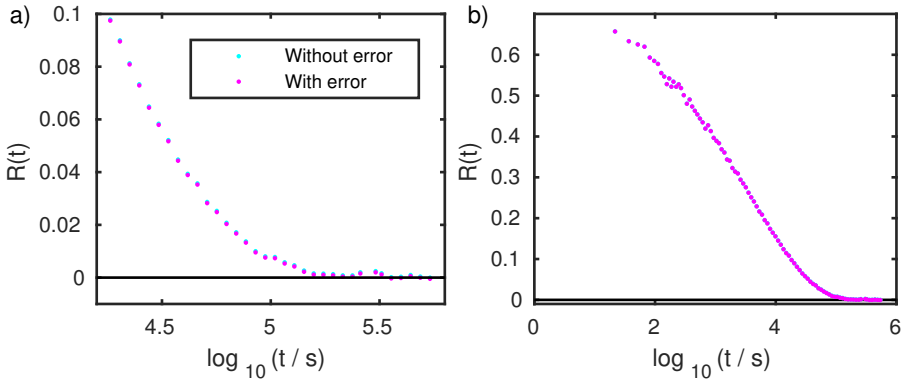

Figure 7.11: Example of the "equilibrium error" for DEP. (a) A zoom of the normalized relaxation function. Different sizes of errors are tried to find a suitable one. (b) An example of how this equilibrium error affects the normalized relaxation function.

$X(t)$ and $\ln(\gamma(t))$ to the first order in $Q(t)$: $\Delta X(t) \cong c_1 \Delta Q(t)$ and $\Delta \ln(\gamma(t)) \cong c_2 \Delta Q(t)$, where c_1 and c_2 are constants. Eliminating $\Delta Q(t)$ in the equations gives $\ln(\gamma(t)) = \ln(\gamma_{\text{eq}}) + \Delta X(t)/X_{\text{const}}$, where $X_{\text{const}} = c_1/c_2$. Using the definition of $R(t)$ (Eq. (7.4)) gives

$$\gamma(t) = \gamma_{\text{eq}} \exp\left(\frac{\Delta X(0)}{X_{\text{const}}} R(t)\right) \tag{7.8}$$

As expected $\gamma(t) \to \gamma_{\text{eq}}$ as $t \to \infty$, because $R(t) \to 0$. Inserting this expression of γ in Eq. (7.7) gives

$$\dot{R} = -F(R)\gamma_{\text{eq}} \exp\left(\frac{\Delta X(0)}{X_{\text{const}}} R(t)\right) \tag{7.9}$$

Rearranging leads to

$$-\frac{\dot{R}}{\gamma_{\text{eq}}} \exp\left(-\frac{\Delta X(0)}{X_{\text{const}}} R(t)\right) = F(R) \tag{7.10}$$

from which the two tests are derived in the following sections.

7.5.1 Test 1 – predicting general jumps from knowledge of a single jump

If the liquid has single parameter aging, this test makes it possible to predict a relaxation curve for one jump using a relaxation curve for another jump. In the following, we use subscripts 1 and 2 to distinguish between the known (measured) relaxation function – jump 1 – and the predicted relaxation functions – jump 2.

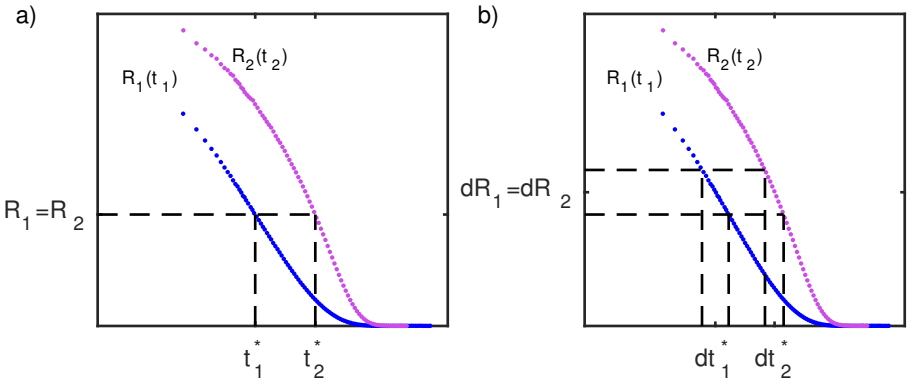

Figure 7.12: Illustration of the steps in the derivation of test 1. Both figures illustrate the normalized relaxation function $R(t)$ on a logarithmic time scale. (a) The times t_1^* and t_2^* corresponding to the same value of R. (b) The time increments dt_1^* and dt_2^* corresponding to an identical change of R ($dR_1 = dR_2$).

Thus, from one jumps relaxation function $R_1(t)$ and its inverse function $t_1(R)$, we derive a method for determining $t_2(R)$ for a different jump $R_2(t)$ using Eq. (7.10).

At times $t_1^*(R)$ and $t_2^*(R)$ where the value of the relaxation functions are the same ($R = R_1 = R_2$) (illustrated in Figure 7.12 (a)), Eq. (7.10) implies

$$-\frac{dR_1}{dt_1^*}\cdot\frac{1}{\gamma_{\mathrm{eq},1}}\cdot\exp\left(-\frac{\Delta X_1(0)}{X_{\mathrm{const}}}R_1(t_1^*)\right) = -\frac{dR_2}{dt_2^*}\cdot\frac{1}{\gamma_{\mathrm{eq},2}}\cdot\exp\left(-\frac{\Delta X_2(0)}{X_{\mathrm{const}}}R_2(t_2^*)\right) \tag{7.11}$$

For time increments dt_1^* and dt_2^* leading to identical changes $dR_1 = dR_2$ (see Figure 7.12 (b)) we can write Eq. (7.11) using the premise that $R_1(t_1^*) = R_2(t_2^*)$ to give

$$dt_2^* = \frac{\gamma_{\mathrm{eq},1}}{\gamma_{\mathrm{eq},2}}\cdot\exp\left(\frac{\Delta X_1(0) - \Delta X_2(0)}{X_{\mathrm{const}}}R_1(t_1^*)\right)dt_1^* \tag{7.12}$$

Integrating this leads to (assuming that both jumps are initiated at time zero)

$$t_2 = \int_0^{t_2} dt_2^* = \frac{\gamma_{\mathrm{eq},1}}{\gamma_{\mathrm{eq},2}}\int_0^{t_1}\exp\left(\frac{\Delta X_1(0) - \Delta X_2(0)}{X_{\mathrm{const}}}R_1(t_1^*)\right)dt_1^* \tag{7.13}$$

which then determines $t_2(t_1) = t_2(t_1(R)) = t_2(R)$ predicting the inverse function $R_2(t)$.

In practice, we do not need to do an inversion. The procedure is to transform a discrete set of measured data points, a time vector $\mathbf{t}_1 = (t_1^1, t_1^2, \ldots, t_1^n)$ and a corresponding relaxation vector $\mathbf{R}_1 = (R_1^1, R_1^2, \ldots, R_1^n)$) to a new time vector $\mathbf{t}_2 = (t_2^1, t_2^2, \ldots, t_2^n)$ corresponding to the measured $\mathbf{R}_1$ points. Plotting $(\mathbf{t}_2, \mathbf{R}_1)$ should then fall on R_2, which can be tested by a separate measurement.

For jumps ending at the same temperature Eq. (7.13) reduces to

$$t_2 = \int_0^{t_1} \exp\left(\frac{\Delta X_1(0) - \Delta X_2(0)}{X_{\text{const}}} R_1(t_1^*)\right) dt_1^* , \tag{7.14}$$

which is the equation used in Hecksher *et al.* [28]. The new generalized test has the disadvantage that one needs to know the clock rate γ_{eq}, which can not be determined exactly (see Section 7.3). In Section 7.6, we show that it is in fact possible to determine γ_{eq} using this test.

The constant X_{const} is found using two normalized relaxation functions, preferably to the same temperature (R_1 and R_2). X_{const} is found by fitting using Eq. (7.14), as the value of X_{const} that gives the best prediction of one jump from the other. In principle, all jumps could be used for this, however, by using two jumps that end at the same temperature, we do not need to know γ_{eq}, since the factor $\gamma_{\text{eq},1}/\gamma_{\text{eq},2}$ is equal to 1 in this case.

7.5.2 Test 2 – unique function of R

Taking the logarithm of Eq. (7.10) leads to (remember $\dot{R} < 0$)

$$\ln\left(-\frac{\dot{R}}{\gamma_{\text{eq}}}\right) - \frac{\Delta X(0)}{X_{\text{const}}} R = \ln(F(R)) \tag{7.15}$$

Since $F(R)$ is a unique function of R, the left hand side of Eq. (7.15) (denoted LHS) is also a unique function of R. This means that LHS plotted against R for the different jumps collapse onto one master curve if a single parameter controls both X and $\ln(\gamma)$. Note that if the jumps ends at the same temperature, $\gamma_{\text{eq},1}$ will be equal $\gamma_{\text{eq},2}$ and it is therefore not necessary to find this.

7.5.3 Initial analysis – find X_{const}

The initial data treatment for the generalized tests of single-parameter aging is to find the constant X_{const}. Two jumps to the same temperature are used (preferrably one up and one down jump). X_{const} is then found as the value that gives the best prediction of one jump from the other using Eq. (7.14).

Figure 7.13 shows the results of the jumps used to find X_{const}. Figure 7.13 (left) shows the predictions of the normalized relaxation functions, and Figure 7.13 (right) shows the left hand side (LHS) of Eq. (7.15) (with $\gamma_{\text{eq}} = 1$) plotted against R.

From this it is seen that all liquids have single-parameter aging to a good approximation, however, with small deviations, especially at short times. This initial investigation corresponds to the tests of single-parameter performed in Hecksher *et al.* (2015) [28]. The next section shows the results of the generalized aging tests.

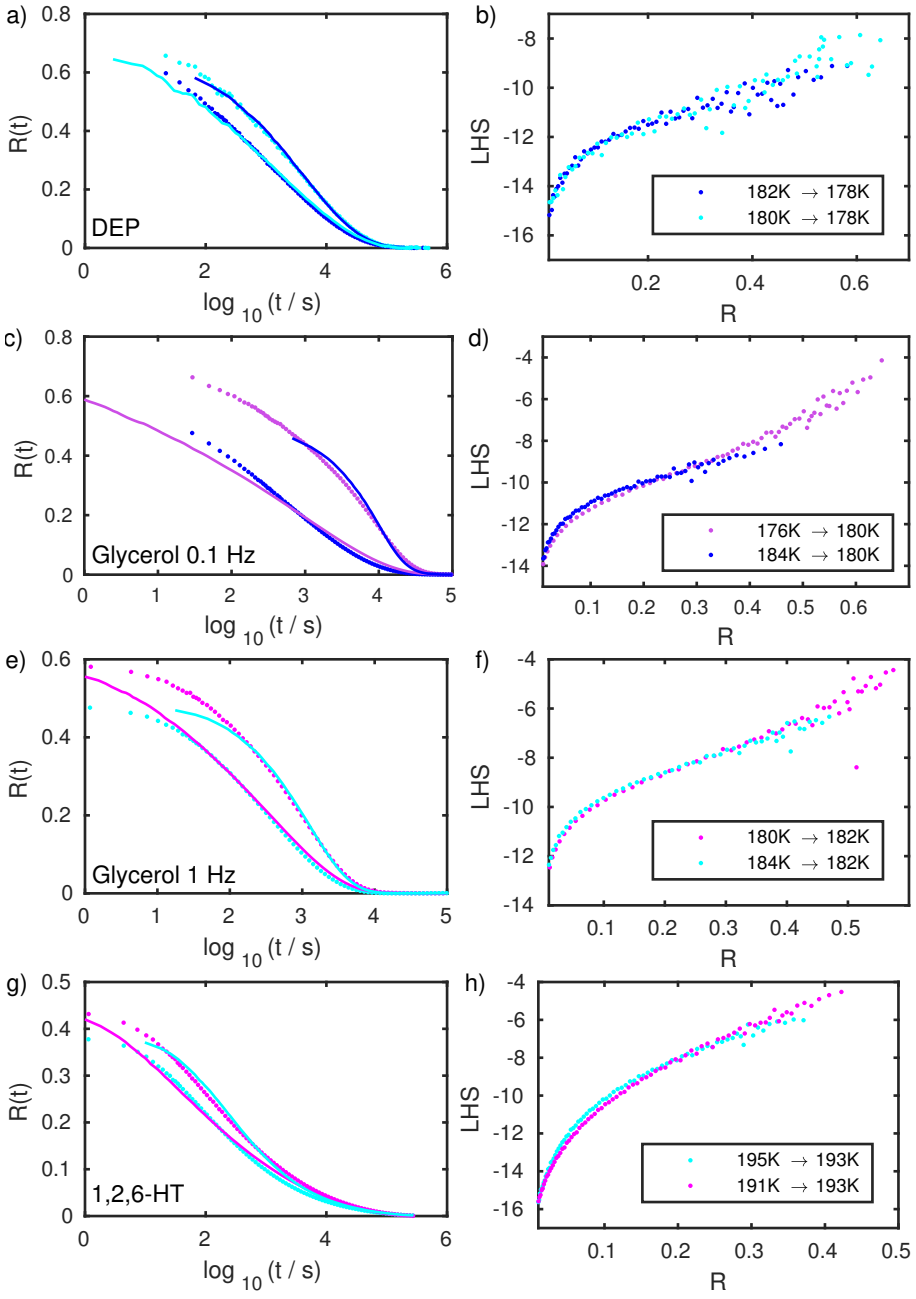

Figure 7.13: Initial analysis to find X_{const} using two jumps to the same temperature. Left: The normalized relaxation function $R(t)$ as a function of time. The jumps are predicted by each other. Dots are data and lines are predictions. Right: Left hand side (LHS) of Eq. (7.15).

7.6 Results

For test 1, one relaxation curve is chosen to predict the relaxation curves for the other jumps. This is chosen to be one of the jumps used to find X_{const} and preferably an up jump. First, the results are shown for glycerol, where we estimated γ_{eq} in Section 7.3. The jump used to predict the other jumps is the jump from 176 K to 180 K, which is shown in Figure 7.14 (a). Figure 7.14 (b) and (c) show the results using γ_{eq} estimated from VFT. For clarity of the figures, the up and down jumps are shown in separate figures. It is seen that the predictions look good, however, with deviations, especially at short times, which was also seen for the van der Waals liquids tested in Hecksher *et al.* (2015) [28]. Note that the 8 K jumps have larger deviations than the smaller jumps (however, still similar to the results on the van der Waals liquids [28]). Since we use a first-order Taylor expansion in the derivation of the test, it is not surprising that the test breaks down somewhat at larger temperature jumps. Note that the two down jumps starting at 184 K both have large deviations at short times, which might be due to the relatively fast relaxation time at this temperature. Therefore, structural relaxation might have occurred during the temperature jump and during the measurements.

Furthermore, it is seen that the predictions for some jumps, e.g. the jumps 180 K to 184 K and 176 K to 184 K, would be improved if the predicted curves are shifted to the left. The value of $\gamma_{\text{eq},1}/\gamma_{\text{eq},2}$ determines the position of the prediction, which means that a wrong estimation of γ_{eq} will lead to a shifted prediction. We instead try to let the constant $\frac{\gamma_{\text{eq},1}}{\gamma_{\text{eq},2}}$ in Eq. (7.13) be a free parameter to find the γ_{eq} that gives the best prediction. The results are seen in Figure 7.14 (d) and (e), where it is seen that the predictions are improved. Figure 7.15 shows γ_{eq} as a function of temperature estimated from the free parameter $\gamma_{\text{eq},1}/\gamma_{\text{eq},2}$ in Eq. (7.13). To invert the parameter $\gamma_{\text{eq},1}/\gamma_{\text{eq},2}$ to γ_{eq} for each temperature, we used the value of γ_{eq} at 184 K found from a VFT-fit. The different jumps to the same temperatures give a slightly different value, which is barely visible in the figure. The found values are compared to the values from the VFT-fit, where it is seen that the estimations have a slightly different curvature.

Predictions for the three other datasets are made with $\gamma_{\text{eq},1}/\gamma_{\text{eq},2}$ as a free parameter. Figure 7.16 shows the predictions. Again, it is seen that the predictions are good, however, still with some deviations, especially at short times. There is no clear difference in whether the liquid is hydrogen-bonded or van der Waals-bonded. Figure 7.17 shows γ_{eq} found as a free parameter.

For test 2, γ_{eq} found from test 1 is used. For each temperature, the found values of γ_{eq} are averaged, so that each temperature has a fixed γ_{eq}. Figure 7.18 shows the results of the test for the four datasets. The data falls onto one master curve. As also seen with test 1, small deviations are seen at short times (large R). The conclusion of this test is that all the tested liquids have single-parameter aging to a good approximation.

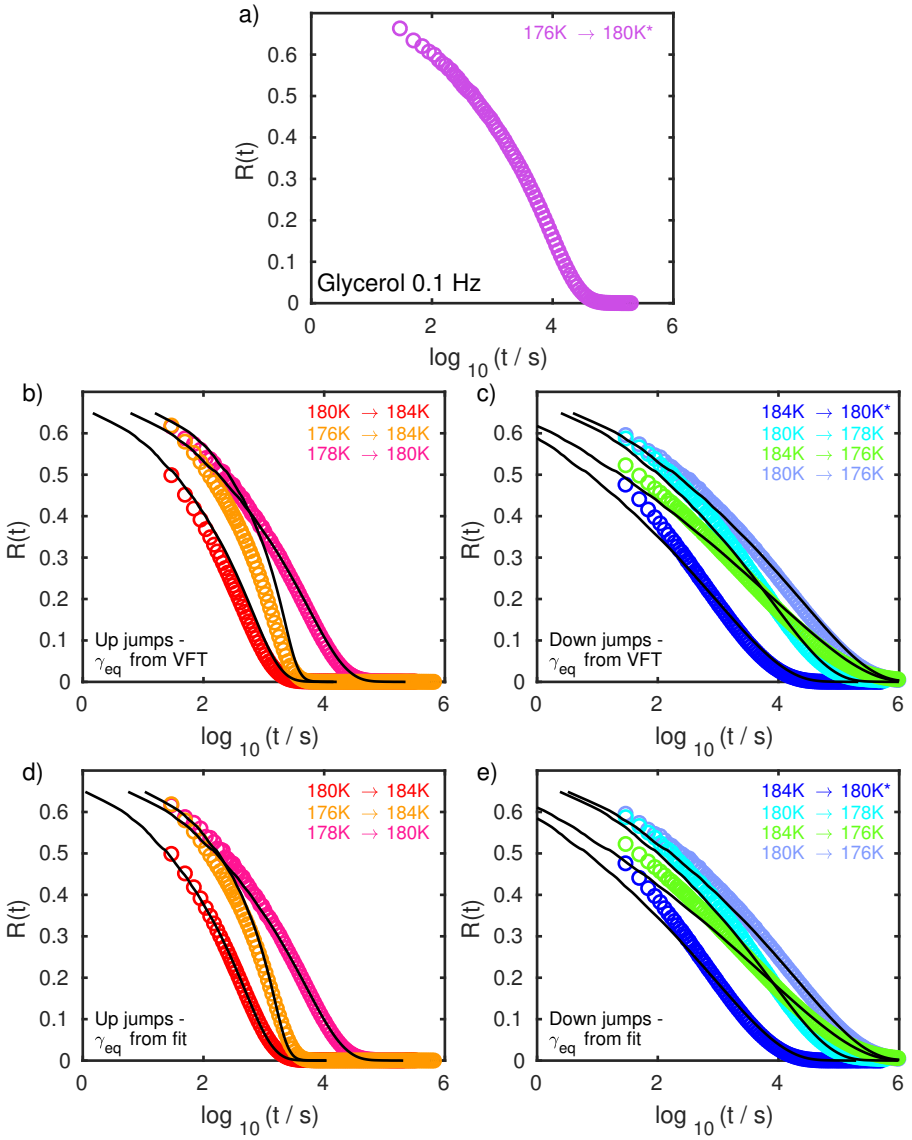

Figure 7.14: Test 1. Prediction of jumps using the jump 176 K to 180 K (shown in (a)). Circles are data and black lines are predictions. The up jump 176 K to 180 K and the down jump 184 K to 180 K were used to find X_{const} (indicated by * in legend). (b) and (c) shows the predictions using γ_{eq} from VFT fit. (d) and (e) shows the predictions with $\gamma_{\text{eq},1}/\gamma_{\text{eq},2}$ as a free parameter.

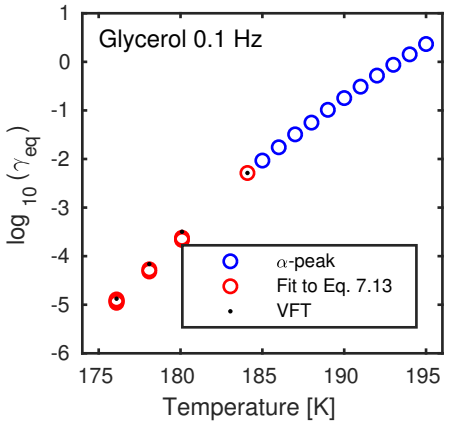

Figure 7.15: The clock rate at equilibrium at the end temperature (γ_{eq}) found from equilibrium spectra (blue circles). The red circles are determined from the free parameter $\gamma_{\mathrm{eq},1}/\gamma_{\mathrm{eq},2}$ in Eq. (7.13). The black dots are extrapolations from a VFT-fit.

7.7 Concluding remarks

The hydrogen-bonded liquids, glycerol and 1,2,6-HT, and the van der Waals-bonded liquid, DEP, were tested for single-parameter aging using the direct tests developed in Hecksher *et al.* (2015) [28]. Hecksher *et al.* 2015 [28] demonstrated single-parameter aging for three different van der Waals liquids. In the present investigation, the tests are applied to hydrogen-bonded liquids for the first time. As part of this investigation, we generalized the single-parameter aging tests to include jumps that do not end at the same temperature.

We conclude that the studied liquids have single-parameter aging to a good approximation, and that there is no difference in whether the liquid is van der Waals or hydrogen bonded. The tests work well also for the large jumps on 4 K and 8 K (performed on glycerol and DEP), where it has been tested beforehand for jumps on maximum 2 K [28]. At the 8 K jumps, single-parameter aging might begin to break down, which is expected, since we use a first-order Taylor expansion in the derivation of the tests.

The data analysis emphasizes that measurements must be precise to use the direct tests of single-parameter aging. It is important that the liquid is in equilibrium at the starting temperature and reach full equilibrium at the ending temperature. Actually, the liquid does not have to reach full equilibrium, if one knows the correct X_{eq}, i.e., where it should end. When performing a large up jump from the glassy state, it is possible to monitor a full relaxation curve where both the plateau in the beginning and the end is present. It is recommended to perform such a jump to predict the other jumps.

Test 1, which predicts the relaxation curves, is the most sensitive test. By

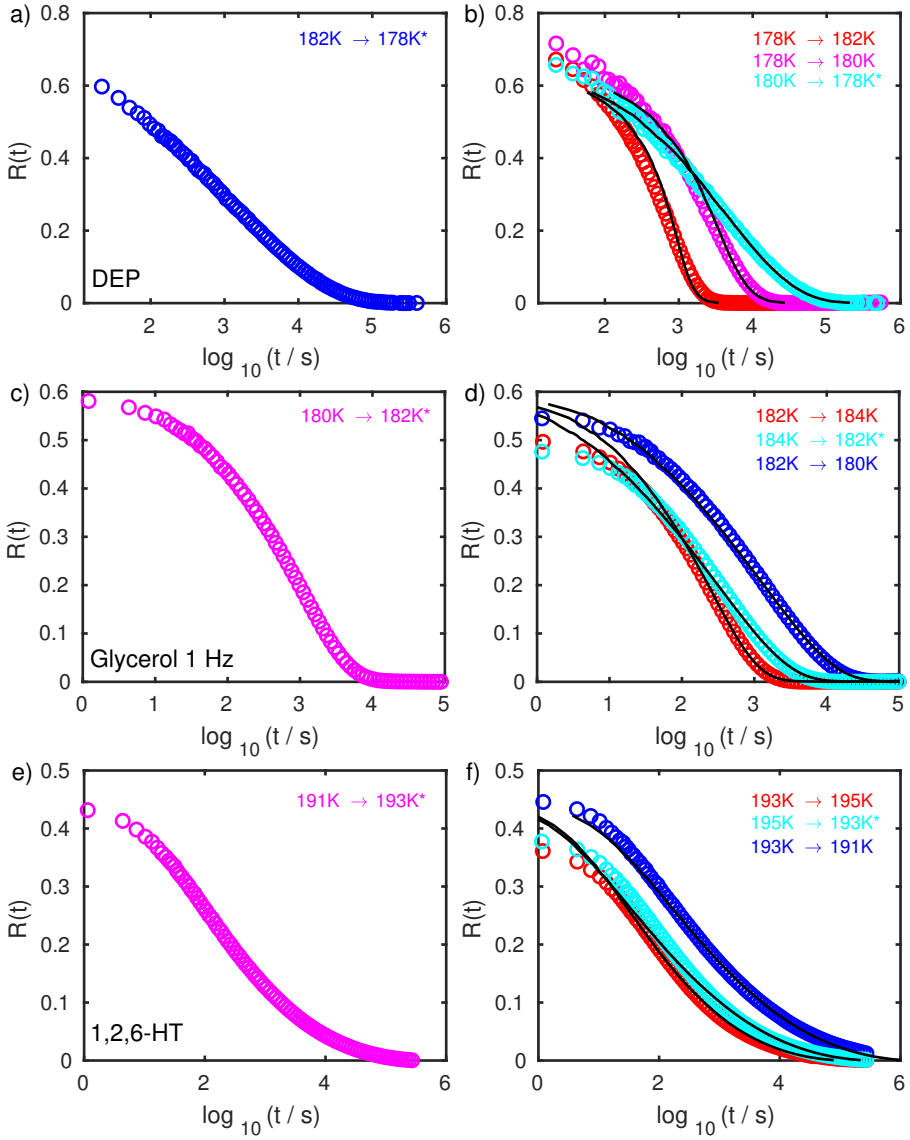

Figure 7.16: Test 1. Prediction of jumps for the three datasets using the jump shown to the left. Circles are data and black lines are predictions. The jumps used to find X_{const} are indicated by * in legend. The predictions are made with $\gamma_{\text{eq},1}/\gamma_{\text{eq},2}$ as a free parameter.

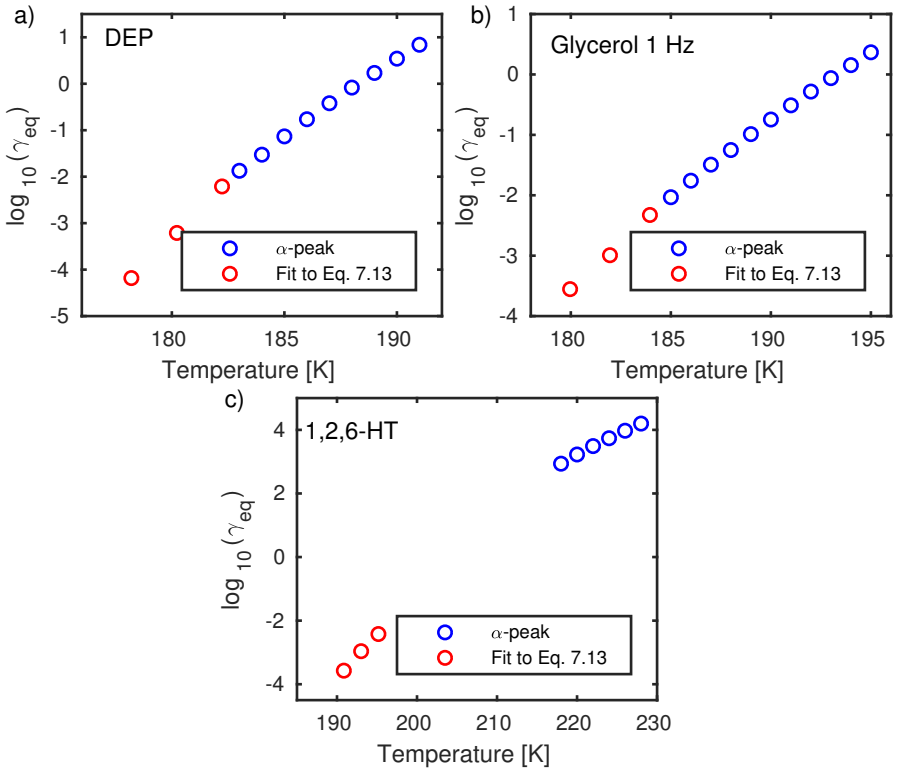

Figure 7.17: The clock rate at equilibrium at the end temperature (γ_{eq}) found from equilibrium spectra (blue circles). The red circles are determined from the free parameter $\gamma_{\mathrm{eq},1}/\gamma_{\mathrm{eq},2}$ in Eq. (7.13).

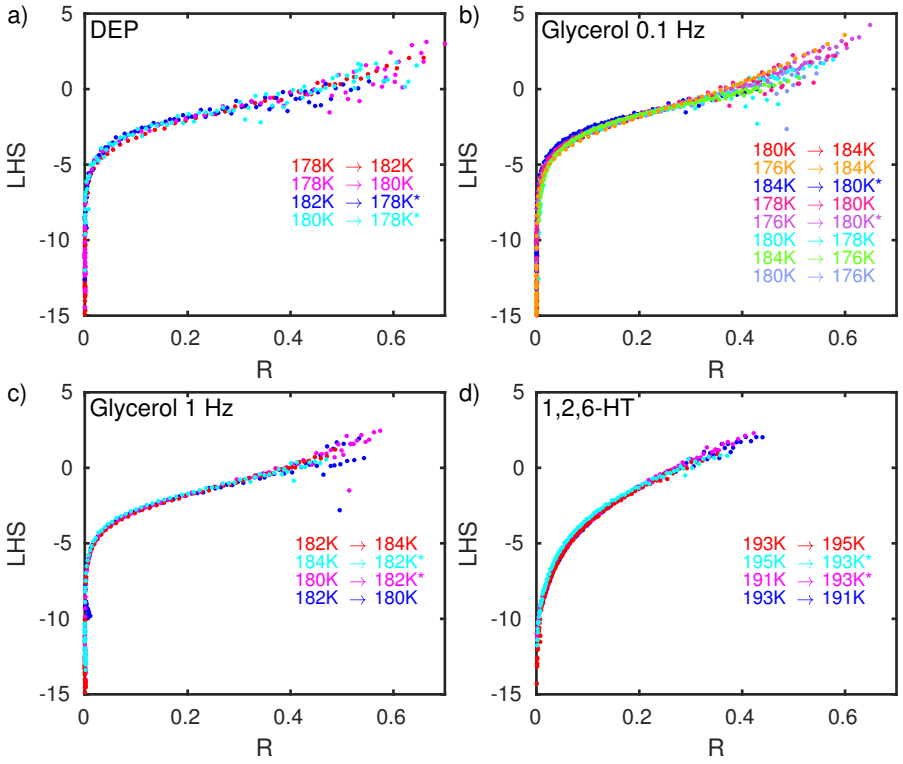

Figure 7.18: Test 2. The left hand side of Eq. (7.15) (LHS) plotted against R. If the liquid has single-parameter aging, the data are predicted to collapse onto one master curve. The two jumps used for determining X_{const} are marked by *.

using test 1, it is possible to find γ_{eq} at temperatures, where the loss peak is outside the available frequency range of the dielectric equilibrium spectrum. However, if one knows γ_{eq} (for example using an extrapolation), an advantage of test 1 is that if a liquid has single-parameter aging, one can use Eq. (7.13) to predict relaxation curves for other jumps. It is necessary to perform two jumps (preferably to the same temperature) to identify the constant X_{const}. Other jumps can then be predicted knowing the clock rate at the end temperature γ_{eq}, the measured quantity at the starting temperature $X(0)$, and the measured quantity at the end temperature X_{eq}. $\Delta X(0) = X(0) - X_{\mathrm{eq}}$ determines the shape of the relaxation, while γ_{eq} determines the position of the relaxation. This prediction is, of course, also limited to small jumps, and possible only in the same temperature range, as the actual jumps are performed in.

Our findings are discussed in relation to the isomorph theory and the simplicity of liquids in Chapter 9.

Chapter 8

Isochronal jump

This chapter describes the investigation of the isochronal jump. By performing the isochronal jump, we want to test one of the most spectacular predictions from the isomorph theory [25]. Namely, that a Roskilde-simple liquid comes into equilibrium instantaneously when jumping from one state point on an isochrone to another state point on the same isochrone (which we refer to as an isochronal jump). Furthermore, the isomorph theory predicts that the relaxation curve for jumps from one isochrone to another along different paths will be the same.

The study of isochronal jump is a study of physical aging as introduced in Chapter 7, where we studied the structural relaxation following temperature jumps. In the present investigation, the jumps are both temperature jumps, pressure jumps, and a combination of the two. As in the investigation of aging followed by temperature jumps, we monitor the aging using the dielectrics at a fixed frequency. In order to monitor the full relaxation curve, we want to perform the temperature and/or pressure jumps as fast as possible (ideally instantaneously). In relation to this, it is important that the time it takes to change state point is much faster that the relaxation time of the liquid, so that we can assume that no structural changes take place in the liquid before thermal/pressure equilibrium is established. See Sections 3.3 and 7.1 for more details on the study of aging.

Note that the equipment used for the temperature aging in Chapter 7 is highly specialized, and that thermal equilibrium is established after only a few seconds when performing a temperature jump. The pressure setup used for the isochronal jump investigation, as described in Section 4.1, does not make it possible to come even close to a few seconds of temperature/pressure equilibrium times. When the temperature is changed using the thermal bath, the temperature of the pressure vessel, the pressure liquid, and, of course, the sample have to change, which takes time. To perform the isochronal jump faster, we develop an temperature regulator placed inside the pressure vessel, which makes it possible to change the temperature of the sample faster. Section 8.2.3 describes this, and tests are performed in Section 8.3.

We also made two attempts to reduce the noise and systematic errors in the measurements, respectively: a new multi-layer capacitor resulting in an increased signal (Section 8.2.1), and a new electronic configuration of the measurement equipment to reduce systematic errors (Section 8.2.2). Section 8.4 shows the final measurements of the isochronal jumps. First, Section 8.1 describes our thoughts and decisions in relation to the experiment.

8.1 Planning the experiment

This section describes the decisions we made in relation to the jump experiment, i.e., the liquid, jumps, relaxation time and measuring frequency.

8.1.1 Liquid

The chosen sample liquid is 5PPE (polyphenyl ether) for several reasons: 5PPE is a van der Waals liquid, which means that we expect it to be Roskilde simple, it has a glass transition temperature on 244 K, which is perfect for the pressure setup due to the temperature range 233 - 333 K, and it has a good signal (compared to other van der Waals liquids). Furthermore, the liquid 5PPE has been used for several investigations in the Glass and Time group at both atmospheric pressure [28, 52, 67, 79, 80, 112, 113] and high pressures [57, 61, 63, 64]. Furthermore, the investigations in Refs. [61, 63, 64, 79] show that 5PPE obey other predictions from the isomorph theory, which furthermore suggest that 5PPE is a Roskilde-simple liquid. The below assumptions and decisions about the experiment is customized to 5PPE.

8.1.2 Jumps

We want to perform different types of jumps in relation to the investigation. These jumps all involve changes in temperature and/or pressure at the pressure setup. We want to perform the jumps as fast as possible, so that no structural relaxation takes place in the liquid during the jump. The time it takes to change the pressure is much faster than the time it takes to change the temperature at the used pressure setup, which is important to take into account when selecting the jumps.

First of all, we want to make the isochronal jump, i.e. a jump from one state point on an isochrone to another state point on the same isochrone. Figure 8.1 (a) illustrates isochronal jumps. There are two possible choices for the isochronal jump: an isochronal up jump, with an up jump in temperature and an up jump in pressure, and an isochronal down jump, with a down jump in temperature and a down jump in pressure. The ideal case would be to perform both jumps. A down jump in pressure can however not be made automatically with the available pump. The pressure should in this case be released manually,

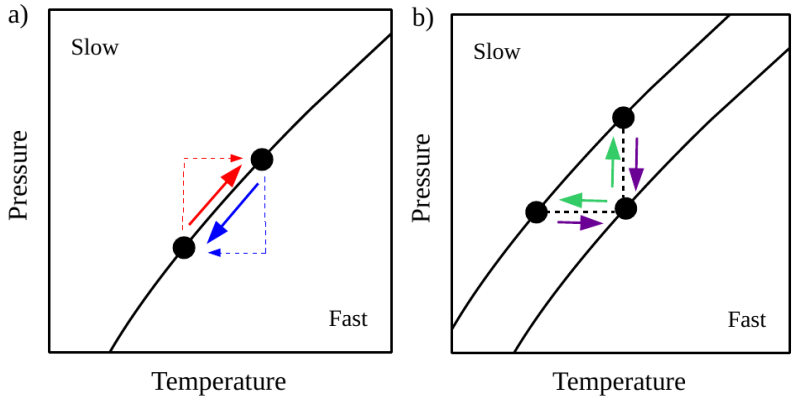

Figure 8.1: Illustration of jumps. (a) Isochronal up (red) and down (blue) jump. Since the pressure changes faster than the temperature, the system will during the different jumps, be in different parts of the phase diagram, as illustrated by the dashed lines. (b) Jumps between two isochrones along different paths in the phase diagram.

and it will be difficult to reach the wanted pressure quickly and precisely. A pressure down jump to atmospheric pressure is, however, a possibility.

A change in pressure leads to a change in temperature. While a pressure up jump increases the temperature, a pressure down jump makes the temperature decrease. This means that both during isochronal up jumps and isochronal down jumps, the pressure change may help decrease the time to reach thermal equilibrium.

There are, however, advantages to performing the isochronal up jump: in this setup, heating is faster than cooling, which means that the temperature jump time is faster for an up jump. Furthermore, since the pressure changes faster than the temperature, we will, during an isochronal up jump, be in the 'slow' part of the phase diagram during the jump (when the pressure has changed, but the temperature is still approaching equilibrium). This is illustrated in Figure 8.1 (a) by the red dashed line. This implies that the assumption that no structural changes take place in the liquid during the time it takes to reach the thermal/pressure equilibrium is best for the isochronal up jump.

Besides doing the actual isochronal jump, we also want to perform other "isomorph" jumps, where we jump from one isochrone to another isochrone along different paths, for example, by different temperature and pressure jumps, as illustrated in Figure 8.1 (b), which illustrates the jumps we perform in Section 8.4.

8.1.3 Jump size

In order to change the state point fast, ideally, we want to make a small jump. However, the size of the jump depends of the stability of the pressure, which is 3 MPa (see Section 4.1). We estimate that a pressure jump of minimum 20 MPa is acceptable. It is, however, also important that the corresponding change in temperature is not too large in order to stay on the isochrone. This can be determined by the slope of the isochrones (Figure 8.1), which depends on the sample liquid.

To estimate the relation between the pressure change ΔP and the temperature change ΔT for 5PPE, the isochrones from the isochronal superposition investigation (Chapter 5) are used. Assuming that the isochrones are linear, gives $\Delta P = \Delta T \cdot a \Leftrightarrow \Delta T = \frac{\Delta P}{a}$. This should be a fine assumption in small P and T intervals. We estimate that $a \approx 5.5$ MPa/K for 5PPE, which means that $\Delta T \approx 3.6$ K when $\Delta P = 20$ MPa. The slope of the isochrones may not be the same in other parts of the phase diagram, but this works as an estimation for the initial tests (during the actual jumps performed in Section 8.4, we found $\Delta T = 3.9$ K for $\Delta P = 20$ MPa).

8.1.4 The relaxation time for the used isochrone

The liquid's relaxation time must be (much) longer than the time it takes to come into thermal/pressure equilibrium, so that we can assume that no structural changes take place in the liquid during the jump. The relaxation time of the liquid at the state points between which the jumps are performed therefore depends on the time it takes to come into thermal/pressure equilibrium after a jump.

Test jumps are made to estimate the temperature and pressure equilibrium times (Section 8.3). From these tests, we conclude that the pressure and thermal equilibrium is established after 200 - 1500 seconds, with the exact time depending on the jump type. We estimate that the relaxation time τ should be at least 20 times slower than the jumping time in order to assume that no structural changes take place in the liquid before thermal/pressure equilibrium is reached. We use the relaxation time $\tau = 16000$ seconds ($\log_{10}(\tau) = 4.2$) (10-80 times slower than the pressure/temperature equilibrium time). The experiments are therefore performed at the isochrone where $\tau = 16000$ s. This corresponds to a loss peak frequency $f_m = 10^{-5}$ Hz using $f_m = \frac{1}{2\pi\tau}$. Note that this is still far from the times used for purely temperature aging where the relaxation time is around 8000 times slower than the thermal equilibrium time.

The state points with $f_m = 10^{-5}$ Hz can not be determined directly from the measurements, since the α-peak is outside the available frequency range. Instead, the state points are estimated using the dielectric equilibrium spectra at higher temperatures (see Section 8.4.1).

8.1.5 The fixed measuring frequency

During the jumps, the dielectrics are measured at a fixed frequency as a function of time to monitor the aging. The fixed measuring frequency is chosen so that the signal of the loss is high, which is close to the α-peak. On the other hand, it is chosen so that the measuring time at this frequency is not too long. The used fixed frequency is chosen as the least-noisy frequency in a small interval of frequencies. The used measuring frequency is 0.0205 Hz, which gives a measuring time of 97 seconds for a point.

8.2 New measurement equipment

The high-pressure setup, as described in Section 4.1, is used for the isochronal jump measurements. This section describes three new improvements of the setup made in relation to this investigation. A new sample cell is designed to increase the signal and thereby reduce the noise, a new electronic setup with a current to voltage converter is implemented to reduce systematic errors, and a new temperature regulator ensures a faster temperature change. The next sections describe these developments.

8.2.1 Sample cell

The aim of the new sample cell is to increase the signal of the capacitance to reduce the noise in the measurements. The new sample cell is a multi-layer parallel-plate capacitor consisting of 12 capacitor plates in copper with a diameter on 20 mm. The plates are stacked on top of each other, which results in 11 layers of liquid. All plates are separated using 4 small Kapton spacers glued on each plate, resulting in liquid layers of 50 μm. The cell, and how the wires are connected, are illustrated in Figure 8.2.1. The sample cell furthermore consists of a cylindrical holder in polyetheretherketone (PEEK), in which the capacitor is assembled. This allows for a reservoir of extra liquid around the sample. The sample cell is wrapped in rubber and Teflon tape to avoid mixing with the pressure liquid. Appendix C.1 provides a detailed description of the assembling of the cell.

The empty capacitance of this capacitor is 11 times the capacitance of a single-layer parallel-plate capacitor with the same diameter and distance between the plates

$$C_{\text{empty}} = 11 \cdot \frac{\varepsilon_0 \cdot A}{d} = 612 \text{ pF} \tag{8.1}$$

where ε_0 is the vacuum permitivity, A is the area of each plate, and d is the distance between the plates. The signal is increased 14 times in comparison to the signal from the sample cell used in the isochronal superposition investigation (Chapter 5).

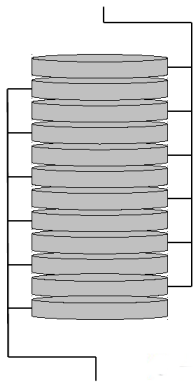

Figure 8.2: Illustration of the new multi-layer parallel-plate capacitor sample cell with 12 plates.

8.2.2 Current to voltage converter

During the isochronal jump measurements, we measure at a low frequency, as described in Section 8.1.5. However, in the low frequency range, systematic errors occur due to leak currents. These leak currents occur because the pressure liquid is conducting, and the wires to connect the sample cell to the electric measuring equipment are running through the pressure liquid.

A multimeter and a voltage divider are normally used for measuring the dielectric signal at frequencies between 0.001 Hz and 100 Hz (see Section 4.2). Figure 8.3 shows our standard electronic setup using a voltage divider where possible leak currents are also illustrated. $\tilde{C}_x$ is the capacitance of the sample and $\tilde{C}_0$ is the capacitance of a prebox consisting of a known capacitor and a known resistor in parallel.

For the measurements of the isochronal jump, we instead use a current to voltage converter to avoid influence of the leak currents in the measurements. Figure 8.4 shows the current to voltage converter setup where possible leak currents are also shown. Compared to the voltage divider, the leak currents R_2 and R_3 will now gather in one leak current R, while the leak current R_1 will not be present. The leak current R will infect the measurements in the same way as conductivity in the pressure liquid. This conductivity does not affect our measurements.

Using the current to voltage converter setup, the capacitance of the sample ($\tilde{C}_x$) is calculated as

$$\tilde{C}_x = -\frac{\tilde{V}_m}{\tilde{V}_g} \cdot \tilde{C}_0 \tag{8.2}$$

where $\tilde{V}_m$ and $\tilde{V}_g$ are the measured and the generated voltage, respectively, and the complex notation implies $V = \mathrm{Re}(\tilde{V}) = \mathrm{Re}(V_0 e^{i(\omega t + \phi_V)})$. $\tilde{C}_0$ is the

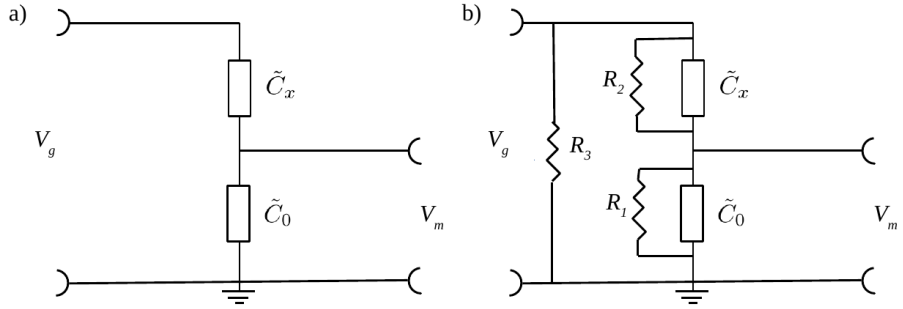

Figure 8.3: The standard electronic setup with voltage divider. $\tilde{C}_x$ illustrates the capacitance of the sample and $\tilde{C}_0$ illustrates a prebox consisting of a known capacitor and a known resistor in parallel. (b) Possible leak currents in this setup.

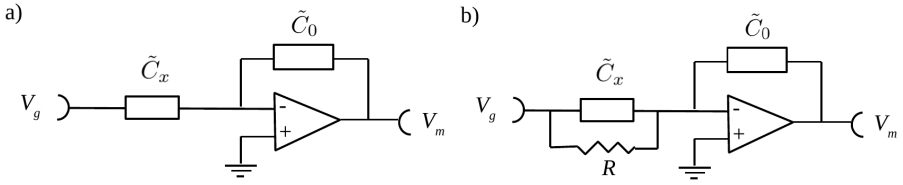

Figure 8.4: The current to voltage converter setup. (b) Possible leak current in this setup.

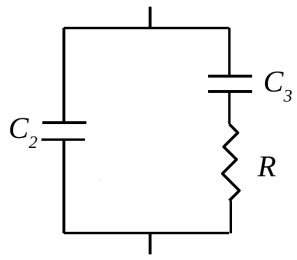

Figure 8.5: Debye circuit. $C_2 = 150$ pF, $C_3 = 68$ pF, and $R = 1$ GΩ.

capacitance of a known capacitor and a known resistor in parallel. $\tilde{C}_0$ is placed in parallel with the operational amplifier.

Before measuring, a calibration is made to find the value of $\tilde{C}_0$. This is done by performing a measurement on a known circuit: a capacitor (1 nF) and a resistor (1 GΩ) in parallel. The exact value of the resistor is measured directly with the multimeter and the exact value of the capacitance is measured directly with the LCR-meter (used for measuring at higher frequencies). The measured voltage ($\tilde{V}_m$) and the generated voltage ($\tilde{V}_g$) are then measured, and the capacitance of $\tilde{C}_0$ is then found as

$$\tilde{C}_0 = -\tilde{C}_{\text{known}} \cdot \frac{\tilde{V}_g}{\tilde{V}_m} \tag{8.3}$$

where $\tilde{C}_{\text{known}}$ is the capacitance of the known circuit.

Test measurements are performed on a 'Debye'-circuit consisting of a capacitor and a resistor in series, in parallel with a capacitor as illustrated in Figure 8.5. This circuit gives a characteristic shape of the real and the imaginary part of the dielectrics, which resemble the ones expected from measurements of a liquid. The values of the capacitor and resistor in series are respectively 68 pF and 1 GΩ, and the value of the capacitor in parallel is 150 pF. These values correspond to the signal from the liquid 5PPE in the high-pressure equipment (with the sample cell used for the isochronal superposition investigation (Chapter 5)). Figures 8.6 (a) and (b) show the expected output of this Debye-circuit.

Test measurements are first conducted in a standard RUC cryostat [56]. The temperature is set to 300 K. 17 spectra are made with respectively the voltage divider setup and the current to voltage converter setup. Figures 8.6 (c) and (d) show the measurements. The calibration of $\tilde{C}_0$ used for the test measurements is not correct, which results in the difference in level in the real part of the capacitance between the two electronic setups. It is seen that the measurements from the current to voltage converter setup have less noise in the low-frequency range than the measurements made with the voltage divider.

Similar test measurements are taken with the same Debye-circuit at the pressure setup at atmospheric pressure. The temperature is set to 300 K, and

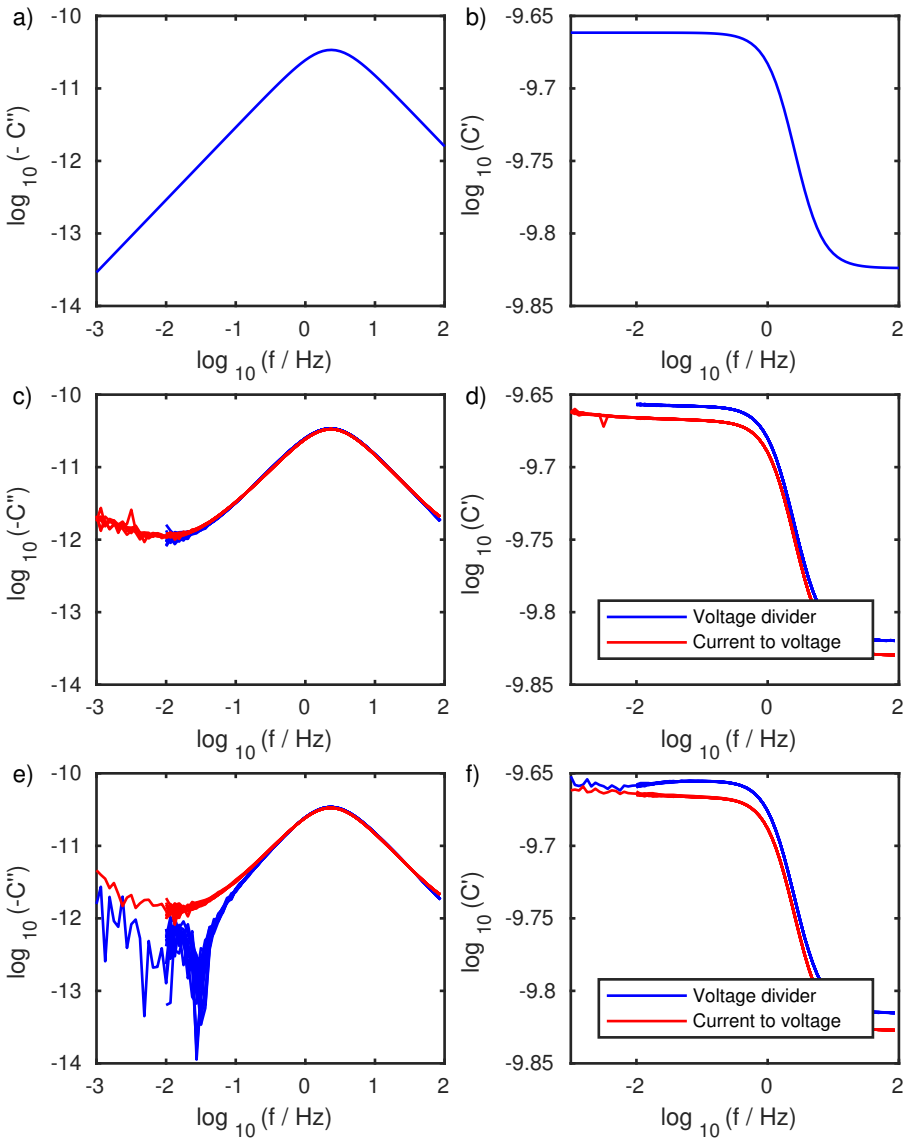

Figure 8.6: Test measurements on a Debye-circuit. (a) and (b) The expected output of measurements on the used Debye-circuit. (c) and (d) Measurements performed in a standard RUC cryostat [56] using respectively the voltage divider setup and the current to voltage converter setup. 17 measurements are made with each method, 7 of the measurements with the current to voltage converter are made in the frequency range 10^{-3} - 10^{2} Hz, while the rest are in the range 10^{-2} - 10^{2} Hz. (e) and (f) Measurements performed in the pressure setup. 13 measurements are made with each method, one measurement of each method is made in the frequency range 10^{-3} - 10^{2} Hz, while the rest are in the range 10^{-2} - 10^{2} Hz.

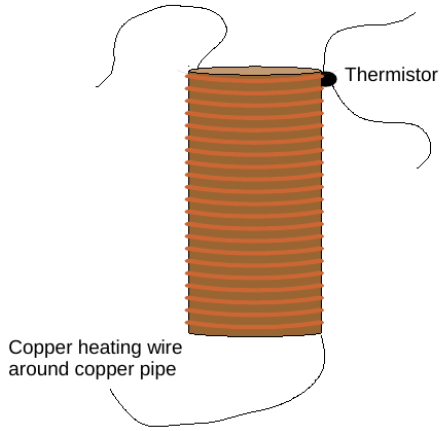

Figure 8.7: Illustration of the heating element for the new temperature regulation. The heating element is placed around the sample.

13 spectra are made with both of the electronic setups. The results are shown in Figures 8.6 (e) and (f), which clearly show that the systematic error at low frequencies are only present in the measurements with the voltage divider setup.

8.2.3 Temperature regulator

We made the temperature regulator with the purpose of changing the temperature fast, but it also has the advantage of keeping the temperature stable. The temperature regulator consists of a heating element made from a copper pipe with a heating wire around it, as illustrated in Figure 8.7. A NTC-thermistor is placed on the copper pipe to measure the temperature. The temperature is controlled using a WEST 4100+ digital temperature controller. The heating element is placed around the cylindrical sample cell.

This temperature regulator only allows for heating to be applied to the sample. The temperature of the thermal bath is therefore held some degrees below (approximately 2 K) the wanted temperature, in order to ensure a stable temperature. We let the bath temperature follow the wanted temperature of the heating element, i.e. if the temperature of the heating element is lowered 4 K, so is the temperature of the bath.

The temperature is monitored using a NTC-thermistor. The temperature T is found from the resistance of the thermistor R using the relation

$$R = R_\infty e^{T_a/T} \tag{8.4}$$

where R_∞ and T_a are constants depending on the thermistor. These constants are found by measuring the temperature in the vessel and the resistance of

the thermistor at a range of temperatures and fit to Eq. (8.4). During this temperature calibration, the temperature is controlled only by the thermal bath.

Tests of the temperature regulation are shown in the next section. These tests show that the speed of a temperature up jump is increased by at least 10 times using the temperature regulator.

8.3 Temperature and pressure tests

It is crucial for our aging investigations, such as the isochronal jump, that the state point is changed instantaneously, or, in practice, as fast as possible. Different tests are conducted in order to investigate the time it takes to change the state point. The pressure is changed quickly relative to the temperature, but tests of how a pressure jump effects the temperature are also performed.

During the test jumps, the temperature is monitored in three different places in the setup as a function of time: in the thermal bath, in the plug of the vessel using a thermocouple, and at the thermistor on the heating element around the sample. In the tests of the temperature regulator, the thermal/pressure equilibrium is also monitored by measuring the dielectrics of the sample liquid at state points with a short relaxation time.

8.3.1 Temperature and pressure tests with thermal bath

The temperature is normally controlled by use of a thermal bath (see Section 4.1). By changing the temperature in the thermal bath, the temperature in the pressure vessel and the sample also changes. Figure 8.8 shows how the measured temperatures evolves respectively after a 5 K up jump and a 5 K down jump made with the thermal bath. It is clear that the temperature change is faster during the up jump. The thermistor placed close to the sample shows that thermal equilibrium is reached after approximately 2500 s for the up jump and 3000 s for the down jump. These times are found as the times where the monitored temperature is 0.01% from the equilibrium temperature.

When the pressure is changed, the temperature in the vessel and thereby the sample also changes. Figure 8.9 show how the temperature is affected by a pressure up jump on 20 MPa. It is seen that pressure equilibrium is established after aproximately 800 s, and that temperature equilibrium is established after approximately 2500 s. This test also shows that it might be difficult to make pure pressure jumps and thereby study aging followed by pressure jumps in this setup (the new temperature regulator, however, helps keep the temperature stable during pressure jump).

When performing an isochronal jump, both the temperature and pressure are changed. An isochronal up jump consists of a pressure up jump and a temperature up jump. This means that the temperature rise caused by the pressure jump may help increase the temperature during the jump. Figure 8.10 shows how the temperature changes during an isochronal jump, where

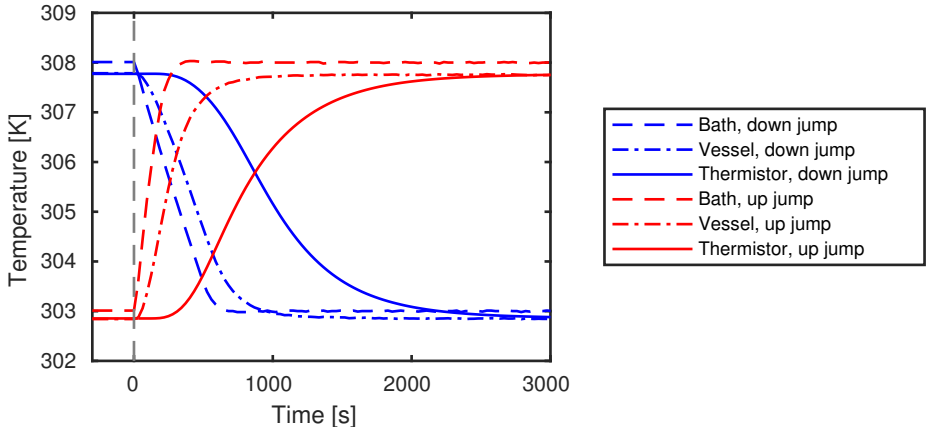

Figure 8.8: Test of the time it takes to change temperature with the thermal bath. Respectively a temperature up jump and a temperature down jump of 5 K are made.

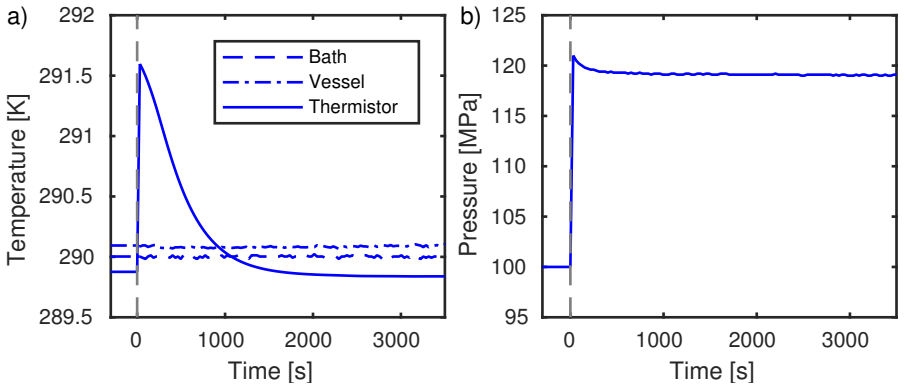

Figure 8.9: Test of pressure jump and its influence on temperature. A pressure up jump on 20 MPa is made. (a) The temperature as a function of time following the pressure jump. (b) The pressure as a function of time.

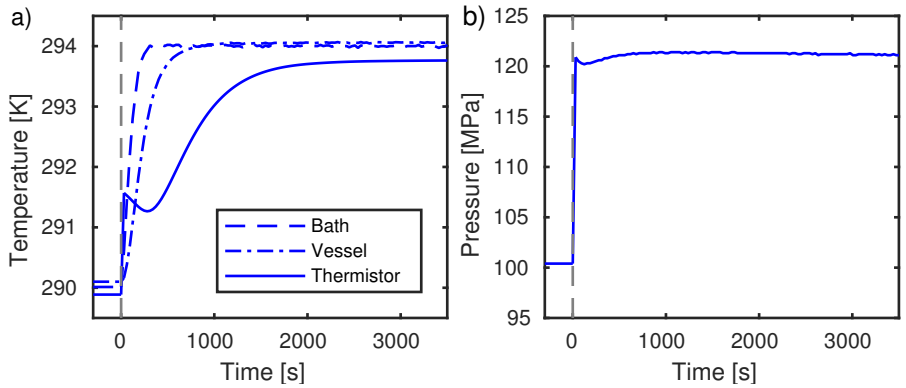

Figure 8.10: An isochronal jump with a temperature up jump on 4 K and a pressure up jump on 20 MPa. (a) The temperature as a function of time. (b) The pressure as a function of time.

both temperature and pressure are raised. The temperature is changed 4 K and the pressure is changed 20 MPa (which we expect corresponds to an isochronal jump for 5PPE (see Section 8.1.3)). The time it takes to come into pressure/temperature equilibrium corresponds to the time for the pressure jump and temperature jump (i.e. approximately 2500 s to reach thermal equilibrium), which means that the pressure jump has no clear effect on the time for reaching thermal equilibrium.

The next section shows temperature and pressure tests with the new temperature regulator.

8.3.2 Temperature and pressure tests with temperature regulator

This section investigates the time it takes to come into thermal/pressure equilibrium after respectively temperature, pressure, and isochronal jumps using the new temperature regulator (Section 8.2.3). During these tests, the dielectrics, at a fixed frequency of the liquid 5PPE, are measured to monitor when the thermal/pressure equilibrium is reached. The state points for these tests are chosen so the relaxation time of the liquid is between 0.02 s and 0.5 s. Therefore no aging occurs, and any change of the dielectrics reflects pressure and temperature changes. Figure 8.11 shows the dielectric spectra at the selected state points along with the chosen measuring frequency 17.8 Hz used for monitoring the liquid.

Five different jumps are made: a temperature up jump, a temperature down jump, a pressure up jump, a pressure down jump, and an isochronal up jump, where both temperature and pressure are raised. Furthermore, different temperature overshoot jumps are performed, where the temperature of the

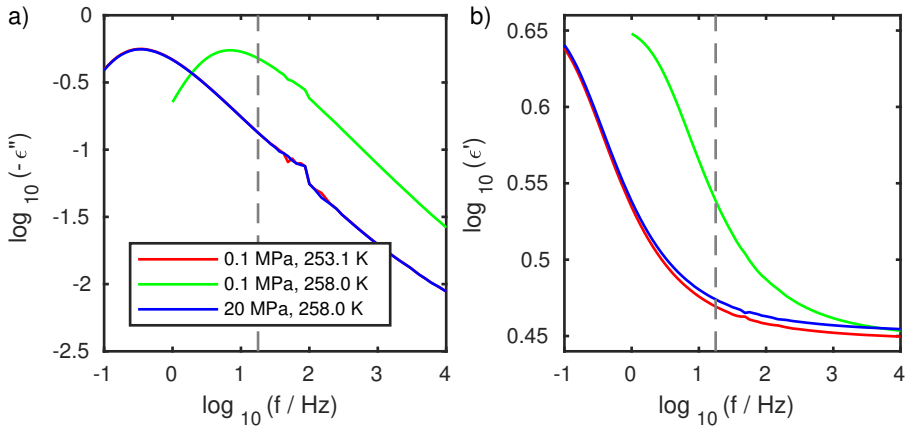

Figure 8.11: The dielectric spectra at three chosen state points used for the temperature tests. The frequency used for monitoring during the jumps is illustrated by the gray line.

regulator is set some degrees above the wanted temperature for a limited time, after which the temperature is set to the wanted temperature. The jumps are illustrated in Figure 8.12 (a).

As an example, the temperature jumps are presented in Figure 8.12 (b), which shows the dielectric loss as a function of time. The other jumps are shown in Appendix C.2. The best overshoot jump for the temperature up jump is also shown. The temperature overshoots for temperature up and isochronal up jump are used in the final measurements. It is clear that the temperature jumps, especially the down jump, requires a long time to reach thermal equilibrium. However, using overshoots of the temperature on the heating element around the sample, most jumps can be performed so that thermal and pressure equilibrium is established within 800 s or less. Only for the temperature down jump and, presumably, also an isochronal down jump the thermal equilibrium is only established in around 1500 s.

Figure 8.12 (c) shows the temperature at the thermistor at the heating element as a function of time. As seen, this temperature comes into equilibrium faster than the sample, which suggests that we can not directly compare the results of the temperature tests with the temperature regulator and the tests with the thermal bath (where we only monitored the temperature using the thermistor). However, it is clear that the jumping time for the temperature up jump, for example, is decreased around 12 times with the temperature regulator.

To ensure that no structural changes take place in the liquid, the relaxation time has to be much slower than the temperature/pressure equilibrium time. It is estimated that the liquid is slow enough when $\log_{10}(\tau/s) = 4.2$, which is more than 20 times the time it takes to change the state point (Section 8.1.4).

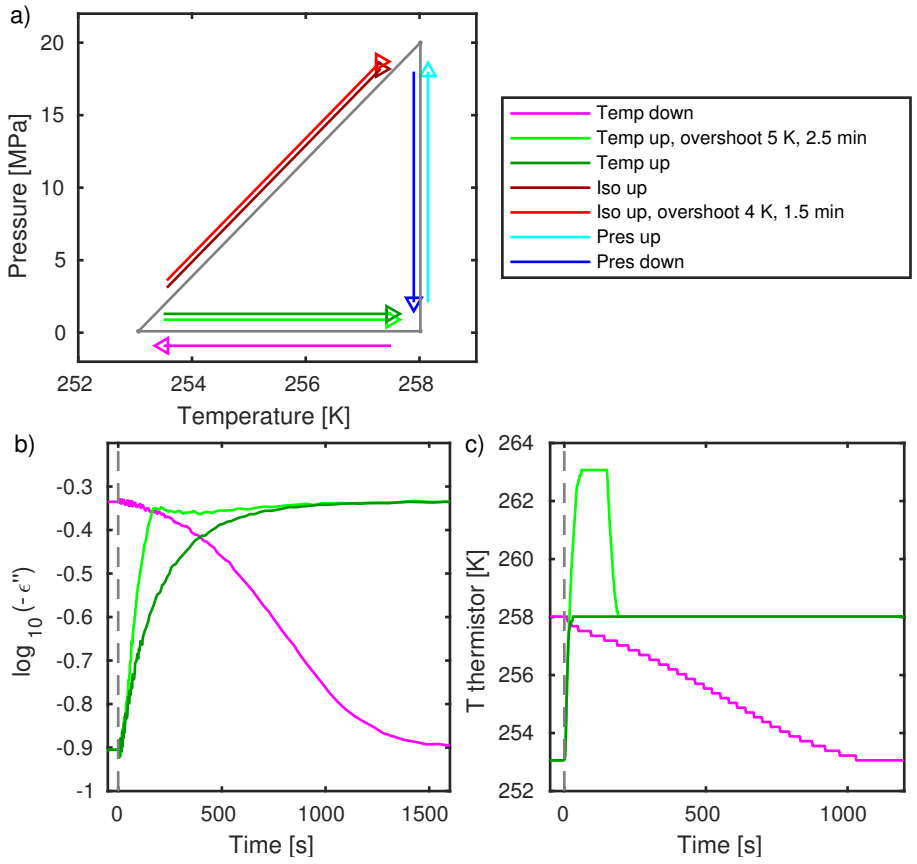

Figure 8.12: Thermal/pressure equilibrium tests with the temperature regulator. (a) Illustration of the used state points and jumps. (b) The dielectric loss as a function of time following the temperature jumps. (c) The temperature at the thermistor at the 'heating element' for temperature regulation.

8.4 Measurements

This section shows the results of the isochronal jump investigation. As described in Section 8.1.3, we make the isochronal jumps with a pressure change of 20 MPa. The jumps are performed between atmospheric pressure (0.1 MPa) and 20 MPa. We make the isochronal jumps along the isochrone with $\log_{10}(\tau) = 4.2$. The sample liquid is 5PPE, and the fixed measuring frequency during the jumps is 0.0205 Hz. Section 8.4.1 shows the dielectric equilibrium spectra at different temperatures along the isobars 0.1 and 20 MPa, and it is estimated at which state points $\log_{10}(\tau) = 4.2$. Section 8.4.2 shows the jump measurements.

8.4.1 Equilibrium spectra

The dielectric equilibrium spectra for 5PPE made, respectively, along the atmospheric pressure isobar (0.1 MPa) and the 20 MPa isobar are seen in Figure 8.13. For the equilibrium spectra at 20 MPa (Figure 8.13 (c) and (d)), four larger gaps between the spectra are seen, even though the temperature interval between all the spectra is around 1 K. This is due to the pressure stability of the pump on 3 MPa, and the larger distances are seen at times where the pump has just pumped the 3 MPa (see Section 4.1). For the spectra where the α-peak is present in the available frequency range, the loss peak frequency f_m is found using a second order polynomial fit. The loss peak frequencies are shown as a function of temperature for the two isobars in Figure 8.14. Again, it is clear in the 20 MPa data that the stability of the pump affects the measurements.

As estimated in Section 8.1.4, we aim for the liquid to have $\log_{10}(f_m) \approx -5$ during the isochronal jump in order to assume that no structural relaxation occurs in the liquid during the temperature/pressure jump. Since this frequency is outside the available frequency range, it is necessary to estimate these state points. We first estimate the state point at atmospheric pressure using the imaginary spectra at atmospheric pressure from Figure 8.13 (a). Three different methods for estimating this temperature are used: a shift-factor method, a linear extrapolation method, and a fit to the Vogel-Fulcher-Tammann (VFT) equation.

For the shift-factor method, a 'main' spectrum is chosen, which is a spectrum where the α-peak is present (see Figure 8.15 (a)). The spectra with longer relaxation times are then shifted to the right until they are on top of the main spectrum as shown in Figure 8.15 (b). The loss peak frequencies f_m are then estimated, assuming that the shift of the loss peak frequencies is the same as the shift of the right flank of the α-peak in the spectra

$$\log_{10}(f_m) = \log_{10}(f_{m,\text{main}}) + \text{shift-factor} \tag{8.5}$$

where $f_{m,\text{main}}$ is the loss peak frequency at the main spectrum and the shift-factor is the temperature-dependent factor that each spectrum is shifted to place it on top of the main spectrum. It is clear that the shift-factor method is not perfect, due to the noise and systematic errors in the spectra. The result

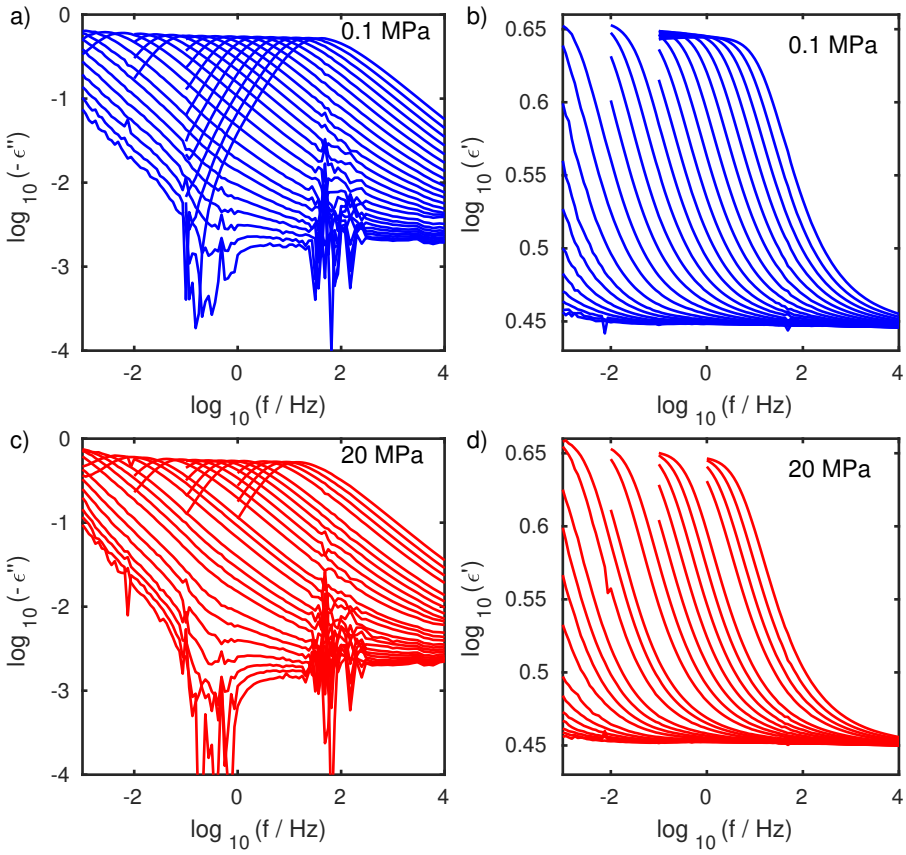

Figure 8.13: Dielectric equilibrium spectra. (a) and (b) Atmospheric pressure with the temperature span 260.9 K - 237.1 K. (c) and (d) 20 MPa with the temperature span 264 K - 240 K.

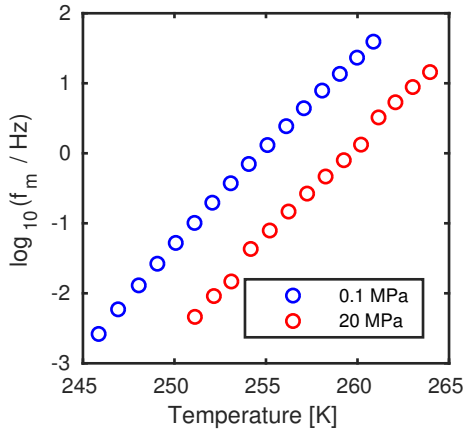

Figure 8.14: Loss peak frequencies f_m as functions of temperature along the two isobars.

is shown in Figure 8.16 (a). Figure 8.16 (b) shows a fit of the data to the Vogel-Fulcher-Tammann (VFT) equation

$$\tau = \tau_0 \cdot \exp\left(\frac{A}{T - T_0}\right) \tag{8.6}$$

where an extrapolation is used to find the wanted temperature. The VFT-fit, however, has been shown only to be good for interpolation and not extrapolation [114], so it is important to notice that this is only an approximation. Figure 8.16 (c) shows a linear extrapolation used to find the wanted temperature. The linear fit is made with the three lowest temperatures. The shift-factor method gives a temperature around 238 K, the linear extrapolation gives a temperature around 238.2 K, and the extrapolation of the VFT-fit gives a temperature around 238.8 K. The used temperature is chosen to be 238.0 K, which is the lowest of the three methods.

The temperature of the corresponding isochronal state point at 20 MPa is chosen so that the dielectric loss at the measuring frequency is the same as for the atmospheric pressure state point (238.0 K, 0.1 MPa). This gives the state point (241.9 K, 20 MPa). Furthermore, the state point (241.9 K, 0.1 MPa) is used to perform pressure and temperature jumps between the two other state points, and, thereby, jumps between two isochrones along different paths. Note that this state point has a shorter relaxation time than the two other state points resulting in the liquid being faster at this state point. The spectra at the three state points are seen in Figure 8.17.

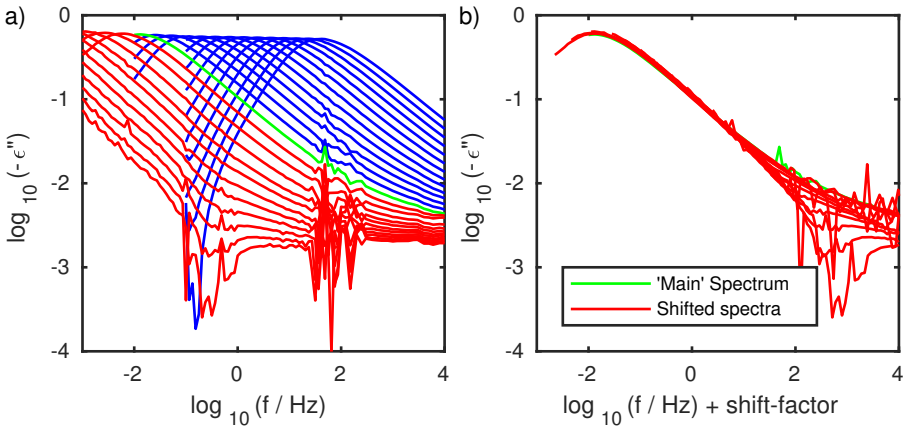

Figure 8.15: Shift-factor method. (a) The spectra at atmospheric pressure. The green spectrum is the 'main'-spectrum, and the red spectra are the spectra that are shifted. (b) The main spectrum and the shifted spectra.

8.4.2 Isochronal jumps

Respectively, up and down isochronal, temperature and pressure jumps are performed between the three chosen state points. Figure 8.18 (a) illustrates the state points and the performed jumps. During the jumps, the dielectrics are measured at $f_{\text{measure}} = 0.0205$ Hz as a function of time. This gives both a real part and an imaginary part of the dielectrics. The data is averaged in the same way as with the aging data following temperature jumps, as described in Section 7.4.

Figures 8.18 (b) and (c) respectively show how the real part of the dielectrics (ε') and the dielectric loss ($-\varepsilon''$) evolve as functions of time. It is clear that the temperature down jump, the pressure up jump and the isochronal down jump have two different regimes in the measured time interval, with a change around $\log_{10}(t/s) \approx 3.3$. The temperature down jump and the pressure up jump both start at the state point with a relaxation time around $\log(\tau/s) = 3.1$. This short relaxation time implies that the liquid reacts immediately to the temperature/pressure change. The second regime occurs when the temperature/pressure equilibrium is established and the change of the dielectrics comes from structural changes. The isochronal down jump has a large relaxation time to begin with, however, since the pressure changes much faster than the temperature, the liquid is brought to a state point with a faster relaxation time before the temperature comes into equilibrium (following the blue dashed line in Figure 8.1 (a)). We can, therefore, not assume that no structural changes take place in the liquid during the isochronal down jump, the temperature down jump, and the pressure up jump, and these jumps can therefore not be considered as instantaneous.

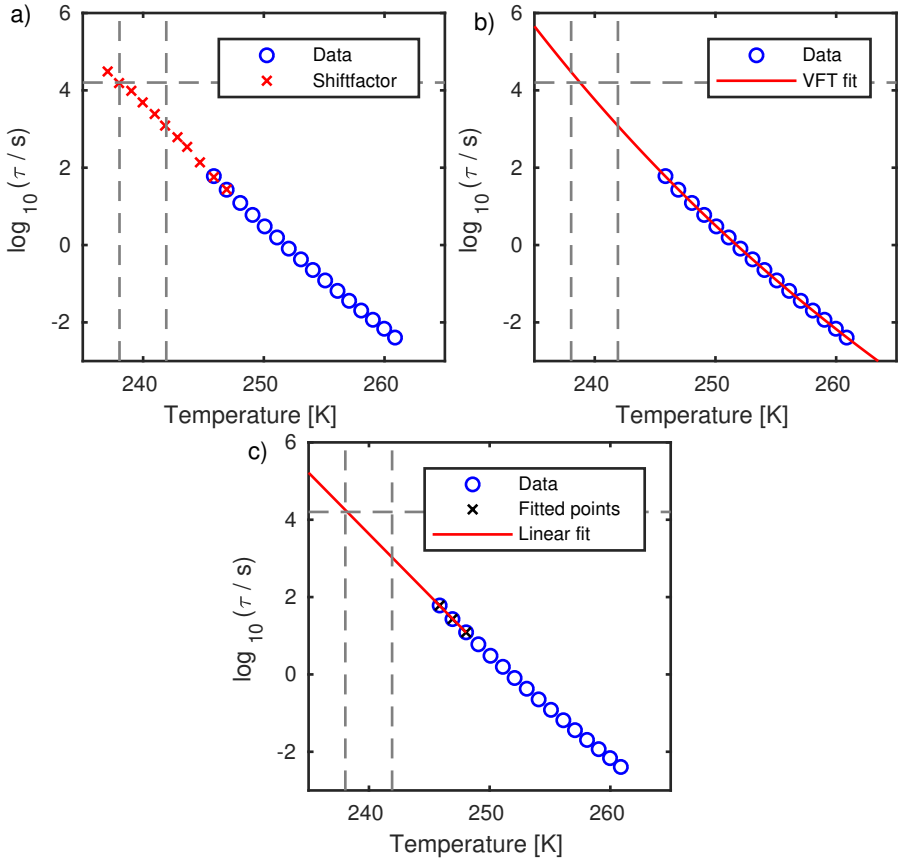

Figure 8.16: Estimation of temperature with $\log_{10}(\tau) = 4.2$ in three different ways. (a) Shift-factor method. (b) Extrapolation of a VFT-fit. (c) Linear extrapolation. The horizontal gray line shows the wanted relaxation time, and the vertical gray lines respectively show the used temperature at the state point, with high relaxation time and the used temperature at the state point with lower relaxation time.

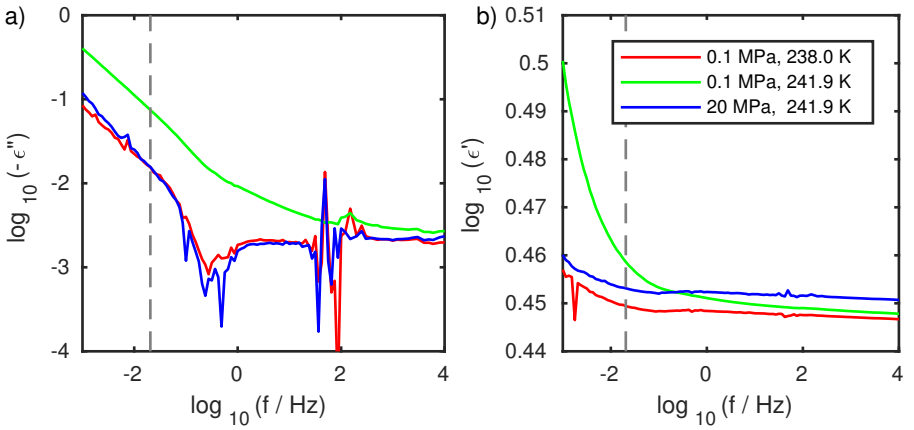

Figure 8.17: Dielectric equilibrium spectra at the three chosen state points. The fixed measuring frequency used for the jumps is illustrated by the gray line.

Jump	$\log_{10}(\tau_{\text{before}})$	$\log_{10}(\tau_{\text{after}})$	$\log_{10}(t_{\text{eq}})$	$\frac{\tau_{\text{before}}}{t_{\text{eq}}}$
Iso up	≈ 4.2	≈ 4.2	≈ 2.9	≈ 20
Iso down	≈ 4.2	≈ 4.2	≈ 3.2	≈ 11
Temp up	≈ 4.2	≈ 3.1	≈ 2.3	≈ 80
Temp down	≈ 3.1	≈ 4.2	≈ 3.2	≈ 0.8
Pres down	≈ 4.2	≈ 3.1	≈ 2.3	≈ 80
Pres up	≈ 3.1	≈ 4.2	≈ 2.8	≈ 2

Table 8.1: Estimated τ_{before} and τ_{after} for the six different jumps. Furthermore, the time to reach temperature/pressure equilibrium (t_{eq}) after each jump type is shown (found in Section 8.3.2). The relationship between these times are stated.

In Table 8.1, the relaxation times at the different state points (estimated from Figure 8.16) are compared to the time it takes to reach thermal/pressure equilibrium after the different jumps (estimated from Section 8.3.2). From the table, it is clear that the relaxation time at the starting point for the temperature down and pressure up jump is about the same size as the time it takes to come into temperature/pressure equilibrium. This again suggests that these jumps can not be considered as instantaneous jumps, and they are therefore not used in the subsequent data treatment. The isochronal down jump is also not used, since structural changes might have taken place during the jump.

Figure 8.19 shows the real and the imaginary part of the dielectrics for the three jumps: isochronal up jump, temperature up jump, and pressure down jump. The part of the measurements where temperature/pressure equilibrium is not established are cut off. The results are shown on both a linear and

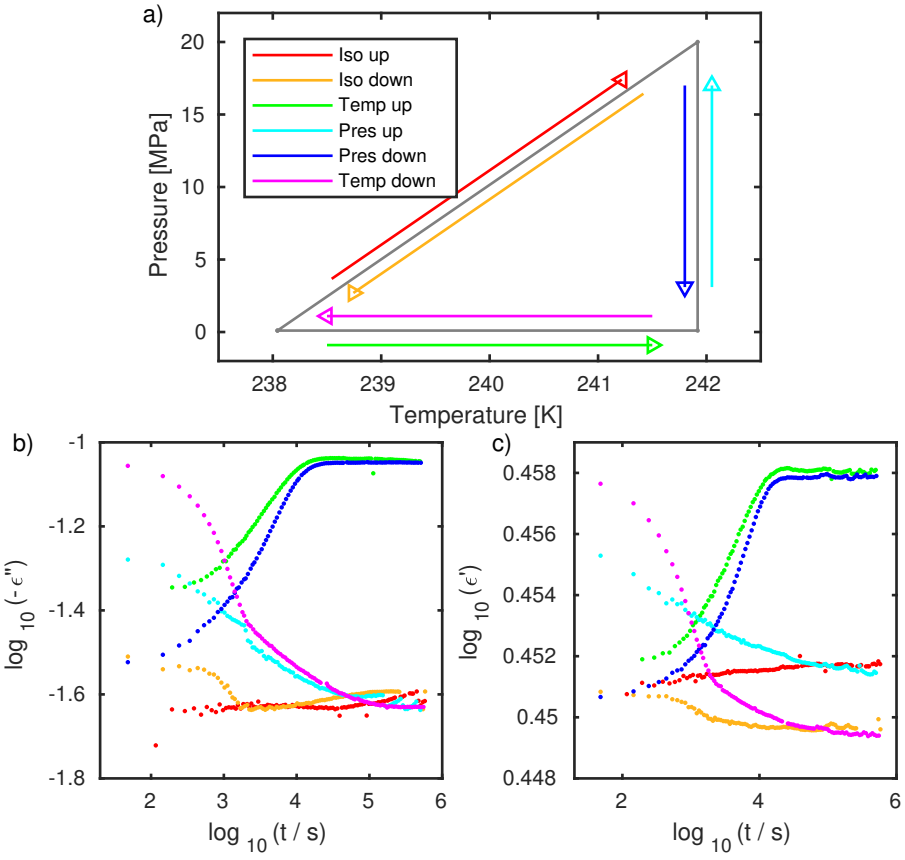

Figure 8.18: (a) Illustration of the used state points and the performed jumps. (b) The dielectric loss at the fixed frequency as a function of time following the different jumps. (c) The real part of the dielectrics at the fixed frequency as a function of time following the different jumps.

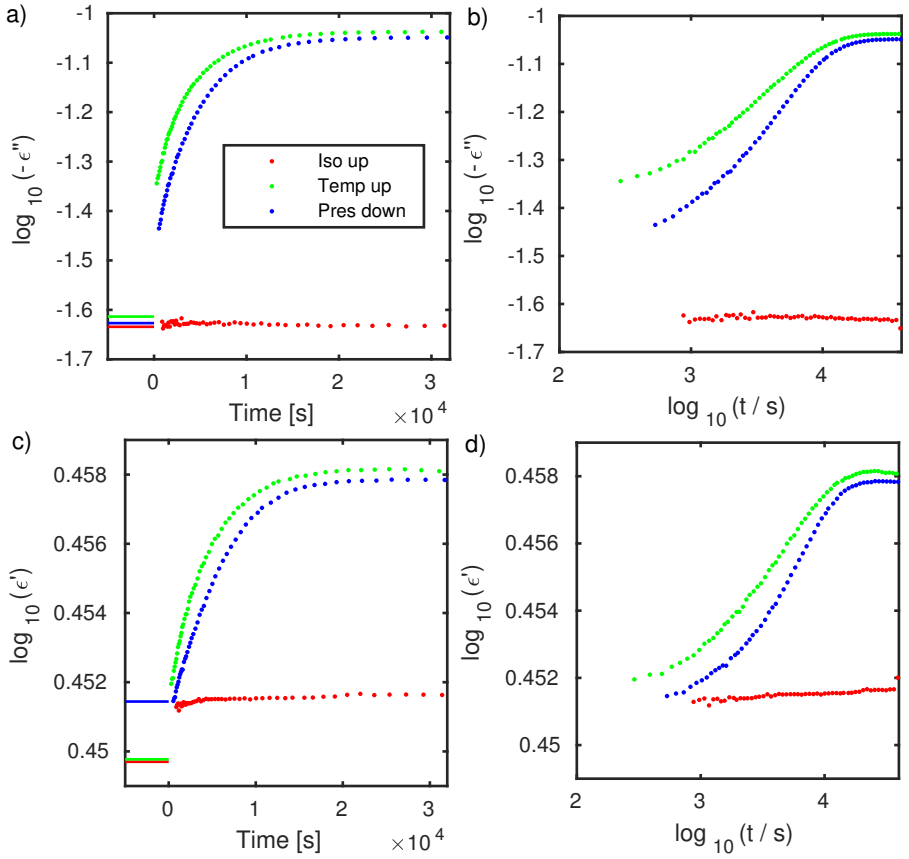

Figure 8.19: The imaginary ((a) and (b)) and real ((c) and (d)) part of the dielectrics following the jumps, shown on respectively a linear (left) and a logarithmic (right) time scale.

a logarithmic time scale. For the isochronal jump, equilibrium is reached instantaneously as predicted by the isomorph theory. Note that the loss should be the same before and after the jump, but for the real part, there should be change (as seen on Figure 8.19 (c)).

The isomorph theory furthermore predicts that the relaxation following jumps from one isochrone to another isochrone along different paths should be the same [25]. This means that we expect that the relaxation for the temperature up jump and the pressure down jump are the same, but as seen on Figure 8.19, this is not the case. For example, it is clear that the instantaneous contribution to the relaxation is different for the two jumps. In order to investigate this further, the normalized relaxation function $R(t)$ is found. The normalized relaxation function for the real part of the dielectrics $R_{\text{real}}(t)$ for a jump from

(T_1, P_1) to (T_2, P_2) is defined as the time-dependent distance to equilibrium over the overall change of the real part of the dielectrics:

$$R_{\text{real}}(t) = \frac{\log_{10}(\varepsilon'(f, T_2, P_2, t)) - \log_{10}(\varepsilon'(f, T_2, P_2, t \to \infty))}{\log_{10}(\varepsilon'(f, T_1, P_1, t = 0)) - \log_{10}(\varepsilon'(f, T_2, P_2, t \to \infty))} \tag{8.7}$$

where f is the fixed measuring frequency and t is the time after the jump is performed. For an isochronal jump, $R_{\text{real}}(t)$ should be 0, if equilibrium is reached instantaneously. The normalized relaxation function for the dielectric loss $(-\varepsilon'')$ $R_{\text{imag}}(t)$ is defined as:

$$R_{\text{imag}}(t) = \frac{\log_{10}(-\varepsilon''(f, T_2, P_2, t)) - \log_{10}(-\varepsilon''(f, T_2, P_2, t \to \infty))}{\log_{10}(-\varepsilon''(f, T_1, P_1, t = 0)) - \log_{10}(-\varepsilon''(f, T_2, P_2, t \to \infty))} \tag{8.8}$$

where f is the fixed measuring frequency and t is the time after the jump is performed. $R_{\text{imag}}(t)$ is not defined for an isochronal jump, since the denominator in this case is 0. The Figures 8.20 (a) and (b) respectively show $R_{\text{imag}}(t)$ and $R_{\text{real}}(t)$. It is seen that the pressure down and the temperature up jump do not collapse, which is, of course, no surprise, because of the difference in the instantaneous contribution for the two jumps. Figure 8.20 (b) also shows that $R_{\text{real}}(t)$ is not 0 for the isochronal jump. However, the change of signal over time is due to the decrease of pressure during the measurements due to the limited stability of the pressure (see Section 4.1).

To further investigate the shape of the relaxation, we try to scale, respectively, $R_{\text{real}}(t)$ and $R_{\text{imag}}(t)$ to place them in top of each other as seen in the Figures 8.20 (c) and (d). This is done by hand. The shape of the relaxation is similar, however, it is difficult to make any final conclusions from the figures.

We believe that the reason for these two jumps not having the same relaxation curve may stem from the different instantaneous contributions to the relaxation. In fact, when looking at Figure 8.19 (c), the instantaneous contribution following the pressure down jump seems to be close to 0. We believe that changes of the geometry of the capacitor may result in a wrong instantaneous contribution. During the pressure down jump, the distance between the capacitor plates may increase as the pressure is released (and they are therefore not pressed together anymore) resulting in a lower signal (since $C = \frac{\varepsilon \varepsilon_0 A}{d}$). However, we need to make further investigations to fully understand the results as described in the next section.

Another study which investigates a systems properties following different paths in the pressure/temperature phase diagram is made in Casalini and Roland (2017) [115]. They studied pressure densification for the van der Waals-bonded liquid DC704, using the real part of the dielectrics at high frequencies from which the density can be determined. The approach is to go from a state point above T_g to a state point below T_g along two different paths. One path is purely cooling between the two state points. The other path is to first compress the liquid, then cool through the glass transition, and at last, decompress again. Because the liquid is Roskilde-simple, it is expected that the measured property

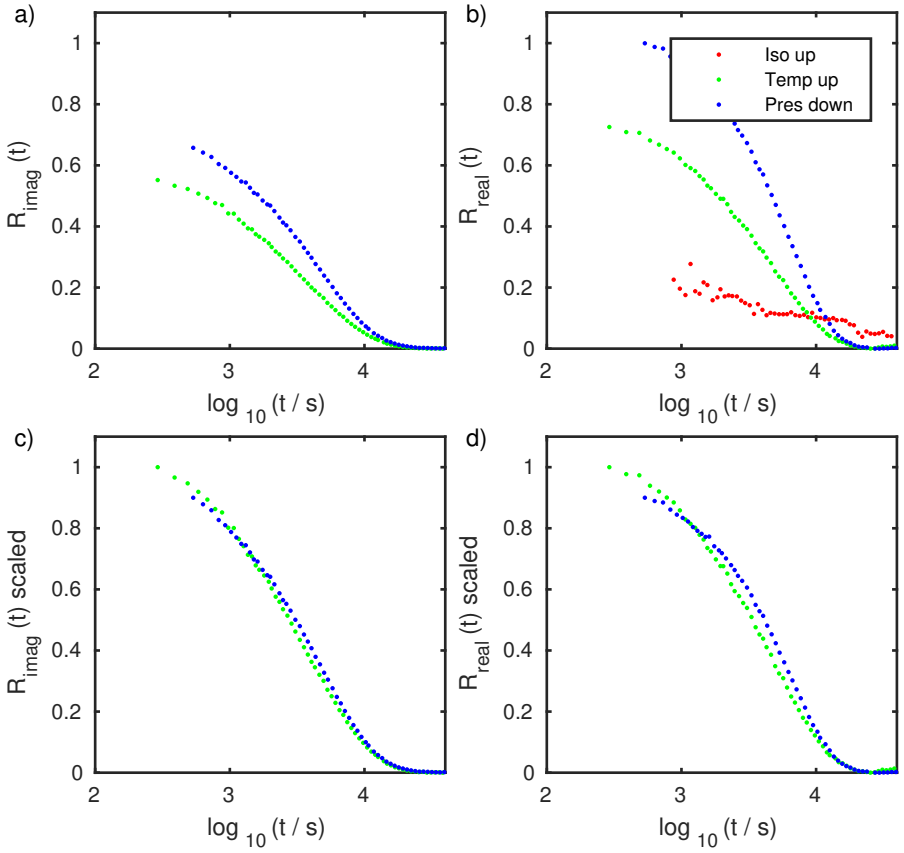

Figure 8.20: The normalized relaxation function $R(t)$. (a) $R_{\mathrm{imag}}(t)$. (b) $R_{\mathrm{real}}(t)$. (c) $R_{\mathrm{imag}}(t)$ where the jumps are scaled to be on top of each other. (d) $R_{\mathrm{real}}(t)$ where the jumps are scaled to be on top of each other.

ends at the same value, regardless of the path. However, Casalini and Roland show that the density is larger following path number two; the liquid, therefore, is said to undergo pressure densification. The capacitor used in Casalini and Roland (2017) [115] has a fixed spacing between the capacitor plates and a reservoir of liquid surrounding the capacitor allowing for liquid to flow into the capacitor. The result of Casalini and Roland (2017) may be rationalized by taking this capacitor geometry into account, and the fact that a system in the glass state cannot flow radially. This results in a higher density and thereby a larger capacitance following path number two [116].

Thus, the present investigation and the study of Casalini and Roland both show that it is important to take the geometry of the capacitor into account when performing high-pressure dielectric spectroscopy in the very viscous/glassy range.

8.5 Concluding remarks and perspective

In this investigation, we performed preliminary measurements of the isochronal jump and jumps between isochrones for the sample liquid 5PPE. We conclude that the liquid comes into instantaneous equilibrium following an isochronal jump as predicted by the isomorph theory. The results are discussed in relation to the isomorph theory in Chapter 9.

As part of the investigation, we made developments on the pressure setup: a new sample cell to increase the signal and thereby reduce noise, a new electronic setup to avoid influence of leak currents, and a temperature regulation that increased the speed of the temperature jump more than 10 times.

We think it would be interesting to perform more jumps to investigate what happens with the relaxation along and across the isochrones. Below, some ideas for investigations are presented. The jumps are illustrated in Figure 8.21.

- Compare two different temperature up jumps from one isochrone to another (the red jumps).
- Compare two different pressure down jumps from one isochrone to another (the green jumps). This will give some challenges with the pump in the existing setup.
- Temperature and pressure jumps, that are not between the two isochrones, but the same size (the dashed jumps).
- Stay in the slow part of the phase diagram during the isochronal jump, i.e. isochronal up jumps. By performing larger isochronal jumps, one might be even more sure to be in the slow part (the blue jump).

The first three points are important to investigate the different instantaneous contributions to the relaxation following temperature and pressure jumps.

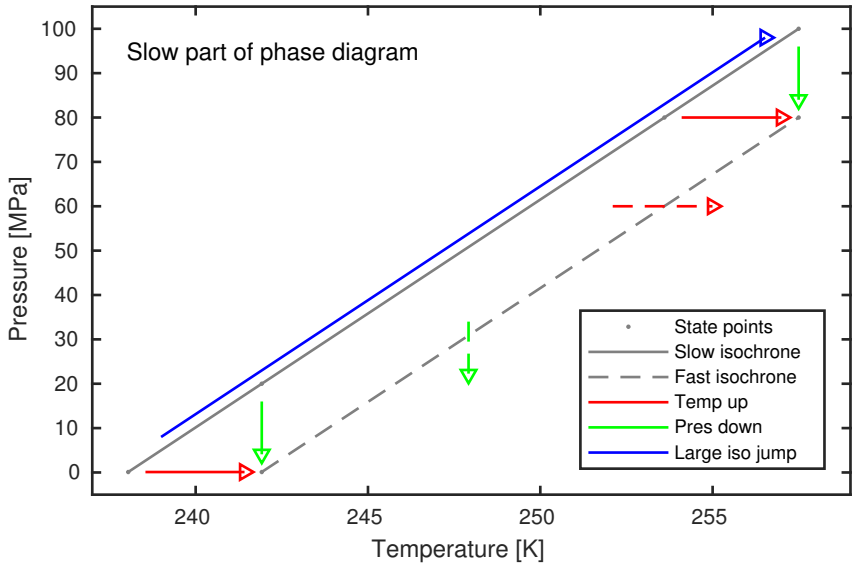

Figure 8.21: Examples of jumps that are interesting to perform.

Furthermore, it is important to measure on more liquids, including different types of liquids, such as hydrogen-bonded liquids that are not expected to be Roskilde-simple.

Chapter 9

Concluding remarks – Simplicity of supercooled liquids and the relation to the isomorph theory

The four investigations carried out in the laboratory at Roskilde University all have the purpose of exploring simple behavior of supercooled liquids. This is, of course, interesting in itself, but the isomorph theory suggested a decade ago predicts simple behavior along isomorphs for Roskilde-simple liquids, resulting in predictions such as density scaling, isochronal superposition, and instantaneous equilibrium following a jump along an isochrone. Van der Waals-bonded liquids are expected to be Roskilde-simple, whereas hydrogen-bonded liquids are not. The isomorph theory does not give predictions for hydrogen-bonded liquids, however, it is still interesting to investigate whether the hydrogen-bonded liquids also have simple behavior. Therefore, both types of liquids are studied in two of the investigations. Below, we gather the results from the investigations, and compare them to the predictions of the isomorph theory. As an overall conclusion of the investigations, the van der Waals liquids follow the predictions from the isomorph theory. Several of the liquids are also shown to have even greater simplicity that was predicted by the isomorph theory. It is also seen that the investigated hydrogen-bonded liquids also have some simple behavior to a good approximation. In fact, we conclude that both types of liquids have single-parameter aging.

9.1 Relaxation spectrum

The investigation of isochronal superposition in Chapter 5 is a direct test of a prediction from the isomorph theory, implying that the shape of the relaxation spectrum is invariant along an isochrone. We test isochronal superposition for both hydrogen-bonded liquids and van der Waals-bonded liquids. We conclude that there is a difference between the two types of liquids' ability to obey isochronal superposition, and that the van der Waals liquids in fact obey isochronal superposition within the experimental uncertainties. This is supported by other investigations of isochronal superposition [13, 14, 16–21], including dielectric and scattering measuring methods. Furthermore, our investigation of isochronal superposition also shows that some of the investigated van der Waals-bonded liquids obey time temperature pressure superposition (TTPS) to a good approximation, implying that the shape of the relaxation spectrum is invariant at all investigated temperatures and pressures. It is furthermore clear that the studied hydrogen-bonded liquids do not obey TTPS.

If a liquid obeys TTPS, it follows that the liquid also obeys time temperature superposition (TTS), where the shape of the relaxation spectrum is temperature invariant. Hecksher *et al.* (2013) [113] showed TTS for the two van der Waals-bonded liquids 5PPE and DC704, using the frequency-dependent bulk modulus and the shear mechanical relaxation, and revealed that the relaxation of these two moduli, in fact, have the same shape. This is all simple behavior that is beyond the predictions from the isomorph theory.

In Xiao *et al.* (2015) [63] they derive and test a direct prediction from the isomorph theory regarding the variation of the amplitude of the dielectric loss along the isochrones. They show that they can predict the amplitude variation for the van der Waals-bonded liquid 5PPE, which therefore obeys the prediction from the isomorph theory.

9.2 Relaxation times from different response functions

Our investigation of comparing the characteristic times of specific heat spectroscopy and dielectric spectroscopy in Chapter 6 is inspired by the isomorph theory, but reveals even simpler behavior for the studied van der Waals-bonded liquid, 5PPE. The isomorph theory predicts that an isochrone for one response function is also an isochrone for another response function, possibly associated with different time scales. This is confirmed by our investigation, which furthermore shows that the time-scale difference between the isochrones of the two methods is constant in all parts of the investigated phase diagram, which is a greater simplicity than predicted by the isomorph theory.

Jakobsen *et al.* (2012) [79] furthermore showed that at ambient pressure, not only the dielectric and specific heat time scales, but also time scales for several other response functions follow each other for the two van der Waals

liquids, 5PPE and DC704. Based on this, we assume that the time scales of all the frequency-dependent response functions of 5PPE have a common temperature and pressure dependence resulting in an "inner clock", meaning that the time scales for the different response functions are proportional. The inner clock theory is also supported by an aging investigation by our group Hecksher *et al.* (2010) [52] which suggests that the studied liquids (all van der Waals bonded) have an "internal clock", meaning that the time scales of the structural relaxation and the dielectric response, respectively, are proportional.

9.3 Aging

Aging is investigated in the Chapters 7 and 8. In Chapter 8, we performed a test of a direct prediction of the isomorph theory, namely that the system comes into instantaneous equilibrium following a jump along an isochrone: an isochronal jump. Our measurements suggest that the used van der Waals-bonded liquid 5PPE come into equilibrium instantaneously following an isochronal jump, and thereby obey the prediction.

In Chapter 7, we studied aging following temperature jumps, where the isomorph theory inspired our hypothesis that van der Waals have simpler behavior than hydrogen-bonded liquids, also during aging. The isomorph theory, however, gives no predictions about this aging following temperature jumps, but work is done to reveal possible relations between aging and the isomorph theory [46]. We investigate whether different liquids have single-parameter aging, meaning that a single parameter controls both the structural relaxation and the measured property. Hecksher *et al.* (2015) [28] demonstrated single-parameter aging to a good approximation for three different van der Waals liquids. Our investigation for the first time applied these test to hydrogen-bonded liquids. We conclude that the studied hydrogen-bonded liquids glycerol and 1,2,6-HT also have single-parameter aging to a good approximation, and that there is no difference between hydrogen-bonded and van der Waals-bonded liquids' ability to obey single-parameter aging.

Chapter 10

Bibliography

[1] G. P. Johari, "Introduction to the glassy state in the undergraduate curriculum," *Journal of Chemical Education*, vol. 51, p. 23, 1974.

[2] R. Cotterill, *The Cambridge guide to the material world*. Cambridge: Cambridge University Press, 1985.

[3] W. Kauzmann, "The nature of the glassy state and the behavior of liquids at low temperatures," *Chemical Reviews*, vol. 43, p. 219, 1948.

[4] J. C. Dyre, "Colloquium: The glass transition and elastic models of glass-forming liquids," *Reviews of Modern Physics*, vol. 78, p. 953, 2006.

[5] P. G. Debenedetti, *Metastable liquids: concepts and principles*. Princeton, N.J.: Princeton University Press, 1996.

[6] S. Brawer, *Relaxation in viscous liquids and glasses, review of phenomenology, molecular dynamics simulations, and theoretical treatment*. Columbus, Ohio: American Ceramic Society, 1985.

[7] K. Niss, C. Dalle-Ferrier, G. Tarjus, and C. Alba-Simionesco, "On the correlation between fragility and stretching in glass-forming liquids," *Journal of Physics: Condensed Matter*, vol. 19, p. 076102, 2007.

[8] C. Dreyfus, A. Aouadi, J. Gapinski, M. Matos-Lopes, W. Steffen, A. Patkowski, and R. Pick, "Temperature and pressure study of brillouin transverse modes in the organic glass-forming liquid orthoterphenyl," *Physical Review E*, vol. 68, p. 011204, 2003.

[9] C. Alba-Simionesco, A. Cailliaux, A. Alegría, and G. Tarjus, "Scaling out the density dependence of the α relaxation in glass-forming polymers," *Europhysics Letters*, vol. 68, p. 58, 2004.

[10] C. Dreyfus, A. Le Grand, J. Gapinski, W. Steffen, and A. Patkowski, "Scaling the α-relaxation time of supercooled fragile organic liquids," *The European Physical Journal B*, vol. 42, p. 309, 2004.

[11] R. Casalini and C. Roland, "Thermodynamical scaling of the glass transition dynamics," *Physical Review E*, vol. 69, p. 062501, 2004.

[12] C. Roland, S. Hensel-Bielowka, M. Paluch, and R. Casalini, "Supercooled dynamics of glass-forming liquids and polymers under hydrostatic pressure," *Reports on Progress in Physics*, vol. 68, p. 1405, 2005.

[13] C. Roland, R. Casalini, R. Bergman, and J. Mattsson, "Role of hydrogen bonds in the supercooled dynamics of glass-forming liquids at high pressures," *Physical Review B*, vol. 77, p. 012201, 2008.

[14] K. Adrjanowicz, J. Pionteck, and M. Paluch, "Isochronal superposition and density scaling of the intermolecular dynamics in glass-forming liquids with varying hydrogen bonding propensity," *RSC Advances*, vol. 6, p. 49370, 2016.

[15] K. Ngai and M. Paluch, "Corroborative evidences of TV γ-scaling of the α-relaxation originating from the primitive relaxation/JG β relaxation," *Journal of Non-Crystalline Solids*, vol. 478, p. 1, 2017.

[16] A. Tölle, "Neutron scattering studies of the model glass former orthoterphenyl," *Reports on Progress in Physics*, vol. 64, p. 1473, 2001.

[17] C. Roland, R. Casalini, and M. Paluch, "Isochronal temperature–pressure superpositioning of the α-relaxation in type-A glass formers," *Chemical Physics Letters*, vol. 367, p. 259, 2003.

[18] S. Pawlus, M. Paluch, M. Sekula, K. Ngai, S. Rzoska, and J. Ziolo, "Changes in dynamic crossover with temperature and pressure in glass-forming diethyl phthalate," *Physical Review E*, vol. 68, p. 021503, 2003.

[19] S. Hensel-Bielowka, S. Pawlus, C. Roland, J. Zioło, and M. Paluch, "Effect of large hydrostatic pressure on the dielectric loss spectrum of type-A glass formers," *Physical Review E*, vol. 69, p. 050501, 2004.

[20] K. Ngai, R. Casalini, S. Capaccioli, M. Paluch, and C. Roland, "Do theories of the glass transition, in which the structural relaxation time does not define the dispersion of the structural relaxation, need revision?," *The Journal of Physical Chemistry B*, vol. 109, p. 17356, 2005.

[21] H. W. Hansen, A. Sanz, K. Adrjanowicz, B. Frick, and K. Niss, "Evidence of a one-dimensional thermodynamic phase diagram for simple glass-formers," *Nature Communications*, vol. 9, p. 518, 2018.

[22] N. P. Bailey, U. R. Pedersen, N. Gnan, T. B. Schrøder, and J. C. Dyre, "Pressure-energy correlations in liquids. I. Results from computer simulations," *The Journal of Chemical Physics*, vol. 129, p. 184507, 2008.

[23] N. P. Bailey, U. R. Pedersen, N. Gnan, T. B. Schrøder, and J. C. Dyre, "Pressure-energy correlations in liquids. II. Analysis and consequences," *The Journal of Chemical Physics*, vol. 129, p. 184508, 2008.

[24] T. B. Schrøder, N. P. Bailey, U. R. Pedersen, N. Gnan, and J. C. Dyre, "Pressure-energy correlations in liquids. III. Statistical mechanics and thermodynamics of liquids with hidden scale invariance," *The Journal of Chemical Physics*, vol. 131, p. 234503, 2009.

[25] N. Gnan, T. B. Schrøder, U. R. Pedersen, N. P. Bailey, and J. C. Dyre, "Pressure-energy correlations in liquids. IV."Isomorphs" in liquid phase diagrams," *The Journal of Chemical Chysics*, vol. 131, p. 234504, 2009.

[26] T. B. Schrøder, N. Gnan, U. R. Pedersen, N. P. Bailey, and J. C. Dyre, "Pressure-energy correlations in liquids. V. Isomorphs in generalized Lennard-Jones systems," *The Journal of Chemical Physics*, vol. 134, p. 164505, 2011.

[27] J. C. Dyre, "Hidden scale invariance in condensed matter," *The Journal of Physical Chemistry B*, vol. 118, p. 10007, 2014.

[28] T. Hecksher, N. B. Olsen, and J. C. Dyre, "Communication: Direct tests of single-parameter aging," *The Journal of Chemical Physics*, vol. 142, p. 241103, 2015.

[29] L. Bøhling, T. S. Ingebrigtsen, A. Grzybowski, M. Paluch, J. C. Dyre, and T. B. Schrøder, "Scaling of viscous dynamics in simple liquids: theory, simulation and experiment," *New Journal of Physics*, vol. 14, p. 113035, 2012.

[30] M. P. Allen and D. J. Tildesley, *Computer simulation of liquids*. Oxford: Oxford University Press, 1987.

[31] J. P. Hansen and I. R. McDonald, *Theory of simple liquids*. London: Academic, 2. ed., 1986.

[32] T. B. Schrøder, U. R. Pedersen, N. P. Bailey, S. Toxvaerd, and J. C. Dyre, "Hidden scale invariance in molecular van der Waals liquids: A simulation study," *Physical Review E*, vol. 80, p. 041502, 2009.

[33] N. P. Bailey, L. Bøhling, A. A. Veldhorst, T. B. Schrøder, and J. C. Dyre, "Statistical mechanics of Roskilde liquids: Configurational adiabats, specific heat contours, and density dependence of the scaling exponent," *The Journal of Chemical Physics*, vol. 139, p. 184506, 2013.

[34] M. L. Samuels and J. A. Witmer, *Statistics for the life sciences*. Upper Saddle River, NJ: Prentice Hall, 3. ed., 2003.

[35] T. S. Ingebrigtsen, T. B. Schrøder, and J. C. Dyre, "What is a simple liquid?," *Physical Review X*, vol. 2, p. 011011, 2012.

[36] A. A. Veldhorst, J. C. Dyre, and T. B. Schrøder, "Scaling of the dynamics of flexible Lennard-Jones chains," *The Journal of Chemical Physics*, vol. 141, p. 054904, 2014.

[37] A. A. Veldhorst, J. C. Dyre, and T. B. Schrøder, "Scaling of the dynamics of flexible Lennard-Jones chains: Effects of harmonic bonds," *The Journal of Chemical Physics*, vol. 143, p. 194503, 2015.

[38] T. S. Ingebrigtsen, T. B. Schrøder, and J. C. Dyre, "Isomorphs in model molecular liquids," *The Journal of Physical Chemistry B*, vol. 116, p. 1018, 2012.

[39] F. Hummel, G. Kresse, J. C. Dyre, and U. R. Pedersen, "Hidden scale invariance of metals," *Physical Review B*, vol. 92, p. 174116, 2015.

[40] D. E. Albrechtsen, A. E. Olsen, U. R. Pedersen, T. B. Schrøder, and J. C. Dyre, "Isomorph invariance of the structure and dynamics of classical crystals," *Physical Review B*, vol. 90, p. 094106, 2014.

[41] U. R. Pedersen, N. Gnan, N. P. Bailey, T. B. Schrøder, and J. C. Dyre, "Strongly correlating liquids and their isomorphs," *Journal of Non-Crystalline Solids*, vol. 357, p. 320, 2011.

[42] D. Gundermann, U. R. Pedersen, T. Hecksher, N. P. Bailey, B. Jakobsen, T. Christensen, N. B. Olsen, T. B. Schrøder, D. Fragiadakis, R. Casalini, C. M. Roland, J. C. Dyre, and K. Niss, "Predicting the density-scaling exponent of a glass-forming liquid from Prigogine-Defay ratio measurements," *Nature Physics*, vol. 7, p. 816, 2011.

[43] U. R. Pedersen, N. P. Bailey, T. B. Schrøder, and J. C. Dyre, "Strong pressure-energy correlations in van der Waals liquids," *Physical Review Letters*, vol. 100, p. 015701, 2008.

[44] T. B. Schrøder and J. C. Dyre, "Simplicity of condensed matter at its core: Generic definition of a Roskilde-simple system," *The Journal of Chemical Physics*, vol. 141, p. 204502, 2014.

[45] T. S. Ingebrigtsen and H. Tanaka, "Effect of energy polydispersity on the nature of Lennard-Jones liquids," *The Journal of Physical Chemistry B*, vol. 120, p. 7704, 2016.

[46] J. C. Dyre, "Isomorph theory of physical aging," *The Journal of Chemical Physics*, vol. 148, p. 154502, 2018.

[47] K. Niss, D. Gundermann, T. Christensen, and J. C. Dyre, "Dynamic thermal expansivity of liquids near the glass transition," *Physical Review E*, vol. 85, p. 041501, 2012.

[48] D. J. Griffiths, *Introduction to Electrodynamics*. Pearson, 3. ed., 2008.

[49] F. Kremer and A. Schönhals, *Broadband Dielectric Spectroscopy*. Berlin New York: Springer, 2003.

[50] G. W. Scherer, *Relaxation in glass and composites*. New York: Wiley, 1986.

[51] K. Niss, "Mapping isobaric aging onto the equilibrium phase diagram," *Physical Review Letters*, vol. 119, p. 115703, 2017.

[52] T. Hecksher, N. B. Olsen, K. Niss, and J. C. Dyre, "Physical aging of molecular glasses studied by a device allowing for rapid thermal equilibration," *The Journal of Chemical Physics*, vol. 133, p. 174514, 2010.

[53] A. Q. Tool, "Relaxation of stresses in annealing glass," *Journal of Research of the National Bureau of Standards (United States)*, vol. 34, p. 199, 1945.

[54] A. Q. Tool, "Relation between inelastic deformability and thermal expansion of glass in its annealing range," *Journal of the American Ceramic Society*, vol. 29, p. 240, 1946.

[55] O. S. Narayanaswamy, "A model of structural relaxation in glass," *Journal of the American Ceramic Society*, vol. 54, p. 491, 1971.

[56] B. Igarashi, T. Christensen, E. H. Larsen, N. B. Olsen, I. H. Pedersen, T. Rasmussen, and J. C. Dyre, "A cryostat and temperature control system optimized for measuring relaxations of glass-forming liquids," *Review of Scientific Instruments*, vol. 79, p. 045105, 2008.

[57] D. Gundermann, *Testing predictions of the isomorph theory by experiment*. PhD thesis, DNRF Centre "Glass & Time", IMFUFA, NSM, Roskilde University, 2013.

[58] Julabo, "Operating Manual F81ME." Julabo Labortechnik, Seelbach, Germany, 2009.

[59] L. A. Roed, "Isochronal superposition - An experimental test of a prediction from the isomorph theory," Master's thesis, IMFUFA, NSM, Roskilde University, 2012.

[60] C. H. Olsen and C. Videnkjær, "Spring op og fald ned på isomorfer." Student project in physics, IMFUFA, NSM, Roskilde University, 2010.

[61] L. A. Roed, D. Gundermann, J. C. Dyre, and K. Niss, "Communication: Two measures of isochronal superposition," *The Journal of Chemical Physics*, vol. 139, p. 101101, 2013.

[62] W. Xiao, J. Tofteskov, and T. V. Christensen, "The dielectric loss strength variation along an isomorph," Master's thesis, IMFUFA, NSM, Roskilde University, 2013.

[63] W. Xiao, J. Tofteskov, T. V. Christensen, J. C. Dyre, and K. Niss, "Isomorph theory prediction for the dielectric loss variation along an isochrone," *Journal of Non-Crystalline Solids*, vol. 407, p. 190, 2015.

[64] L. A. Roed, K. Niss, and B. Jakobsen, "Communication: High pressure specific heat spectroscopy reveals simple relaxation behavior of glass forming molecular liquid," *The Journal of Chemical Physics*, vol. 143, p. 221101, 2015.

[65] B. Igarashi, T. Christensen, E. H. Larsen, N. B. Olsen, I. H. Pedersen, T. Rasmussen, and J. C. Dyre, "An impedance-measurement setup optimized for measuring relaxations of glass-forming liquids," *Review of Scientific Instruments*, vol. 79, p. 045106, 2008.

[66] A. I. Nielsen, S. Pawlus, M. Paluch, and J. C. Dyre, "Pressure dependence of the dielectric loss minimum slope for ten molecular liquids," *Philosophical Magazine*, vol. 88, p. 4101, 2008.

[67] B. Jakobsen, K. Niss, and N. B. Olsen, "Dielectric and shear mechanical alpha and beta relaxations in seven glass-forming liquids," *The Journal of Chemical Physics*, vol. 123, p. 234511, 2005.

[68] K. Niss and B. Jakobsen, "Dielectric and shear mechanical relaxation in glass forming liquids. A thorough analysis and experimental test of the DiMarzio-Bishop model," Master's thesis, IMFUFA, Roskilde University, 2003.

[69] A. I. Nielsen, T. Christensen, B. Jakobsen, K. Niss, N. B. Olsen, R. Richert, and J. C. Dyre, "Prevalence of approximate $\sqrt{t}$ relaxation for the dielectric α process in viscous organic liquids," *The Journal of Chemical Physics*, vol. 130, p. 154508, 2009.

[70] P. W. Bridgman, "Volume-temperature-pressure relations for several non-volatile liquids," *Proceedings of the American Academy of Arts and Sciences*, vol. 67, p. 1, 1932.

[71] J. Papini, "Unpublished data on 1,2,6 hexanetriol." Roskilde University, 2012.

[72] H. Forsman, "Dielectric relaxation of 1, 2, 6-hexanetriol at frequencies from 1 mHz to 10 MHz and at pressures to 1 GPa," *Molecular Physics*, vol. 63, p. 65, 1988.

[73] H. Forsman, P. Andersson, and G. Bäckström, "Dielectric relaxation of glycerol and n-propyl alcohol at high pressure," *Journal of the Chemical Society, Faraday Transactions 2: Molecular and Chemical Physics*, vol. 82, p. 857, 1986.

[74] M. Paluch, S. Rzoska, P. Habdas, and J. Ziolo, "Isothermal and high-pressure studies of dielectric relaxation in supercooled glycerol," *Journal of Physics: Condensed Matter*, vol. 8, p. 10885, 1996.

[75] M. Paluch, J. Ziolo, S. Rzoska, and P. Habdas, "The influence of pressure on dielectric relaxation for phthalate derivatives in the supercooled state," *Journal of Physics: Condensed Matter*, vol. 9, p. 5485, 1997.

[76] S. Capaccioli, K. Kessairi, D. Prevosto, M. Lucchesi, and P. Rolla, "Correlation of structural and Johari–Goldstein relaxations in systems vitrifying along isobaric and isothermal paths," *Journal of Physics: Condensed Matter*, vol. 19, p. 205133, 2007.

[77] A. I. Nielsen, *The primary relaxation in glass-forming liquids. An empirical investigation of dielectric data.* PhD thesis, DNRF Centre "Glass & Time", IMFUFA, NSM, Roskilde University, 2009.

[78] D. Davidson and R. H. Cole, "Dielectric relaxation in glycerine," *The Journal of Chemical Physics*, vol. 18, p. 1417, 1950.

[79] B. Jakobsen, T. Hecksher, T. E. Christensen, N. B. Olsen, J. C. Dyre, and K. Niss, "Communication: Identical temperature dependence of the time scales of several linear-response functions of two glass-forming liquids," *The Journal of Chemical Physics*, vol. 136, p. 081102, 2012.

[80] B. Jakobsen, N. B. Olsen, and T. Christensen, "Frequency-dependent specific heat from thermal effusion in spherical geometry," *Physical Review E*, vol. 81, p. 061505, 2010.

[81] H. Gobrecht, K. Hamann, and G. Willers, "Complex plane analysis of heat capacity of polymers in the glass transition region," *Journal of Physics E: Scientific Instruments*, vol. 4, p. 21, 1971.

[82] C. Angell and L. Torell, "Short time structural relaxation processes in liquids: Comparison of experimental and computer simulation glass transitions on picosecond time scales," *The Journal of Chemical Physics*, vol. 78, p. 937, 1983.

[83] N. O. Birge and S. R. Nagel, "Specific-heat spectroscopy of the glass transition," *Physical Review Letters*, vol. 54, p. 2674, 1985.

[84] T. Christensen, "The frequency dependence of the specific heat at the glass transition," *Journal de Physique Colloques*, vol. 46, p. C8, 1985.

[85] N. O. Birge, "Specific-heat spectroscopy of glycerol and propylene glycol near the glass transition," *Physical Review B*, vol. 34, p. 1631, 1986.

[86] J. K. Nielsen and J. C. Dyre, "Fluctuation-dissipation theorem for frequency-dependent specific heat," *Physical Review B*, vol. 54, p. 15754, 1996.

[87] M. Settles, F. Post, D. Müller, A. Schulte, and W. Doster, "Solvent damping of internal processes in myoglobin studied by specific heat spectroscopy and flash photolysis," *Biophysical Chemistry*, vol. 43, p. 107, 1992.

[88] I. Moon, Y. H. Jeong, and S. Kwun, "The 3ω technique for measuring dynamic specific heat and thermal conductivity of a liquid or solid," *Review of Scientific Instruments*, vol. 67, p. 29, 1996.

[89] T. Christensen and N. B. Olsen, "Thermoviscoelasticity of glass-forming liquids," *Journal of Non-Crystalline Solids*, vol. 235, p. 296, 1998.

[90] L. Carpentier, O. Bustin, and M. Descamps, "Temperature-modulated differential scanning calorimetry as a specific heat spectroscopy," *Journal of Physics D: Applied Physics*, vol. 35, p. 402, 2002.

[91] E. H. Bentefour, C. Glorieux, M. Chirtoc, and J. Thoen, "Broadband photopyroelectric thermal spectroscopy of a supercooled liquid near the glass transition," *Journal of Applied Physics*, vol. 93, p. 9610, 2003.

[92] A. Minakov, S. Adamovsky, and C. Schick, "Advanced two-channel ac calorimeter for simultaneous measurements of complex heat capacity and complex thermal conductivity," *Thermochimica Acta*, vol. 403, p. 89, 2003.

[93] H. Leyser, A. Schulte, W. Doster, and W. Petry, "High-pressure specific-heat spectroscopy at the glass transition in o-terphenyl," *Physical Review E*, vol. 51, p. 5899, 1995.

[94] D. V. Schroeder, *An introduction to thermal physics*. San Francisco, CA: Addison Wesley, 2000.

[95] T. Christensen, N. B. Olsen, and J. C. Dyre, "Conventional methods fail to measure $c_p(\omega)$ of glass-forming liquids," *Physical Review E*, vol. 75, p. 041502, 2007.

[96] T. Christensen and J. C. Dyre, "Solution of the spherically symmetric linear thermoviscoelastic problem in the inertia-free limit," *Physical Review E*, vol. 78, p. 021501, 2008.

[97] B. Jakobsen, "Lecture note on the course Technical Physics at Roskilde University: Exercise in thermal analysis," 2011.

[98] "Scientific Instrument Services: Santovac 5P ultra and Santovac 5 polyphenyl ether vacuum pump fluid." http://www.sisweb.com/vacuum/sis/satovc5p.htm, 2015.

[99] B. Jakobsen, "Unpublished note on the temperature correction made in Ref. [79]." Roskilde University, 2012.

[100] "Glass & Time - Data repository." http://glass.ruc.dk/data/, Roskilde University, 2018.

[101] J. C. Dyre, "Narayanaswamy's 1971 aging theory and material time," *The Journal of Chemical Physics*, vol. 143, p. 114507, 2015.

[102] P. Lunkenheimer, R. Wehn, and A. Loidl, "Dielectric spectroscopy on aging glasses," *Journal of Non-Cystalline Solids*, vol. 352, p. 4941, 2006.

[103] R. Richert, P. Lunkenheimer, S. Kastner, and A. Loidl, "On the derivation of equilibrium relaxation times from aging experiments," *The Journal of Physical Chemistry B*, vol. 117, p. 12689, 2013.

[104] E. Schlosser and A. Schönhals, "Dielectric relaxation during physical ageing," *Polymer*, vol. 32, p. 2135, 1991.

[105] U. Schneider, R. Brand, P. Lunkenheimer, and A. Loidl, "Excess wing in the dielectric loss of glass formers: A Johari-Goldstein β relaxation?," *Physical Review Letters*, vol. 84, p. 5560, 2000.

[106] P. Lunkenheimer, R. Wehn, U. Schneider, and A. Loidl, "Glassy aging dynamics," *Physical Review Letters*, vol. 95, p. 055702, 2005.

[107] R. Wehn, P. Lunkenheimer, and A. Loidl, "Broadband dielectric spectroscopy and aging of glass formers," *Journal of Non-Crystalline Solids*, vol. 353, p. 3862, 2007.

[108] A. Alegría, E. Guerrica-Echevarria, L. Goitiandía, I. Tellería, and J. Colmenero, "α-relaxation in the glass transition range of amorphous polymers. 1. Temperature behavior across the glass transition," *Macromolecules*, vol. 28, p. 1516, 1995.

[109] A. Alegría, L. Goitiandía, I. Tellería, and J. Colmenero, "α-relaxation in the glass-transition range of amorphous polymers. 2. Influence of physical aging on the dielectric relaxation," *Macromolecules*, vol. 30, p. 3881, 1997.

[110] L. Goitiandía and A. Alegría, "The Adam-Gibbs equation and the out-of-equilibrium α relaxation of glass forming systems," *The Journal of Chemical Physics*, vol. 121, p. 1636, 2004.

[111] D. Cangialosi, M. Wübbenhorst, J. Groenewold, E. Mendes, and S. Picken, "Diffusion mechanism for physical aging of polycarbonate far below the glass transition temperature studied by means of dielectric spectroscopy," *Journal of Non-Crystalline Solids*, vol. 351, p. 2605, 2005.

[112] K. Niss, B. Jakobsen, and N. B. Olsen, "Dielectric and shear mechanical relaxations in glass-forming liquids: A test of the Gemant-DiMarzio-Bishop model," *The Journal of Chemical Physics*, vol. 123, p. 234510, 2005.

[113] T. Hecksher, N. B. Olsen, K. A. Nelson, J. C. Dyre, and T. Christensen, "Mechanical spectra of glass-forming liquids. I. Low-frequency bulk and shear moduli of DC704 and 5-PPE measured by piezoceramic transducers," *The Journal of Chemical Physics*, vol. 138, p. 12A543, 2013.

[114] T. Hecksher, A. I. Nielsen, N. B. Olsen, and J. C. Dyre, "Little evidence for dynamic divergences in ultraviscous molecular liquids," *Nature Physics*, vol. 4, p. 737, 2008.

[115] R. Casalini and C. Roland, "Pressure densification of a simple liquid," *Journal of Non-Crystalline Solids*, vol. 475, p. 25, 2017.

[116] A. Sanz, J. Dyre, and K. Niss, "The challenge of studying pressure densification by dielectric spectroscopy." Unpublished, Roskilde University, 2018.

Appendix A

Isochronal superposition

A.1 Qualitative analysis of isochronal superposition

A qualitative picture of whether the liquids obey isochronal superposition or not is obtained by normalizing the dielectric relaxation spectra, such that they have the same maximum, which is also what Roland *et al.* [17] and Ngai *et al.* [20] have done in their data treatment with state points that are almost on the same isochrone. We normalize all the used dielectric relaxation spectra for each liquid, such that it is also seen whether the liquids obey isochronal superposition better than time-temperature-pressure superposition (TTPS), where the shape of the spectra are invariant for all state points. This type of data treatment is also used in Ref. [7].

For each liquid, all the used raw data are normalized, and plotted in the same figure (Figures A.1, A.2, A.3, A.4, A.5, and A.6). Measurements that are from same isochrone have the same color. The figures thereby provide a qualitative picture of how close the relaxation spectra on the same isochrone are to each other, as well as giving a qualitative idea of whether the relaxation spectra are more equal on the isochrones than in general.

From the figures, it is clear that 1,2,6-HT obeys isochronal superposition better than TTPS. This is also the case for glycerol and DBP, although more clearly with 1,2,6-HT. With 5PPE, DEP, and DC704 this also seems to be the case, but it is difficult to quantify.

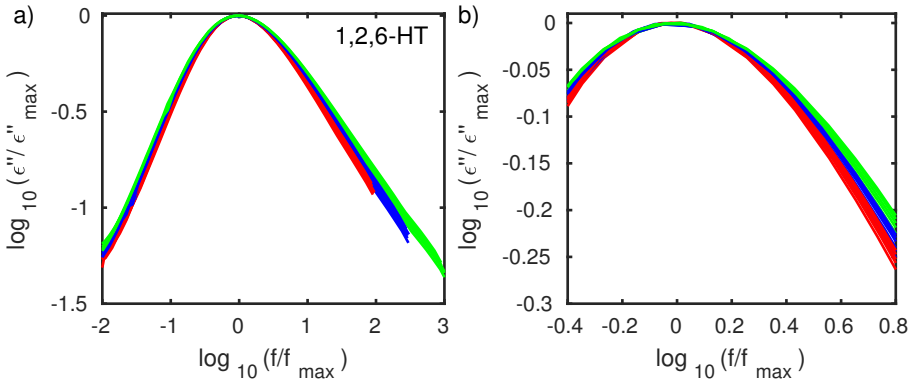

Figure A.1: The normalized relaxation spectra for 1,2,6-HT. The three different colors show the three isochrones. The figure to the right is a zoom of the peak. The red spectra are measurements with $\log_{10}(f_m) \simeq 4$, the blue spectra are measurements with $\log_{10}(f_m) \simeq 3.6$, and the green spectra are measurements with $\log_{10}(f_m) \simeq 3$.

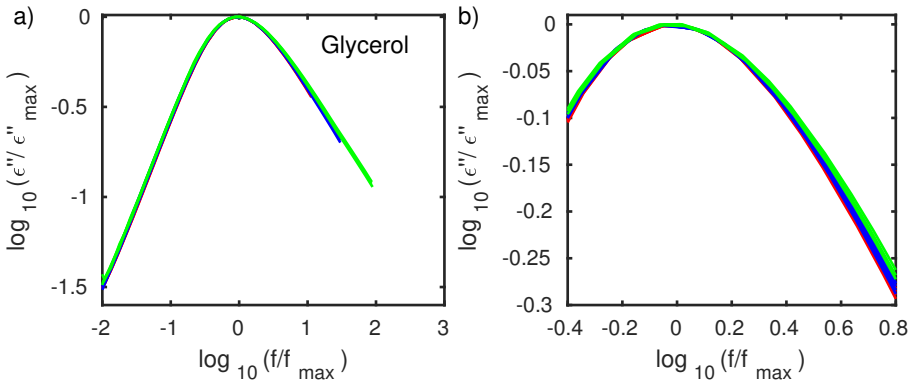

Figure A.2: The normalized relaxation spectra for glycerol. The three different colors show the three isochrones. The figure to the right is a zoom of the peak. The red spectra are measurements with $\log_{10}(f_m) \simeq 5$, the blue spectra are measurements with $\log_{10}(f_m) \simeq 4.5$, and the green spectra are measurements with $\log_{10}(f_m) \simeq 4$.

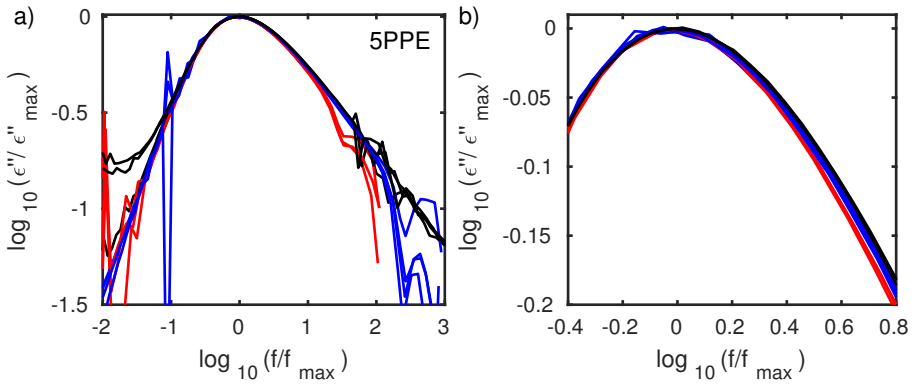

Figure A.3: The normalized relaxation spectra for 5PPE. The three different colors show the three isochrones. The figure to the right is a zoom of the peak. The red spectra are measurements with $\log_{10}(f_m) \simeq 4$, the blue spectra are measurements with $\log_{10}(f_m) \simeq 3.1$, and the black spectra are measurements with $\log_{10}(f_m) \simeq 0.2$.

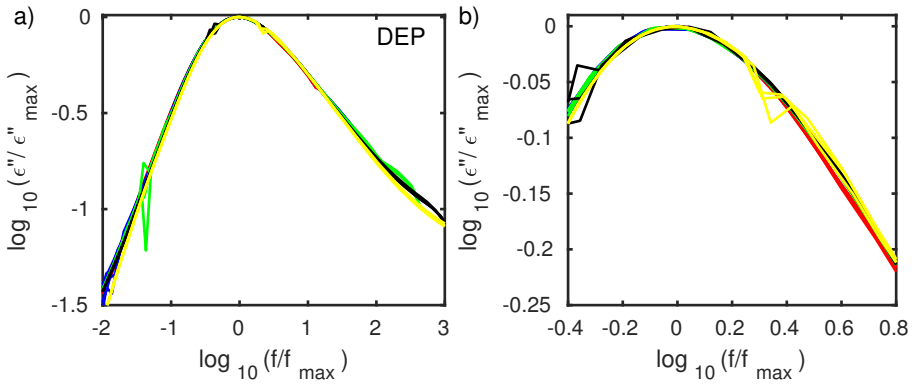

Figure A.4: The normalized relaxation spectra for DEP. The five different colors show the five isochrones. The figure to the right is a zoom of the peak. The red spectra are measurements with $\log_{10}(f_m) \simeq 4.9$, the blue spectra are measurements with $\log_{10}(f_m) \simeq 4.3$, the green spectra are measurements with $\log_{10}(f_m) \simeq 3.4$, the black spectra are measurements with $\log_{10}(f_m) \simeq 2.4$, and the yellow spectra are measurements with $\log_{10}(f_m) \simeq 1.7$.

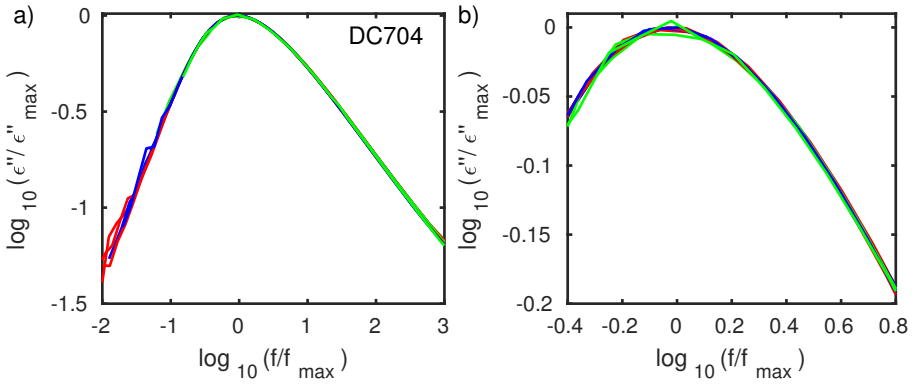

Figure A.5: The normalized relaxation spectra for DC704. The three different colors show the three isochrones. The figure to the right is a zoom of the peak. The red spectra are measurements with $\log_{10}(f_m) \simeq 2$, the blue spectra are measurements with $\log_{10}(f_m) \simeq 1$, and the green spectra are measurements with $\log_{10}(f_m) \simeq 0.3$.

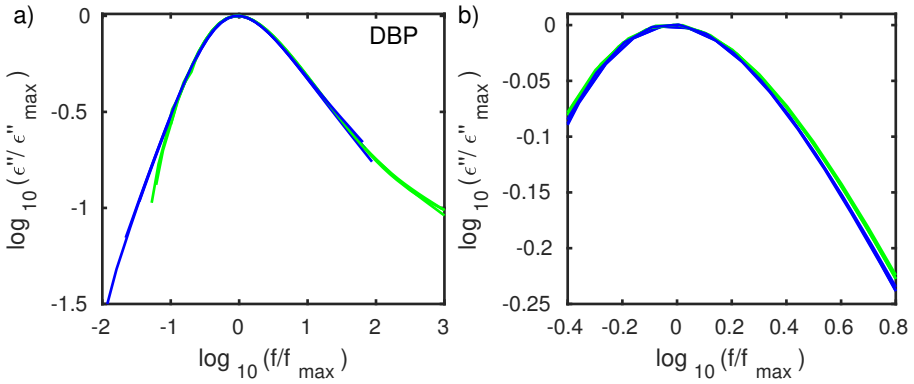

Figure A.6: The normalized relaxation spectra for DBP. The two different colors show the two isochrones. The figure to the right is a zoom of the peak. The blue spectra are measurements with $\log_{10}(f_m) \simeq 4.1$, and the green spectra are measurements with $\log_{10}(f_m) \simeq 2.6$.

A.2 Data of the selected measurements

1,2,6-HT

$\log_{10}(f_m)$	T (K)	p (MPa)
4.05	240.5	99
4.03	243.0	150
4.02	245.3	199
4.06	248.0	248
4.07	250.5	298
3.53	235.6	101
3.54	238.0	150
3.54	240.5	198
3.52	242.8	250
3.56	245.3	298
4.65	248.5	347
2.96	235.6	198
2.95	237.9	251
2.99	240.5	301
3.04	243.2	351
3.05	245.3	399

Glycerol

$\log_{10}(f_m)$	T (K)	p (MPa)
4.94	242.4	100
4.95	244.7	151
4.94	246.3	200
4.96	248.6	249
4.96	250.4	298
4.52	237.5	100
4.54	240.0	152
5.52	241.4	199
4.52	243.5	249
4.53	245.3	300
4.05	236.6	198
4.07	238.6	249
4.06	240.4	299

5PPE

$\log_{10}(f_m)$	T (K)	p (MPa)
3.98	271.9	0.1
3.96	295.3	97
3.96	317.9	199
3.05	267.1	0.1
3.05	290.4	99
3.06	312.0	198
3.09	332.4	300
0.30	255.6	0.1
0.21	277.7	101
0.17	297.3	199
0.26	316.9	301

DEP

$\log_{10}(f_m)$	T (K)	p (MPa)
4.88	237.3	149
4.93	245.4	200
4.89	251.3	248
4.88	258.2	298
4.85	263.9	347
4.91	270.9	398
4.34	240.5	200
4.26	246.3	251
4.31	253.2	299
4.30	259.1	350
4.25	265.0	401
3.37	239.5	248
3.40	246.3	299
3.39	252.2	351
3.40	258.2	400
2.43	240.4	300
2.36	245.2	348
2.37	251.4	400
1.69	236.4	300
1.66	241.3	347
1.70	247.5	399

DC704

$\log_{10}(f_m)$	T (K)	p (MPa)
1.89	253	104.3
2.22	263	155.3
1.84	283	255.9
0.90	253	132.0
1.05	263	178.7
1.11	283	274.4
0.21	253	144.5
0.33	263	192.4
0.23	283	294.7

DBP

$\log_{10}(f_m)$	T (K)	p (MPa)
4.06	206	0
4.16	219.3	108
4.19	236.3	251
2.61	206	85
2.68	219.3	200
2.40	236.3	389

Appendix B

Specific heat spectroscopy

B.1 The fitting parameter r

Figure B.1 shows the spectra and the loss peak frequencies using the two different fitting methods with, respectively, r as a free parameter and r fixed. It is seen that the different methods influence the high-frequency end of the spectra. The fitting method with r fixed is chosen since the spectra from this procedure look the best, and theoretically, it also seems to be more correct to fix r since it should not change with temperature.

B.2 Different values of $Z_{\mathbf{liq,0}}$

The spectra and the loss peak frequencies using the two different ways to find $Z_{\mathrm{liq},0}$ (respectively the low-frequency limit of Z_{liq} and the fitting parameter) are shown in Figure B.2. It is seen that the value of $Z_{\mathrm{liq},0}$ especially affects the low-frequency part of the spectra, and that the spectra with $Z_{\mathrm{liq},0}$ found from the low-frequency limit of Z_{liq} looks more correct.

B.3 Fitting parameters 300 MPa

Figure B.3 shows the fitting parameters of the dataset at 300 MPa, using a fit to the seven-parameter model.

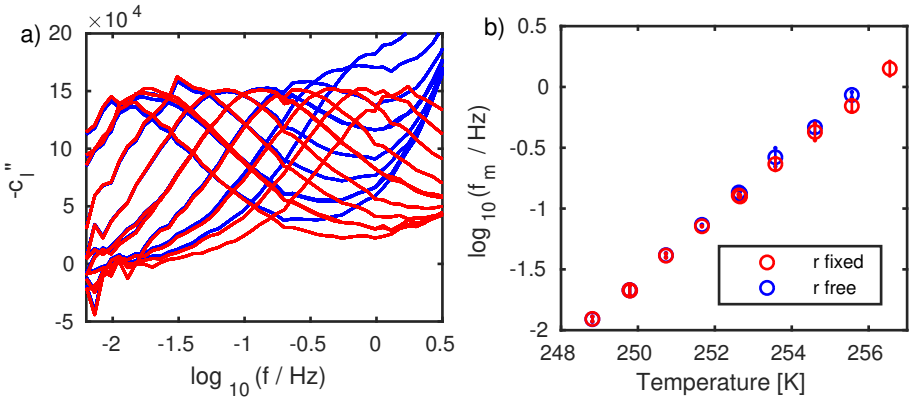

Figure B.1: Two different fitting methods with, respectively, r fixed and r free. (a) The imaginary part of the specific heat. (b) The loss peak frequencies.

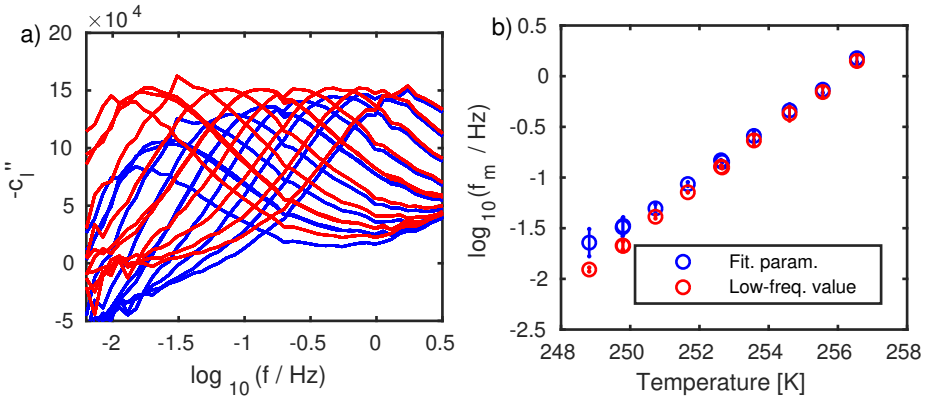

Figure B.2: Results using the two different $Z_{\mathrm{liq},0}$. (a) The imaginary part of the specific heat. (b) The loss peak frequencies.

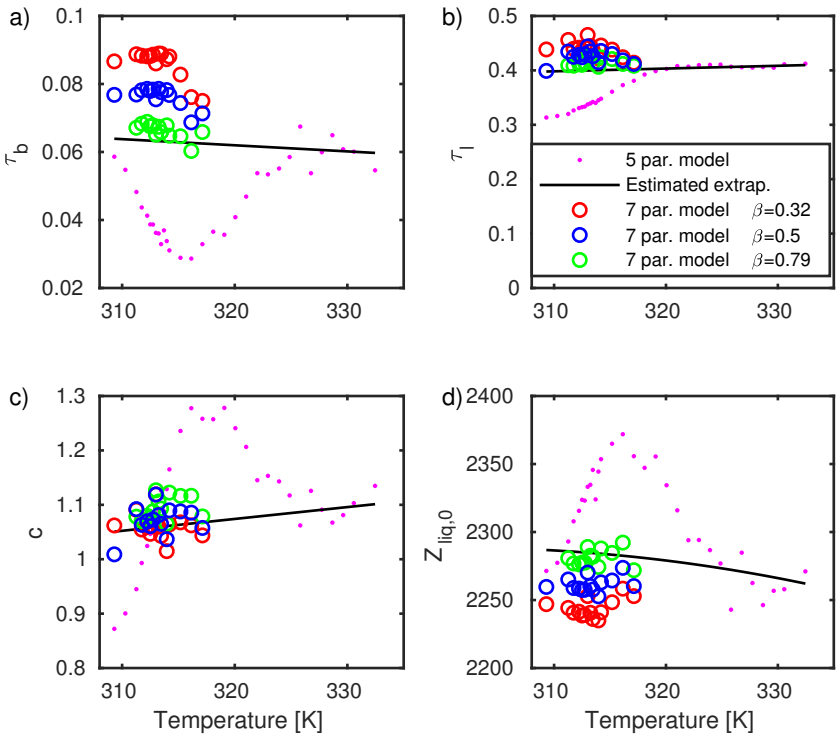

Figure B.3: The fitting parameters of the dataset at 300 MPa. The fitting parameters from the five-parameter fit, the extrapolations estimated from the 0.1 MPa and 150 MPa extrapolations, and the fitting parameters using the seven-parameter fit with respectively $\beta = 0.32$, $\beta = 0.5$, and $\beta = 0.79$ are shown.

Appendix C

Isochronal jump

C.1 Detailed description of the sample cell

This appendix describes the new multi-layer capacitor sample cell in detail, including how to fill it, and how to wrap it to protect it against pressure liquid. The cell consists of 12 capacitor plates in copper, which results in 11 liquid layers. The cell, and how the wires are connected are illustrated here:

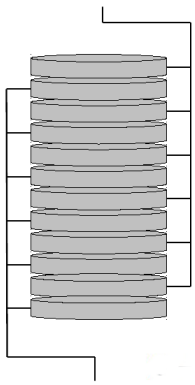

Two of the plates are 'end'-plates, which have a tip used to collect and connect the wires from the other plates. The remaining 10 plates have wires connected, which are of different lengths. On all the plates (except one of the end-plates) four small Kapton spacers are glued onto one side of the plate.

The sample cell furthermore consists of a cylindrical holder with top and bottom made in PEEK, in which the capacitor is assembled. The wires on the thin plates prevent the plates from rotating in the holder. The end-plates have a tip in the side, ensuring that they do not rotate when the cell is assembled. Below,

the different parts of the cell are shown along with a special holder for assembling.

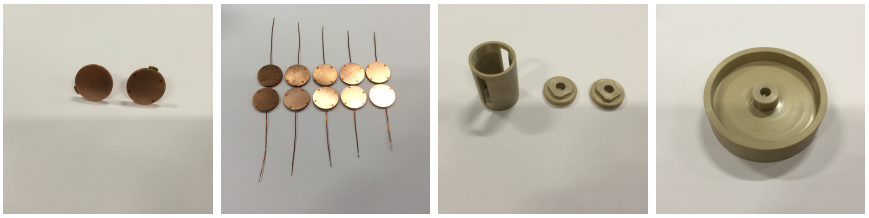

Assembling of the cell

First, one of the end-plates is placed in the cylindrical PEEK holder, and the bottom of the cylindrical holder is screwed into the holder. The cell is then placed in a holder made especially for assembling of the cell. The sample liquid is then placed on the end-plate. There should be enough liquid to fill the volume between the two plates, and it is good if there is too much liquid (so that it will flow out in the sides).

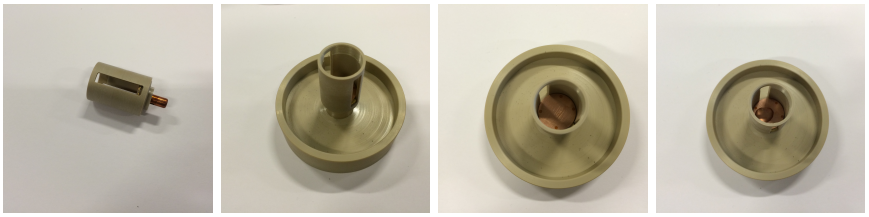

A thin plate is then placed in top of the end-plate. Since the wire of this plate should be connected to the end-plate in the other end of the sample cell, the wire should be one of the two plates with longest wires. The plate should turn correctly so that there are spacers, but only one set of spacers, between the plates. Sample liquid is then placed in top of the plate.

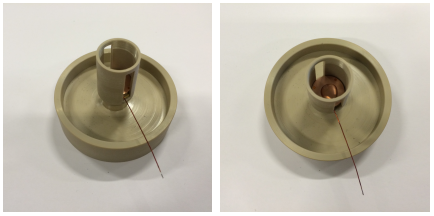

A new plate is then placed in the holder. This plate should be connected to the first end-plate, and it should therefore be one of the two plates with shortest wire. The wire should come out of the holder in the opposite direction of the first wire (so that in the end all wires going to one end-plate are in one side,

and all the wires going to the other end-plate are in the other side). A drop of liquid is then placed in top of the plate.

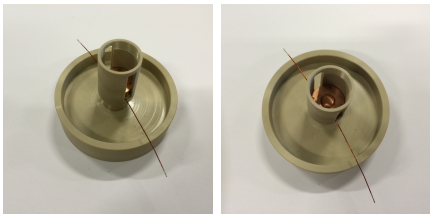

Now the rest of the plates and sample liquid are placed in the holder. The plates are placed so that the length of the wire on the plates corresponds to the position in the capacitor.

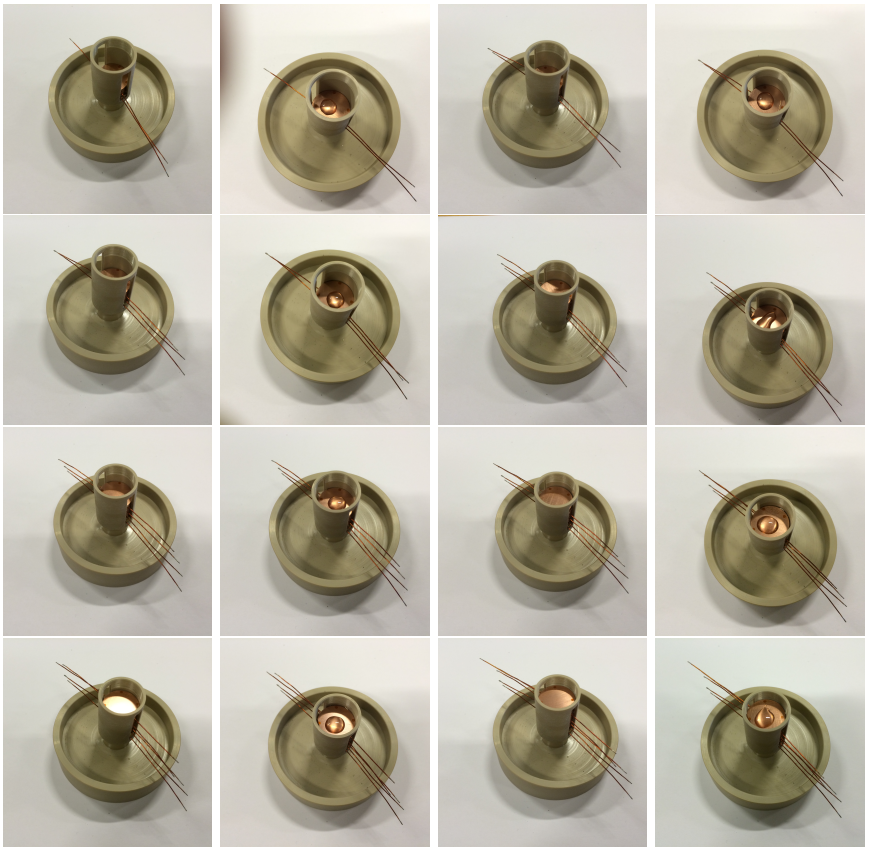

The other end-plate is then placed in the top, and the top of the cylindrical PEEK holder is screwed into the holder.

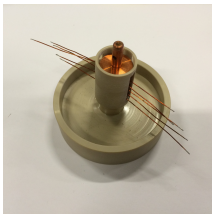
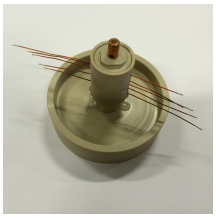

The wires from one side of the capacitor are then collected and placed in a hole in the tip in the corresponding end-plate. The wires are tightened to the end-plate by use of a screwdriver (in the top of the tip). The same procedure is done for the wires in the other side.

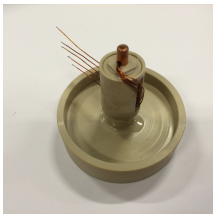
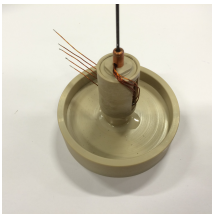


Wrapping of the sample cell

After the cell is assembled, the next step is to "wrap" the cell to prevent mixture of sample and pressure liquid. The things used for wrapping are three rubber fingers from rubber gloves, Teflon tape, and strips as seen below.

First, one layer of rubber is placed around the cell. Some extra liquid can now be added in the sides of the sample cell to ensure that it is filled with sample liquid. Possible air is removed by smoothing the rubber out, and it is then closed temporarily by use of Teflon tape.

The sample cell is then wrapped smoothly in Teflon tape (except at the tips in top and bottom).

Another rubber finger is then placed around the cell, which is also closed temporarily. The cell in then wrapped in another layer of Teflon tape.

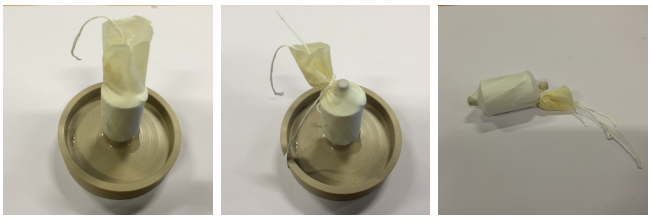

A final layer of rubber is then wrapped around the cell and closed temporarily.

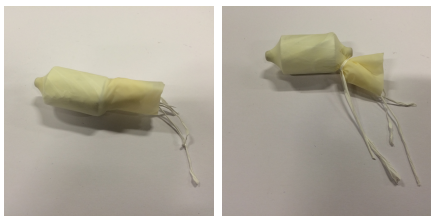

The temporary closing of the rubber is then removed, and closed using three strips.

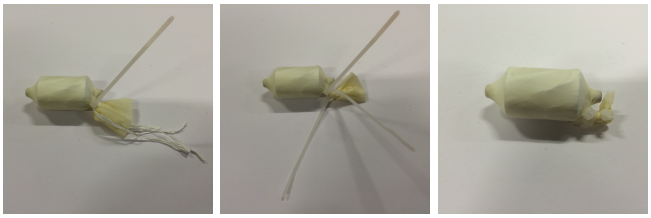

Connecting wires to the sample cell

The wires for the measurement equipment are then connected to the cell. The equipment used for this is seen below.

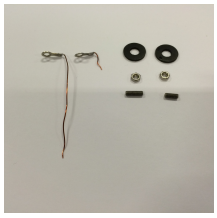

A small o-ring is placed around the tip of the end-plates (this is probably not necessary). A small screw is then screwed into the top of the tip (pressed through the rubber). The wire, which is connected to a metal o-ring is placed around the screw and a nut is placed at the screw, so that the wire is now connected to the sample cell. The same procedure is used for the other end of the cell.

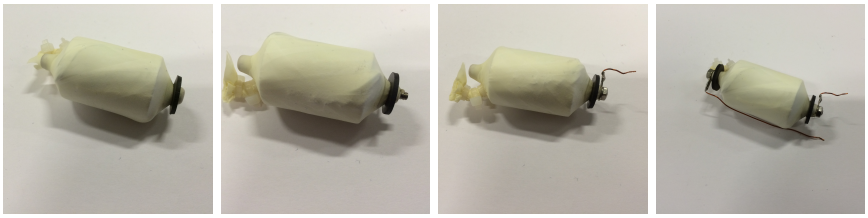

The cell is now ready to be connected to the plug.

C.2 Test with temperature regulator

The test of the temperature regulator using different jumps is seen in Figure C.1.

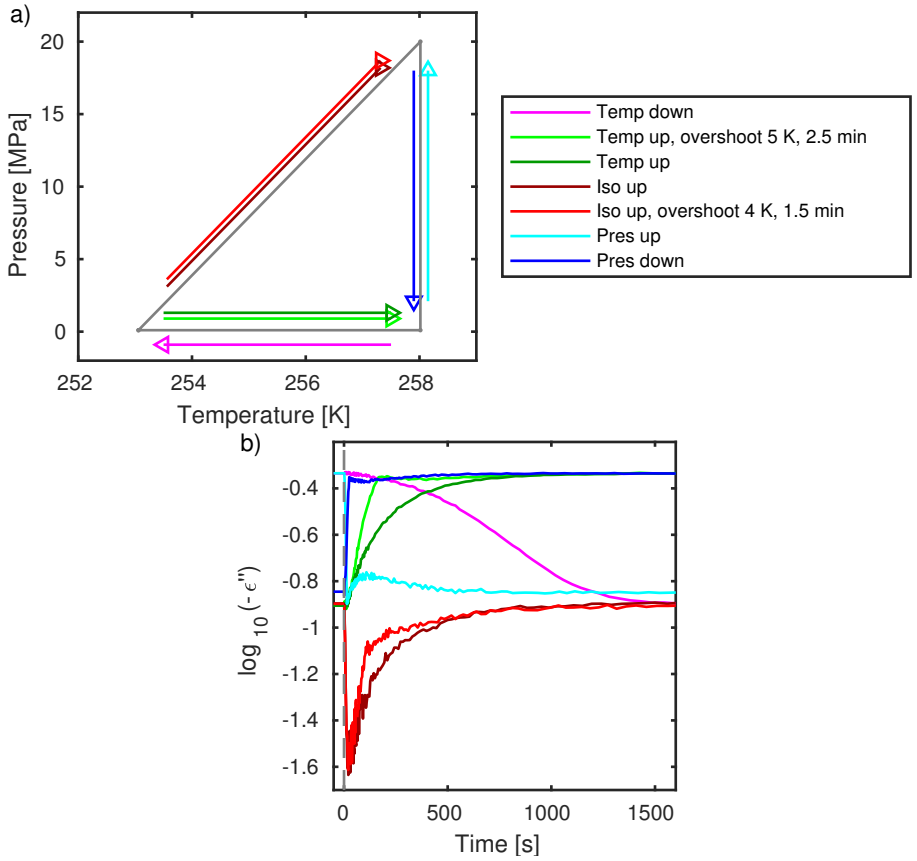

Figure C.1: Thermal/pressure equilibrium tests with temperature regulator. (a) Illustration of the used state points and jumps. (b) The imaginary part of the dielectrics as a function of time following the different jumps.

Appendix D

Reprints of articles

THE JOURNAL OF CHEMICAL PHYSICS **139**, 101101 (2013)

Communication: Two measures of isochronal superposition

Lisa Anita Roed, Ditte Gundermann, Jeppe C. Dyre, and Kristine Niss
DNRF Centre "Glass and Time", IMFUFA, Department of Sciences, Roskilde University, Postbox 260, DK-4000 Roskilde, Denmark

(Received 5 July 2013; accepted 29 August 2013; published online 13 September 2013)

A liquid obeys isochronal superposition if its dynamics is invariant along the isochrones in the thermodynamic phase diagram (the curves of constant relaxation time). This paper introduces two quantitative measures of isochronal superposition. The measures are used to test the following six liquids for isochronal superposition: 1,2,6 hexanetriol, glycerol, polyphenyl ether, diethyl phthalate, tetramethyl tetraphenyl trisiloxane, and dibutyl phthalate. The latter four van der Waals liquids obey isochronal superposition to a higher degree than the two hydrogen-bonded liquids. This is a prediction of the isomorph theory, and it confirms findings by other groups. © *2013 AIP Publishing LLC*. [http://dx.doi.org/10.1063/1.4821163]

The relaxation time of a supercooled liquid depends strongly on temperature and pressure. Different thermodynamic state points with same relaxation time are said to be on the same isochrone. A liquid obeys "isochronal superposition" if its dynamics is invariant along the isochrones. More precisely, a liquid obeys isochronal superposition (IS) if the complex, frequency-dependent response function $R(\omega, Q)$ in question at state point Q can be written

$$R(\omega, Q) = R_0(Q)\tilde{R}(\omega, \tau(Q)) + K_0(Q). \quad (1)$$

Here $R_0(Q)$ and $K_0(Q)$ are state-point dependent real constants. The function $\tilde{R}(\omega, \tau(Q))$ describes the shape of the relaxation spectrum; this function depends on the state point Q only via its relaxation time $\tau(Q)$. For the imaginary part of the response function, IS implies $R''(\omega, Q) = R_0(Q)\tilde{R}''(\omega, \tau(Q))$. This paper suggests two quantitative measures of how well IS is obeyed and applies them to test six glass-forming liquids for IS.

Tölle first demonstrated IS for a single liquid, orthoterphenyl, in data for the intermediate scattering function determined by neutron scattering.[1] Soon after, systematic investigations of IS were initiated by Roland *et al.*[2] and Ngai *et al.*[3] using dielectric spectroscopy. These seminal papers established IS for the van der Waals liquids studied, but reported that hydrogen-bonded liquids often violate IS. This was a striking discovery presenting a serious challenge to theory: Why would some liquids, for which the relaxation time spectrum generally varies throughout the thermodynamic phase diagram, have invariant spectra along its isochrones? And why do other liquids disobey IS?

By visually comparing the imaginary part of response functions along a liquid's isochrones the analysis of IS has traditionally followed the age-old method for investigating time-temperature superposition (TTS). The present paper takes the analysis one step further by suggesting two measures of the *degree of IS* — such measures are relevant because one does not expect any liquid to obey IS with mathematical rigor. First, however, a few experimental details are given (further details are given in the supplementary material[4]).

We studied four van der Waals liquids: polyphenyl ether (5PPE), diethyl phthalate (DEP), dibutyl phthalate (DBP), and tetramethyl tetraphenyl trisiloxane (DC704), as well as two hydrogen-bonded liquids: 1,2,6 hexanetriol (1,2,6-HT) and glycerol (details are given in Table I). New measurements have been obtained for four of the liquids, while the data on DC704 are from Ref. 10 and the data on DBP are from Ref. 11. The four liquids studied in this work were all studied before, also by use of dielectric spectroscopy under high pressure.[9,12–16]

Glycerol was dried in an exicator for 20 h and 1,2,6-HT was dried for 2 h; the other liquids were used as acquired from Sigma Aldrich. The experiments were performed on the high-pressure equipment described in Refs. 9 and 17. The electrical measurement equipment is described in Ref. 18. Pressures go up to 600 MPa, temperatures range from 233 to 333 K. The sample cell consists of two round stainless steel plates with a diameter of 19.5 mm separated by a 0.05 mm thick Kapton spacer, which has inner diameter 17.5 mm and outer diameter 19.5 mm. To document reproducibility all measurements were repeated. The relaxation time was identified from the dielectric loss-peak frequency.

Hydrogen-bonded liquids have generally much larger dipole moment than van der Waals liquids, which leads to much better dielectric relaxation signals for the former liquids. Figure 1 shows typical dielectric relaxation data for the six liquids studied.

To develop quantitative measures of IS, consider first perfect IS. A loss peak is characterized by, in principle, infinitely many shape parameters $X, Y, Z, \ldots$. In practice, a few parameters are enough to characterize the shape, for instance fitting-model based parameters such as the stretching exponent β, the Havriliak-Negami parameters, the Cole-Davidson β_{CD}, etc., or model-independent parameters such as the half width at half depth or the loss peak area in a log-log plot. Perfect IS is characterized by constant shape parameters along an isochrone: $0 = dX|_\tau = dY|_\tau = dZ|_\tau = \ldots$, in which $|_\tau$ signals that the variation is considered at constant relaxation time.

In order to determine how much a given shape parameter X varies along an isochrone, we assume that a metric ds

TABLE I. The liquids studied. "H" is hydrogen bonded and "vdW" is van der Waals bonded. Where no reference is given, $\Delta\varepsilon$ is from our measurements. Details on the density data are given in the supplementary material.[4]

Liquid	Abbr.	Bonding	T_g (K)	$\Delta\varepsilon$	T (K)	p (MPa)	Density	Ref.
1,2,6 hexanetriol	1,2,6-HT	H	203[5]	~40	236–251	100–400	This work	This work
Glycerol		H	193[6]	~60	237–250	100–300	Ref. 7	This work
Polyphenyl ether	5PPE	vdW	245[8]	~2[8]	255–332	0.1–400	Ref. 9	This work
Diethyl phthalate	DEP	vdW	187[6]	~8	235–271	100–400	This work	This work
Tetramethyl tetraphenyl trisiloxane	DC704	vdW	211[8]	~0.2[8]	253–283	39–304	Ref. 9	Ref. 10
Dibutyl phthalate	DBP	vdW	177[11]	~8	206–254	0–389	Ref. 7	Ref. 11

has been defined in the thermodynamic phase diagram. Since $d\ln X = dX/X$ gives the relative change of X, the rate of relative change of X along an isochrone is given by the operator L defined by

$$L(X) \equiv \left| \frac{d\ln X}{ds} \right|_\tau . \tag{2}$$

How to define a reasonable metric ds? A state point is characterized by its temperature T and pressure p, so one option is $ds^2 = dT^2 + dp^2$. This metric depends on the unit system used, however, which is not acceptable. This problem may be solved by using logarithmic distances, i.e., defining $ds^2 = (d\ln T)^2 + (d\ln p)^2$. Actually, using pressure is not optimal because there are numerous decades of pressures below ambient pressure where little change of the physics take place; furthermore, a logarithmic pressure metric does not allow for negative pressures. For these reasons we instead quantify state points by their temperature and density ρ, and use the following metric:

$$ds^2 \equiv (d\ln T)^2 + (d\ln \rho)^2 . \tag{3}$$

Equations (2) and (3) define a quantitative measure of IS. In practice, suppose an experiment results in data for the shape parameter X along an isochrone. This gives a series of numbers X_1, $X_2, \ldots$, corresponding to the state points (T_1, ρ_1), $(T_2, \rho_2), \ldots$. Since $\ln X_{i+1} - \ln X_i = \ln(X_{i+1}/X_i)$, etc., the discrete version of the right-hand side of Eq. (2) is $|\ln(X_{i+1}/X_i)/\sqrt{\ln^2(T_{i+1}/T_i) + \ln^2(\rho_{i+1}/\rho_i)}|$.

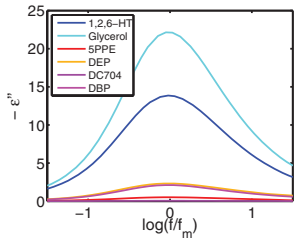

FIG. 1. One dielectric relaxation spectrum for each of the six liquids plotted on a linear scale. The hydrogen-bonded liquids (blue) have much larger signals than the van der Waals liquids (reddish). The spectrum of DC704 is too small to be visible.

An alternative measure of IS corresponding to the purely temperature-based metric $ds^2 = (d\ln T)^2$ is defined by

$$L_T(X) \equiv \left| \frac{d\ln X}{d\ln T} \right|_\tau . \tag{4}$$

This measure is considered because density data are not always available. If the density-scaling exponent $\gamma \equiv (d\ln T/d\ln \rho)|_\tau$ is known for the range of state points in question, Eq. (3) implies $ds^2 = (d\ln T)^2(1 + 1/\gamma^2)$. This leads to the following relation between the two IS measures:

$$L(X) = \frac{L_T(X)}{\sqrt{1 + 1/\gamma^2}} . \tag{5}$$

This relation is useful in the (common) situation where gamma is reported in the literature but the original density data are difficult to retrieve.

As one shape parameter we used the half width at half depth, $W_{1/2}$, defined as the number of decades of frequency from the frequency of maximum dielectric loss to the higher frequency (denoted $f_{1/2}$) where the loss value is halved: $W_{1/2} \equiv \log(f_{1/2}/f_m)$.[6] Here and henceforth "log" is the logarithm with base 10.

The $W_{1/2}$-values are plotted in Fig. 2(a) as functions of temperature for each isochrone studied. This figure suggests that IS is not obeyed for the two hydrogen-bonded liquids (blue), but for the four van der Waals liquids. There is more scatter in the values for the van der Waals liquids than for the hydrogen-bonded liquids, which is due to the smaller dielectric signals (see Fig. 1).

From Fig. 2(a) it is seen that the $W_{1/2}$ is almost constant at all state points for DEP and DC704, suggesting that IS in these cases is a consequence of TTS (or more specifically, time-temperature-pressure superposition). However, the isochrones in Fig. 2(a) are separated from one another in the case of 5PPE and DBP, just as they are in the case of 1,2,6-HT and glycerol. This shows that IS can apply even when the spectra broaden upon supercooling, which is also supported by earlier works where IS has been found for systems without TTS.[10,19]

For a quantitative IS analysis, we apply the L and L_T operators to the shape parameter $W_{1/2}$ (Figs. 2(b) and 2(c)). From these figures it is clear that the measures for the hydrogen-bonded liquids are higher than for the van der Waals liquids. It is not straightforward to estimate the systematic uncertainties involved in the measurements, but an attempt to do so is presented in the supplementary material.[4] We see from Fig. 2

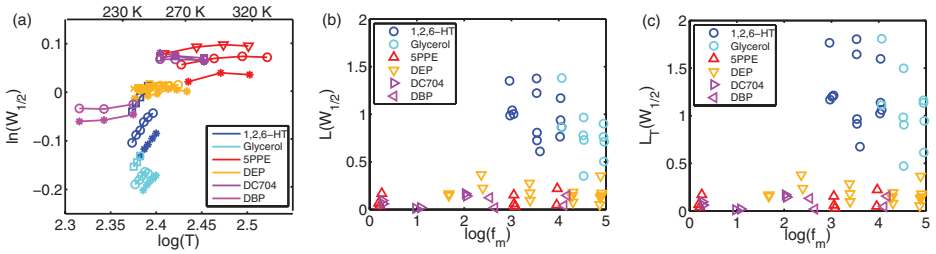

FIG. 2. Analysis of isochronal superposition (IS) based on the half width at half depth of the dielectric loss peak, $W_{1/2}$. (a) Data for $W_{1/2}$ along isochrones marked by connecting lines as functions of temperature. (b) The measure $L(W_{1/2})$ giving the rate of relative change of $W_{1/2}$ along an isochrone. (c) The measure $L_T(W_{1/2})$. Both measures are considerably higher for the hydrogen-bonded liquids than for the van der Waals liquids; thus the latter obey IS to a higher degree than the hydrogen-bonded liquids.

that the two measures $L(W_{1/2})$ and $L_T(W_{1/2})$ lead to similar overall pictures and the same conclusion.

Invariance of one shape parameter such as $W_{1/2}$ is not enough to prove IS. As a second, model-independent shape parameter we used the area of dielectric loss over maximum loss in a log-log plot, denoted by A. We integrated from -0.4 decades below the loss peak frequency to 1.0 decade above it. This was done by adding data for the logarithm of the dielectric loss taken at -0.4, -0.2, 0.2, 0.4, 0.6, 0.8, and 1.0 decades relative to the loss peak frequency. This area measure focuses on the high-frequency side of the peak. This is motivated in part by the occasional presence of dc conductivity on the low-frequency side of the peak, in part by the fact that for molecular-liquids this side of the peak is generally characterized by a slope close to unity, i.e., it varies little from liquid to liquid.[20] In Fig. 3, the measures $L(A)$ and $L_T(A)$ are shown. Clearly, the measures are higher for the hydrogen-bonded liquids than for the van der Waals liquids. Thus also with respect to the area shape parameter, the van der Waals liquids obey IS to a higher degree than the hydrogen-bonded liquids.

As a third parameter, we used the model-dependent shape parameter β_{DC} from the Cole-Davidson fitting function.[21] Details on the fits are given in the supplementary material.[4] Results from using the L operators on β_{CD} are shown in Fig. 4. It is seen that also with respect to the model-dependent shape parameter β_{CD} the van der Waals liquids obey IS to a higher degree than the hydrogen-bonded liquids.

The conclusion that van der Waals liquids obey IS better than hydrogen-bonded liquids is not new. This was reported as a clear tendency in the pioneering papers on IS from 2003 and 2005 by Roland *et al.*[2] and Ngai *et al.*[3] In 2009, this finding was given a theoretical basis via the isomorph theory,[22,23] which applies for liquids that have strong correlations between their virial and potential-energy equilibrium fluctuations at constant volume.[24–26] Due to the directional nature of hydrogen bonds, liquids dominated by these do not show strong virial potential-energy correlations.[24] The isomorph theory predicts that density scaling, as well as IS, applies for van der Waals liquids, but not for hydrogen-bonded liquids, a result that is consistent with previous experiments.[27–30] Only few experimental studies have yet been made with the explicit purpose of testing the isomorph theory, see, e.g., Ref. 31, which supports the theory.

In this paper, we have focused on systems with no visible beta relaxation or excess wing. Capaccioli *et al.*[19] demonstrated IS in systems with beta relaxation, suggesting that the beta and alpha relaxations are connected. This result can be rationalized in terms of the isomorph theory, which predicts IS to hold for all intermolecular modes. It would be interesting to use the quantitative measures suggested in this paper for systems with a beta relaxation.

To summarize, we have proposed two measures of isochronal superposition that quantify the relative change of a given relaxation-spectrum shape parameter along an isochrone. The measures were tested for six liquids with re-

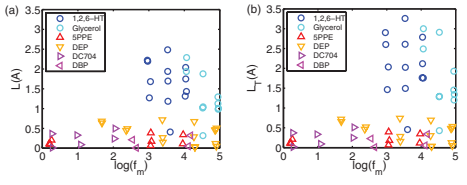

FIG. 3. The measures of isochronal superposition based on the area A of the dielectric loss peak plotted in a normalized log-log plot, obtained by integrating from -0.4 to $+1.0$ decades around the loss-peak frequency. (a) The measure $L(A)$. (b) The measure $L_T(A)$.

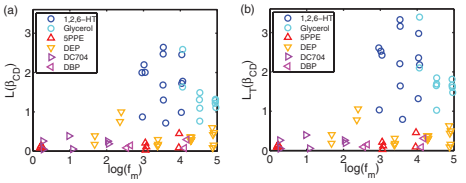

FIG. 4. The measures of isochronal superposition based on the shape parameter of the Cole-Davidson function β_{CD}. (a) The measure $L(\beta_{CD})$. (b) The measure $L_T(\beta_{CD})$.

gard to two model-independent shape parameters characterizing dielectric loss peaks, the half width at half depth and the loss-peak area in a normalized log-log plot, and one model-dependent shape parameter, the Cole-Davidson β_{CD}. The two measures lead to similar overall pictures; in particular both support the conclusion that van der Waals liquids obey IS to a higher degree than hydrogen-bonded liquids.

We thank Albena Nielsen for providing data to this study, Bo Jakobsen for help with the data analysis, and Ib Høst Pedersen for help in relation to the high-pressure setup. L.A.R. and K.N. wish to acknowledge The Danish Council for Independent Research for supporting this work. The center for viscous liquid dynamics "Glass and Time" is sponsored by the Danish National Research Foundation's Grant No. DNRF61.

[1] A. Tölle, Rep. Prog. Phys. **64**, 1473 (2001).
[2] C. M. Roland, R. Casalini, and M. Paluch, Chem. Phys. Lett. **367**, 259 (2003).
[3] K. L. Ngai, R. Casalini, S. Capaccioli, M. Paluch, and C. M. Roland, J. Phys. Chem. B **109**, 17356 (2005).
[4] See supplementary material at http://dx.doi.org/10.1063/1.4821163 for experimental details and further results.
[5] Estimated from calorimetric data measured in our lab.
[6] A. I. Nielsen, T. Christensen, B. Jakobsen, K. Niss, N. B. Olsen, R. Richert, and J. C. Dyre, J. Chem. Phys. **130**, 154508 (2009).
[7] P. W. Bridgman, Proc. Am. Acad. Arts Sci. **67**, 1 (1932).
[8] B. Jakobsen, K. Niss, and N. B. Olsen, J. Chem. Phys. **123**, 234511 (2005).
[9] D. Gundermann, Ph.D. thesis, Roskilde University, DNRF Centre "Glass & Time," IMFUFA, NSM, 2012.
[10] A. I. Nielsen, S. Pawlus, M. Paluch, and J. C. Dyre, Philos. Mag. **88**, 4101 (2008).
[11] K. Niss, C. Dalle-Ferrier, G. Tarjus, and C. Alba-Simionesco, J. Phys.: Condens. Matter **19**, 076102 (2007).
[12] H. Forsman, Mol. Phys. **63**, 65 (1988).
[13] H. Forsman, P. Andersson, and G. Bäckström, J. Chem. Soc., Faraday Trans. 2 **82**, 857 (1986).
[14] M. Paluch, S. J. Rzoska, P. Habdas, and J. Ziolo, J. Phys.: Condens. Matter **8**, 10885 (1996).
[15] M. Paluch, J. Ziolo, S. J. Rzoska, and P. Habdas, J. Phys.: Condens. Matter **9**, 5485 (1997).
[16] S. Pawlus, M. Paluch, M. Sekula, K. L. Ngai, S. J. Rzoska, and J. Ziolo, Phys. Rev. E **68**, 021503 (2003).
[17] L. A. Roed, Master's thesis, Roskilde University, IMFUFA, NSM, 2012.
[18] B. Igarashi, T. Christensen, E. H. Larsen, N. B. Olsen, I. H. Pedersen, T. Rasmussen, and J. C. Dyre, Rev. Sci. Instrum. **79**, 045106 (2008).
[19] S. Capaccioli, K. Kessairi, M. Lucchesi, and P. A. Rolla, J. Phys.: Condens. Matter **19**, 205133 (2007).
[20] A. I. Nielsen, Ph.D. thesis, Roskilde University, DNRF Centre "Glass & Time," IMFUFA, NSM, 2009.
[21] D. W. Davidson and R. H. Cole, J. Chem. Phys. **18**, 1417 (1950).
[22] N. Gnan, T. B. Schrøder, U. R. Pedersen, N. P. Bailey, and J. C. Dyre, J. Chem. Phys. **131**, 234504 (2009).
[23] T. B. Schrøder, N. Gnan, U. R. Pedersen, N. P. Bailey, and J. C. Dyre, J. Chem. Phys. **134**, 164505 (2011).
[24] N. P. Bailey, U. R. Pedersen, N. Gnan, T. B. Schrøder, and J. C. Dyre, J. Chem. Phys. **129**, 184507 (2008).
[25] N. P. Bailey, U. R. Pedersen, N. Gnan, T. B. Schrøder, and J. C. Dyre, J. Chem. Phys. **129**, 184508 (2008).
[26] T. B. Schrøder, N. P. Bailey, U. R. Pedersen, N. Gnan, and J. C. Dyre, J. Chem. Phys. **131**, 234503 (2009).
[27] C. Dreyfus, A. L. Grand, J. Gapinski, W. Steffen, and A. Patkowski, Eur. Phys. J. B **42**, 309 (2004).
[28] R. Casalini and C. M. Roland, Phys. Rev. E **69**, 062501 (2004).
[29] C. Alba-Simionesco, A. Cailliaux, A. Alegría, and G. Tarjus, Europhys. Lett. **68**, 58 (2004).
[30] C. M. Roland, R. Casalini, R. Bergman, and J. Mattsson, Phys. Rev. B **77**, 012201 (2008).
[31] D. Gundermann, U. R. Pedersen, T. Hecksher, N. P. Bailey, B. Jakobsen, T. Christensen, N. B. Olsen, T. B. Schrøder, D. Fragiadakis, R. Casalini, C. M. Roland, J. C. Dyre, and K. Niss, Nat. Phys. **7**, 816 (2011).

THE JOURNAL OF CHEMICAL PHYSICS **143**, 221101 (2015)

Communication: High pressure specific heat spectroscopy reveals simple relaxation behavior of glass forming molecular liquid

Lisa Anita Roed, Kristine Niss, and Bo Jakobsen[a)]
DNRF Centre "Glass and Time," IMFUFA, Department of Sciences, Roskilde University, P.O. Box 260, DK-4000 Roskilde, Denmark

(Received 22 October 2015; accepted 18 November 2015; published online 9 December 2015)

The frequency dependent specific heat has been measured under pressure for the molecular glass forming liquid 5-polyphenyl-4-ether in the viscous regime close to the glass transition. The temperature and pressure dependences of the characteristic time scale associated with the specific heat is compared to the equivalent time scale from dielectric spectroscopy performed under identical conditions. It is shown that the ratio between the two time scales is independent of both temperature and pressure. This observation is non-trivial and demonstrates the existence of specially simple molecular liquids in which different physical relaxation processes are both as function of temperature and pressure/density governed by the same underlying "inner clock." Furthermore, the results are discussed in terms of the recent conjecture that van der Waals liquids, like the measured liquid, comply to the isomorph theory. © *2015 AIP Publishing LLC.* [http://dx.doi.org/10.1063/1.4936867]

The viscosity of liquids close to the glass transition is strongly temperature dependent — just a few percent decrease in temperature can lead to several decades increase in viscosity. Coupled to the increase in viscosity is a slowing down of the molecular structural relaxation time (the alpha relaxation time), leading to a time scale separation between the fast iso-structural degrees of freedom and the slow structural degrees of freedom. The glass transition occurs at the temperature where the slow degrees of freedom are no longer accessible on the experimental time scale. This gives rise to a drop in the measured specific heat which is a classical signature of the glass transition.[1] The time scale separation in the highly viscous liquid just above the glass transition temperature leads to time or equivalently frequency dependence of physical properties which couple to the structural relaxation; the mechanical moduli and the dielectric constant are, for example, frequency dependent. Even though heat capacity is a classical probe of the glass transition, the awareness of the fact that the specific heat is also a frequency dependent response function which shows relaxation is surprisingly young and only dates back to the 1980s (some of the earliest discussions are given in Refs. 2–7). The first experimental specific heat spectroscopic techniques for studying viscous liquids were also developed in the 1980s by Birge and Nagel[4] and Christensen.[5] The amount of data on frequency dependent specific heat is still very limited today 30 years later, probably because no standard commercial technique has been available. (The following list is not a comprehensive list of all specific heat spectroscopy studies of glass forming liquids but covers to the best of our knowledge all groups that have addressed the issue, Refs. 4, 5, and 8–14).

The workhorse in the study of frequency dependent response of glass forming liquids is dielectric spectroscopy both when it comes to studies of the temperature dependence of the alpha relaxation (e.g., Refs. 15–17) and the spectral shape of the relaxation (i.e., stretching[18,19] and beta-relaxation[20]). The use of dielectric spectroscopy is particularly dominant when it comes to high pressure studies, which have become increasingly important during the last couple of decades. Today, it is clear that the dynamics of viscous liquids should be understood as function of both temperature and pressure/density because this is the only way to disentangle the effect of density from that of thermal energy. Two key findings from high pressure studies are: density scaling (e.g., Refs. 21–24), and isochronal superposition (e.g., Refs. 25–30). These results are almost exclusively based on dielectric data because dielectric spectroscopy is easily adapted to high pressure and commercial equipment is available.[31]

Different physical properties probe the microscopic dynamics in different ways. An example is that dielectric spectroscopy only is sensitive to degrees of freedom which involve reorientation of dipoles in the liquid while specific heat measures those degrees of freedom which couple to changes in energy. This naturally leads to differences in the observed characteristic time scales for different properties it is, e.g., well-known that shear-mechanical relaxation is faster than dielectric relaxation (e.g., Ref. 32 and references therein).

While all the liquid dynamics slows down upon cooling (or compression) it is by no means trivial that all time scales follow each other as a function of temperature and pressure. A well-known example is the pronounced decoupling between translational and rotational motions which has been confirmed in many systems, also under pressure (e.g., Ref. 33). Even time scales which at a first coarse look seem to follow each other over many decades have been shown to have differences in the temperature dependence when analyzed in detail (e.g., Refs. 32 and 34). Moreover, there is an increasing amount of evidence for dynamical heterogenities in viscous liquids

a)Electronic mail: boj@dirac.ruc.dk

(e.g., Ref. 35). Different physical properties will *a priori* "see" and average differently over the dynamical heterogeneities. This would imply different temperature-dependence of the time scales as the dynamical heterogenities evolve with cooling and lead to the picture suggested by Angell in 1991, namely, a series of decoupling temperatures as the liquid is cooled down.[36]

An example of the pitfall of exclusively basing analysis on one response function is the understanding of the dynamics in monohydroxy alcohols. It was for a long time thought that the main dielectric relaxation peak was the signature of the structural relaxation, leading to puzzling observations about monohydroxy alcohols (e.g., in Ref. 18). This was only resolved when other response functions were analyzed, showing that the dominant process in the dielectric spectrum is not related to the structural molecular relaxation[37] seen in specific heat[38] and shear modulus.[39,40]

It is in itself a fundamental question whether the liquid relaxation seen in different techniques behaves in the same way. Additionally, it is important to establish whether dielectric results especially at elevated pressures can be generalized and viewed as generic information about the alpha relaxation.

Experimentalists have often attempted to find general (universal) behaviors and correlations in the effort to guide theory and models for the viscous slowing down.[18,41–43] However, as more and more systems are studied, these results are usually found to hold only for a limited class of systems.[44–48] Another trend is to focus on exotic phenomena seen in complicated systems like the notorious counter example water.[49,50] The emerging picture is that while the viscous slowing down and the glass transition as such are universal features which (at least in principle) can be observed in all systems independent of chemical details, there is also a myriad of specific behaviors and it seems unlikely to capture all this in one simple model. Based on this understanding our proposal is to address the question of what the simplest behavior is? Or put in other words what are the features that should be included in the "ideal gas model" of glass forming liquids?

In this work, we present frequency dependent specific heat measurements taken as function of both temperature and pressure up to 300 MPa on the molecular glass former 5-polyphenyl-4-ether (*5PPE*) and compare to existing dielectric data[30,51] taken in the same pressure equipment ensuring consistency of absolute temperature and pressure. To the best of our knowledge, these are the first ever high pressure data where both dielectric and specific heat spectroscopy are taken under identical conditions, allowing for a detailed comparison.

5PPE has been studied intensively by the "Glass and time" group over the past years (at atmospheric pressure,[14,32,52–55] and at high pressures[30,56,57]) and has been found to have a particular simple behavior. One of these findings was that no decoupling is seen in 5PPE when comparing the temperature dependence of 6 different time scales.[54] This result was later supported by result from the group of Schick who compared dielectric and specific heat spectroscopy with lower accuracy but over larger range in dynamics.[58]

The data in the current paper extend these studies to high pressures. Hereby addressing the question of whether the alpha relaxation time is uniquely determined independent of probe in the entire phase space.

The strong temperature dependence of the characteristic time scales of liquids close to the glass transition has the consequence that even small temperature/pressure differences will lead to large errors in the measured time scales. In order to make detailed comparisons, it is therefore crucial to measure different response functions under the same conditions (see e.g., Ref. 59). To the best of our knowledge there is only one previous study of frequency dependent specific heat at elevated pressures, in which Leyser *et al.*[60] 20 years ago investigated orthoterphenyl in a limited pressure range up to 105 MPa, and compared to existing literature data.[61] Their data show that the time scales do follow rather closely along the investigated paths in phase space; however, some systematic changes are seen. Due to the limited pressure/temperature range investigated and the fact that the dielectric data they compare to is from a different study, it is not possible to conclude if the ratio between the two time scales is constant or changing for this liquid.

Our unique specific heat spectroscopy technique is based on measuring the thermal impedance at a spherical surface in the liquid (the relation between heat flow into the liquid from the surface, and the temperature at the same surface). The method is inspired by the method developed by Birge and Nagel 30 years ago.[4,62] Our version of the technique[14] utilize a spherical geometry, and a liquid layer much thicker than the thermal wavelength (the thermally thick limit). In this case, the outer thermal and mechanical boundaries do not influence the measured property.[63] What is measured is the longitudinal volume specific heat c_l[63,64] which is approximately equal to the isobaric specific heat.[65] By the 3omega technique a temperature dependent resistor is utilized as heat generator and thermometer simultaneous.[14,62]

The method is well suited to be adopted to different sample environments with little requirements to the mechanical properties of the sample cell and electrical connections. Altogether this makes the method perfect for integration in existing pressure equipment.

The measurements were performed using commercial high-pressure equipment from Unipress Equipment (Warsaw, Poland). The pressure is applied using a pressure liquid, which is separated from the sample cell by a shielding of rubber and Teflon. Pressures go up to 600 MPa with a stability of 3 MPa, temperatures ranges from 233 to 333 K (for further details see Refs. 51, 56, and 66). A spherical NTC-thermistor bead (a temperature dependent resistor, with "Negative Temperature Coefficient") is used as heat generator and thermometer and is placed in the middle of the sample cell with a distance of ≈10 mm from the closest sides ensuring approximately thermally thick conditions down to the millihertz range. The 5PPE liquid studied is the diffusion pump oil 5-polyphenyl-4-ether acquired from Santovac. The liquid was dried for one hour under vacuum before use.

The specific heat measurements are performed at different temperatures along the isobars; 0.1 MPa (atmospheric pressure), 150 MPa, and 300 MPa. The initial data analysis

was performed as in Ref. 14. Examples of the imaginary part of the frequency dependent longitudinal specific heat at different temperatures and pressures are shown in Fig. 1(a). The peak frequency of the imaginary part, $f_{c_l,\mathrm{lp}}$ (the loss-peak frequency), defines a directly experimental accessible characteristic time scale ($\tau_{c_l} = 1/(2\pi f_{c_l,\mathrm{lp}})$) for the specific heat relaxation. Figure 1(b). shows the relaxation times for all measured temperatures and pressures. The extreme temperature and pressure dependences of the relaxation time are clearly seen in this representation. The shown error bars refer to limitations in precision of the specific heat technique.[14] There is moreover approximately 0.1 decade uncertainty on the relaxation time due to the limited stability of the pressure of 3 MPa.

The comparable dielectric spectroscopy measurements were taken in relation to Refs. 30 and 51 utilizing the same pressure equipment. The dielectric measurements were performed along the isobars; 0.1 MPa, 100 MPa, 200 MPa, 300 MPa, and 400 MPa. The relaxation time is again defined from the loss-peak frequency ($\tau_\epsilon = 1/(2\pi f_{\epsilon,\mathrm{lp}})$). Figure 2 shows the relaxation time as a function of temperature at the different pressures for both the specific heat and for the dielectric measurements. As mentioned earlier the fact that the data are taken under the same thermal and pressure conditions gives a unique possibility for directly comparing

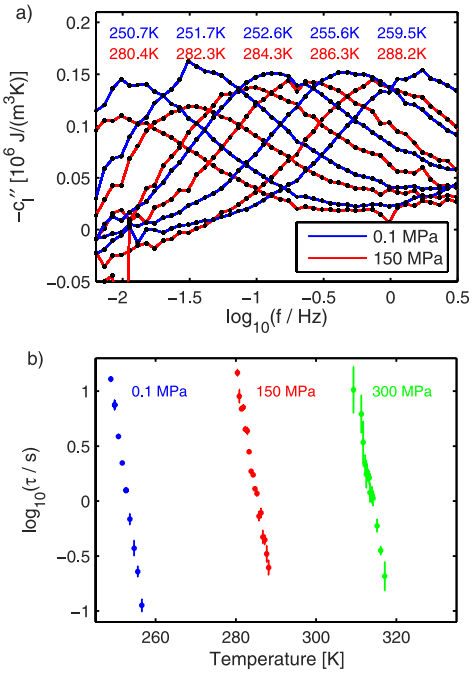

FIG. 1. Specific heat data. (a) The imaginary part of the longitudinal specific heat at the indicated temperatures and pressures. (b) The relaxation time τ, based on the loss-peak frequency, as a function of temperature for all studied temperatures and pressures.

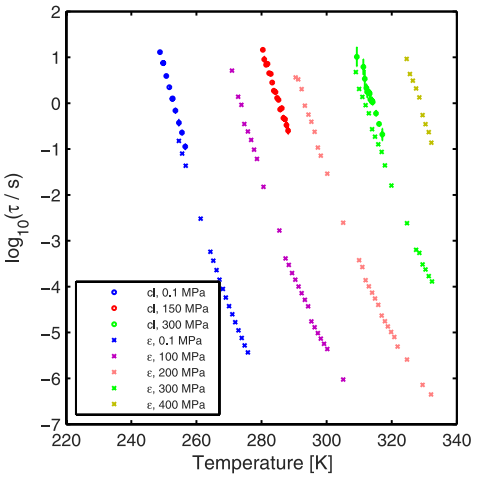

FIG. 2. Comparison of the relaxation times (τ) for the specific heat measurements (same data as on Fig. 1) and the dielectric measurements at the indicated pressures.

the temperature and pressure dependence of the time scale from dielectric and specific heat spectroscopy over a rather wide pressure range.

From Fig. 2, it is seen that the temperature dependence of the relaxation times from the two methods closely follows each other at all investigated pressures. It is also seen that the dielectric relaxation time is faster than the specific heat relaxation time at all pressures. This shows that the ambient pressure observation of identical temperature dependence of dielectric and specific heat relaxation time presented by some of us in Jakobsen *et al.* (2012)[54] on 5PPE also holds at elevated pressures.

Figure 3 presents the same data using isochrones, which are lines in the phase diagram of constant relaxation time; that is contour lines of the relaxation time map, $\tau(T,P)$. The isochrones are illustrated for both methods, and it is seen that the isochrones for the two response functions are parallel.

The *main result* of this communication is that the τ_ϵ/τ_{c_l} ratio is constant within error bars for all investigated temperatures and pressures for 5PPE. This result is obtained by combining the observation from Fig. 2 (and Ref. 54) and Fig. 3 as described below. Combining the data from the present study and from Ref. 54 yields $\log_{10}(\tau_\epsilon/\tau_{c_l}) = -0.4 \pm 0.1$, with the major contribution to the uncertainty coming from pressure instabilities.

The relaxation time is a smooth function of temperature and pressure, and parallel isochrones therefore imply that an isochrone for one of the two response functions is also an isochrone for the other but with a different time scale, as the dielectric relaxation is faster than the specific heat relaxation at a given state point.

The difference between the time scales associated with the isochrones is not *a priory* the same for different isochrones. The observation that the τ_ϵ/τ_{c_l} ratio is constant along the

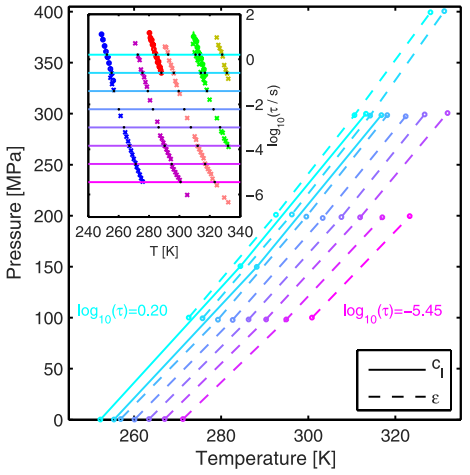

FIG. 3. Isochrones for specific heat (full lines) and dielectric (dashed lines). The two slowest isochrones are found for both the specific heat and dielectric, but the six fastest isochrones are only found for the dielectric measurements. The inset shows the same data as Fig. 2 where the vertical lines illustrate eight chosen relaxation times. The temperatures used for the isochrones are found by interpolation (indicated by small solid points on the inset).

isobars as shown in Fig. 2 (and illustrated even more clearly at atmospheric pressure in Ref. 54) is therefore an additional simplicity. Since any isobar crosses all the isochrones, we can conclude that the time scale difference associated with the isochrones indeed is the same in all of the explored part of the phase diagram for this liquid (it is enough to shown that it is constant along one curve, crossing the isochrones).

The observation that the isochrones from one of the methods are also isochrones for the other method is a direct prediction of the isomorph theory developed in the "Glass and Time" group.[67–69] The theory predicts the existence of isomorphs which are curves in the phase diagram of simple (called *Roskilde simple*) liquids along which a number of properties are invariant. The isochrones of any response function will in the viscous regime (or in reduced units) coincide with an isomorphs, which means that an isochrone from one response function is also an isochrone for another response function, as all dynamics are invariant along an isomorph.[30]

Simple van der Waals liquids as 5PPE are expected to be Roskilde simple.[67,68,70] We have in Refs. 30, 56, and 57 shown that 5PPE corroborates other isomorph predictions, this together with the present result indicating that 5PPE indeed is a good example of a Roskilde simple liquid.

In Jakobsen *et al.* (2012)[54] some of us showed that at ambient pressure, not only specific heat and dielectric but also several other thermo-viscoelastic responses have time scales which follow closely with temperature for 5PPE. Based on this, we hypothesize that the time scales of all the frequency dependent response functions of 5PPE have a common temperature and pressure dependence in the viscous regime. An interpretation of this observation is that the structural relaxation time is governed by one "inner clock" and implies a greater simplicity than predicted by the isomorph theory. It is also a challenge to understand how all response functions can couple so closely if the underlying dynamics is heterogeneous with a growing length scale along with viscous slowing down — since the different macroscopic responses could very well average differently over the heterogeneities.

5PPE has other simple behaviors which are beyond isomorph theory. The spectral shape of the dielectric signal obeys Time Temperature Pressure Superposition (TTPS), thus it is independent of pressure and temperature in a range where τ_ϵ changes by 7 orders of magnitude.[30,51] Time temperature superposition is moreover found in frequency dependent bulk modulus and the shear mechanical relaxation, and these two moduli in fact have the same spectral shape.[55] Finally 5PPE is also found to obey time aging time superposition.[53]

The simple behavior of 5PPE is obviously not universal for all glass-forming liquids, it might not even be a general behavior of van der Waals bonded liquids. Yet 5PPE exhibits the hallmarks of glass forming liquids; it has a non-Arrhenius temperature dependence (fragility index m = 80–85)[71] and a non-exponential relaxation (high frequency power law −0.5).[32] This means that models and theories for understanding non-Arrhenius non-exponential relaxation need to be consistent with a simple behavior where there is no decoupling of different time scales and no increase in the broadening of the relaxations in the entire viscous range (defined as time scales ranging from a microsecond up to a kilosecond).

To summarize, we have presented specific heat spectroscopy data over an unprecedented pressure range, with accompanying dielectric data taken under the same thermal and pressure conditions. The main experimental results are that the characteristic time scale of the specific heat and the dielectric relaxation follow each other closely as function of temperature at all investigated pressures and that isochrone curves for specific heat and dielectric spectroscopy coincide. The consequence of these two observations is that the τ_ϵ/τ_{c_l} ratio is constant over the investigated temperature and pressure ranges, with the dielectric spectroscopy being the fastest.

Altogether 5PPE seems to have the simplest possible behavior in respect to differences in time scales between response functions, namely, that one common inner clock controls the different relaxations, and the only difference is a temperature and pressure independent ratio between the different time scales.

L.A.R. and K.N. wish to acknowledge The Danish Council for Independent Research for supporting this work. The center for viscous liquid dynamics "Glass and Time" is sponsored by the Danish National Research Foundation's Grant No. DNRF61.

[1]W. Kauzmann, Chem. Rev. **43**, 219 (1948).
[2]H. Gobrecht, K. Hamann, and G. Willers, J. Phys. E: Sci. Instrum. **4**, 21 (1971).
[3]C. A. Angell and L. M. Torell, J. Chem. Phys. **78**, 937 (1983).
[4]N. O. Birge and S. R. Nagel, Phys. Rev. Lett. **54**, 2674 (1985).
[5]T. Christensen, J. Phys. Colloq. **46**, C8-635 (1985).
[6]N. O. Birge, Phys. Rev. B **34**, 1631 (1986).
[7]J. K. Nielsen and J. C. Dyre, Phys. Rev. B **54**, 15754 (1996).

[8]M. Settles, F. Post, D. Muller, A. Schulte, and W. Doster, Biophys. Chem. **43**, 107 (1992).
[9]I. K. Moon, Y. H. Jeong, and S. I. Kwun, Rev. Sci. Instrum. **67**, 29 (1996).
[10]T. Christensen and N. B. Olsen, J. Non-Cryst. Solids **235-237**, 296 (1998).
[11]L. Carpentier, O. Bustin, and M. Descamps, J. Phys. D: Appl. Phys. **35**, 402 (2002).
[12]E. H. Bentefour, C. Glorieux, M. Chirtoc, and J. Thoen, J. Appl. Phys. **93**, 9610 (2003).
[13]A. A. Minakov, S. A. Adamovsky, and C. Schick, Thermochim. Acta **403**, 89 (2003).
[14]B. Jakobsen, N. B. Olsen, and T. Christensen, Phys. Rev. E **81**, 061505 (2010).
[15]R. Richert and C. A. Angell, J. Chem. Phys. **108**, 9016 (1998).
[16]T. Hecksher, A. I. Nielsen, N. B. Olsen, and J. C. Dyre, Nat. Phys. **4**, 737 (2008).
[17]Y. S. Elmatad, D. Chandler, and J. P. Garrahan, J. Phys. Chem. B **113**, 5563 (2009).
[18]R. Bohmer, K. L. Ngai, C. A. Angell, and D. J. Plazek, J. Chem. Phys. **99**, 4201 (1993).
[19]A. I. Nielsen, T. Christensen, B. Jakobsen, K. Niss, N. B. Olsen, R. Richert, and J. C. Dyre, J. Chem. Phys. **130**, 154508 (2009).
[20]G. P. Johari and M. Goldstein, J. Chem. Phys. **53**, 2372 (1970).
[21]C. Dreyfus, A. Aouadi, J. Gapinski, M. Matos-Lopes, W. Steffen, A. Patkowski, and R. M. Pick, Phys. Rev. E **68**, 011204 (2003).
[22]C. Alba-Simionesco, A. Cailliaux, A. Alegría, and G. Tarjus, Europhys. Lett. **68**, 58 (2004).
[23]R. Casalini and C. M. Roland, Phys. Rev. E **69**, 062501 (2004).
[24]C. M. Roland, S. Hensel-Bielowka, M. Paluch, and R. Casalini, Rep. Prog. Phys. **69**, 1405 (2005).
[25]A. Tölle, Rep. Prog. Phys. **64**, 1473 (2001).
[26]C. Roland, R. Casalini, and M. Paluch, Chem. Phys. Lett. **367**, 259 (2003).
[27]S. Pawlus, M. Paluch, M. Sekula, K. L. Ngai, S. J. Rzoska, and J. Ziolo, Phys. Rev. E **68**, 021503 (2003).
[28]K. L. Ngai, R. Casalini, S. Capaccioli, M. Paluch, and C. M. Roland, J. Phys. Chem. B **109**, 17356 (2005).
[29]C. M. Roland, R. Casalini, R. Bergman, and J. Mattsson, Phys. Rev. B **77**, 012201 (2008).
[30]L. A. Roed, D. Gundermann, J. C. Dyre, and K. Niss, J. Chem. Phys. **139**, 101101 (2013).
[31]Examples of commercial high pressure dielectric equipment are a full dielectric high pressure system from "NOVOCONTROL Technologies GmbH" and high pressure vessels with electrical feed throughs from "Unipress Equipment."
[32]B. Jakobsen, K. Niss, and N. B. Olsen, J. Chem. Phys. **123**, 234511 (2005).
[33]S. H. Bielowka, T. Psurek, J. Ziolo, and M. Paluch, Phys. Rev. E **63**, 062301 (2001).
[34]F. Stickel, E. W. Fischer, and R. Richert, J. Chem. Phys. **104**, 2043 (1996).
[35]M. D. Ediger, Annu. Rev. Phys. Chem. **51**, 99 (2000).
[36]C. A. Angell, J. Non-Cryst. Solids **131-133**, 13 (1991).
[37]R. Böhmer, C. Gainaru, and R. Richert, Phys. Rep. **545**, 125 (2014).
[38]H. Huth, L.-M. Wang, C. Schick, and R. Richert, J. Chem. Phys. **126**, 104503 (2007).
[39]B. Jakobsen, C. Maggi, T. Christensen, and J. C. Dyre, J. Chem. Phys. **129**, 184502 (2008).
[40]T. Hecksher and B. Jakobsen, J. Chem. Phys. **141**, 101104 (2014).
[41]A. P. Sokolov, E. Rössler, A. Kisliuk, and D. Quitmann, Phys. Rev. Lett. **71**, 2062 (1993).
[42]T. Scopigno, G. Ruocco, F. Sette, and G. Monaco, Science **302**, 849 (2003).
[43]V. N. Novikov and A. P. Sokolov, Nature **431**, 961 (2004).
[44]S. N. Yannopoulos and G. N. Papatheodorou, Phys. Rev. B **62**, 3728 (2000).
[45]D. H. Huang and G. B. McKenna, J. Chem. Phys. **114**, 5621 (2001).
[46]U. Buchenau and A. Wischnewski, Phys. Rev. B **70**, 092201 (2004).
[47]K. Niss, C. Dalle-Ferrier, G. Tarjus, and C. Alba-Simionesco, J. Phys.: Condens. Matter **19**, 076102 (2007).
[48]C. Dalle-Ferrier, K. Niss, A. P. Sokolov, B. Frick, J. Serrano, and C. Alba-Simionesco, Macromolecules **43**, 8977 (2010).
[49]P. G. Debenedetti, J. Phys.: Condens. Matter **15**, R1669 (2003).
[50]C. A. Angell, Science **319**, 582 (2008).
[51]L. A. Roed, "Isochronal superposition - an experimental test of a prediction from the isomorph theory," Master's thesis, NSM, IMFUFA, Physics, Roskilde University, Denmark, 2012.
[52]K. Niss, B. Jakobsen, and N. B. Olsen, J. Chem. Phys. **123**, 234510 (2005).
[53]T. Hecksher, N. B. Olsen, K. Niss, and J. C. Dyre, J. Chem. Phys. **133**, 174514 (2010).
[54]B. Jakobsen, T. Hecksher, T. Christensen, N. B. Olsen, J. C. Dyre, and K. Niss, J. Chem. Phys. **136**, 081102 (2012).
[55]T. Hecksher, N. B. Olsen, K. A. Nelson, J. C. Dyre, and T. Christensen, J. Chem. Phys. **138**, 12A543 (2013).
[56]D. Gundermann, "Testing predictions of the isomorph theory by experiment," Ph.D. thesis, Roskilde University, DNRF Centre "Glass & Time", IMFUFA, NSM, 2013).
[57]W. Xiao, J. Tofteskov, T. V. Christensen, J. C. Dyre, and K. Niss, J. Non-Cryst. Solids **407**, 190 (2015).
[58]E. Shoifet, G. Schulz, and C. Schick, Thermochim. Acta **603**, 227 (2015).
[59]R. Richert, Chem. Phys. Lett. **199**, 355 (1992).
[60]H. Leyser, A. Schulte, W. Doster, and W. Petry, Phys. Rev. E **51**, 5899 (1995).
[61]M. Naoki, H. Endou, and K. Matsumoto, J. Phys. Chem. **91**, 4169 (1987).
[62]N. O. Birge, P. K. Dixon, and N. Menon, Thermochim. Acta **304–305**, 51 (1997).
[63]T. Christensen and J. C. Dyre, Phys. Rev. E **78**, 021501 (2008).
[64]T. Christensen, N. B. Olsen, and J. C. Dyre, Phys. Rev. E **75**, 041502 (2007).
[65]The longitudinal volume specific heat c_l is related to the isochoric specific heat (c_v) by $c_l = \frac{K_S + \frac{4}{3}G}{K_T + \frac{4}{3}G} c_v$ where K_S and K_T respectively are the adiabatic and the isothermal bulk moduli, and G is the shear modulus. At state points where relaxation occurs G will differ from 0, which means that c_l and c_P differs. However, the difference in characteristic timescale is very small (see supplementary material of Ref. 54).
[66]B. Igarashi, T. Christensen, E. H. Larsen, N. B. Olsen, I. H. Pedersen, T. Rasmussen, and J. C. Dyre, Rev. Sci. Instrum. **79**, 045106 (2008).
[67]N. Gnan, T. B. Schrøder, U. R. Pedersen, N. P. Bailey, and J. C. Dyre, J. Chem. Phys. **131**, 234504 (2009).
[68]J. C. Dyre, J. Phys. Chem. B **118**, 10007 (2014).
[69]T. B. Schrøder and J. C. Dyre, J. Chem. Phys. **141**, 204502 (2014).
[70]T. S. Ingebrigtsen, T. B. Schrøder, and J. C. Dyre, Phys. Rev. X **2**, 011011 (2012).
[71]K. Niss and B. Jakobsen, "Dielectric and shear mechanical relaxation in glass forming liquids — a thorough analysis and experimental test of the DiMarzio-Bishop model," Master thesis, Roskilde University (2003), text nr. 424 in "Tekster fra IMFUFA."

Generalized single-parameter aging tests and their application to glycerol

Lisa Anita Roed, Tina Hecksher, Jeppe C. Dyre, and Kristine Niss
Glass and Time, IMFUFA, Department of Science and Environment,
Roskilde University, Postbox 260, DK-4000 Roskilde, Denmark

(Dated: October 19, 2018)

Abstract

Physical aging of glycerol following temperature jumps is studied by dielectric spectroscopy at temperatures just below the glass transition temperature. The data are analyzed using two single-parameter aging tests developed by Hecksher *et al.* [J. Chem. Phys. **142**, 241103 (2015)]. We generalize these tests to include jumps ending at different temperatures. Moreover, four times larger jumps than previously are studied. The single-parameter aging tests are for the first time applied to a hydrogen-bonded liquid. We conclude that glycerol obeys single-parameter aging to a good approximation.

I. INTRODUCTION

Supercooled liquids are liquids cooled with a cooling rate fast enough to avoid crystallization[1]. As the glass transition is approached the liquid becomes more and more viscous, and at the glass transition temperature (T_g) the molecules effectively stop moving on the experimental time scale[2]. Supercooled liquids are often studied using linear response experiments as for example dielectric spectroscopy, where a change in the electric field (a perturbation) leads to a change in polarization (a response). The perturbation is in this case usually small in order to ensure that the response depends linearly on the applied perturbation, and the measured response function is connected to the dynamics in equilibrium via the fluctuation dissipation theorem. In contrast to linear response experiments, aging is the response following a large perturbation, where the liquid is brought out of equilibrium, and the study of aging is a study of how the properties of a system change over time as it relaxes towards equilibrium[3]. In contrast to linear response studies, aging is highly non-linear, since the relaxation rate itself changes as the liquid equilibrates. Most aging studies, including the work presented in this paper, are studies of how the system responds to a change in temperature. The experiments are performed close to and below the glass transition temperature, where aging takes place on time scales that are slow enough to measure, yet fast enough to follow all (or a substantial part) of the relaxation towards equilibrium. Close to the glass transition temperature, the rate of the structural relaxation depends strongly on temperature, and this has the consequence that aging is non-linear even for fairly small temperature steps. For a jump down in temperature the structural relaxation becomes slower as time evolves, whereas for an jump up in temperature the rate of structural relaxation increases as time evolves.

The study of aging has a very practical root – the out-of-equilibrium nature of glasses has the consequence that the properties of all glassy materials age, even if it is sometimes very slow. The standard formalism for describing this was first set out by Narayanaswamy, an engineer at Ford Motor Company who needed a method for predicting how the frozen-in stresses in a wind-shield depend on the glass' thermal history[4]. Today this is referred to as the Tool-Narayanaswamy (TN) formalism. Besides the obvious importance for application of glasses, aging experiments have the potential to yield new information about fundamental outstanding questions regarding the equilibrium

relaxation (e.g. Ref.[5]).

The analysis in this paper is based on the above-mentioned Tool-Narayanaswamy (TN) aging formalism[3,4,6,7]. The TN-formalism interprets aging in terms of a material time ξ. The material time may be thought of as a time measured on a clock with a clock rate that changes with time as the system ages. The material time is defined from the clock rate $\gamma(t)$ by[4,7]

$$d\xi = \gamma(t)dt. \tag{1}$$

In terms of the material time, the fundamental idea is that the non-linear aging curve is given by a master curve as follows: $R(t) = \phi(\xi(t))$, with $\phi(\xi)$ being a unique function independent of temperature and aging time, t. Inspired by Tool, Narayanaswamy introduced a single-parameter aging assumption in terms of a fictive temperature[8]. The central hypothesis of single-parameter aging is that the clock-rate out of equilibrium, $\gamma(t)$, depends only on one structural parameter, and that this parameter also controls the measured quantity.

In 2015 two of us[8] derived tests of the single-parameter assumption, which are used and further developed below. The starting point of the tests is an "ideal aging experiment" in which aging is measured from equilibrium to a new equilibrium after an "instantaneous" jump in temperature. In the experimental section we discuss how to perform an experiment that comes close to the ideal aging experiment. The tests from 2015 have the advantage that it is not necessary to calculate the material time explicitly in order to test for single-parameter aging. Moreover, the tests can be performed without any additional assumptions regarding the shape of the relaxation curve $\phi(\xi)$ and the temperature dependence of the relaxation rate in equilibrium $\gamma_{eq}(T)$. The tests are in these respects similar to tests we developed in 2010[9] and 2017[5]. The unique feature of one of the 2015-tests is that if a liquid has single-parameter aging, then this can be used to predict relaxation curves. This implies that it is possible to predict linear relaxation curves from the non-linear curves. The linear response to a temperature jump is not easy to measure because it requires a very small temperature change. In this paper we extend the tests and procedures from Hecksher *et al.* 2015 to work also for jumps with different final temperature.

Hecksher *et al.*[8] concluded that the three van der Waals liquids investigated all conform to single-parameter aging to a good approximation. It is of interest to test whether

hydrogen-bonded liquids also have single-parameter aging. The difference between van der Waals bonded liquids and hydrogen-bonded liquids is of interest in relation to the isomorph theory[10,11], which predicts that van der Waals liquids have simple behavior along isochrones, whereas no predictions are given for hydrogen-bonded liquids. This is particularly interesting following the development of isomorph theory of physical aging by one of us[12].

TN-formalism was originally developed for oxide glasses, which are covalently bonded systems, i.e., they have strongly directional bonds. With that in mind it would not be surprising to find that it works also for hydrogen-bonding systems. On the other hand, the single-parameter tests we use today are are performed on high precision data and the tests are developed to have no free fitting parameters. So far we have only performed these high precision parameter free tests on van der Waals bonded liquids[5,8,9], but in this paper we present data and tests on the hydrogen bonding liquid, glycerol.

Glycerol (propane-1,2,3-triol) is a small molecule with three hydroxyl groups. It is the molecular liquid which is used most often in studies of glassy dynamics, e.g. Refs.[13–18], and it is of importance in technology, notably due to its cryoprotectant properties[19–21]. For these reasons it sometimes referred to as an archetypical glass former. Yet, it is also known that glycerol supports the formation of a 3D hydrogen-bonded network penetrating the bulk liquid[22] and some of us have recently shown that glycerol exihibits a low frequency mode in the mechanical relaxation spectra[23]. This means that there is dynamics on a slower time scale than the main relaxation - possibly due to the hydrogen bonding network. This could influence the structural state of the liquid and thereby the number of parameters involved in physical aging.

Section II gives an overview over the experimental details. Section III presents the data and initial data treatment. Generalized single-parameter aging tests are derived in Sec. IV, where also the results of the tests are shown. Section V discusses the generalized single-parameter aging tests and their ability to predict jumps. The results are furthermore discussed in light of the isomorph theory.

II. EXPERIMENTAL PROTOCOL AND DETAILS

A. General considerations on the protocol

We ideally want to perform the temperature jump instantaneously. Since this is not possible, we instead aim for the time it takes to change the temperature and reach thermal equilibrium throughout the sample, to be much smaller than the structural relaxation time of the liquid. Thereby, one can assume that no structural changes takes place in the liquid during the temperature jump, and that the liquid experiences the jump as "instantaneous".

In order to study aging, it is important to apply the perturbation at the right temperature. If the temperature is too far below T_g, the liquid will not reach equilibrium in an experimental time scale (depending on the time of the experiment). Because of the strong temperature dependence of τ, this can be impossible. On the other hand, if the perturbation is applied at a temperature far above T_g, the liquid will come into equilibrium almost instantaneously and the aging will be too fast to be measurable. This of course depends on how fast one can measure. If the relaxation time is close to the time it takes to make a measurement, structural relaxation will occur during the measurement. This leaves only a small temperature interval where measurements can be performed. The starting temperature is a few degrees below the conventional glass transition temperature (where the relaxation time is 100 s[24]). At the temperatures studied the relaxation time of the liquid is between $\log(\tau) = 2.3$ and $\log(\tau) = 4.9$ (see Table. I).

B. Temperature control

In order to change the temperature fast, we use a specially designed microregulator as sample cell[5,8,9,25]. The microregulator is placed in a main cryostat[26]. By using the microregulator temperature fluctuations are kept below 100 μK and the characteristic thermal equilibrium time is 2 s. More details are given in Ref.[9]. In the studied temperature range the time it takes to change temperature is below the relaxation time of the liquid. We can therefore assume that no structural relaxation take place in the liquid during the temperature change with the possible exception at jumps starting at 184 K, where the relaxation time is only 100 times slower that the thermal equilibrium time.

End temp.	Jump	Annealing time	τ_{eq} at end temp.
184 K	180 K $\rightarrow$ 184 K	$\log(t) = 3.7 \approx 1.4$ hours	$\log(\tau_{eq}) = 2.3 \approx 3$ min
	176 K $\rightarrow$ 184 K	$\log(t) = 3.9 \approx 2.2$ hours	
180 K	184 K $\rightarrow$ 180 K	$\log(t) = 4.8 \approx 18$ hours	$\log(\tau_{eq}) = 3.6 \approx 1.2$ hours
	178 K $\rightarrow$ 180 K	$\log(t) = 4.8 \approx 18$ hours	
	176 K $\rightarrow$ 180 K	$\log(t) = 5.0 \approx 30$ hours	
178 K	180 K $\rightarrow$ 178 K	$\log(t) = 5.5 \approx 90$ hours	$\log(\tau_{eq}) = 4.3 \approx 5.5$ hours
176 K	184 K $\rightarrow$ 176 K	$\log(t) = 6.3 \approx 550$ hours	$\log(\tau_{eq}) = 4.9 \approx 23$ hours
	180 K $\rightarrow$ 176 K	$\log(t) = 6.2 \approx 440$ hours	

TABLE I: Times. The annealing time for each jump ranges from a couple of hours to more than 20 days. τ_{eq} is found from Eq. (8).

C. Permitivity – the monitored property

An aging experiment monitors how a selected quantity evolves over time. In this work we monitor the dielectric permitivity at a fixed frequency. The dielectric signal is a useful probe because it can be measured with high precision and it has therefore been used to monitor aging in several earlier works e.g. Schlosser and Schönhals[27], Loidl and Lunkenheimer *et al.*[28–31], Richert *et al.*[32], Alegría *et al.*[33–35], and Cangialosi *et al.*[36]. We use dielectric spectroscopy with a parallel plate capacitor with diameter 10 mm and liquid layer on 50 μm. The electrical measurement equipment is described in Ref.[37]. In order to perform the measurements fast, a single measuring frequency is chosen, where the dielectric loss is measured as a function of time to monitor the aging. The frequency is chosen to be on the right flank of the α-peak but below any excess wing. Figure 1 (a) shows the dielectric equilibrium spectra at the temperatures where the jumps are performed, marking the frequency used for monitoring 0.1 Hz, which corresponds to a measuring time on 20 s. For most measurements, we can assume that no structural changes take place in the liquid during the measurement; however, for the measurements starting at the highest temperature (184 K) where the relxation time is 200 s, some structural relaxation may occur during the measurements.

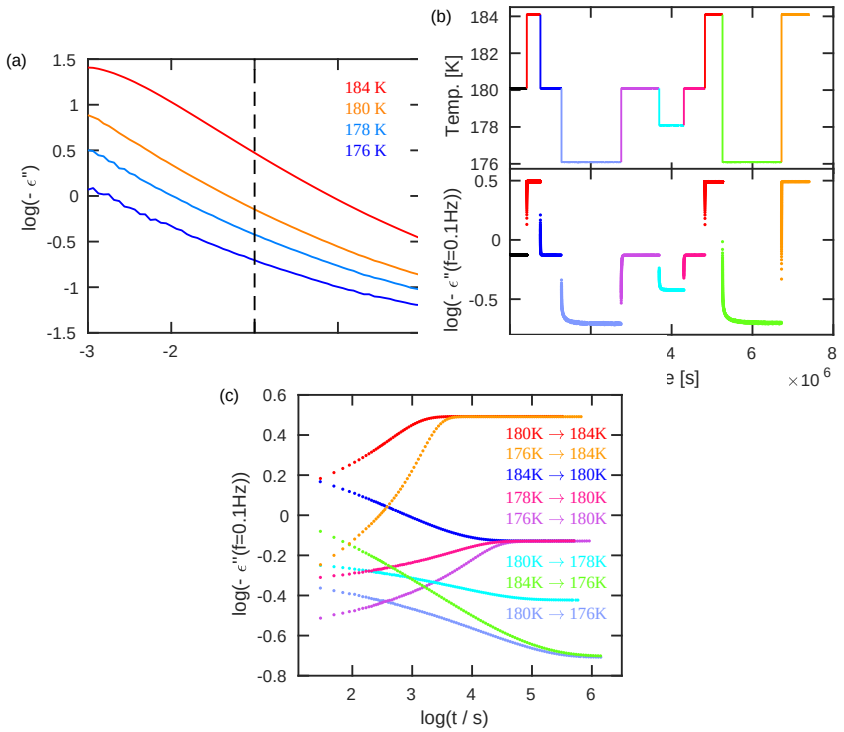

FIG. 1: Raw data. (a) The dielectric loss as a function of frequency in the equilibrium state at the temperatures where jumps are performed between. The dashed black line marks the frequency 0.1 Hz used for monitoring aging. (b) The temperature and the measured quantity ($\log(-\varepsilon''(f = 0.1\text{Hz}))$) as functions of time. (c) The jumps on a logarithmic time scale. The data have been averaged in order to reduce noise as described in the text.

D. Sample

Glycerol was acquired from Fluka and placed in an exicator for 18 h before the experiment. In order to prevent the liquid taking up water from the surrounding air, the cryostat is heated to 300 K before use. It is then flushed with liquid nitrogen, after which the microregulator with sample is placed in the cryostat while the temperature is lowered to 245 K (which is below the melting temperature of water).

III. MEASUREMENTS AND INITIAL DATA ANALYSIS

A. Protocol and raw data

The measuring protocol is the following: The liquid is brought into equilibrium at the starting temperature 180 K (a few degrees below $T_g \approx 185$ K). We used 35 days ($\log(t_{anneal}/s) = 6.5$) of annealing; equilibrium spectra were taken at different temperatures while cooling to estimate the right starting temperature. A jump in temperature is performed, and the liquid is monitored until equilibrium is established. A new jump is then performed. During the jumps the dielectric loss at the measuring frequency is monitored as a function of time ($\log(-\varepsilon''(f = 0.1\text{Hz}, t))$). The jump magnitudes are 2 K, 4 K, and 8 K.

The measuring protocol and the raw data of the aging measurements are seen in Fig. 1 (b), where each color represents a jump. Throughout the paper up jumps are reddish and down jumps are bluish. The jump from 180 K to 184 K is made twice, which makes it possible to check for reproducibility, but only the first jump is used in the further data treatment. Note that the time scale of the measurements is several months. The data are available on Glass and Time's data repository (glass.ruc.dk). Table I shows the annealing time for each jump which ranges from a couple of hours to more than 20 days.

B. Initial data analysis

Figure 1 (c) shows the data on a logarithmic time scale. The data are here averaged in order to reduce noise, which is done on a logarithmic scale. The first 15 raw data points are kept, then the $\log(time)$-scale are divided into 90 equal sized intervals over which the raw data are averaged. Figure 1 (c) shows that jumps ending af the same temperature reach the same equilibrium value. It is on the other hand not visible, that jumps starting at the same temperature have the same starting value. This is due to the instantanous contribution to the aging. Note that same size up and down jumps are not symmetric, which is due to the non-linearity already seen with small jumps.

For the further data treatment some notation is now introduced. The jump is performed from the starting temperature T_{start} and ends at the temperature T_{end}. The measured time-dependent quantity is denoted $X(t) = \log(-\varepsilon''(f = 0.1\text{Hz}, t))$. When the liq-

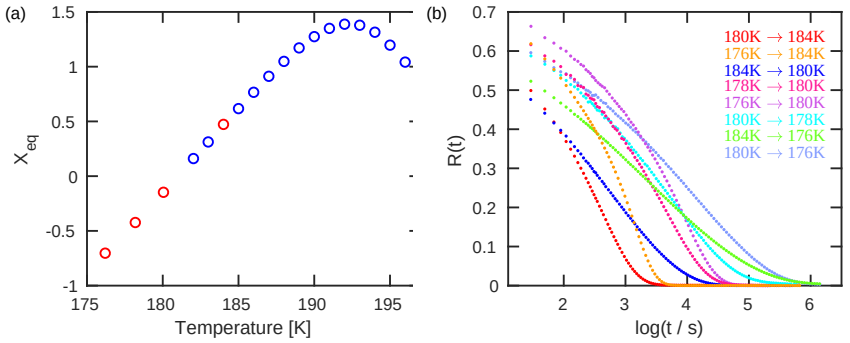

FIG. 2: Quantities used in the data analysis to perform single-parameter tests. (a) The measured quantity ($\log(-\varepsilon''(f = 0.1\text{Hz}, t))$) at equilibrium at the end temperature (X_{eq}) as a function of temperature. The red circles indicate the four temperatures at which jumps are performed. The peak appearing between 190 K and 195 K is due to the α-peak moving across the measuring frequency. (b) The normalized relaxation functions as functions of time for the jumps.

uid is in equilibrium at T_{end} as $t \to \infty$, the measured quantity is X_{eq}. Figure 2 (a) shows X_{eq} as a function of temperature. The time-dependent distance to equilibrium at T_{end} is denoted $\Delta X(t) = X(t) - X_{eq}$. $\Delta X(0)$ thereby defines the total change of the measured quantity from T_{start} to T_{end}.

The normalized relaxation function $R(t)$ is defined as the time-dependent distance to equilibrium over the overall change from start to end of the measured quantity[3,4]

$$R(t) = \frac{\Delta X(t)}{\Delta X(0)} \tag{2}$$

It is seen that $R(0) = 1$ and that $R(t) \to 0$ as $t \to \infty$. Figure 2 (b) shows $R(t)$ for all jumps. According to the TN formalism $R(t)$ is a unique function of the material time ξ.

IV. GENERALIZED SINGLE-PARAMETER AGING TESTS

Two single-parameter aging tests were derived by Hecksher *et al.* 2015[8] for jumps ending at the same temperature. In this investigation we study jumps to different temperatures, and the single-parameter aging tests are therefore generalized below.

According to the single-parameter assumption, both the measured quantity $X(t)$ and

the clock rate $\gamma(t)$ are controlled by the same parameter $Q(t)$. Hecksher *et al.*[8] assumed that the temperature jumps are small, that it is reasonable to Taylor expand both $X(t)$ and $\ln\gamma(t)$ to the first order in $Q(t)$: $\Delta X(t) \cong c_1 \Delta Q(t)$ and $\Delta \ln\gamma(t) \cong c_2 \Delta Q(t)$, where c_1 and c_2 are constants. Eliminating $\Delta Q(t)$ in the equations gives $\ln\gamma(t) = \ln\gamma_{eq} + \Delta X(t)/X_{const}$, where $X_{const} = c_1/c_2$. Using the definition of $R(t)$ (Eq. (2)) gives

$$\gamma(t) = \gamma_{eq} \exp\left(\frac{\Delta X(0)}{X_{const}} R(t)\right) \tag{3}$$

As expected $\gamma(t) \to \gamma_{eq}$ as $t \to \infty$ because $R(t) \to 0$. Hecksher *et al.*[8] derived following expression for the time-derivative of R from the TN-formalism

$$\dot{R} = -F(R)\gamma(t) \tag{4}$$

where $F(R)$ is a unique function of R i.e. independent of start and end temperature. Since $R(t)$ goes from 1 to 0, $\dot{R} < 0$. Inserting the expression for γ (Eq. (3)) and rearranging leads to

$$-\frac{\dot{R}}{\gamma_{eq}} \exp\left(-\frac{\Delta X(0)}{X_{const}} R(t)\right) = F(R) \tag{5}$$

from which the two generalized tests are derived in the following sections.

A. Test 1 - Predicting general jumps from knowledge of a single jump

If single-parameter aging is obeyed, it possible to predict the relaxation function for one jump from the relaxation function of another jump. In the following we use subscripts 1 and 2 to distinguish between the known (measured) relaxation function – jump 1 – and the predicted relaxation functions – jump 2. Thus, from one jump relaxation function $R_1(t)$ and its inverse function $t_1(R)$, we derive a method for determining $t_2(R)$ for a different jump $R_2(t)$ using Eq. (5).

At times $t_1^*(R)$ and $t_2^*(R)$ where the value of the relaxation functions are the same ($R = R_1 = R_2$), Eq. (5) implies

$$-\frac{dR_1}{dt_1^*} \cdot \frac{1}{\gamma_{eq,1}} \cdot \exp\left(-\frac{\Delta X_1(0)}{X_{const}} R_1(t_1^*)\right) = -\frac{dR_2}{dt_2^*} \cdot \frac{1}{\gamma_{eq,2}} \cdot \exp\left(-\frac{\Delta X_2(0)}{X_{const}} R_2(t_2^*)\right). \tag{6}$$

For time increments dt_1^* and dt_2^* leading to identical changes $dR_1 = dR_2$ we can write Eq. (6) using the premise that $R_1(t_1^*) = R_2(t_2^*)$ to give

$$dt_2^* = \frac{\gamma_{eq,1}}{\gamma_{eq,2}} \cdot \exp\left(\frac{\Delta X_1(0) - \Delta X_2(0)}{X_{const}} R_1(t_1^*)\right) dt_1^*. \tag{7}$$

Integrating this leads to (assuming that both jumps are initiated at time zero)

$$t_2 = \int_0^{t_2} dt_2^* = \frac{\gamma_{eq,1}}{\gamma_{eq,2}} \int_0^{t_1} \exp\left(\frac{\Delta X_1(0) - \Delta X_2(0)}{X_{const}} R_1(t_1^*)\right) dt_1^*, \tag{8}$$

which then determines $t_2(t_1) = t_2(t_1(R)) = t_2(R)$ predicting the inverse function $R_2(t)$.

In practice, we do not need to do an inversion. The procedure is to transform a discrete set of measured data points, a time vector $\mathbf{t}_1 = (t_1^1, t_1^2, \ldots, t_1^n)$ and a corresponding relaxation vector $\mathbf{R}_1 = (R_1^1, R_1^2, \ldots, R_1^n)$) to a new time vector $\mathbf{t}_2 = (t_2^1, t_2^2, \ldots, t_2^n)$ corresponding to the measured $\mathbf{R}_1$ points. Plotting $(\mathbf{t}_2, \mathbf{R}_1)$ should then fall on R_2, which can be tested by a separate measurement.

For jumps ending at the same temperature Eq. (8) reduces to

$$t_2 = \int_0^{t_1} \exp\left(\frac{\Delta X_1(0) - \Delta X_2(0)}{X_{const}} R_1(t_1^*)\right) dt_1^*, \tag{9}$$

which is the equation used in Hecksher *et al.*[8].

The new generalized test has the disadvantage that one needs to know the equilibrium clockrate γ_{eq}. By assuming an internal clock[9,38], one may define the clock rate at T_{end} (γ_{eq}) as the dielectric inverse relaxation time ($\gamma_{eq} = 1/\tau$), where the relaxation time is determined from the maximum frequency at the α-peak (f_m) as $\tau = 1/(2\pi f_m)$. At the temperatures where jumps are performed, we cannot find τ directly, since the α-peak is outside the available frequency range (see Fig. 1 (a)). One may find γ_{eq} using an extrapolation from a fitting function e.g. Vogel-Fulcher-Tammann (VFT) or determine γ_{eq} in another way. Below we let the constant $\frac{\gamma_{eq,1}}{\gamma_{eq,2}}$ in Eq. (8) be a free parameter to find the γ_{eq} that gives the best prediction (which is very close to the VFT prediction seen in Fig. 4).

The constant X_{const} was identified using two jumps to the same temperature; the down jump 184 K to 180 K and the up jump 176 K to 180 K. A fit is made using Eq. (9) to find the X_{const} that gives the best prediction of one jump from the other. This gives $X_{const} = 0.16$, which was used for all jumps.

The result of the test is shown in Fig. 3. The up jump 176 K to 180 K (Fig. 3 (a)) is used to predict the other jumps. The predictions are good, however with some deviations especially at short times, which was also seen for the van der Waals liquids tested in Hecksher *et al.* 2015[8]. The 8 K jumps have larger deviations than the smaller jumps (however, still similar to the results on the van der Waals liquids[8]). Since we use a first-order Taylor expansion in the derivation of the test, it is not surprising that the test breaks

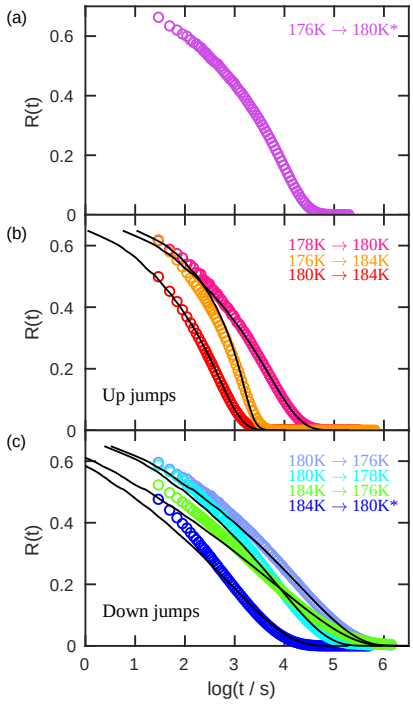

FIG. 3: Test 1. Prediction of jumps based on the jump 176 K to 180 K (shown in (a)). In (b) and (c) circles are data and black lines are predictions. The up jump 176 K to 180 K and the down jump 184 K to 180 K were used to find X_{const} (indicated by * in legend), while $\gamma_{eq}(T)$ was a fitting parameter (Fig. 4).

down somewhat at large temperature jumps.

Note that the two down jumps starting at 184 K both have large deviations at short times. This might be due to the relative fast relaxation time at this temperature and structural relaxation may have occured during the jump and during the first measurements.

Figure 4 shows γ_{eq} as a function of temperature found from the free parameter $\gamma_{eq,1}/\gamma_{eq,2}$ in Eq. (8). To determine γ_{eq} for each temperature, we used a value of γ_{eq} at 184 K found from a VFT-fit to higher temperature data. The different jumps to the different temperatures give a slightly different value, which is barely visible in the figure. The

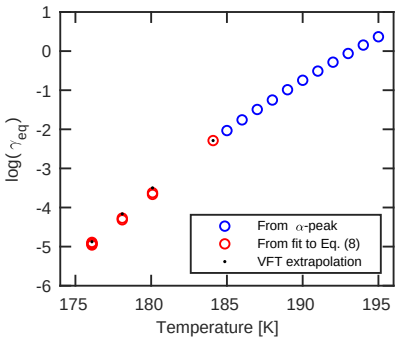

FIG. 4: The clock rate at equilibrium at the end temperature (γ_{eq}) found from equilibrium spectra (blue circles). The red circles are determined from the free parameter $\gamma_{eq,1}/\gamma_{eq,2}$ in Eq. (8). Since we have two jumps to 180 K and 176 K this results in two values of γ_{eq} at these temperatures, however, the difference is barely visible. The black dots are the predictions from the VFT-fit.

found values look realistic, however, varies slighty from the predictions of γ_{eq} from VFT. The values of γ_{eq} is stated in Table II.

B. Test 2 - Unique function of R

Taking the logarithm of Eq. (5) leads to (remember $\dot{R} < 0$)

$$\ln\left(-\frac{\dot{R}}{\gamma_{eq}}\right) - \frac{\Delta X(0)}{X_{const}} R = \ln(F(R)) \tag{10}$$

Since $F(R)$ is a unique function of R, the left hand side of Eq. (10) (denoted LHS following Hecksher *et al.* 2015[8]) is also a unique function of R. This means that LHS plotted against R for the different jumps collapse onto one master curve if a single parameter controls both $X(t)$ and $\gamma(t)$. γ_{eq} found from Test 1 is used. For each temperature the found values of γ_{eq} is now averagered, so that each temperature has a fixed γ_{eq}.

Figure 5 shows the result of the test. The data falls onto one master curve. As also seen with test 1, small deviations are observed at short times (large R).

Temperature	$\log(\gamma_{eq})$ from Eq. (8)	Average $\log(\gamma_{eq})$ from Eq. (8)	$\log(\gamma_{eq})$ from VFT
184 K			-2.28
180 K	-3.62	-3.64	-3.50
	-3.67		
178 K	-4.27	-4.29	-4.16
	-4.31		
176 K	-4.92	-4.92	-4.88
	-4.96		
	-4.89		
	-4.93		

TABLE II: The equilibrium clockrate at the end temperature γ_{eq} determined from Eq. (8). To invert $\gamma_{eq,1}/\gamma_{eq,2}$ to γ_{eq}, we first used the value of γ_{eq} at 184 K found from a VFT-fit to estimate γ_{eq} at 180 K (resulting in two values because there are two jumps to 184 K). The estimated γ_{eq} at 180 K are then used to determine γ_{eq} at 178 K and 176 K. Different jumps to the same temperature gives a slightly different value of γ_{eq}. Furthermore, extrapolations of VFT-fit are stated.

V. DISCUSSION & CONCLUSION

A. How to test the single-parameter assumption

The data analysis emphasizes that measurements must be precise to use the direct tests of single-parameter aging. It is important that the liquid is in equilibrium at the starting temperature and reaches full equilibrium at the ending temperature. Actually, the liquid does not have to reach full equilibrium, if one knows the correct X_{eq}; i.e., where it should end. Our analysis revealed that it is crucia to have the correct X_{eq}. When performing a large up jump from the glassy state it is possible to monitor a full relaxation curve where both the plateau in the beginning and the end is present. It is recommended to use such a jump for predicting other jumps.

Test 1, which is used to predict the curves, is the most sensitive test. By using test 1 it is possible to find γ_{eq} at temperatures where the peak is not present in the dielectric equilibrium spectrum. If one knows γ_{eq} (for example using an extrapolation), an advantage of test 1 is that if a liquid has single-parameter aging, one can use Eq. (8) to predict

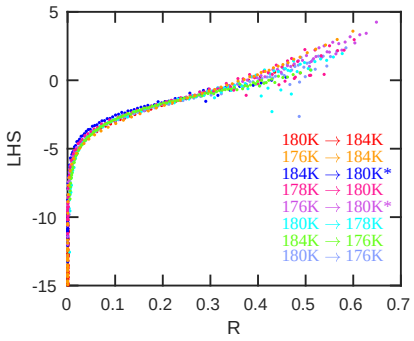

FIG. 5: Test 2. The left hand side of Eq. (10) (LHS) plotted against R. If the liquid has single-parameter aging, the data are predicted to collapse onto one master curve which is seen to apply to a good approximation. The two jumps used for determining X_{const} are marked by *.

relaxation curves. It is necessary to perform two jumps (preferably to the same temperature) to identify X_{const}. Other jumps can then be predicted knowing the clock rate at the end temperature (γ_{eq}), the measured quantity at the starting temperature ($X(0)$), and the measured quantity at the end temperature (X_{eq}). $\Delta X(0) = X(0) - X_{eq}$ determines the shape of the relaxation, while γ_{eq} determines the position of the relaxation. This is of course also limited to small jumps, and possible only in the same temperature range, as the actual jumps are performed in.

B. The scope of single-parameter aging

Hecksher *et al.* 2015[8] demonstrated single-parameter aging for three different van der Waals liquids. In the present investigation the tests are for the first time applied to a hydrogen-bonded liquid. The comparison of hydrogen-bonded liquids and van der Waals bonded liquids is interesting in view of the isomorph theory, which states that R-simple liquids have simple behavior along isochrones[10,11]. Van der Waals bonded liquids are expected to be R-simple, whereas hydrogen-bonded liquids are not. The isomorph theory was suggested a decade ago, and since it has been tested in a number of investigations e.g.[39–44]. Earlier investigations of density scaling[45–48] and isochronal superposition[49–53] also follow the predictions of the isomorph theory. The understand-

ing of aging in computer simulation has been connected to isomorph theory already in 2010[54] and recently experimental results[5] and theory of aging[12] were also analyzed and developed in the framework of isomorph theory. Based on these earlier works we expected that single-parameter aging might not work for a hydrogen bonding network-forming system like glycerol. However, based on the tests presented above we find that single-parameter aging works to a good approximation also for glycerol. The degree of agreement with the predictions from the single-parameter aging found for glycerol is in fact very similar to that found for three van der Waals bonding liquids in Ref.[8]. This finding suggests that single-parameter aging works for a wider range of systems than those complying to isomorph theory, which also means that single-parameter aging needs to be understood in a more general theoretical framework.

The tests work well also for the large jumps (4 K and 8 K), while it previously has been tested only for jumps of maximum 2 K[8]. At the 8 K jumps single-parameter aging may begin to break down, which is not surprising, since a first-order Taylor expansion is used in the derivation of the tests. For future works higher order Taylor expansions could be introduced in the tests.

VI. ACKNOWLEDGEMENT

L. A. R. and K. N. want to thank The Danish Council for Independent Research for supporting this work. The center for viscous liquid dynamics "Glass and Time" was sponsored by the Danish National Research Foundation's Grant No. DNRF61. T. H. and J. C. D. are supported by the VILLUM Foundation's Matter grant (16515).

[1] R. Cotterill, *The Cambridge guide to the material world* (Cambridge University Press, Cambridge, 1985), ISBN 0521246407.

[2] S. Brawer, *Relaxation in viscous liquids and glasses, review of phenomenology, molecular dynamics simulations, and theoretical treatment* (American Ceramic Society, Columbus, Ohio, 1985), ISBN 0916094685.

[3] G. W. Scherer, *Relaxation in glass and composites* (Wiley, New York, 1986), ISBN 0471819913.

[4] O. S. Narayanaswamy, J. Am. Ceram. Soc. **54**, 491 (1971).

[5] K. Niss, Phys. Rev. Lett. **119**, 115703 (2017).

[6] A. Q. Tool, J. Am. Ceram. Soc. **29**, 240 (1946).

[7] J. C. Dyre, J. Chem. Phys. **143**, 114507 (2015).

[8] T. Hecksher, N. B. Olsen, and J. C. Dyre, J. Chem. Phys. **142**, 241103 (2015).

[9] T. Hecksher, N. B. Olsen, K. Niss, and J. C. Dyre, J. Chem. Phys. **133**, 174514 (2010).

[10] N. Gnan, T. B. Schrøder, U. R. Pedersen, N. P. Bailey, and J. C. Dyre, J. Chem. Phys. **131**, 234504 (2009).

[11] J. C. Dyre, J. Phys. Chem. B **118**, 10007 (2014).

[12] J. C. Dyre, J. Chem. Phys. **148**, 154502 (2018).

[13] G. E. Gibson and W. F. Giauque, **45**, 93 (1923).

[14] C. H. Wang and R. B. Wright, J. Chem. Phys. **55**, 1617 (1971).

[15] B. Schiener, R. Böhmer, A. Loidl, and R. Chamberlin, Science **274**, 752 (1996).

[16] L. Berthier, G. Biroli, J.-P. Bouchaud, L. Cipelletti, D. E. Masri, D. L'Hôte, F. Ladieu, and M. Pierno, Science **310**, 1797 (2005).

[17] T. Pezeril, C. Klieber, S. Andrieu, and K. A. Nelson, Phys. Rev. Lett. **102**, 107402 (2009).

[18] S. Albert, T. Bauer, M. Michl, G. Biroli, J.-P. Bouchaud, A. Loidl, P. Lunkenheimer, R. Tourbot, C. Wiertel-Gasquet, and F. Ladieu, Science **352**, 1308 (2016).

[19] R. W. Salt, Nature **181**, 1281 (1958).

[20] J. L. Dashnau, N. V. Nucci, K. A. Sharp, and J. M. Vanderkooi, The Journal of Physical Chemistry B **110**, 13670 (2006).

[21] D.-X. Li, B.-L. Liu, Y. shu Liu, and C. lung Chen, Cryobiology **56**, 114 (2008).

[22] J. J. Towey, A. K. Soper, and L. Dougan, Phys. Chem. Chem. Phys. **13**, 9397 (2011).

[23] M. H. Jensen, C. Gainaru, C. Alba-Simionesco, T. Hecksher, and K. Niss, Phys. Chem. Chem. Phys. **20**, 1716 (2018).

[24] P. G. Debenedetti, *Metastable liquids, concepts and principles*, Physical chemistry (Princeton University Press, Princeton, N.J, 1996), ISBN 0691085951.

[25] K. Niss, D. Gundermann, T. Christensen, and J. C. Dyre, Phys. Rev. E **85**, 041501 (2012).

[26] B. Igarashi, T. Christensen, E. H. Larsen, N. B. Olsen, I. H. Pedersen, T. Rasmussen, and J. C. Dyre, Rev. Sci. Instrum. **79**, 045105 (2008).

[27] E. Schlosser and A. Schönhals, Polymer **32**, 2135 (1991).

[28] U. Schneider, R. Brand, P. Lunkenheimer, and A. Loidl, Phys. Rev. Lett. **84**, 5560 (2000).

[29] P. Lunkenheimer, R. Wehn, U. Schneider, and A. Loidl, Phys. Rev. Lett. **95**, 055702 (2005).

[30] P. Lunkenheimer, R. Wehn, and A. Loidl, J. Non-Cryst. Solids **352**, 4941 (2006).

[31] R. Wehn, P. Lunkenheimer, and A. Loidl, J. Non-Cryst. Solids **353**, 3862 (2007).

[32] Richert Ranko, Lunkenheimer Peter, Kastner Stefan, and Loidl Alois, J. Phys. Chem. B **117**, 12689 (2013).

[33] A. Alegría, E. Guerrica-Echevarria, L. Goitiandia, I. Telleria, and J. Colmenero, Macromolecules **28**, 1516 (1995).

[34] Alegría A., Goitiandía L., Tellería I., and Colmenero J., Macromolecules **30**, 3881 (1997).

[35] L. Goitiandia and A. Alegría, J. Chem. Phys. **121**, 1636 (2004).

[36] D. Cangialosi, M. Wübbenhorst, J. Groenewold, E. Mendes, and S. Picken, J. Non-Cryst. Solids **351**, 2605 (2005).

[37] B. Igarashi, T. Christensen, E. H. Larsen, N. B. Olsen, I. H. Pedersen, T. Rasmussen, and J. C. Dyre, Rev. Sci. Instrum. **79**, 045106 (2008).

[38] B. Jakobsen, T. Hecksher, T. E. Christensen, N. B. Olsen, J. C. Dyre, and K. Niss, J. Chem. Phys. **136** (2012).

[39] D. Gundermann, U. R. Pedersen, T. Hecksher, N. P. Bailey, B. Jakobsen, T. Christensen, N. B. Olsen, T. B. Schrøder, D. Fragiadakis, R. Casalini, et al., Nat. Phys. **7**, 816 (2011).

[40] L. A. Roed, D. Gundermann, J. C. Dyre, and K. Niss, J. Chem. Phys. **139**, 101101 (2013).

[41] W. Xiao, J. Tofteskov, T. V. Christensen, J. C. Dyre, and K. Niss, J. Non-Cryst. Solids **407**, 190 (2015).

[42] L. A. Roed, K. Niss, and B. Jakobsen, J. Chem. Phys. **143**, 221101 (2015).

[43] K. Adrjanowicz, J. Pionteck, and M. Paluch, RSC Adv. **6**, 49370 (2016).

[44] H. W. Hansen, A. Sanz, K. Adrjanowicz, B. Frick, and K. Niss, Nat. Commun. **9**, 518 (2018).

[45] C. Dreyfus, A. Aouadi, J. Gapinski, M. Matos-Lopes, W. Steffen, A. Patkowski, and R. M. Pick, Phys. Rev. E **68**, 011204 (2003).

[46] C. Alba-Simionesco, A. Cailliaux, A. Alegría, and G. Tarjus, Europhys. Lett. **68**, 58 (2004).

[47] R. Casalini and C. M. Roland, Phys. Rev. E **69**, 062501 (2004).

[48] C. M. Roland, S. Hensel-Bielowka, M. Paluch, and R. Casalini, Rep. Prog. Phys. **69**, 1405 (2005).

[49] A. Tölle, Rep. Prog. Phys. **64**, 1473 (2001).

[50] C. M. Roland, R. Casalini, and M. Paluch, Chem. Phys. Lett. **367**, 259 (2003).

[51] S. Pawlus, M. Paluch, M. Sekula, K. L. Ngai, S. J. Rzoska, and J. Ziolo, Phys. Rev. E **68**, 021503

(2003).

[52] K. L. Ngai, R. Casalini, S. Capaccioli, M. Paluch, and C. M. Roland, J. Phys. Chem. B **109**, 17356 (2005).

[53] C. M. Roland, R. Casalini, R. Bergman, and J. Mattsson, Phys. Rev. B **77**, 012201 (2008).

[54] N. Gnan, C. Maggi, T. B. Schrøder, and J. C. Dyre, Phys. Rev. Lett. **104**, 125902 (2010).